

Technical Reports



CENTRO EURO-MEDITERRANEO
PER I CAMBIAMENTI CLIMATICI

ISC – Impatti sul Suolo e sulle Coste

AMRA: Numerical analyses on the response of slopes subjected to rainfall - Typical geomorphological scenarios in Campania Region

prof. Luciano Picarelli

Analisi e Monitoraggio del Rischio Ambientale, AMRA

prof. Filippo Vinale

Analisi e Monitoraggio del Rischio Ambientale, AMRA



AMRA:

**Numerical analyses on the response of slopes subjected to rainfall -
Typical geomorphological scenarios in Campania Region**

Summary

This report contains the results of some numerical analyses aimed to investigate the factors which govern the response of typical slopes in Campania Region subjected to rainfall. In particular, the results show how geometrical features, rainfall characteristics, soil properties, initial and boundary conditions influence the slope behaviour, determining different consequences in terms of time and size of failure.

The analyses of the transient infiltration due to the rainfall have been performed thanks to the finite element code SEEP/W, produced by GEO-SLOPE International Ltd. The input data have been obtained by literature and previous reports on the same subject.

Keywords: rainfall-induced landslides, pyroclastic soils, numerical simulation

JEL Classification:

Address for correspondence:

prof. Luciano Picarelli
E-mail: luciano.picarelli@amracentre.com

prof. Filippo Vinale
E-mail: filippo.vinale@amracentre.com

A.M.R.A. S.c.a.r.l.
Via Nuova Agnano, 11
80125 Napoli, Italy



CONTENTS

1. Foreword.....	4
2. Theoretical aspects.....	4
2.1 Infiltration model.....	4
2.2 Slope stability model.....	7
3. Examined cases.....	9
3.1. Results.....	15
4. Conclusive remarks.....	34
5. References.....	35
 ATTACHMENT A.....	 36
 ATTACHMENT B.....	 49
 ATTACHMENT C.....	 62
 ATTACHMENT D.....	 68
 ATTACHMENT E.....	 81
 ATTACHMENT F.....	 95
 ATTACHMENT G.....	 105
 ATTACHMENT H.....	 117
 ATTACHMENT I.....	 130



1. Foreword

During the last decades, several rainfall events have mobilized shallow pyroclastic deposits which cover many slopes in Campania Region (Southern Italy), sometimes causing victims and huge economical damages. The analyses included in this report intend to stress the role of the main factors which affect the stability of slopes.

The analyses concern the study of the transient flow induced by the rainfall coupled with a stability analysis. In particular, the seepage analysis has been performed by the SEEP/W code, produced by the GEO-SLOPE International Ltd. The code is a finite element program able to model both saturated and unsaturated 2D seepage. The input data needed by the code have been taken from literature and reports in the context of this research.

2. Theoretical aspects

2.1 Infiltration model

The equations which govern the seepage problems modelled by SEEP/W are:

- conservation of the mass law;
- Darcy's flow law.

Referring for a given X-Y (horizontal-vertical) coordinate system (2D problem), the conservative law of the mass is regulated by the equation:

$$\frac{\partial}{\partial x} v_x + \frac{\partial}{\partial y} v_y + Q = -\frac{\partial \theta}{\partial t} \quad [2.1]$$

where

- v_x [L/T] is the hydraulic velocity in the x -direction;
- v_y [L/T] is the water velocity in the y -direction;
- Q [(L/T)/L] is the imposed boundary flux;
- θ is volumetric water content;
- t [T] is the time.

The equation [2.1] states that the change in the water flux seeping through an elemental volume at a point is equal, at any time, to the change in the volumetric water content of the soil.

According to the Darcy's flow law (1856), the hydraulic velocities v_x and v_y are related to the gradient of fluid through the equations:

$$v_x = -k_x \cdot \frac{\partial H}{\partial x} \quad [2.2]$$

$$v_y = -k_y \cdot \frac{\partial H}{\partial y} \quad [2.3]$$

where

- k_x is the hydraulic conductivity in the x-direction;
- k_y is the hydraulic conductivity in the y-direction;
- H is the total head

The equations [2.2] and [2.3], originally applied by Darcy to saturated soils, were later on validated by other researcher (Richards, 1931; Childs and Collins-George, 1950) also for unsaturated soils. In such a case, the hydraulic conductivity k is not a constant, but a function of the water content and consequently of the pore-water pressure (Fig. 2.1).

Combining the equations [2.2] and [2.3] with the [2.1], the following equation is obtained

$$\frac{\partial}{\partial x} \left[k_x \cdot \frac{\partial H}{\partial x} \right] + \frac{\partial}{\partial y} \left[k_y \cdot \frac{\partial H}{\partial y} \right] + Q = \frac{\partial \theta}{\partial t} \quad [2.4]$$

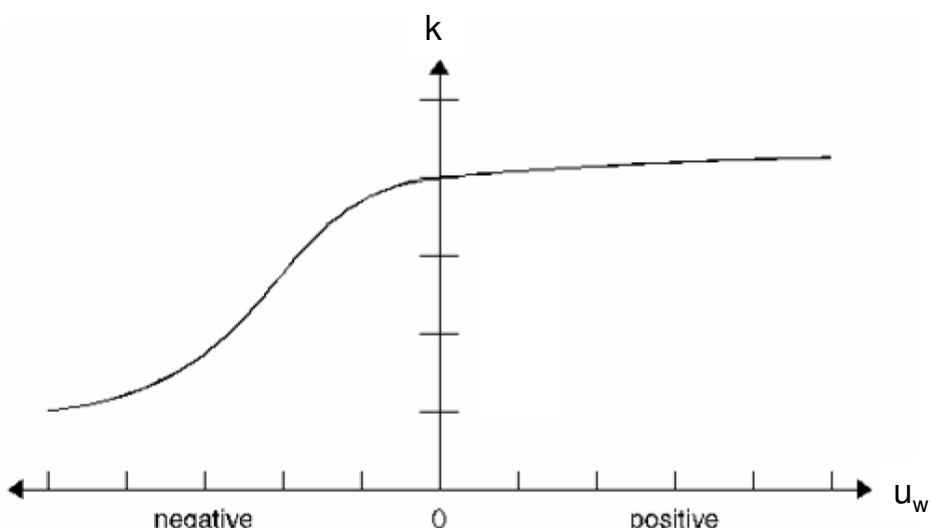


Figure 2.1. Relationship between the hydraulic conductivity k and the pore-water pressure u_w (permeability function)

The knowledge of the constitutive model of the soil allow to relate any change with time of the volumetric water content to change of the stress state and of the properties of soil. In particular, according to Fredlund and Morgenstern (1976), the stress state for a unsaturated soil can be described through the stress state variables

- $(s - u_a)$, which is the net normal stress
- $(u_a - u_w)$, which is the matric suction

where s is the total stress, u_a is the pore-air pressure, u_w is the pore-water pressure. The solutions of the equation [2.4] are furnished by SEEP/W, under further assumptions:

- the total stress s doesn't change during the transient seepage;
- the pore-air pressure u_a is equal to the atmospheric pressure.

Accordingly any change in water content θ depends only by a change in pore-water pressure u_w , through the equation

$$\partial\theta = m_w \cdot \partial u_w \quad [2.5]$$

where m_w is the slope of the so called soil-water "characteristic curve" (Fig. 2.2).

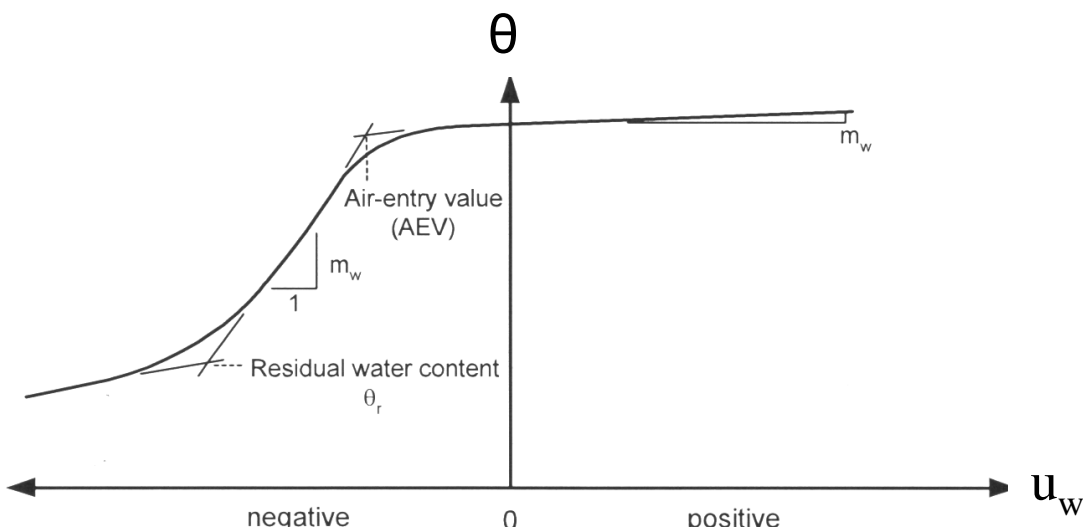


Figure 2.2. Relationship between the volumetric water content and the pore-water pressure u_w (soil-water characteristic curve)

The pore-water pressure u_w can be defined as

$$u_w = \gamma_w \cdot (H - y) \quad [2.6],$$

where

- γ_w is the unit weight of water
- y is the elevation.

Using the equations [2.5] and [2.6], the governing differential equation [2.4] becomes

$$\frac{\partial}{\partial x} \left[k_x \cdot \frac{\partial H}{\partial x} \right] + \frac{\partial}{\partial y} \left[k_y \cdot \frac{\partial H}{\partial y} \right] + Q = m_w \cdot \gamma_w \cdot \frac{\partial H}{\partial t} \quad [2.7]$$

The analysis is performed through the finite element method. In particular, SEEP/W assumes that the head distribution within each element follows the same interpolating functions adopted for the elements themselves. The finite element equation derives from the Weighted Residual Method of Galerkin.

2.2 Slope stability model

Slope stability is carried out using the infinite-slope model, which applies only if the thickness of the landslide is small with respect to its length and width (Fig. 2.3): taking into account of the characteristics of pyroclastic slopes in the Campania Region, this hypothesis can be considered quite reliable. From a numerical point of view, this assumption applies very well in the middle of the domain and far enough from the lateral boundaries (Fig. 2.3).

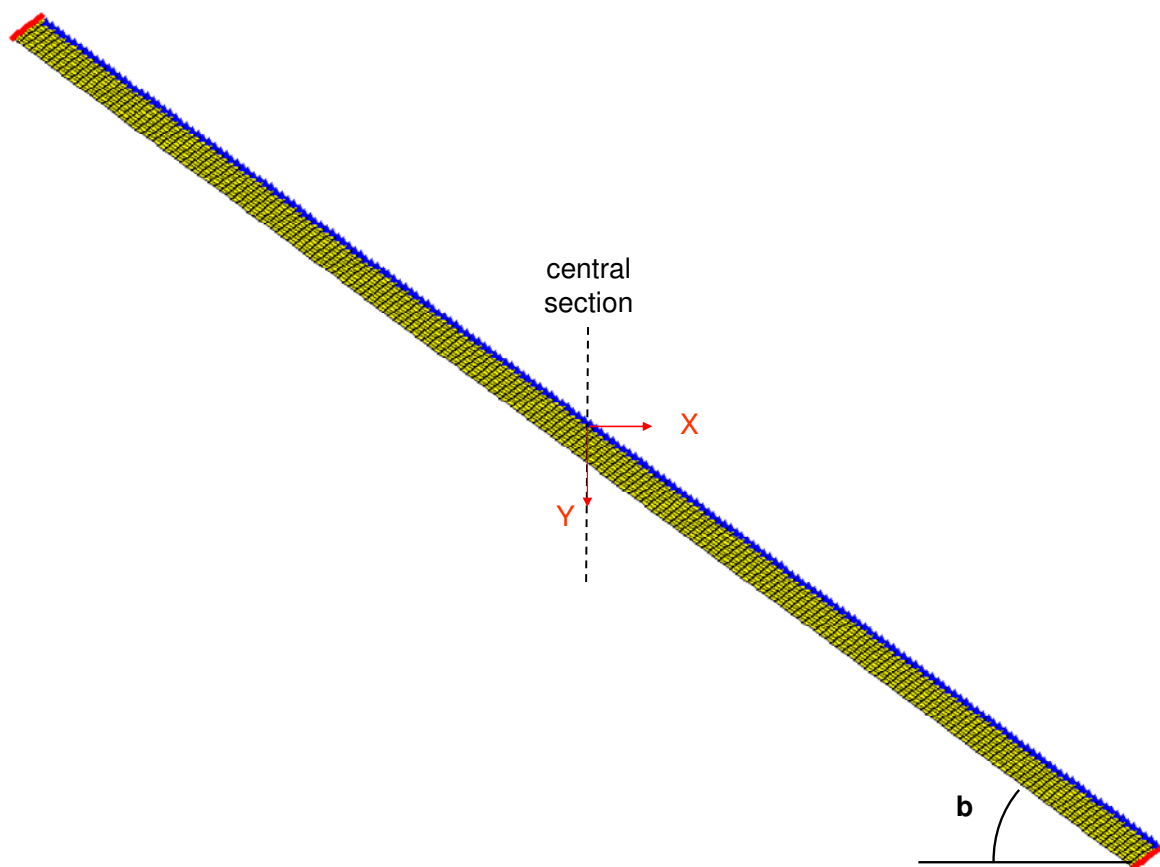


Figure 2.3. Infinite-slope model: the output data have been taken from the vertical central section

The factor of safety $FS(Y;t)$ is the ratio of the resisting shear stress τ_{lim} and the driving shear stress τ acting on the considered plane located at a depth Y parallel to the ground surface

$$FS(Y;t) = \frac{\tau_{lim}(Y;t)}{\tau(Y)} [2.8]$$

Fredlund (1979) has furnished the following formulation for the shear strength envelope of unsaturated soils



$$\tau_{\text{lim}} = [c' + (u_a - u_w) \cdot \chi \cdot \tan \varphi'] + (\sigma - u_a) \cdot \tan \varphi' \quad [2.9]$$

where

- τ_{lim} is the shear strength;
- c' and φ' are the shear strength parameters for saturated conditions;
- $(u_a - u_w)$ is the matric suction,
- χ is a coefficient function of various factors, such as confining total stress, suction, degree of saturation, void ratio, etc.;
- $(\sigma - u_a)$ is the net normal stress.

The coefficient χ has been expressed through the equation proposed by Vanapalli et al. (1996)

$$\chi = \Theta^k \quad [2.10]$$

where

- $\Theta = \frac{\theta - \theta_r}{\theta_s - \theta_r}$ is the relative volumetric water content;
- θ is the volumetric water content;
- θ_s is the saturated volumetric water content;
- θ_r is the residual volumetric water content;
- k is a fitting parameter.

Therefore, the equation [2.8] takes the following expression

$$FS(Y; t) = \frac{\tau_{\text{lim}}(Y; t)}{\tau(Y)} = \frac{c(Y; t) + [\sigma(Y) - u_a] \cdot \tan \varphi'}{\gamma \cdot Y \cdot \sin \beta \cdot \cos \beta} \quad [2.11]$$

where:

- $c(Y; t)$ is the intercept of cohesion, function of the matric suction $u_a - u_w(Y; t)$, according to the equation

$$c = c' + (u_a - u_w) \cdot \Theta^k \cdot \tan \varphi' \quad [2.12]$$

- $s(Y) = g \cdot Y \cdot \cos^2 \beta$ is the total normal stress, acting at the depth Y in the direction normal to the slope;
- β is the inclination of the slope;
- γ is the unit weight of soil;
- u_a , which is the relative air pressure, has been assumed equal to the atmospheric pressure ($u_a = 0$).

Due to the dependence by time of matric suction, then of intercept of cohesion, the factor of safety is a time-function.

If the soil is saturated, the coefficient χ is equal to 1.



3. Examined cases

In order to investigate the influence of different factors on the response of the slope subjected to rainfall, different hypotheses have been made about

- slope angle;
- mechanical and hydraulic properties of the soil;
- thickness of the soil;
- stratigraphy;
- rainfall intensity;
- initial hydraulic conditions;
- boundary hydraulic conditions.

Slope angle

Four slope angles have been considered: 20°; 30°; 40°; 45°.

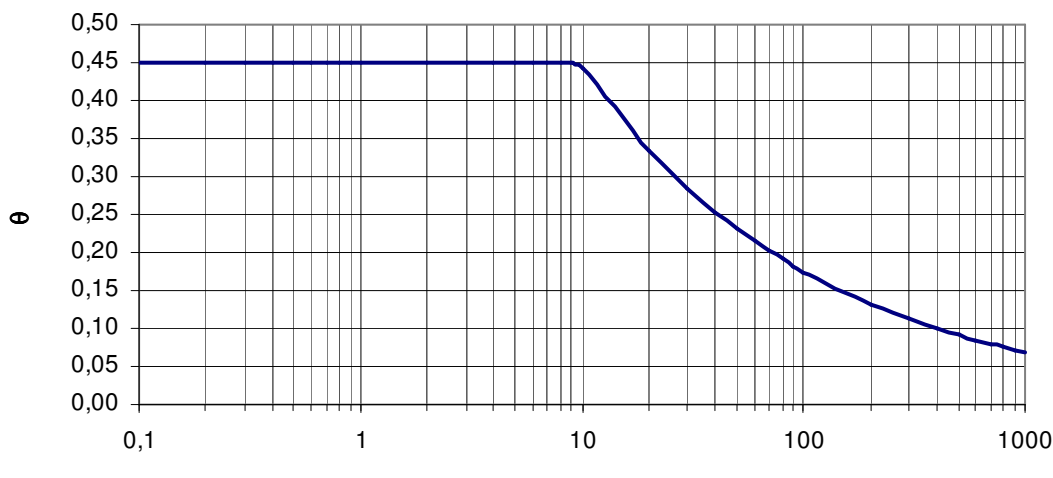
Mechanical and hydraulic properties of the soil

Two classes of soils, respectively named soil nr.1 and soil nr.2, have been studied.

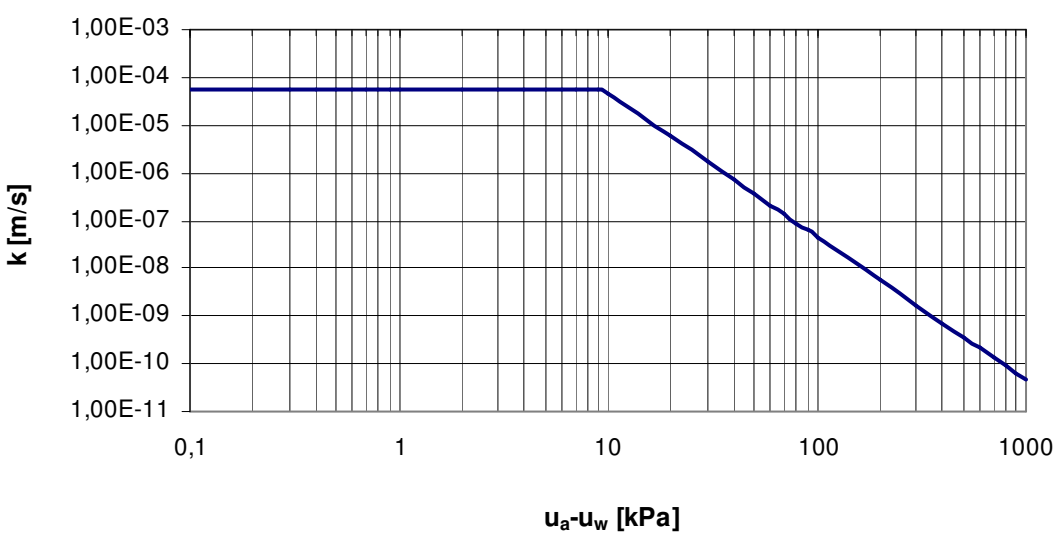
The properties of soil nr.1 are typical of the pyroclastic ashes of the Phlegraean Fields (Evangelista and Scotto di Santolo, 2001), while the properties of soil nr.2 are typical of the air-fall ashes of Cervinara (Olivares and Tommasi, 2008). Their properties are reported in Table 3.1 and in the Figures 3.1 and 3.2.

Table 3.1 Considered properties of soil

	unit weight, g [kN/m³]	hydraulic properties						strength properties	
		k_{ws} [m/s]	θ_{ws}	θ_{wr}	λ	α [kPa a⁻¹]	$(u_a - u_w)_e$ [kPa]	permeability, K [m/s]	intercept of cohesion, c [kPa]
soil nr.1	13	5.40·10⁻⁵	0,45	0,00	0,4019	0,1053	9,5	k_{ws}	$c = (u_a - u_w) \cdot \Theta^2 \cdot \operatorname{tg} \varphi'$
soil nr.2		3.73·10⁻⁷	0,70	0,10	0,4200	0,3333	3,0	$k_{ws} \cdot [\alpha \cdot (u_a - u_w)]^{-(2+5\lambda/2)}$	35 $c = (u_a - u_w) \cdot \Theta^{1,2} \cdot \operatorname{tg} \varphi'$ 38

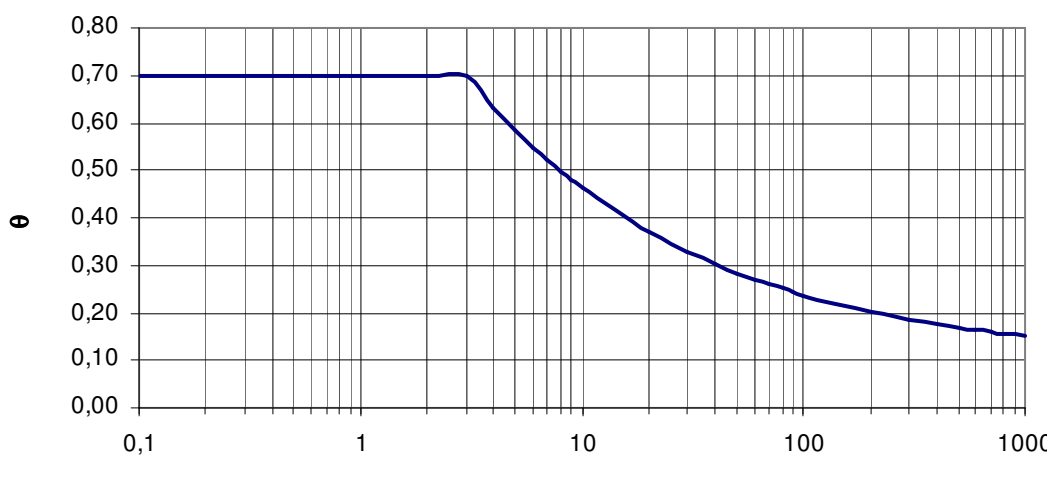


a)

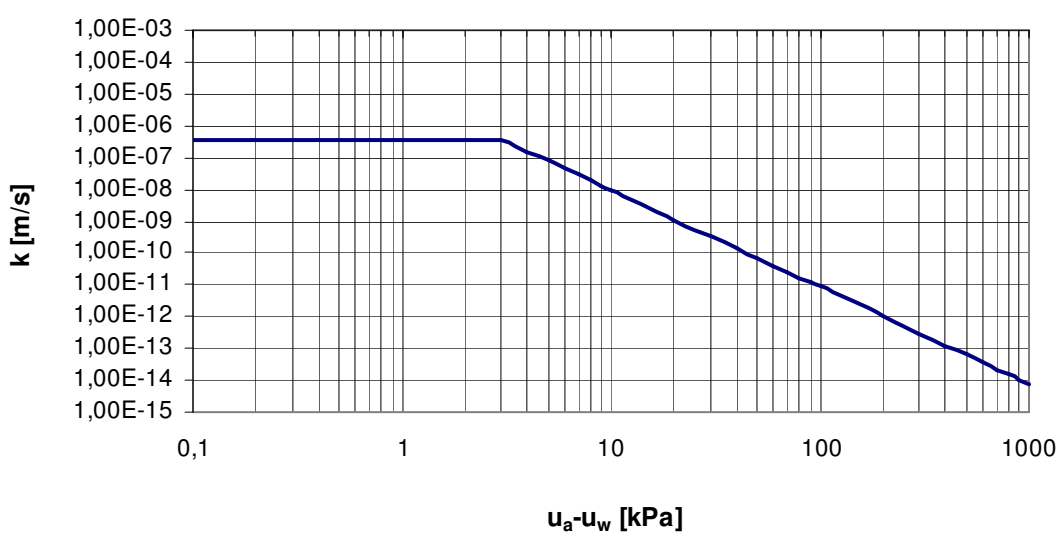


b)

Figure 3.1. Soil-water characteristic curve (a) and permeability function (b) of soil nr.1



a)



b)

Figure 3.2. Soil water characteristic curve (a) and permeability function (b) of the soil nr.2



Thickness of the soil

Four thicknesses h have been considered: 0.5 m; 1.0 m; 2.0 m; 4.0 m.

Stratigraphy

Two hypotheses have been made:

- homogeneous deposit;
- layered deposit.

In the second hypothesis, a layer with a higher saturated permeability k_{sat} , named soil nr.3, has been interbedded between two layers characterized by the properties of soil nr.1. This scenario reproduces the sequences that show pumice layers (more pervious in saturated conditions) interbedded between pyroclastic ashes (less pervious in saturated conditions).

In order to assign the soil-water characteristic curve to soil nr.3, the van Genuchten's equation (1980) has been adopted

$$\frac{\theta - \theta_r}{\theta_s - \theta_r} = \left[\frac{1}{1 + \alpha \cdot |h|^n} \right]^m \quad [3.1] \quad [h] = [cm]$$

with $\theta_s = 0.55$; $\theta_r = 0.25$; $m = 0.3$; $n = 7$; $\alpha = 3.3$. For the permeability function of soil nr.3, the Gardner's equation (1958) has been adopted

$$k = k_{sat} \cdot \frac{1}{1 + a \cdot (u_a - u_w)^n} \quad [3.2] \quad [u_a - u_w] = [kPa] \\ [k] = [m/s]$$

with $k_{sat} = 5.40 \cdot 10^{-3}$ m/s, $a = 1$, $n = 0.80$.

Rainfall intensity

Different rainfall intensities have been imposed at the upper boundary of the slope model. Such intensities vary within the range 0.972 ÷ 97.20 mm/h, whose limits respectively correspond to the 0.5% and the 50% of the saturated permeability of soil nr.1 ($k_{sat} = 5.40 \cdot 10^{-5}$ m/s).

Initial hydraulic conditions

The characteristics of the initial steady state can strongly influence the response of a slope to rainfall.

Under the hypothesis of initial water flow parallel to the ground surface, three initial suctions $(u_a - u_w)_0$ have been imposed at the ground surface: 95 kPa, 42.49 kPa and 19 kPa. In particular, the highest and the lowest values are respectively 10 and 2 times bigger than the air-entry value of soil nr.1 $(u_a - u_w)_e = 9.5$ kPa.



Boundary hydraulic conditions

Two hypotheses have been made about the lower boundary condition: impervious and pervious bottom. The “impervious hypothesis” is representative of slopes resting on non fractured bedrock or on fine-grained soils; the “pervious hypothesis” enables to consider the case of pyroclastic covers laying on highly fractured rock.

The scenarios have been examined through different analyses, as reported in Table 3.2.

The different hypotheses about slope angle β , thickness of the deposit h and suction at the ground surface ($u_a - u_w$)₀ obviously let the safety factor FS_0 to assume different initial values, which vary within the interval 1.18 ÷ 3.90 (Figs. 3.3a and 3.3b).

The results of the analyses are reported in attachments. In the follow the most significant results will be commented.

Table 3.2. Examined cases: β is the slope angle; h is the thickness of the deposit

Hypothesis	Case	$h = 4.0 \text{ m}$	$h = 2.0 \text{ m}$	$h = 1.0 \text{ m}$	$h = 0.5 \text{ m}$
1) $\beta = 45^\circ$; soil nr.1	a		x		
	b			x	
	c			Δ	
	d				x
2) $\beta = 30^\circ$; soil nr.1	a		x		
	b		o		
3) $\beta = 20^\circ$; soil nr.1	a	x			
	b		x		
4) $\beta = 40^\circ$; soil nr.2			x		

x : homogeneous deposit - impervious bottom

Δ : homogeneous deposit - pervious bottom

o : layered deposit - impervious bottom

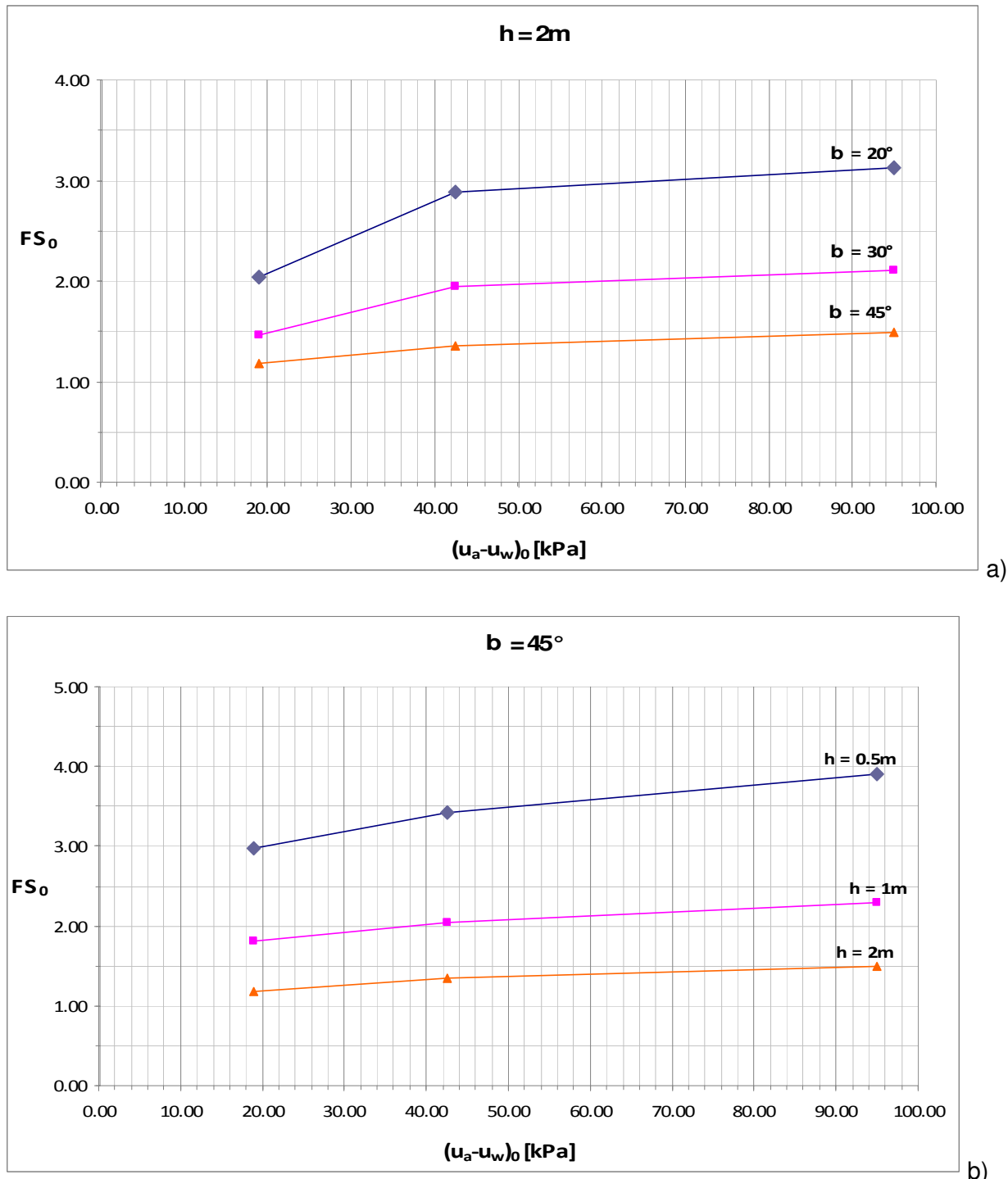


Figure 3.3. Initial safety factor FS_0 , as a function of the initial suction at the ground surface $(u_a - u_w)_0$.

3.1 Results



Once applied the transient boundary condition of constant intensity rainfall precipitation, each analysis has been stopped at the onset of slope failure, i.e. when the calculated factor of safety FS attains a value equal to 1.

The results have been reported through different diagrams:

- relative volumetric water content Θ vs. time t , $\Theta = \Theta(t)$;
- pore-water pressure u_w vs. time t , $u_w = u_w(t)$;
- factor of safety FS vs. time t , $FS = FS(t)$.

The corresponding critical thresholds curves have been plotted in the plane rainfall intensity I – duration D , as functions of the initial suction $(u_a - u_w)_0$ at the ground surface.

a) Homogeneous deposit (soil nr.1)- impervious bottom

The number of analyses enables to draw general considerations. In particular, the critical duration D of every assigned rainfall increases with:

- the initial suction $(u_a - u_w)_0$, for b and h constants (Figs. from 3.4 to 3.8);
- the slope angle b , for $(u_a - u_w)_0$ and h constants (Figs. from 3.9 to 3.11);
- the soil thickness h , for $(u_a - u_w)_0$ and b constants (Figs. from 3.12 to 3.14).

After a comparison with the empirical thresholds, obtained by Guadagno (1991) and by Calcaterra et al. (2000)

$$\text{Guadagno (1991)} \quad I = 176.40 \cdot D^{-0.90} \quad [I] = [\text{mm/h}]; 0.10 \text{ h} \leq D \leq 1000 \text{ h}$$

$$\text{Calcaterra et al. (2000)} \quad I = 28.10 \cdot D^{-0.74} \quad [I] = [\text{mm/h}]; 1 \text{ h} \leq D \leq 600 \text{ h}$$

which are both based on documented landslide events occurred in Campania Region, we have observed that the calculated critical thresholds are in rather good agreement with the bound obtained by Calcaterra et al., only for $(u_a - u_w)_0 > 42.49 \text{ kPa}$ and $h > 0.5 \text{ m}$, while they look ever lower than the bound obtained by Guadagno.

Therefore, the maximum difference ΔD_{\max} between the maximum and the minimum critical duration, respectively calculated in correspondence of the maximum initial suction $(u_a - u_w)_0 = 95 \text{ kPa}$ and the minimum initial suction $(u_a - u_w)_0 = 19 \text{ kPa}$, tends to increase with:

- the slope angle b , for h constant (Fig. 3.15);
- the soil thickness h , for b constant (Fig. 3.16).

At the same time, the maximum difference ΔD_{\max} between the maximum and the minimum critical duration, respectively calculated in correspondence of the maximum soil thickness $h = 2 \text{ m}$ and the minimum soil thickness $h = 0.5 \text{ m}$, tends to decrease with the initial suction $(u_a - u_w)_0$, for b constant (Fig. 3.17).

Such an information is useful to assess the magnitude of the potential error in the prediction of landslide triggering. In particular, the results show that it decreases with the rainfall-intensity I .

As a matter of fact, if the bottom is impervious, two phenomena simultaneously occur during a precipitation:



- increase of the pore-water pressure from the ground surface toward the impervious bottom, caused by the rain that directly falls on the ground surface;
- increase of the pore-water pressure from the impervious bottom toward the ground surface, due to the water flow within the landslide body coming from upslope.

The prevailing of one of these two phenomena, related to different factors (intensity of rainfall, geometry, geotechnical properties of the soils, etc.) is responsible of a consequent mechanical aspect. In particular, with regard to the characteristics of the landslide body at the onset of the failure, we have noted three possible scenarios:

- fully saturation of the entire body;
- superficial failure;
- failure at the base of the body.

The fully saturation of the entire body has been found with reference to the simultaneous presence of high intensity of rainfall and thickness of the deposit less than 4 m. With reference to the case $h = 0.5$ m (see attachment D), this kind of failure occurs also if the intensity of rainfall is low (Fig. 3.18).

The superficial failure occurs if a slipping surface next to the ground surface is activated before the rainfall is able to infiltrate along the entire deposit. We have found this situation with reference to the simultaneous presence of very high intensity of rainfall and big thickness $h = 4$ m (Fig. 3.19). Only the portion of the landslide body set above the slipping surface is saturated.

On the other side, if the intensity is not so high, the velocity of rising up of pore-water pressures from the bottom toward the ground surface is high enough to produce failure at the base of the landslide body. The landslide body is not fully saturated (Fig. 3.20).

b) Homogeneous deposit (soil nr.2)- impervious bottom

The soil nr.2 is essentially characterized by a permeability lower than soil nr.1. This causes a strongly delay of the onset of failure (see attachment I), and also influences the characteristics of the landslide, that is ever superficial (Fig. 3.21).

c) Homogeneous deposit (soil nr.1) - pervious bottom

In the case of "pervious bottom", the failure is never attained (see attachment C). In fact, that considered boundary condition forces the water flow to reach a steady-state condition characterized by a factor of safety higher than 1 (Fig. 3.22).

d) Layered deposit (soil nr.1) - impervious bottom

The analyses carried out for layered cover (see attachment F) shows that this acts as a "screen", delaying water infiltration in the lowermost layer. According to the intensity I of the rainfall, the failure may be superficial (high intensity) or deep (low intensity) (Figs. 3.23 and 3.24): if compared with the homogeneous deposit ($b=30^\circ$; $h=2$ m), in the first case the failure is anticipated (Fig. 3.25), while in the second case the failure is delayed (Fig. 3.26). For lower rainfall intensity (less than 9.72 mm/h), the failure is never attained (Fig. 3.27)

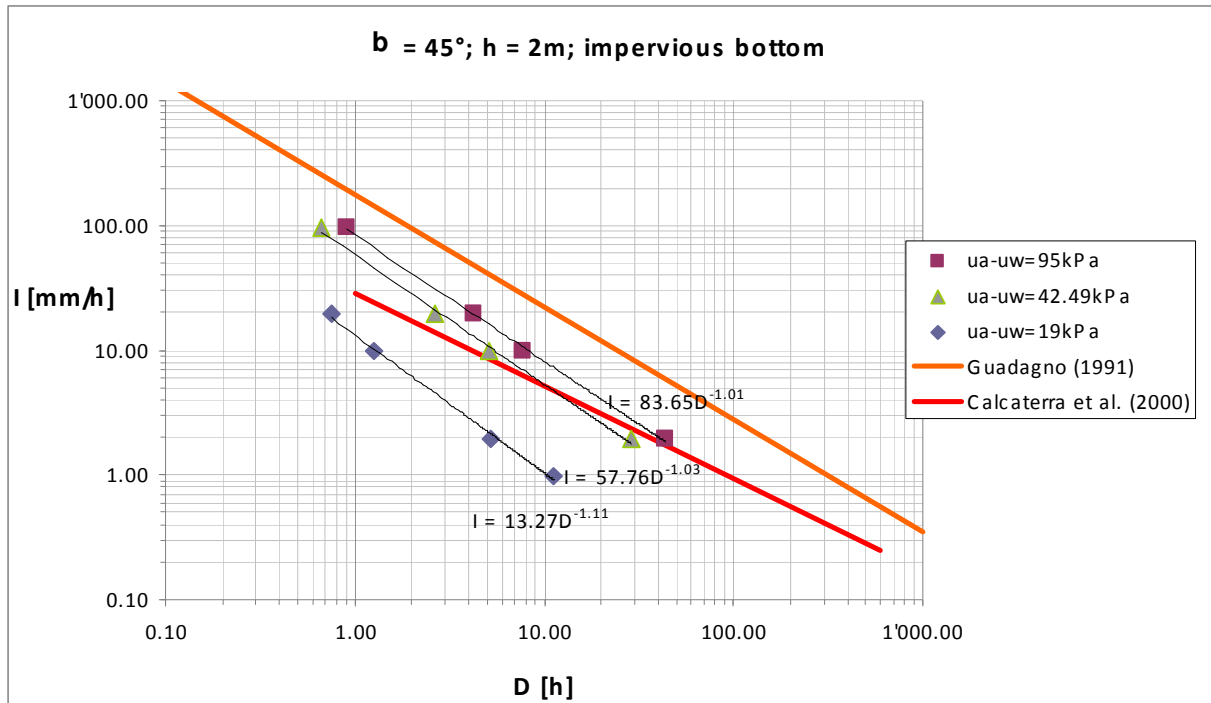


Figure 3.4. Critical thresholds, rainfall intensity I – duration D, triggering slope failure: slope angle $b=45^\circ$; soil thickness $h=2\text{m}$; impervious bottom. The empirical thresholds from Guadagno (1991) and Calcaterra et al. (2000), based on landslide events in Campania Region are also reported.

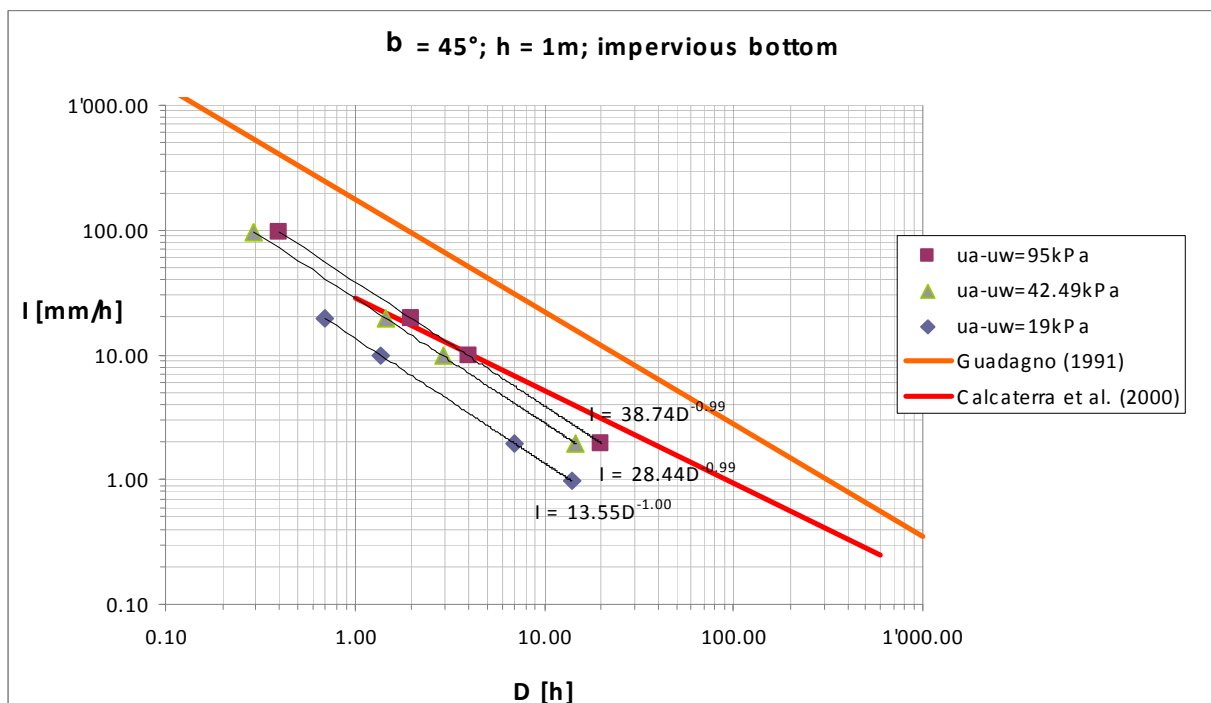


Figure 3.5. Critical thresholds, rainfall intensity I – duration D, triggering slope failure: slope angle $b=45^\circ$; soil thickness $h=1\text{m}$; impervious bottom. The empirical thresholds from Guadagno (1991) and Calcaterra et al. (2000), based on landslide events in Campania Region, are also reported.

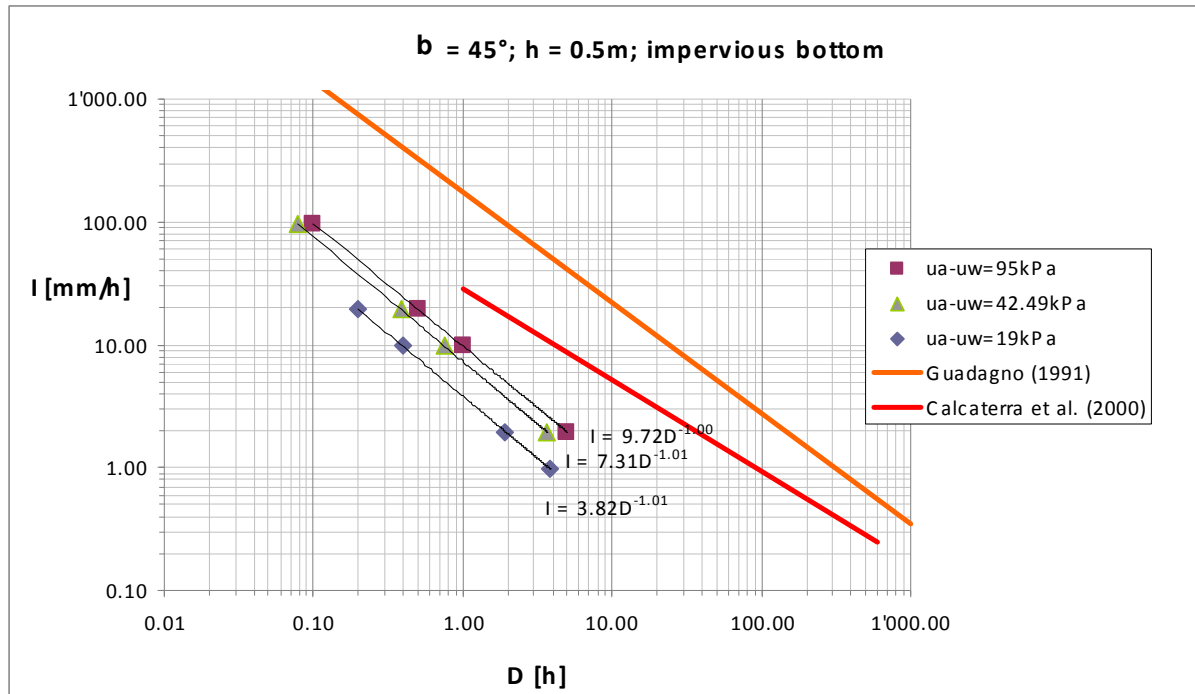


Figure 3.6. Critical thresholds, rainfall intensity I – duration D, triggering slope failure: slope angle $b=45^\circ$; soil thickness $h=0.5\text{m}$; impervious bottom. The empirical thresholds from Guadagno (1991) and Calcaterra et al. (2000), based on landslide events in Campania Region, are also reported.

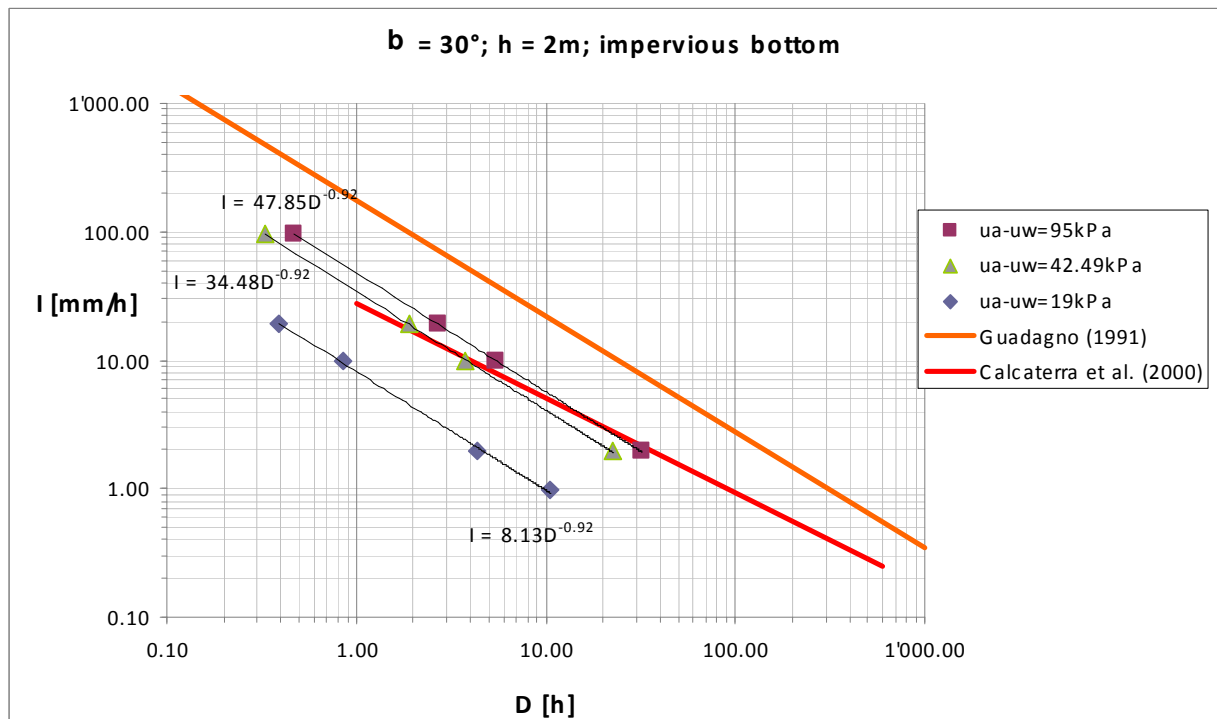


Figure 3.7. Critical thresholds, rainfall intensity I – duration D, triggering slope failure: slope angle $b=30^\circ$; soil thickness $h=2\text{m}$; impervious bottom. The empirical thresholds from Guadagno (1991) and Calcaterra et al. (2000), based on landslide events in Campania Region, are also reported.

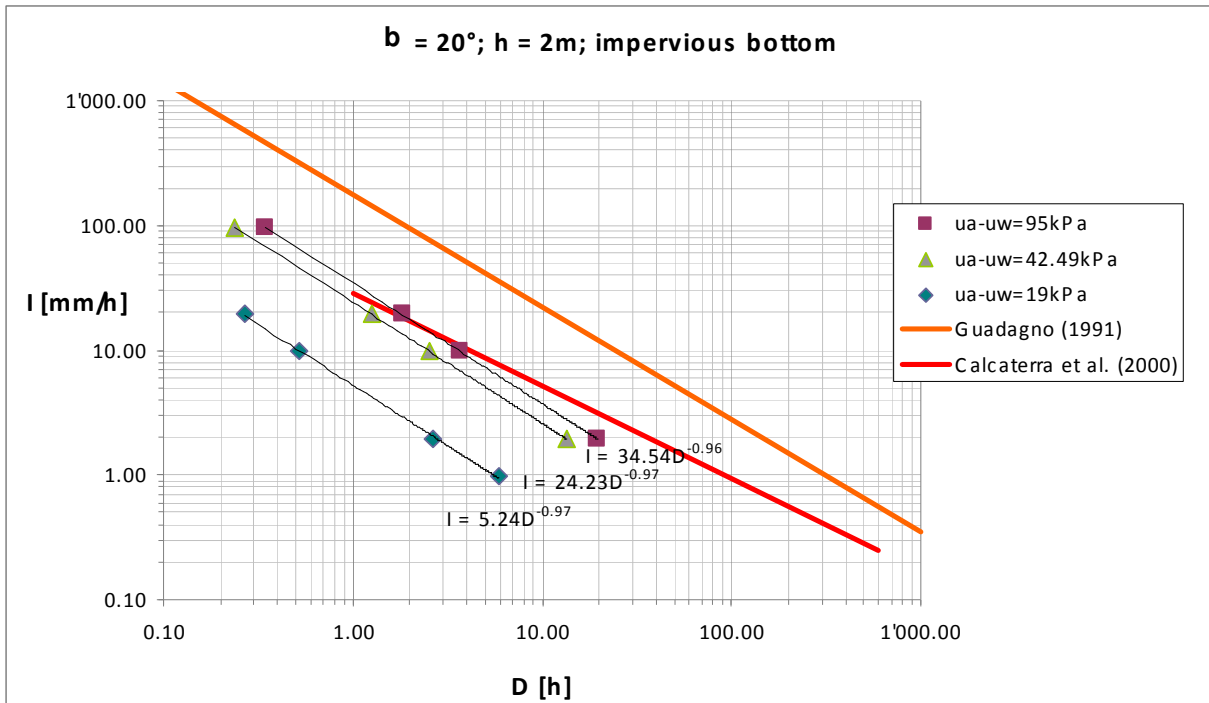


Figure 3.8. Critical thresholds, rainfall intensity I – duration D , triggering slope failure: slope angle $b=20^\circ$; soil thickness $h=2\text{m}$; impervious bottom. The empirical thresholds from Guadagno (1991) and Calcaterra et al. (2000), based on landslide events in Campania Region, are also reported.

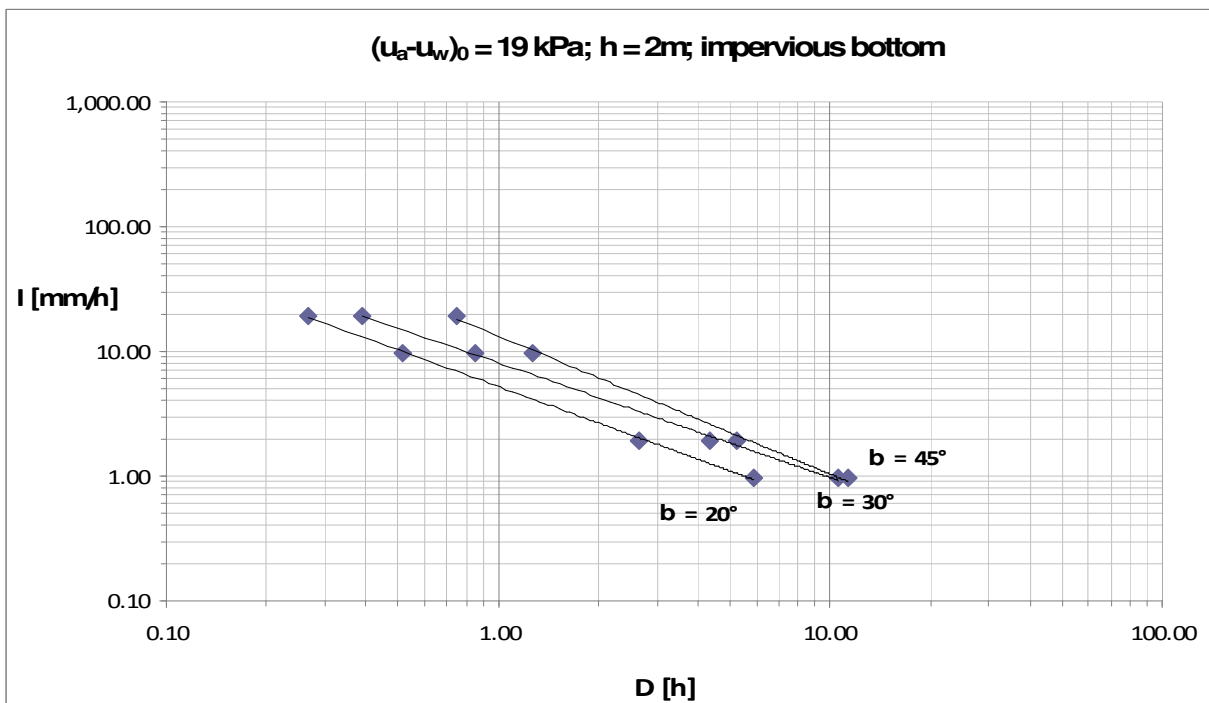


Figure 3.9. Critical thresholds, rainfall intensity I – duration D , triggering slope failure: initial suction at the ground surface $(u_a-u_w)_0=19\text{kPa}$; soil thickness $h=2\text{m}$; impervious bottom.

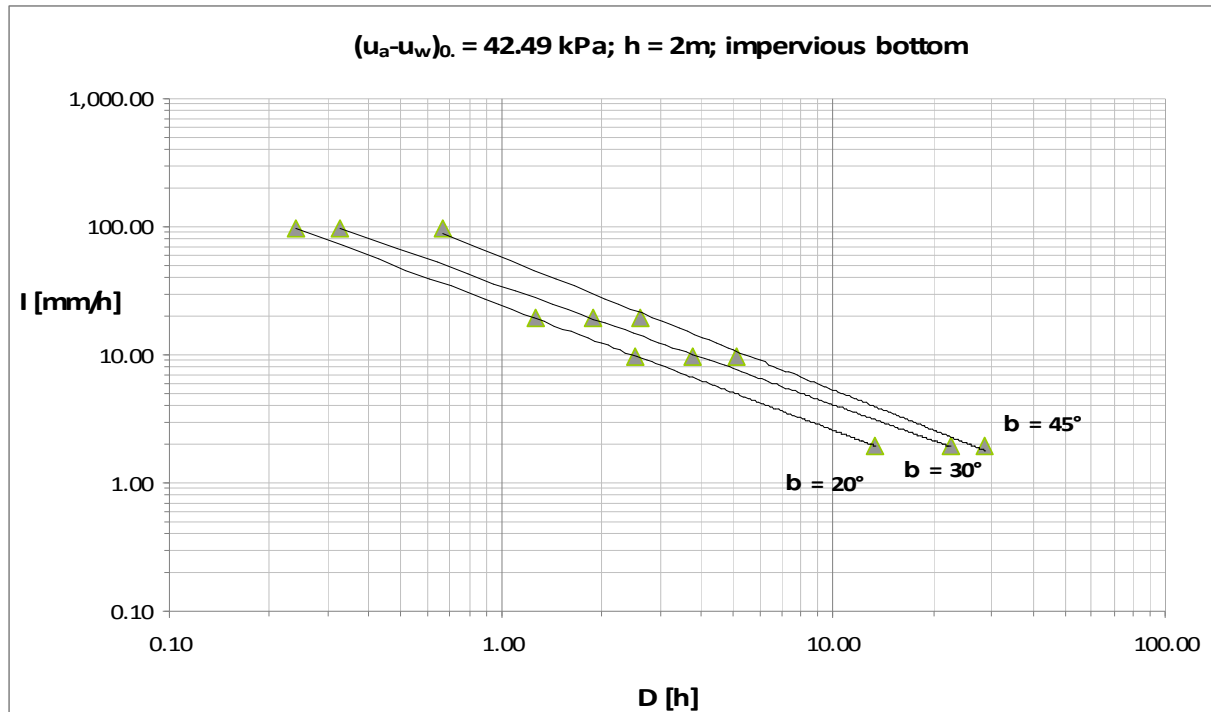


Figure 3.10. Critical thresholds, rainfall intensity I – duration D , triggering slope failure: initial suction at the ground surface $(u_a - u_w)_0 = 42.49 \text{ kPa}$; soil thickness $h = 2\text{m}$; impervious bottom.

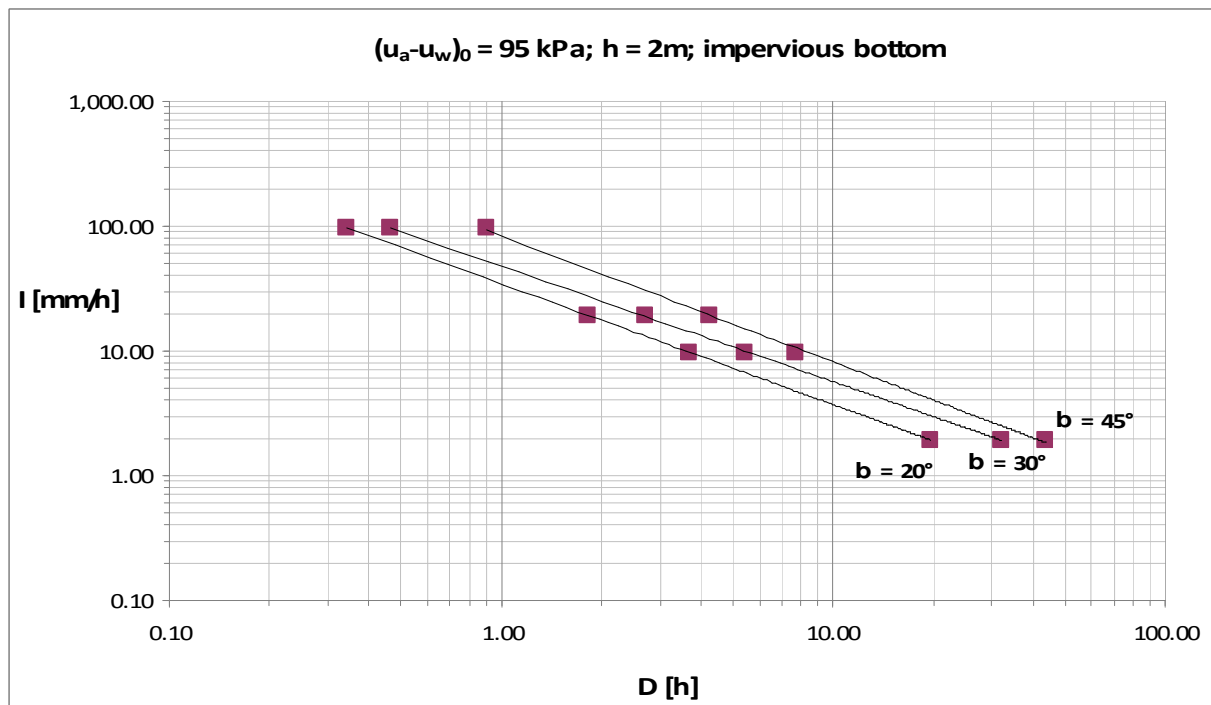


Figure 3.11. Critical thresholds, rainfall intensity I – duration D , triggering slope failure: initial suction at the ground surface $(u_a - u_w)_0 = 95 \text{ kPa}$; soil thickness $h = 2\text{m}$; impervious bottom.

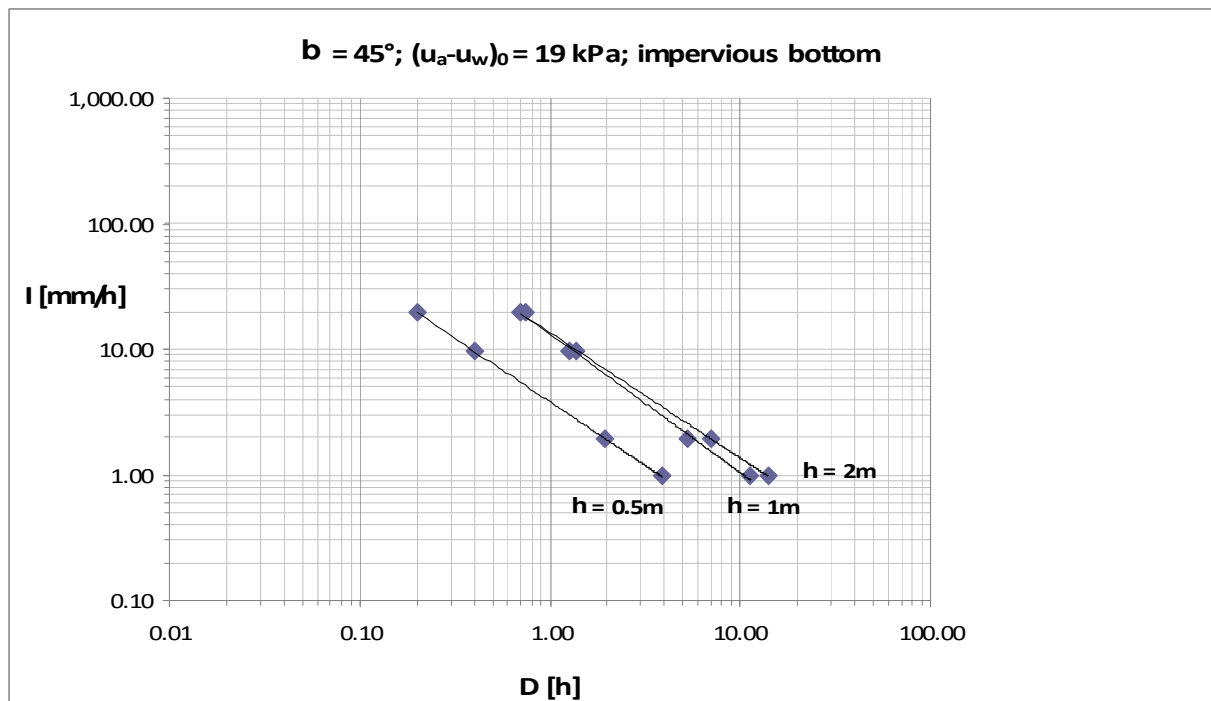


Figure 3.12. Critical thresholds, rainfall intensity I – duration D , which triggering slope failure: slope angle $b=45^\circ$; initial suction at the ground surface $(u_a - u_w)_0=19\text{kPa}$; impervious bottom.

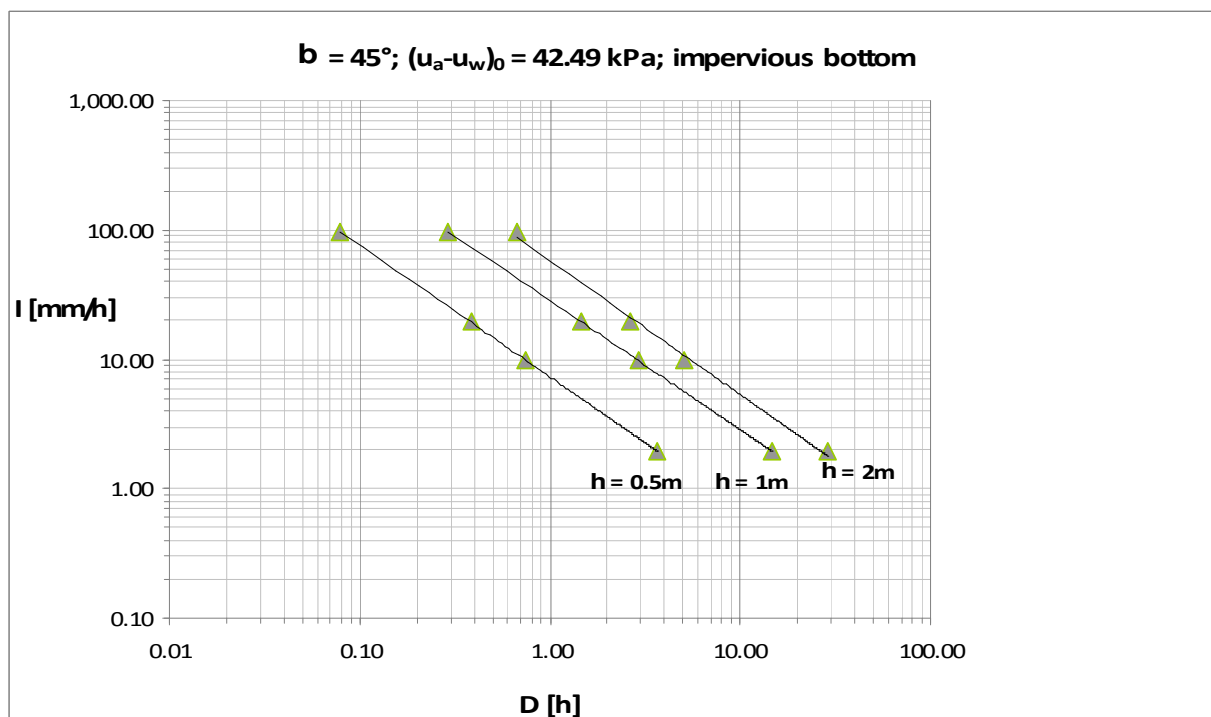


Figure 3.13. Critical thresholds, rainfall intensity I – duration D , triggering slope failure: slope angle $b=45^\circ$; initial suction at the ground surface $(u_a - u_w)_0=42.49\text{kPa}$; impervious bottom.

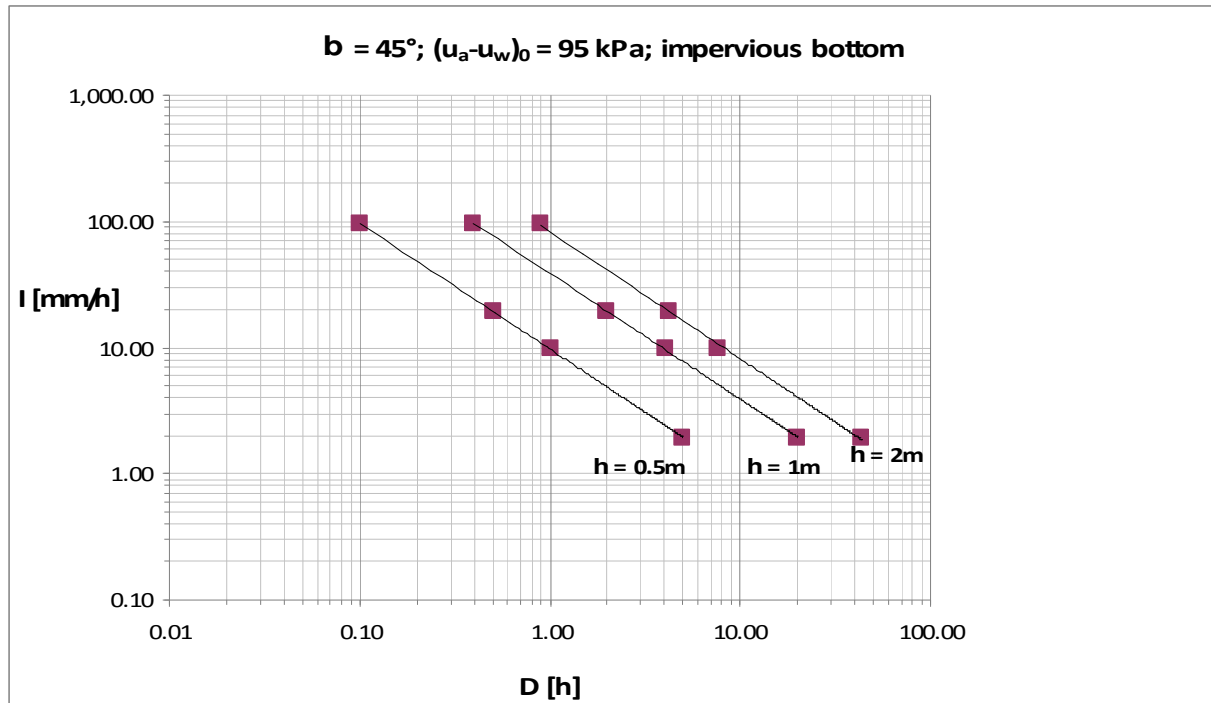


Figure 3.14. Critical thresholds, rainfall intensity I – duration D , triggering slope failure: slope angle $b=45^\circ$; initial suction at the ground surface $(u_a - u_w)_0=95\text{kPa}$; impervious bottom.

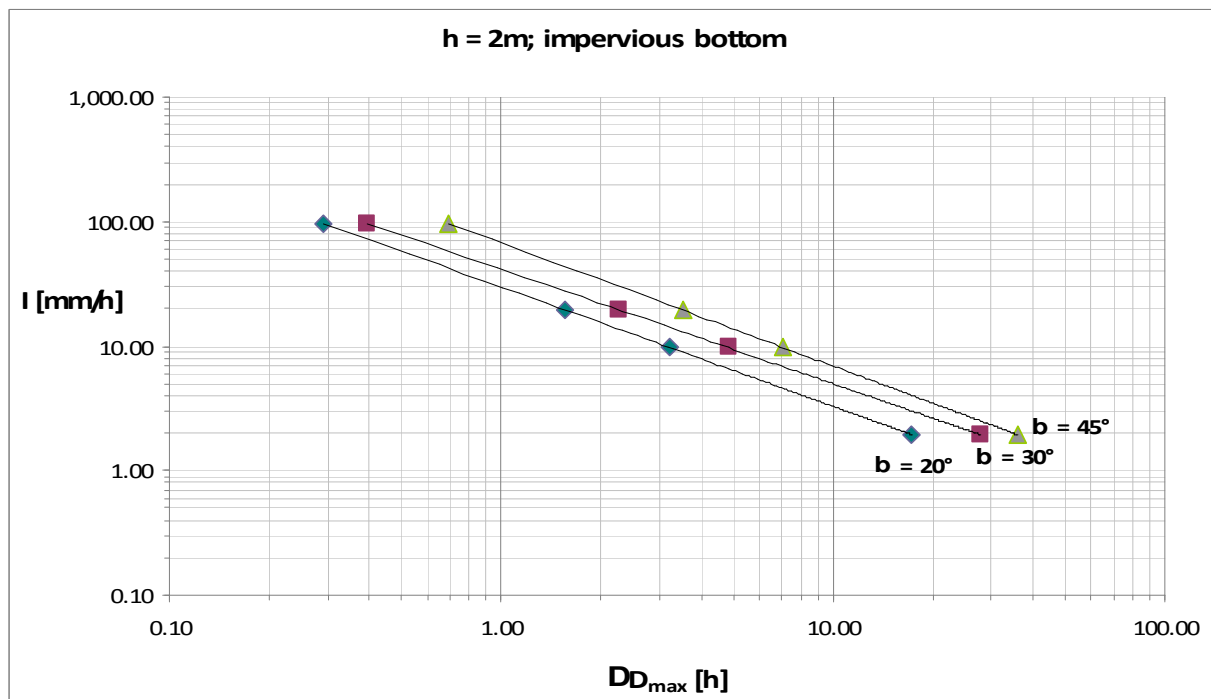


Figure 3.15. Maximum difference of the calculated critical duration DD_{max} , as a function of the considered initial suction at the ground surface $((u_a - u_w)_0=19-95\text{kPa})$: soil thickness $h=2\text{m}$; impervious bottom.

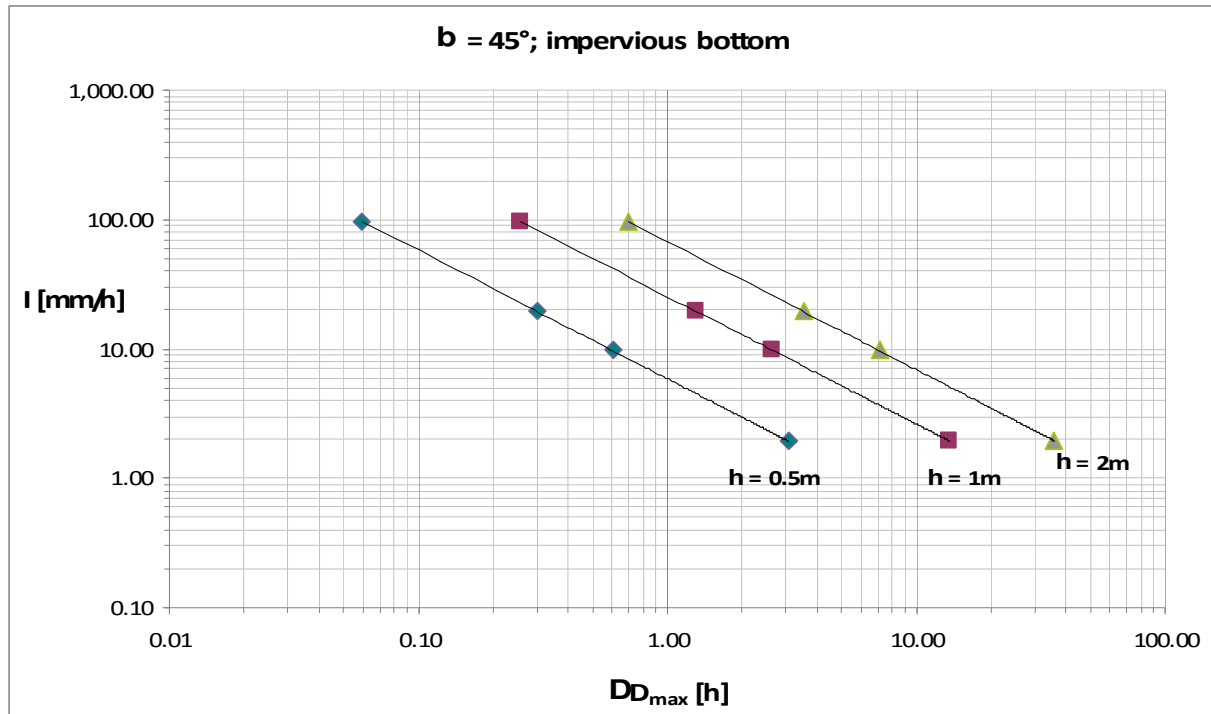


Figure 3.16. Maximum difference of the calculated critical duration DD_{\max} , as a function of the considered initial suction at the ground surface ($(u_a - u_w)_0 = 19-95 \text{ kPa}$): slope angle $b = 45^\circ$; impervious bottom.

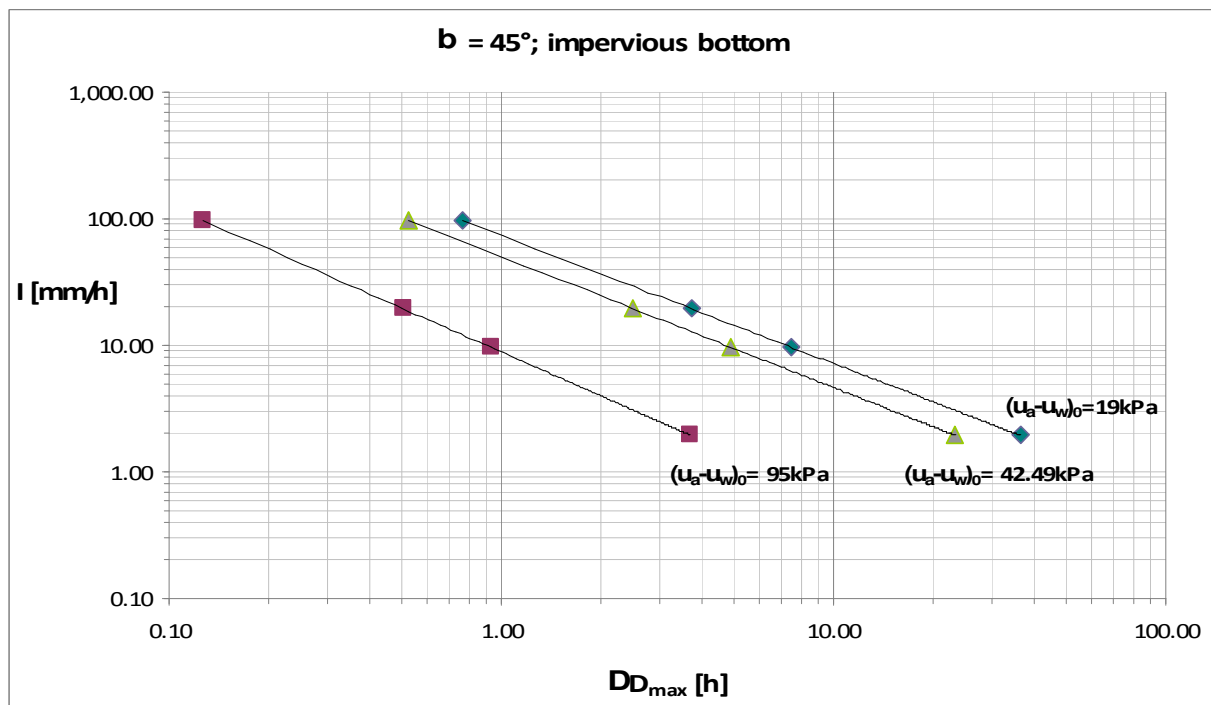


Figure 3.17. Maximum difference of the calculated critical duration DD_{\max} , as a function of the considered soil thickness ($h = 0.5-2.0 \text{ m}$): slope angle $b = 45^\circ$; impervious bottom.

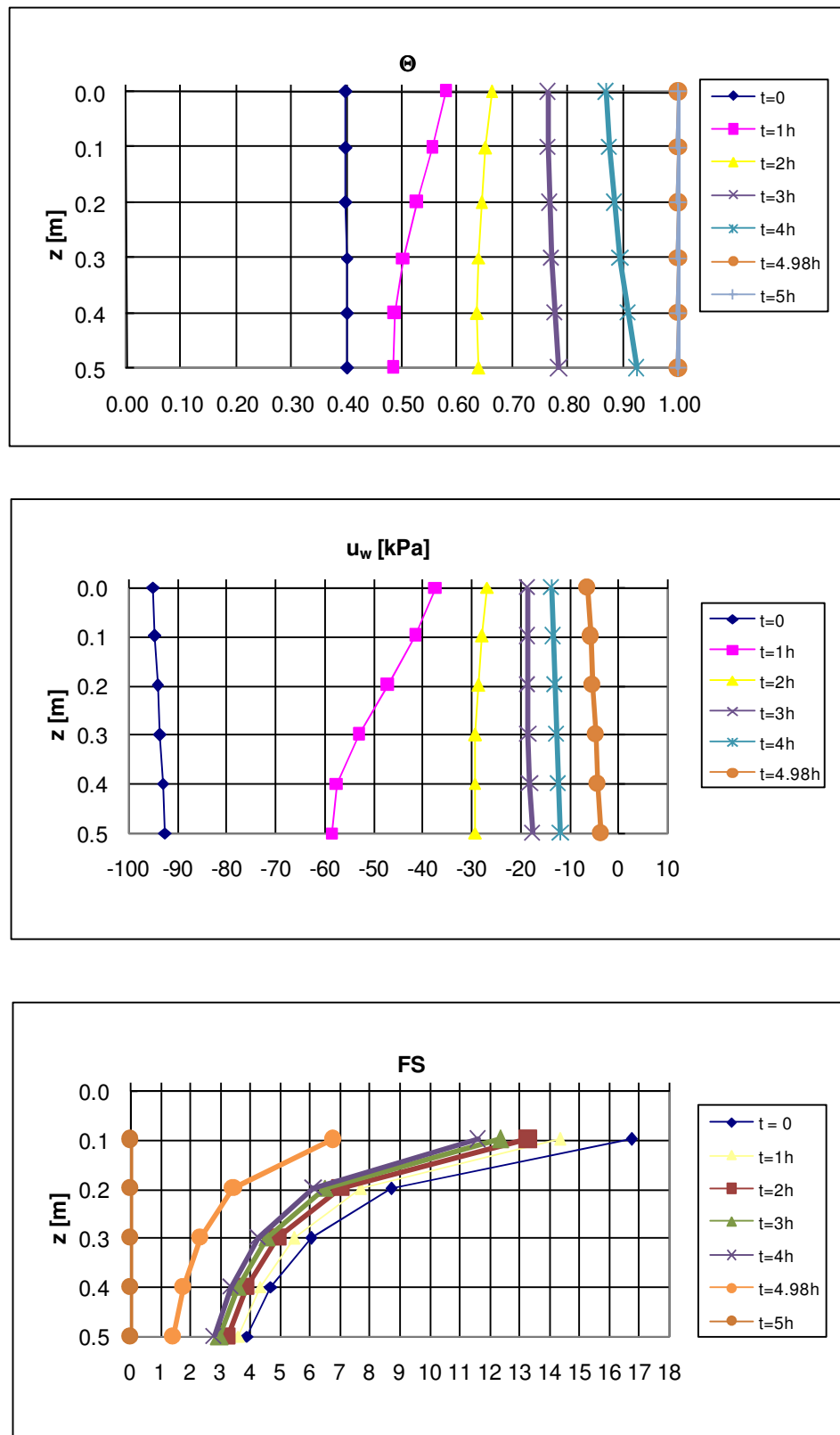


Figure 3.18. Homogeneous deposit – impervious bottom (soil nr.1; $b=45^\circ$; $h=0.5\text{m}$; $(u_a-u_w)_0 = 95 \text{ kPa}$; $I = 1.94 \text{ mm/h}$): changing with time of the relative volumetric water content Θ , the pore-water pressure u_w and the factor of safety FS along the depth z .

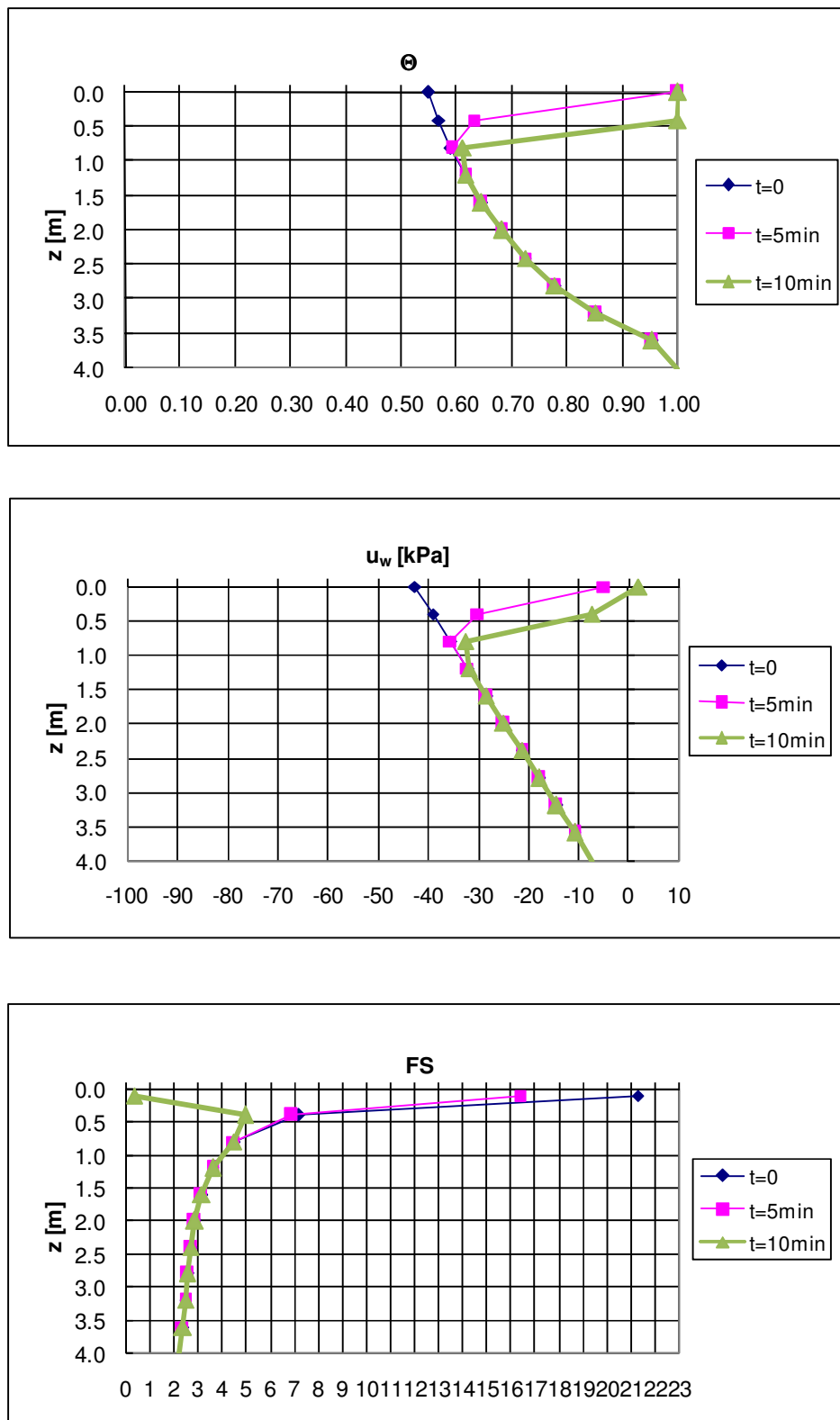


Figure 3.19. Homogeneous deposit – impervious bottom (soil nr.1; $b=20^\circ$; $h=4\text{m}$; $(u_a-u_w)_0 = 42.49 \text{ kPa}$; $I = 97.20 \text{ mm/h}$): changing with time of the relative volumetric water content Θ , the pore-water pressure u_w and the factor of safety FS along the depth z .

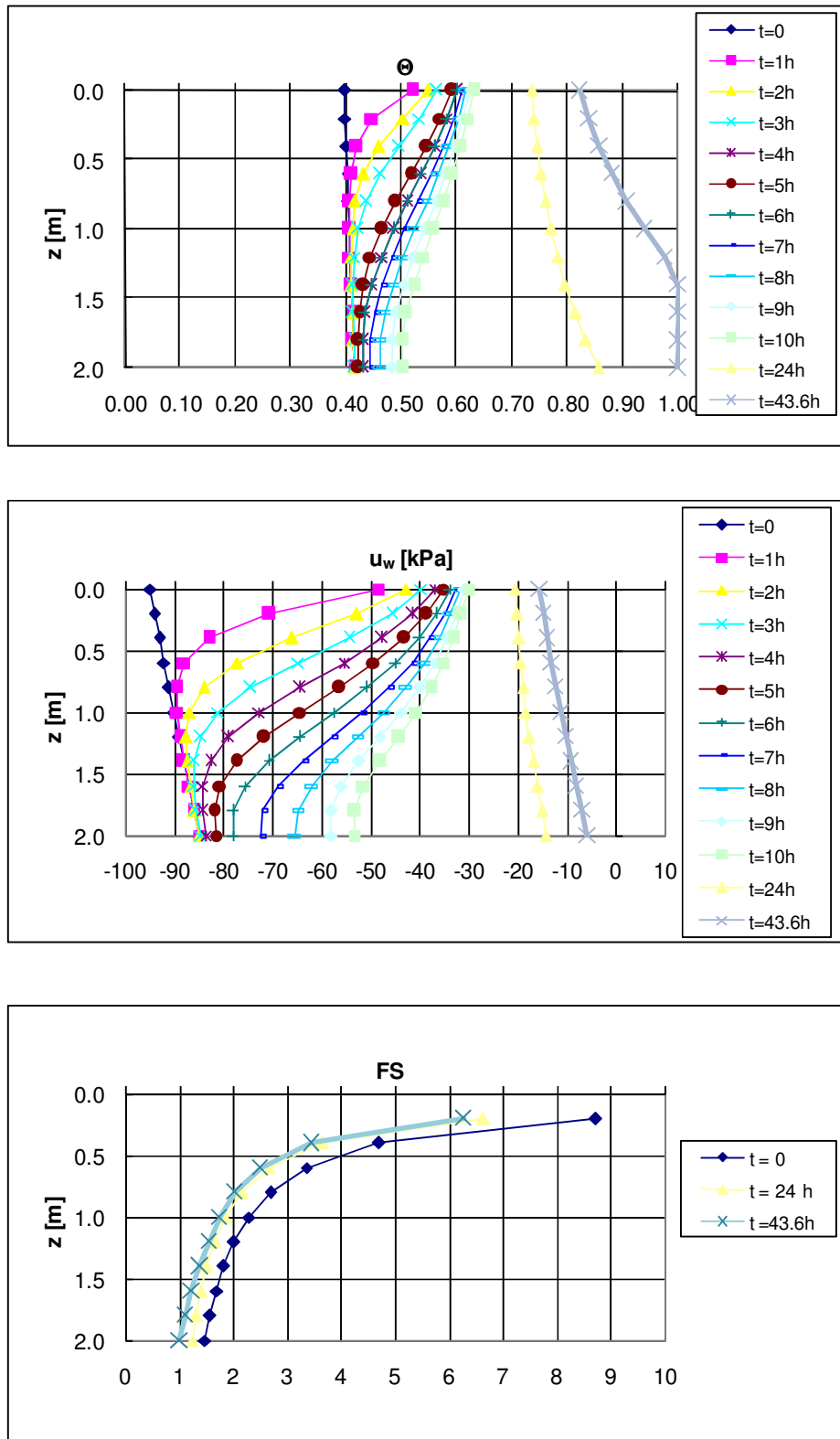


Figure 3.20. Homogeneous deposit – impervious bottom (soil nr.1; $b=45^\circ$; $h=2m$; $(u_a-u_w)_0 = 95$ kPa; $I = 1.94$ mm/h): changing with time of the relative volumetric water content Θ , the pore-water pressure u_w and the factor of safety FS along the depth z .

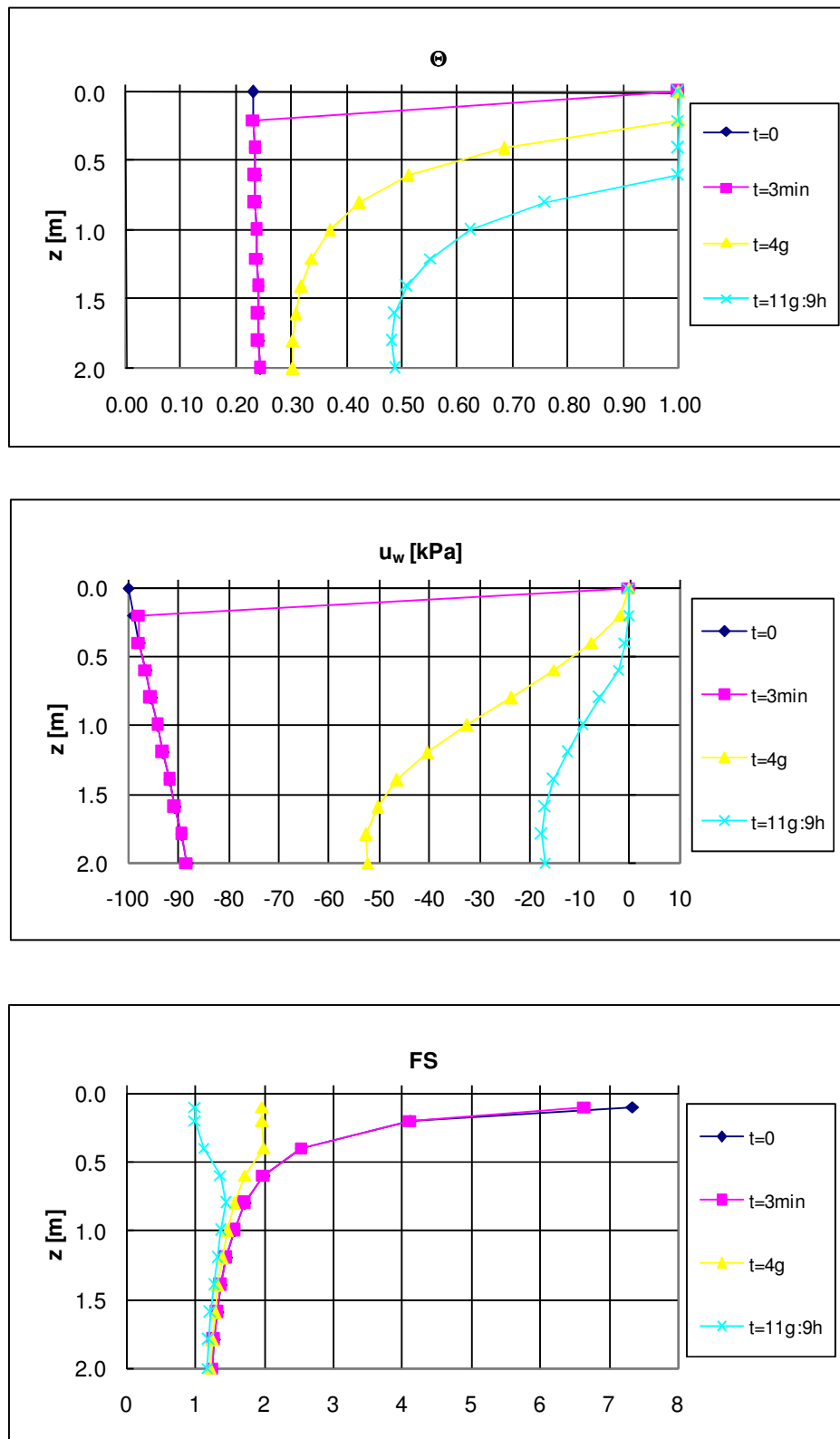


Figure 3.21. Homogeneous deposit – impervious bottom (soil nr.2; $b=40^\circ$; $h=2\text{m}$; $(u_a-u_w)_0 = 100$ kPa; $I = 97.20 \text{ mm/h}$): changing with time of the relative volumetric water content Θ , the pore-water pressure u_w and the factor of safety FS along the depth z .

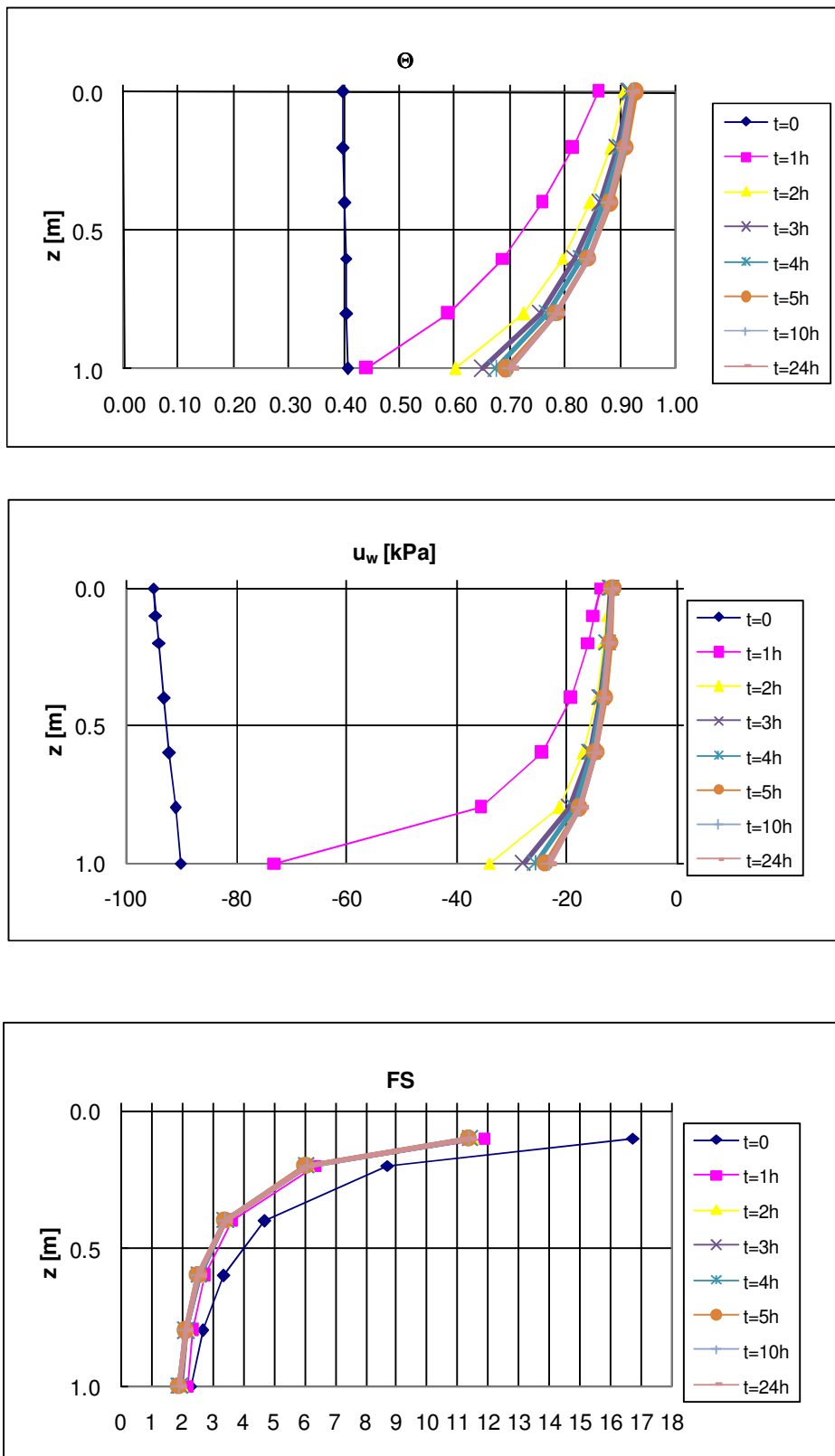


Figure 3.22. Homogeneous deposit – pervious bottom (soil nr.1; $b=45^\circ$; $h=1\text{m}$; $(u_a-u_w)_0 = 95 \text{ kPa}$; $I = 19.44 \text{ mm/h}$): changing with time of the relative volumetric water content Θ , the pore-water pressure u_w and the factor of safety FS along the depth z .

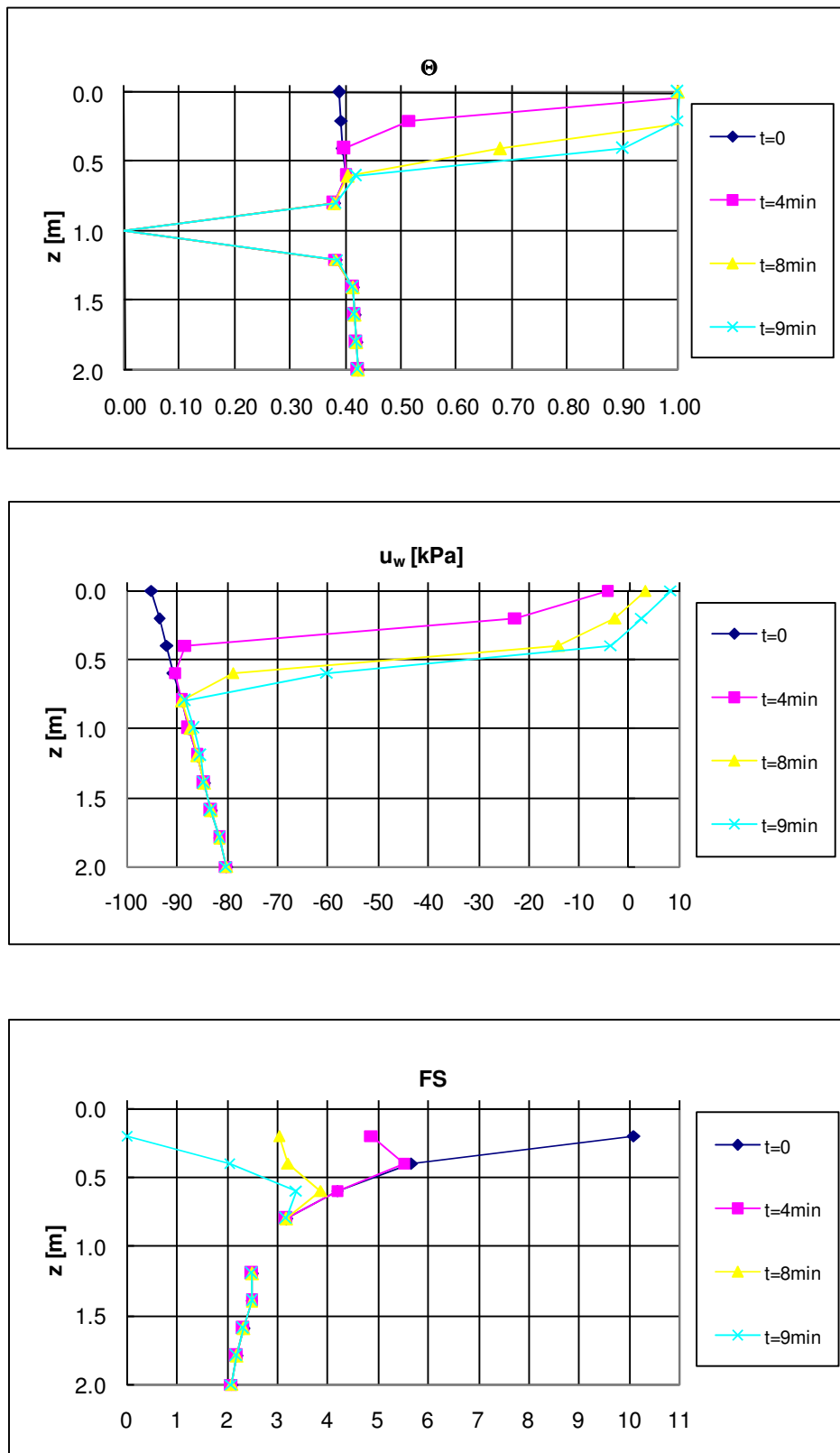


Figure 3.23. Layered deposit – impervious bottom (soil nr.1; $b=30^\circ$; $h=2\text{m}$; $(u_a-u_w)_0 = 95 \text{ kPa}$; $I = 97.20 \text{ mm/h}$): changing with time of the relative volumetric water content Θ , the pore-water pressure u_w and the factor of safety FS along the depth z .

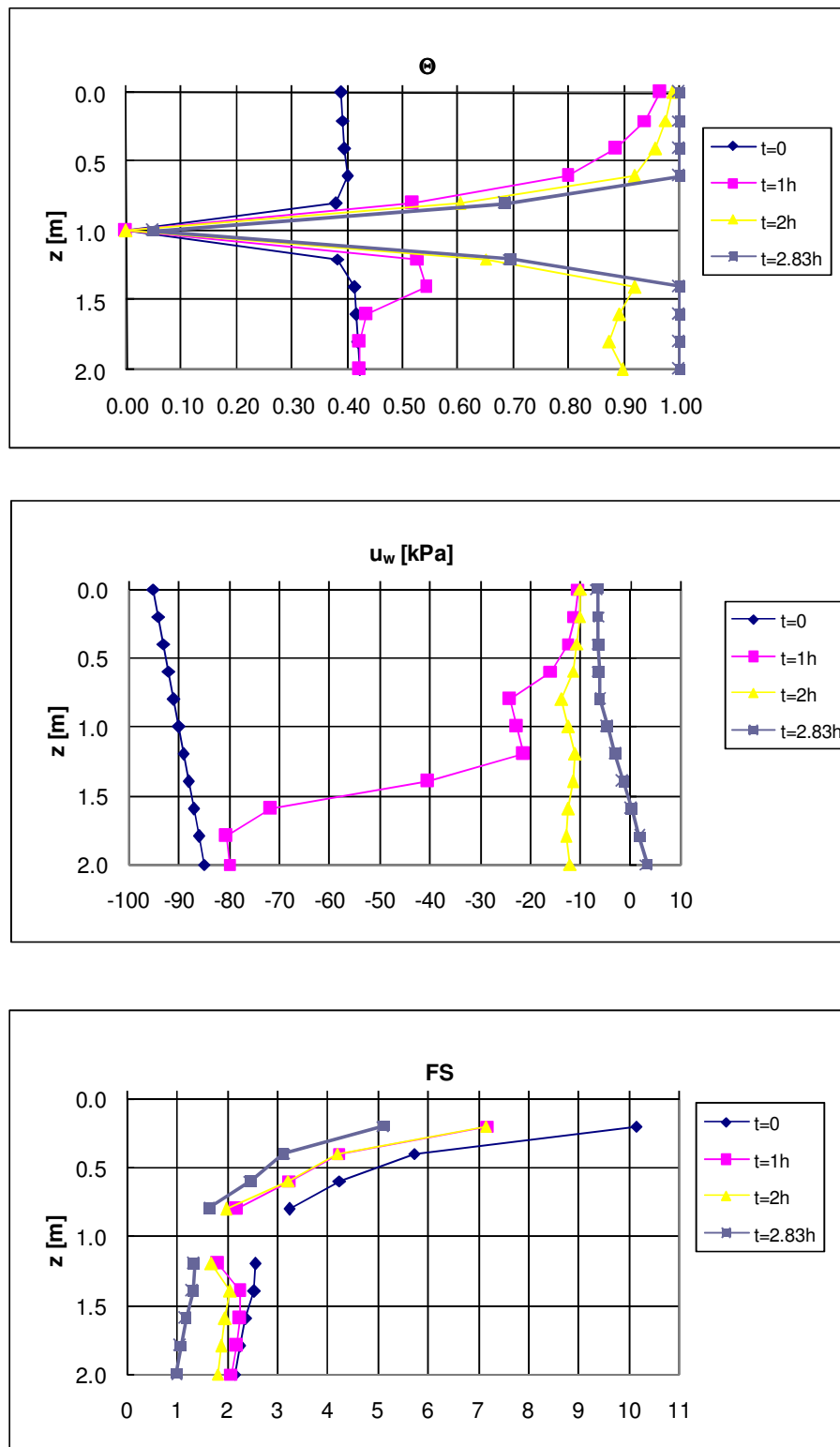


Figure 3.24. Layered deposit – impervious bottom (soil nr.1; $b=30^\circ$; $h=2\text{m}$; $(u_a-u_w)_0 = 95 \text{ kPa}$; $I = 19.44 \text{ mm/h}$): changing with time of the relative volumetric water content Θ , the pore-water pressure u_w and the factor of safety FS along the depth z .

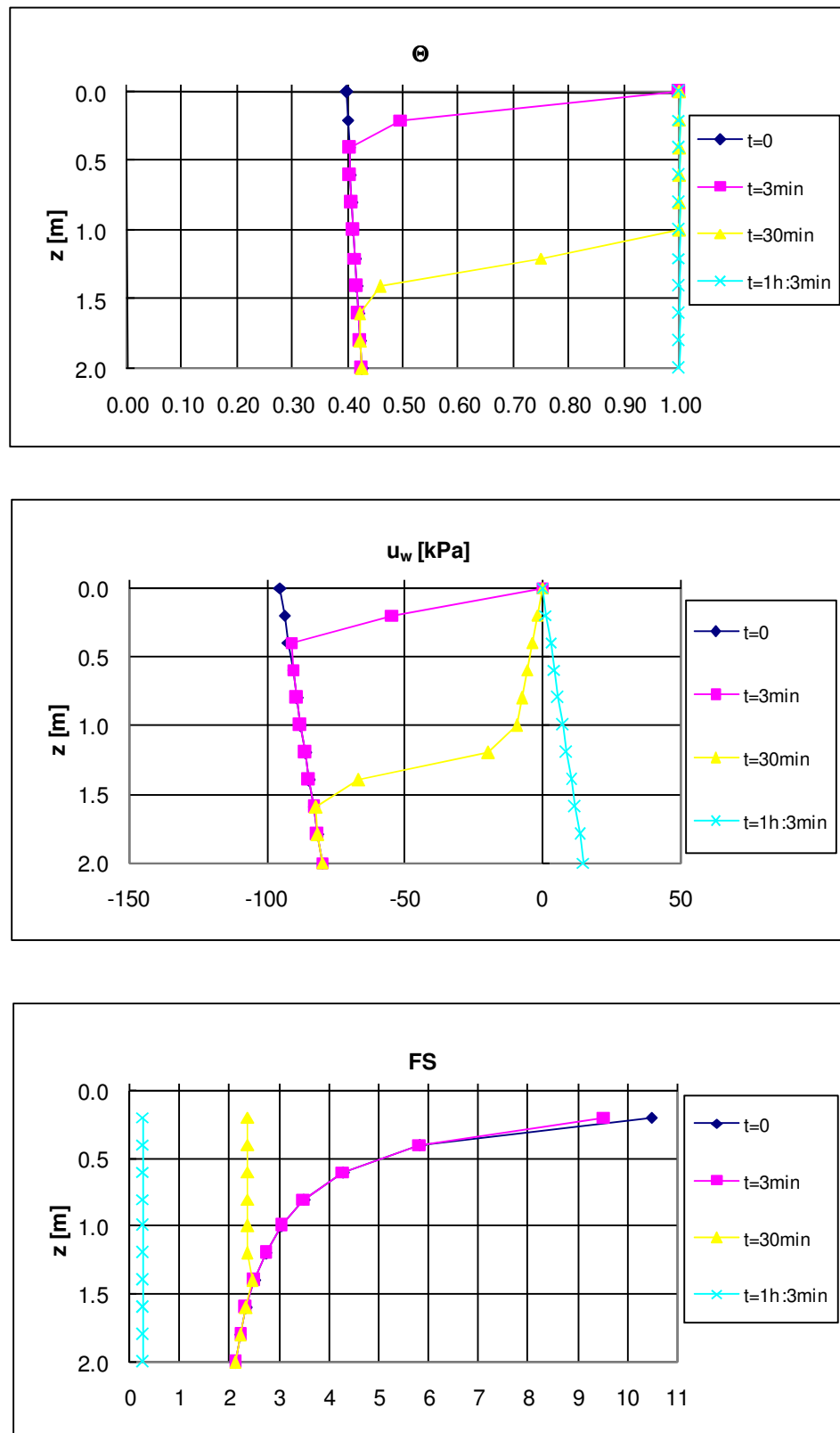


Figure 3.25. Homogeneous deposit – impervious bottom (soil nr.1; $b=30^\circ$; $h=2\text{m}$; $(u_a-u_w)_0 = 95$ kPa; $I = 97.20 \text{ mm/h}$): changing with time of the relative volumetric water content Θ , the pore-water pressure u_w and the factor of safety FS along the depth z .

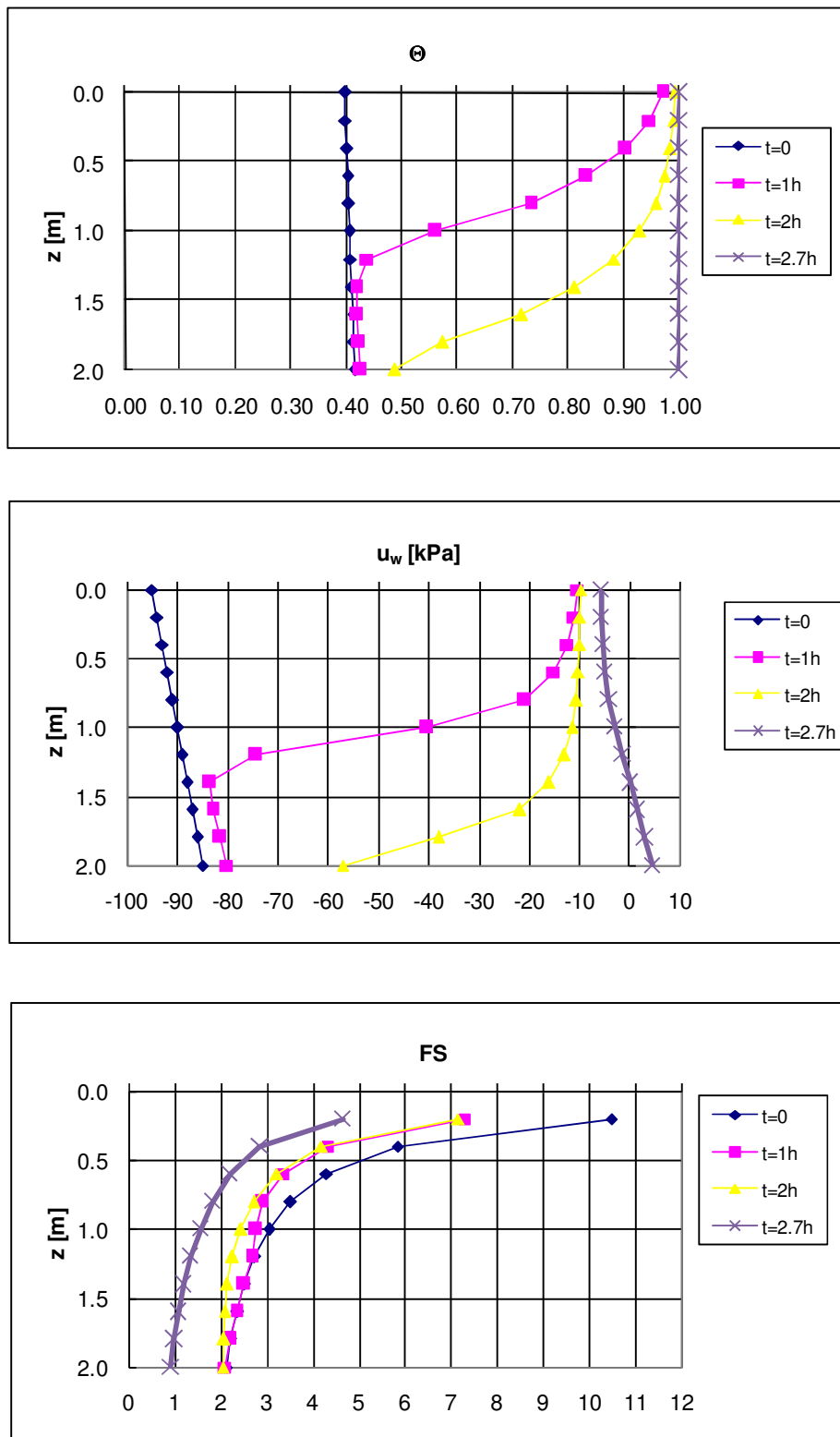


Figure 3.26. Homogeneous deposit – impervious bottom (soil nr.1; $b=30^\circ$; $h=2\text{m}$; $(u_a-u_w)_0 = 95$ kPa; $I = 19.44 \text{ mm/h}$): changing with time of the relative volumetric water content Θ , the pore-water pressure u_w and the factor of safety FS along the depth z .

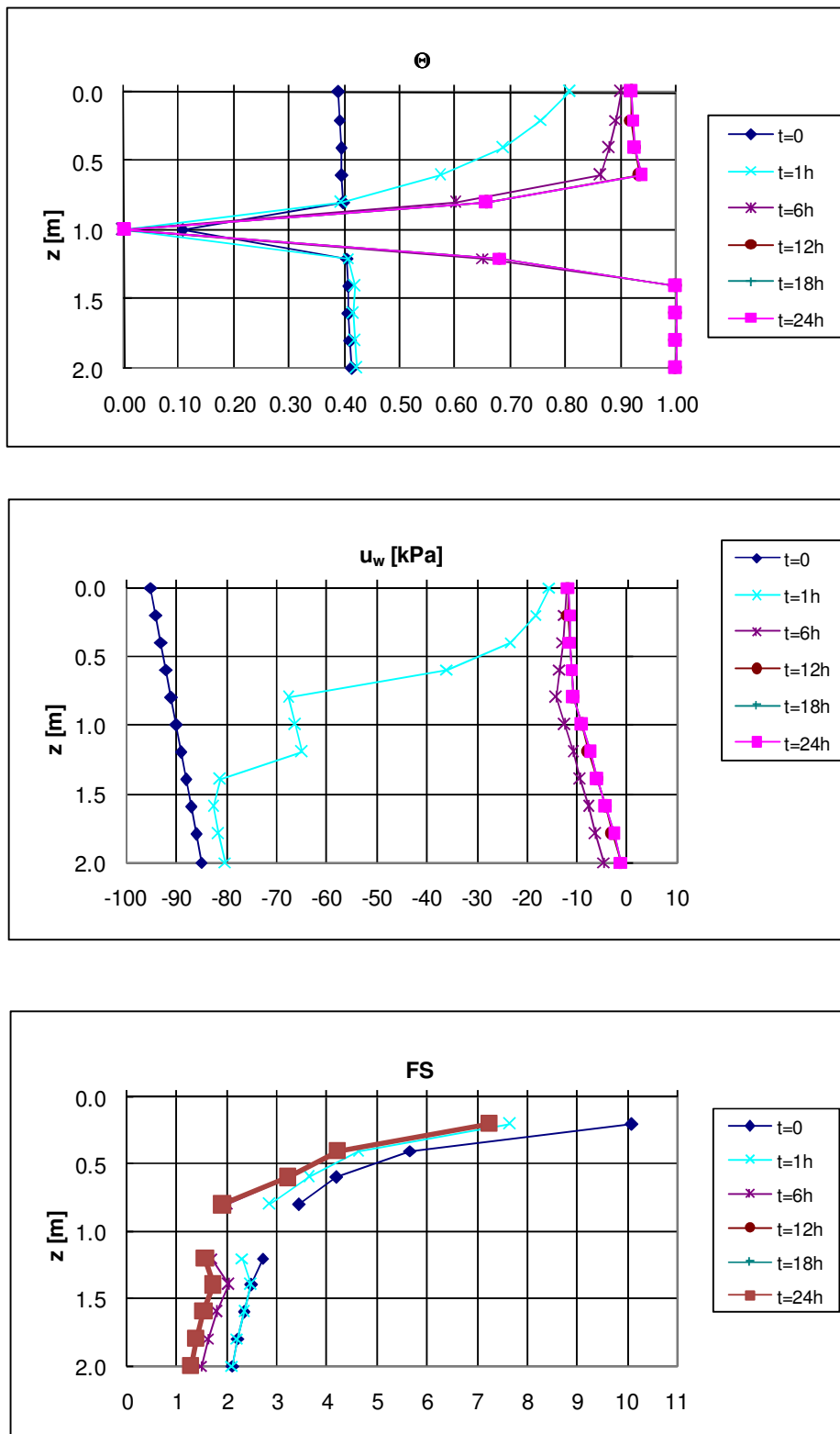


Figure 3.27. Layered deposit – impervious bottom (soil nr.1; $b=30^\circ$; $h=2\text{m}$; $(u_a-u_w)_0 = 95 \text{ kPa}$; $I = 9.72 \text{ mm/h}$): changing with time of the relative volumetric water content Θ , the pore-water pressure u_w and the factor of safety FS along the depth z .



4. Conclusive remarks

This Technical Report illustrates the results of some numerical analyses aimed to assess the response of slopes subjected to rainfall, in typical geomorphological scenarios in Campania Region.

Several factors, like geometrical aspects, rainfall characteristics, soil properties, initial conditions, boundary conditions, affect the slope behaviour. The analyses have shown that different combinations of these factors lead to totally different consequences in terms of:

- time of failure;
- depth of failure.

For example, the magnitude of error in the prediction of the time of failure increases with the slope angle and the thickness of soil, while it decreases with the intensity of the rainfall and the initial suction at the ground surface.

Moreover, the landslide can involve the entire deposit or only a superficial part of it. With regard to the first scenario, if the bottom is impervious, at the onset of the failure the soil is typically:

- saturated if the rainfall intensity is high and the thickness is small;
- not saturated if the rainfall intensity is low.

On the contrary, the failure is typically shallow if:

- the thickness is high;
- the deposit includes an intermediate pumice layer, which acts as a “screen”, delaying water infiltration in the lowermost layers.

These aspects are particularly important, because they govern the depth and the time of the triggered landslide.



5. References

- Calcaterra D, Parise M, Palma B, Pelella L (2000). The Influence of Meteoric Events in Triggering Shallow Landslides in Pyroclastic Deposits of Campania, Italy. Proc. 8th Int. Conf. on Landslides, Cardiff, vol. 1, pp. 209-214
- Childs EC and Collins-George N (1950). The Permeability of Porous Materials. Proceedings of the Royal Society, pp. 392-405
- Darcy H (1856). Détetermination des lois d'écoulement de l'eau à travers le sable. pp. 590–594. In Les Fontaines Publiques de la Ville de Dijon. Victor Dalmont, Paris
- Evangelista A and Scotto di Santolo A (2001). Mechanical behaviour of unsaturated pyroclastic soil. Proc. Int. Conf. Landslides: Causes, Impacts and Countermeasures, Davos, pp. 35-44
- Fredlund DG (1979). Second Canadian geotechnical colloquium: Appropriate concepts and technology for unsaturated soils. Canadian Geotechnical Journal, 16, pp. 121-139
- Fredlund DG and Morgenstern NR (1976). Constitutive Relations for Volume Change in Unsaturated Soils. Canadian Geotechnical Journal. Vol. 13, pp. 261-276
- Gardner WR (1958). Some steady state solutions of the unsaturated moisture flow equation with application to evaporation from water table. Soil Sci., 85(4), pp. 228-232
- Guadagno F (1991). Debris flows in the Campanian volcaniclastic soils (Southern Italy). Proc. Int. Conf. on Slope stability eng. develop. and applications, Isle of Wight, pp. 109-114.
- Olivares L and Tommasi P (2008). The role of suction and its changes on stability of steep slopes in unsaturated granular soils. Proc. of the 10th International Symposium On Landslides And Engineered Slopes, pp. 203-215
- Richards LA (1931). Capillary Conduction of Liquids Through Porous Mediums. Physics, Vol.1
- SEEP/W. User's Guide. GEO-SLOPE International Ltd, Canada
- van Genuchten MTh (1980). A closed-form equation for predicting the hydraulic conductivity of unsaturated soils. Soil Sci. Soc. Am. J. 44, pp. 892-898
- Vanapalli SK, Fredlund DG, Pufahl DE and Clifton AW (1996). Model for the prediction of shear strength with respect to soil suction. Canadian Geotechnical Journal, 33, pp. 379-392



ATTACHMENT A

Hypothesis 1

Slope angle $\beta = 45^\circ$
Soil nr.1

Case a

Thickness $h = 2$ m
Impervious bottom

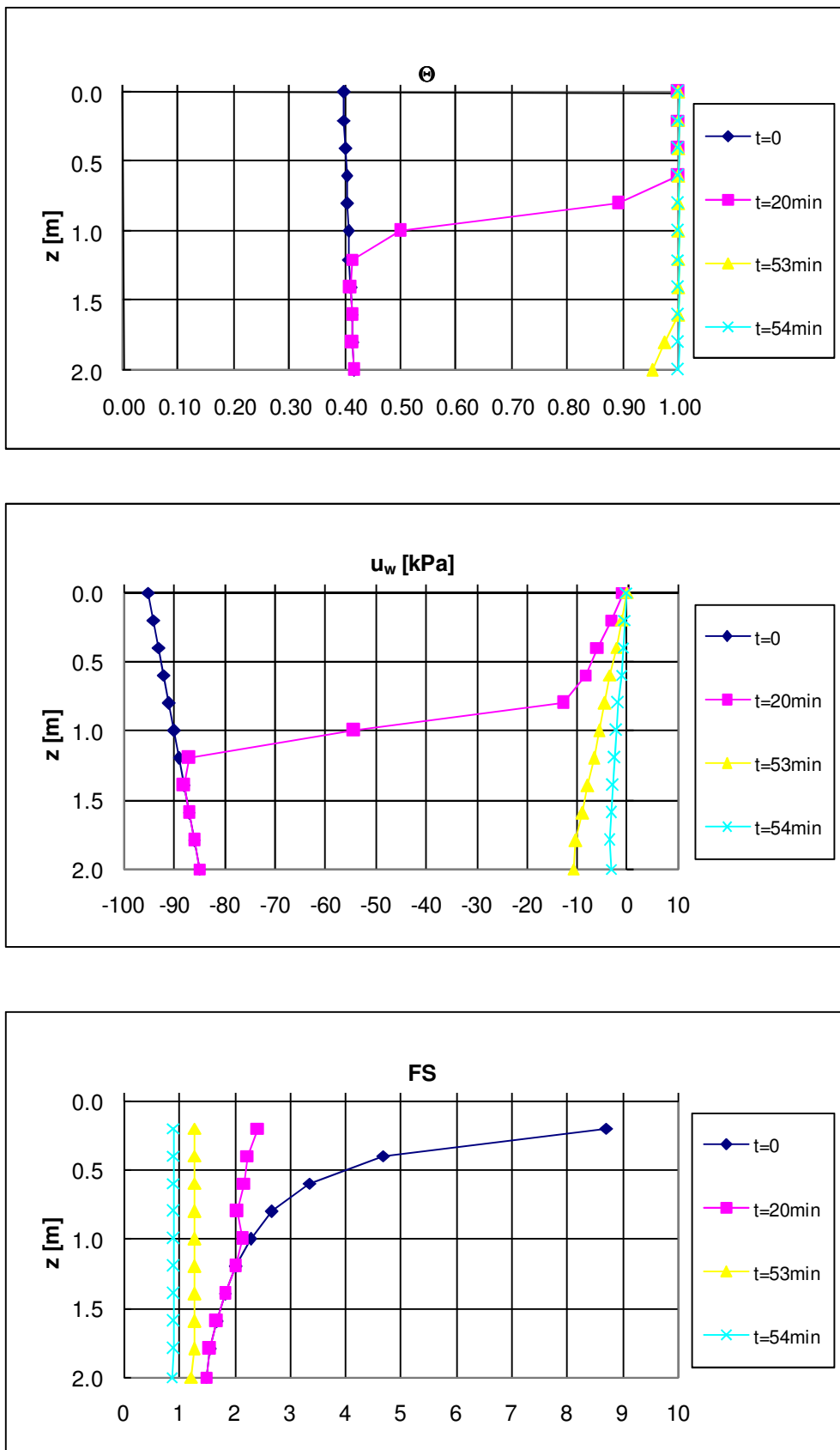


Fig. A1: $(u_a - u_w)_0 = 95 \text{ kPa}; I = 97.20 \text{ mm/h}$

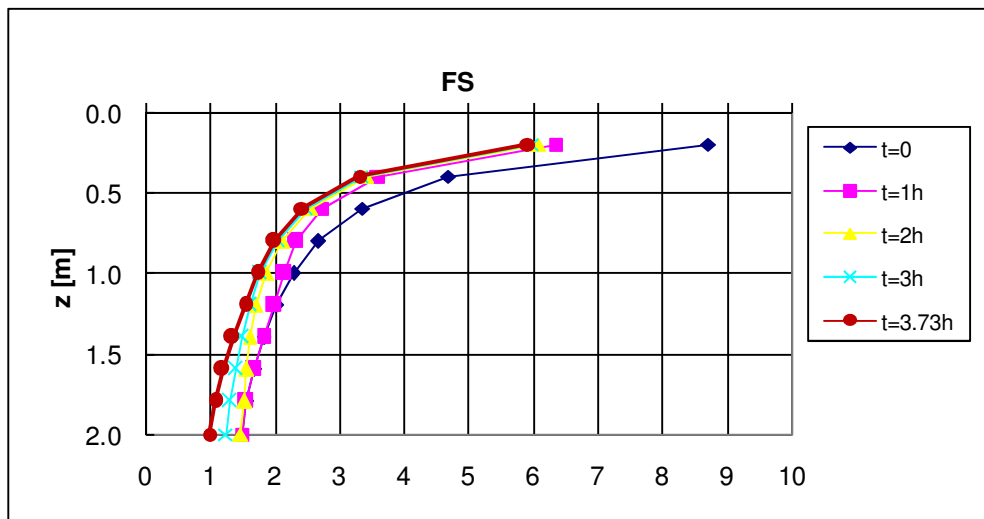
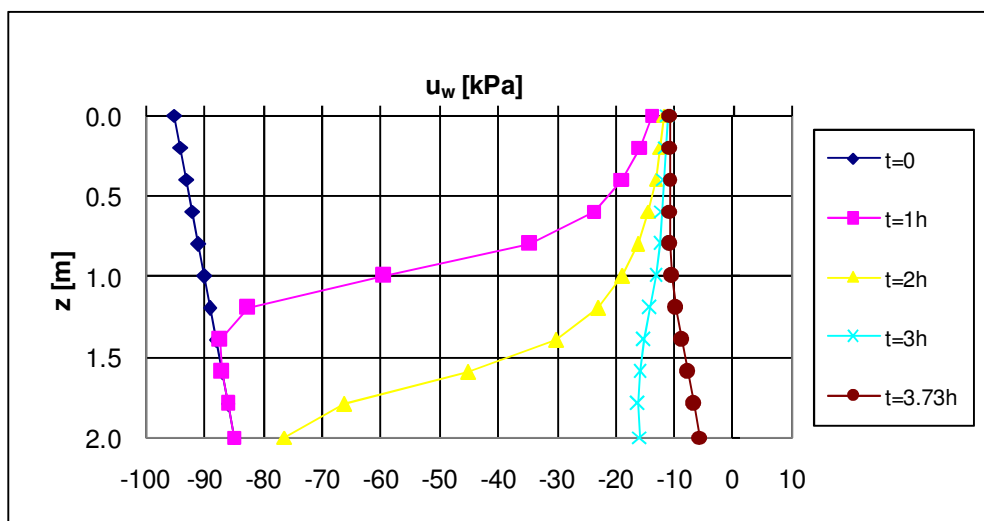
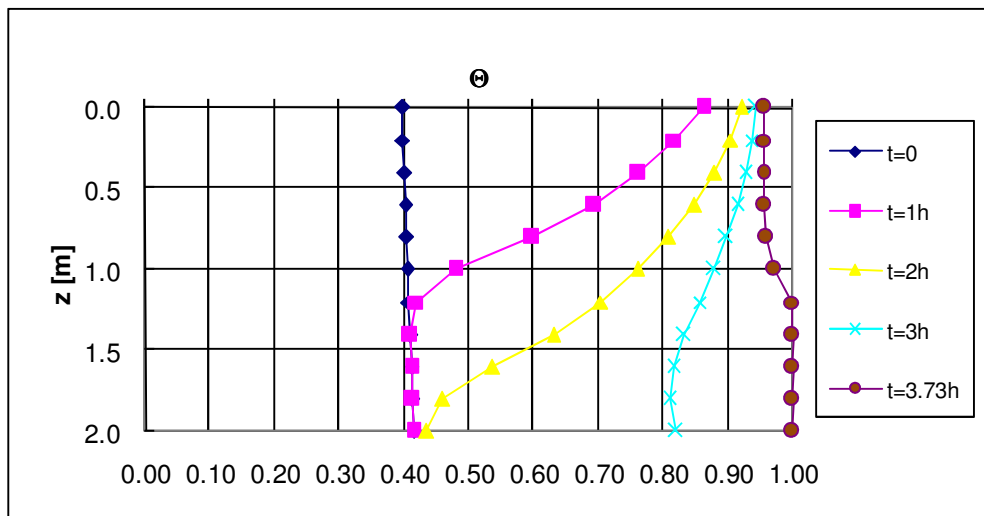


Fig. A2: $(u_a - u_w)_0 = 95 \text{ kPa}; I = 19.44 \text{ mm/h}$

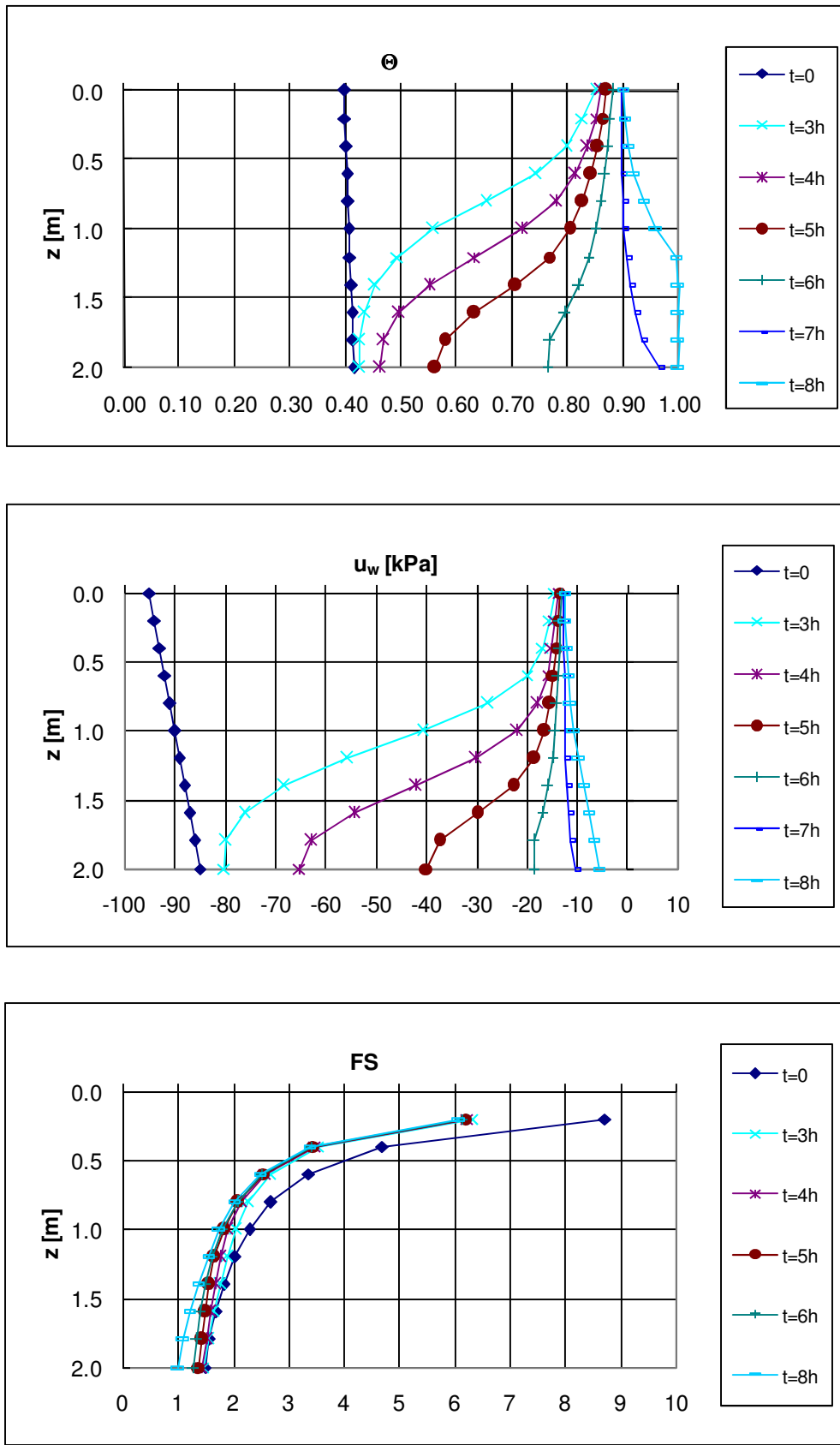


Fig. A3: $(u_a - u_w)_0 = 95 \text{ kPa}$; $I = 9.72 \text{ mm/h}$

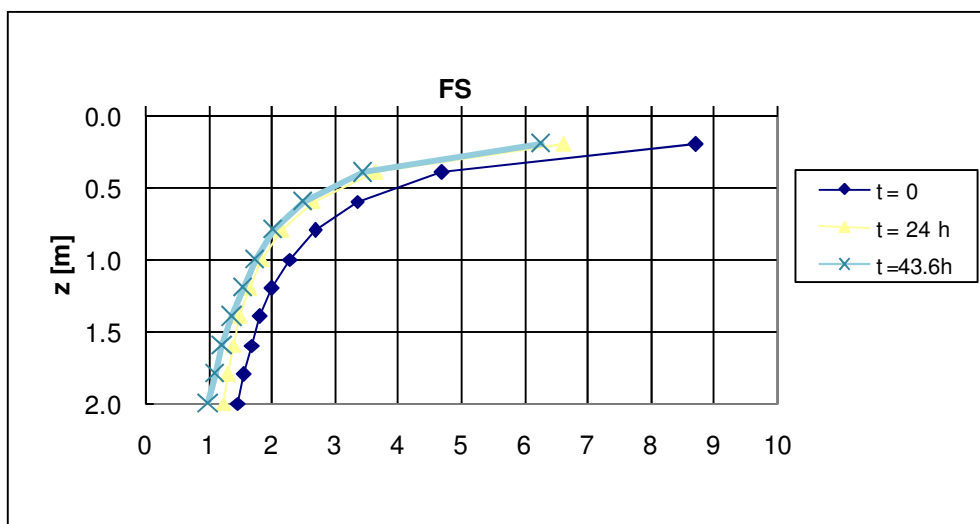
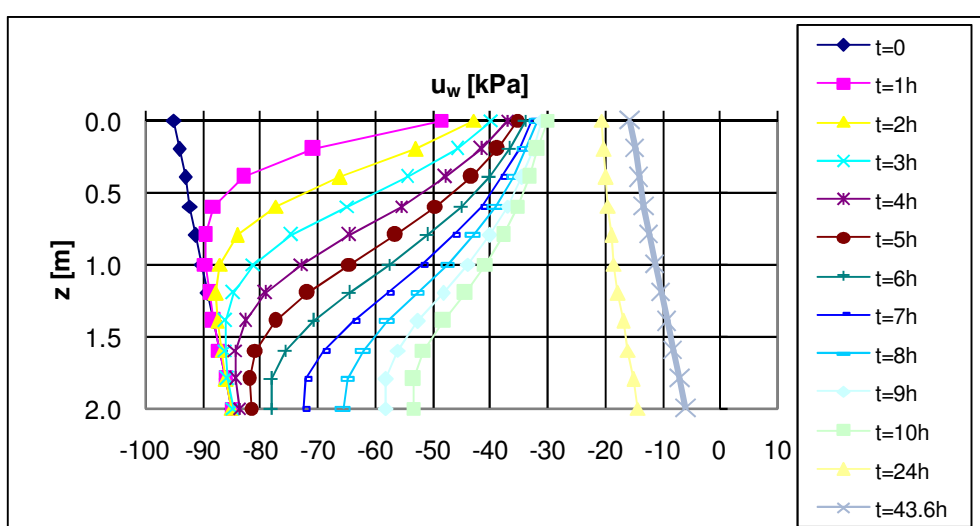
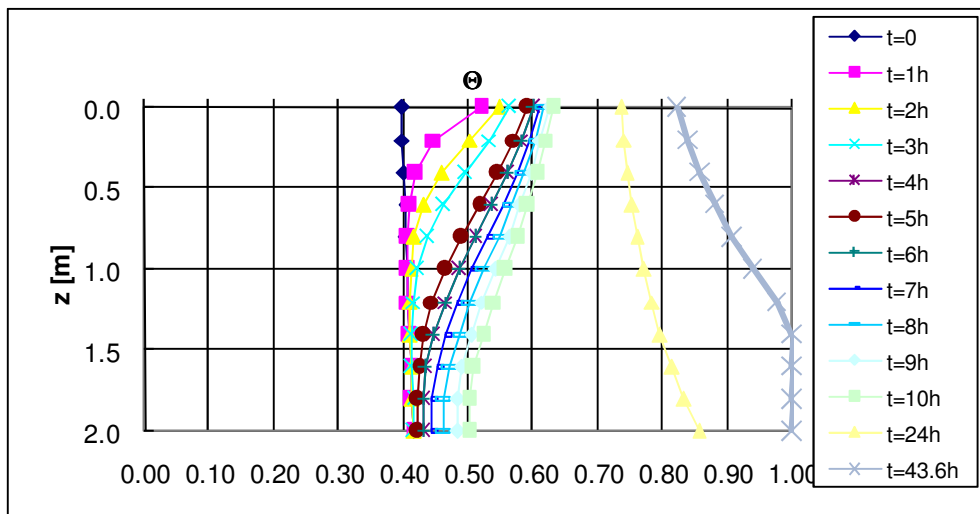


Fig. A4: $(u_a - u_w)_0 = 95 \text{ kPa}$; $I = 1.94 \text{ mm/h}$

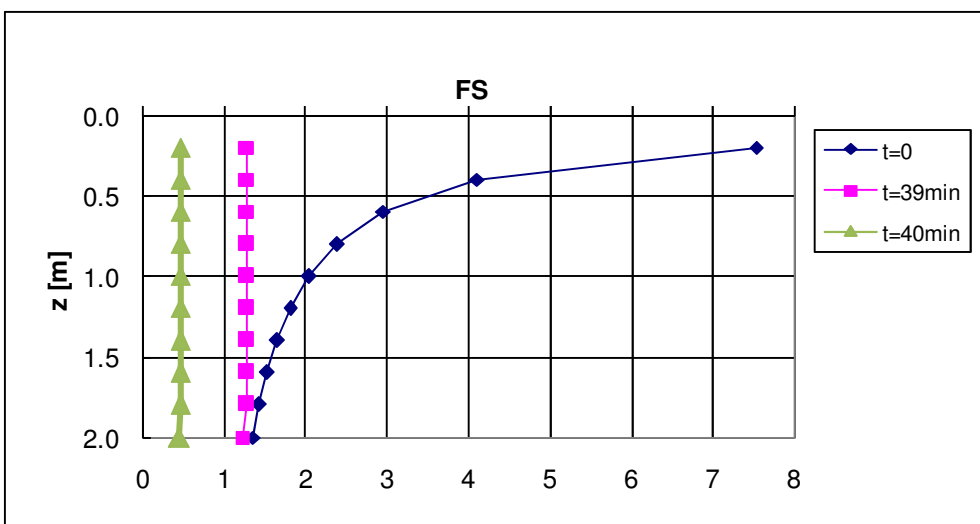
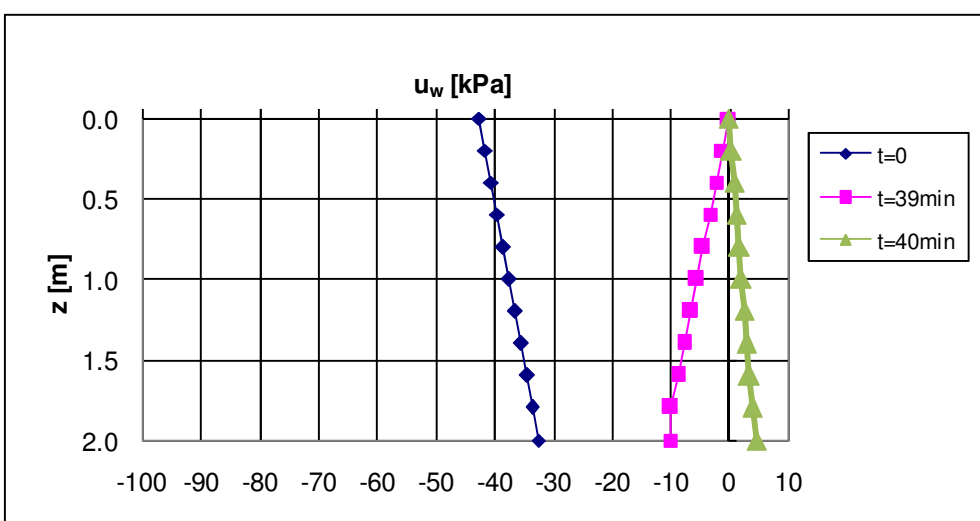
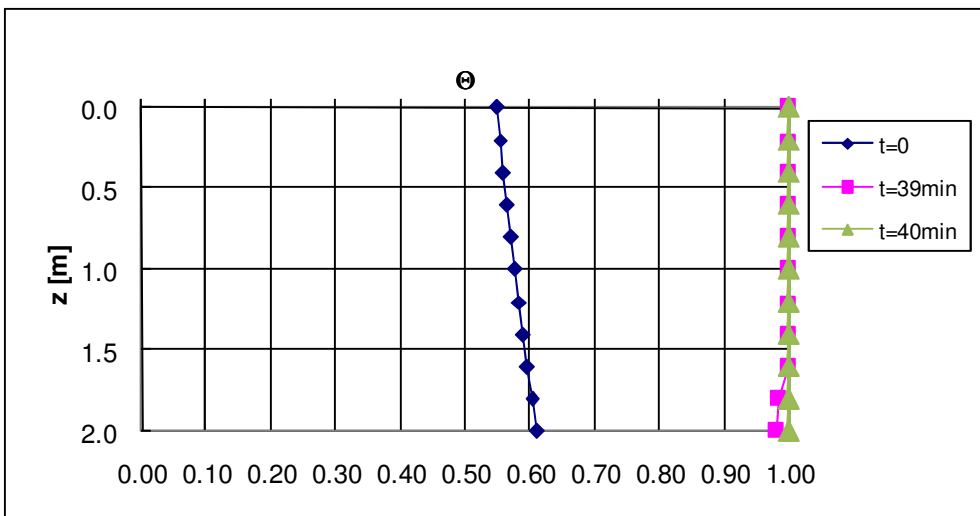


Fig. A5: $(u_a - u_w)_0 = 42.49 \text{ kPa}; I = 97.20 \text{ mm/h}$

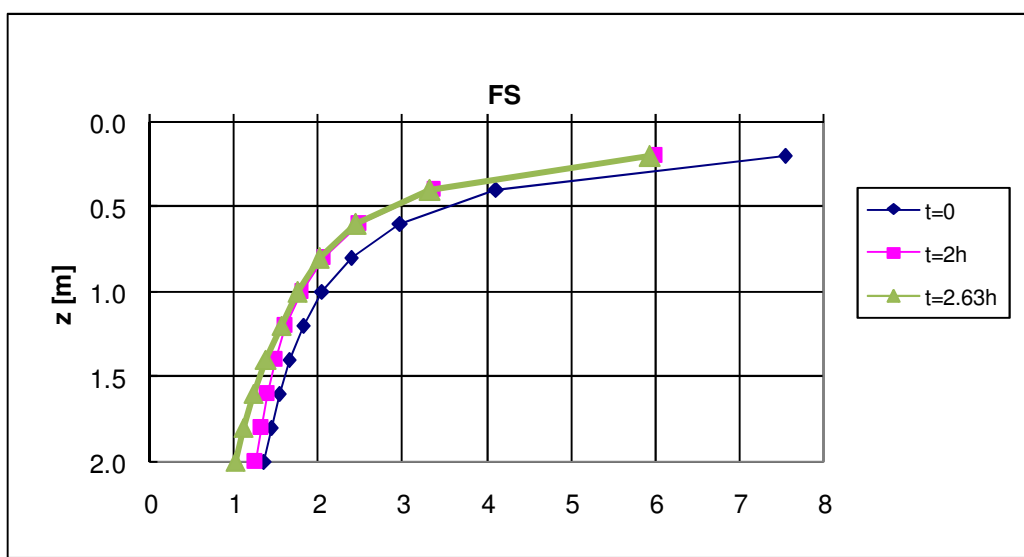
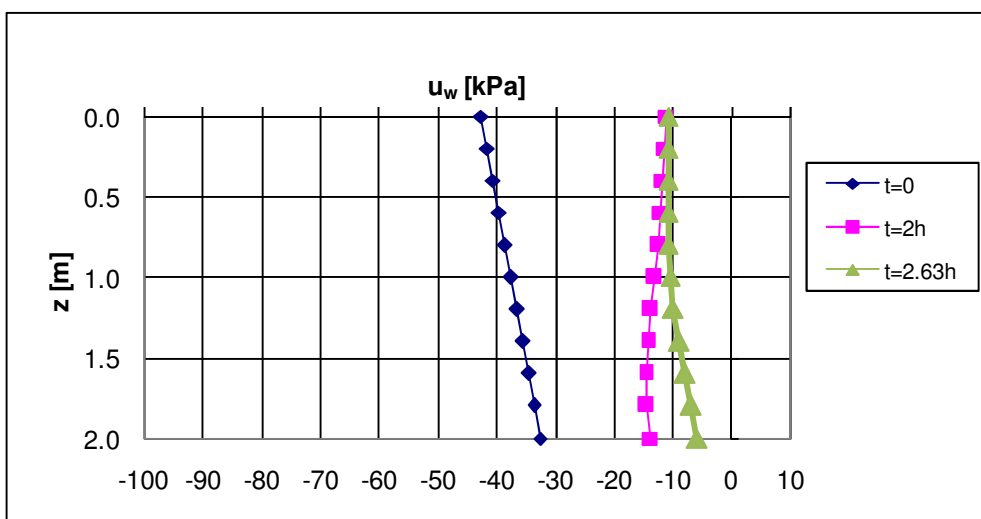
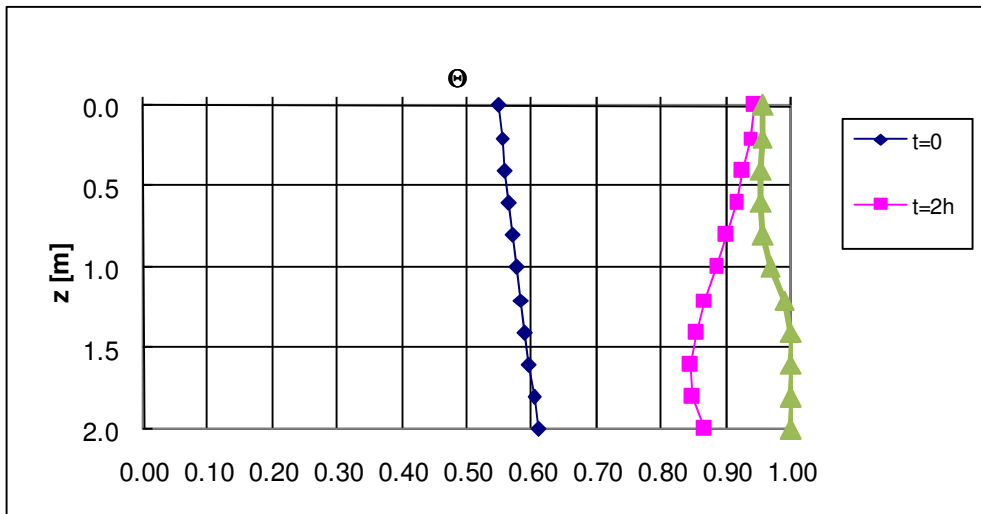


Fig. A6: $(u_a - u_w)_0 = 42.49$ kPa; $I = 19.44$ mm/h

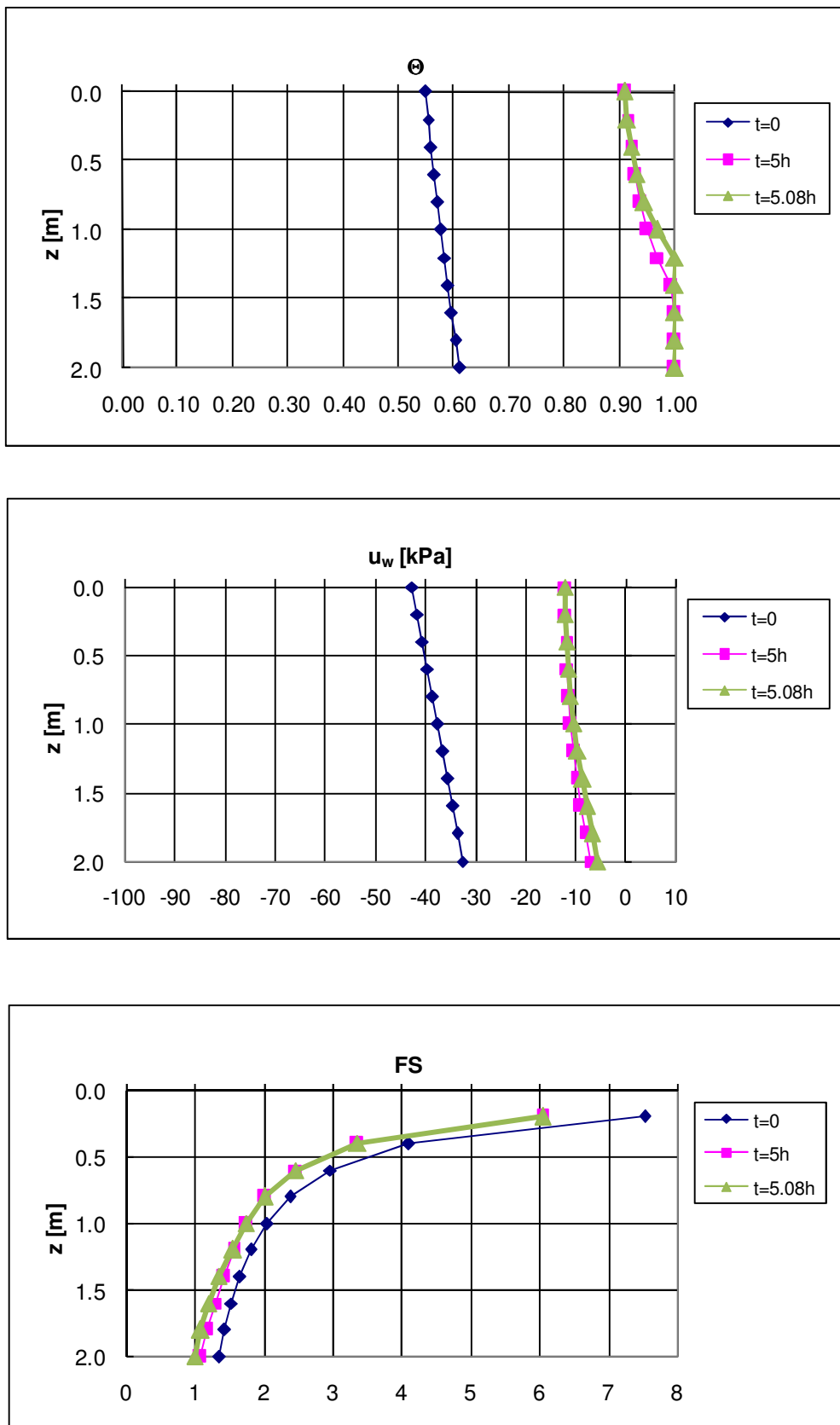


Fig. A7: $(u_a - u_w)_0 = 42.49 \text{ kPa}$; $I = 9.72 \text{ mm/h}$

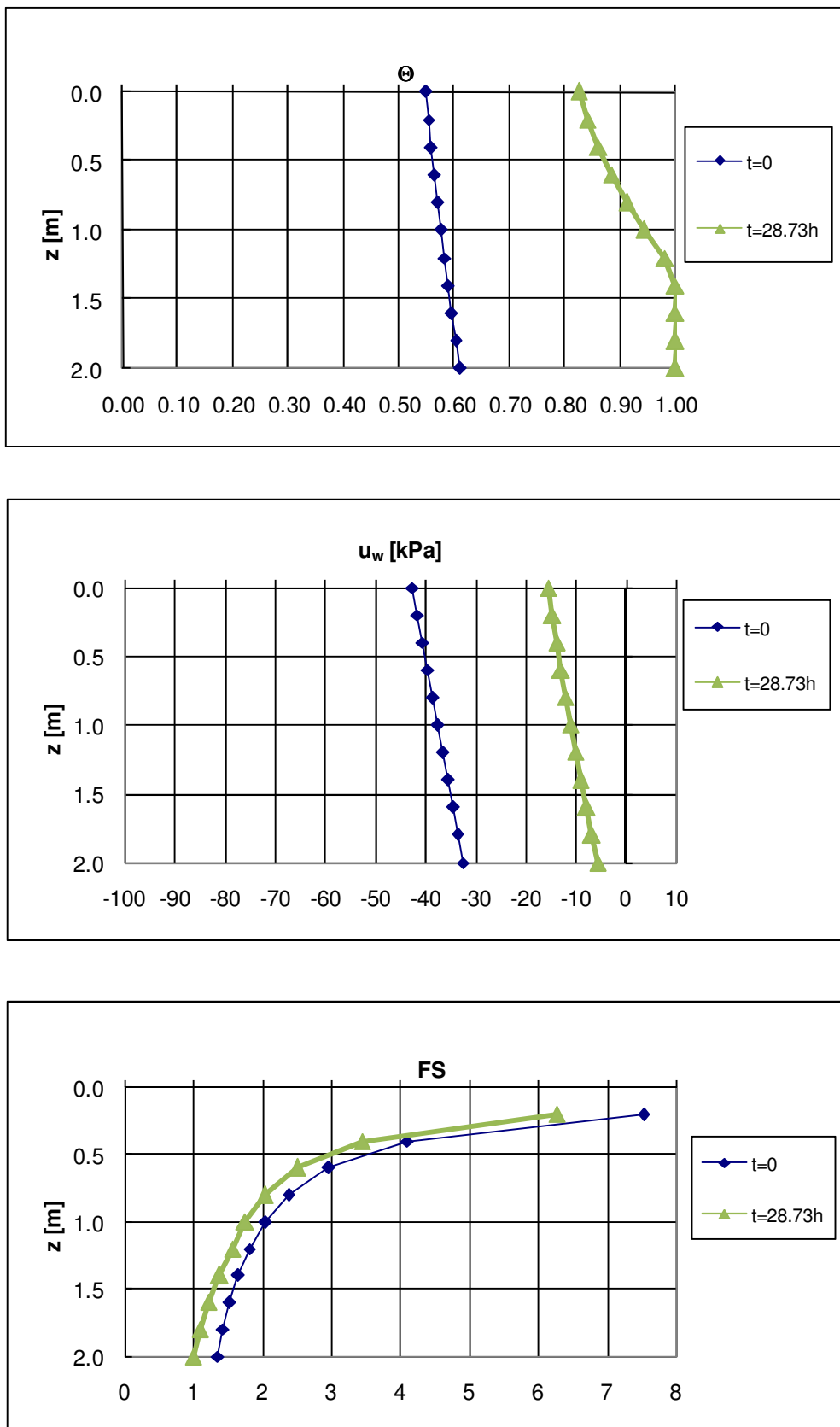


Fig. A8: $(u_a - u_w)_0 = 42.49 \text{ kPa}$; $I = 1.94 \text{ mm/h}$

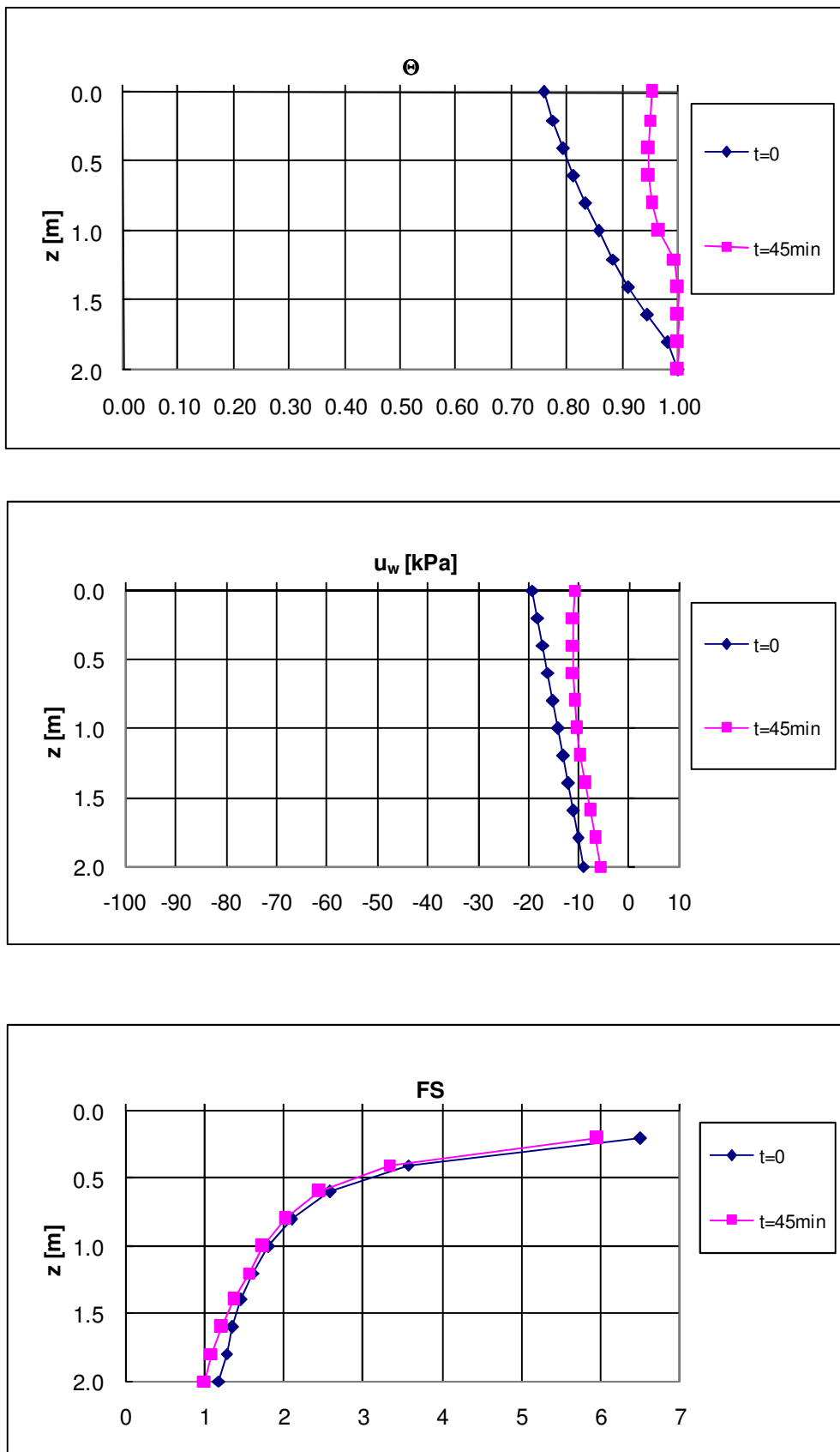


Fig. A9: $(u_a - u_w)_0 = 19 \text{ kPa}; I = 19.44 \text{ mm/h}$

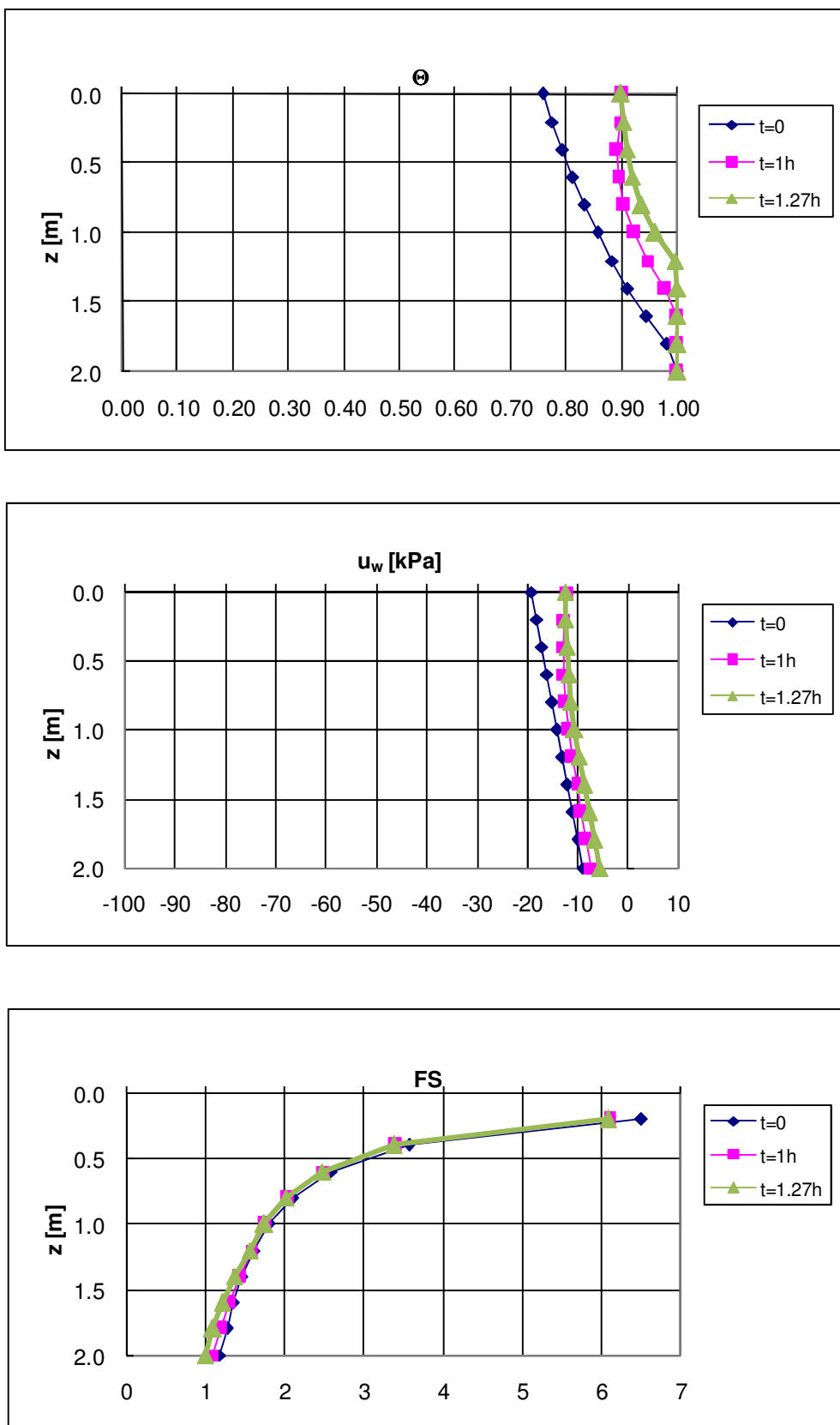


Fig. A10: $(u_a - u_w)_0 = 19 \text{ kPa}$; $I = 9.72 \text{ mm/h}$

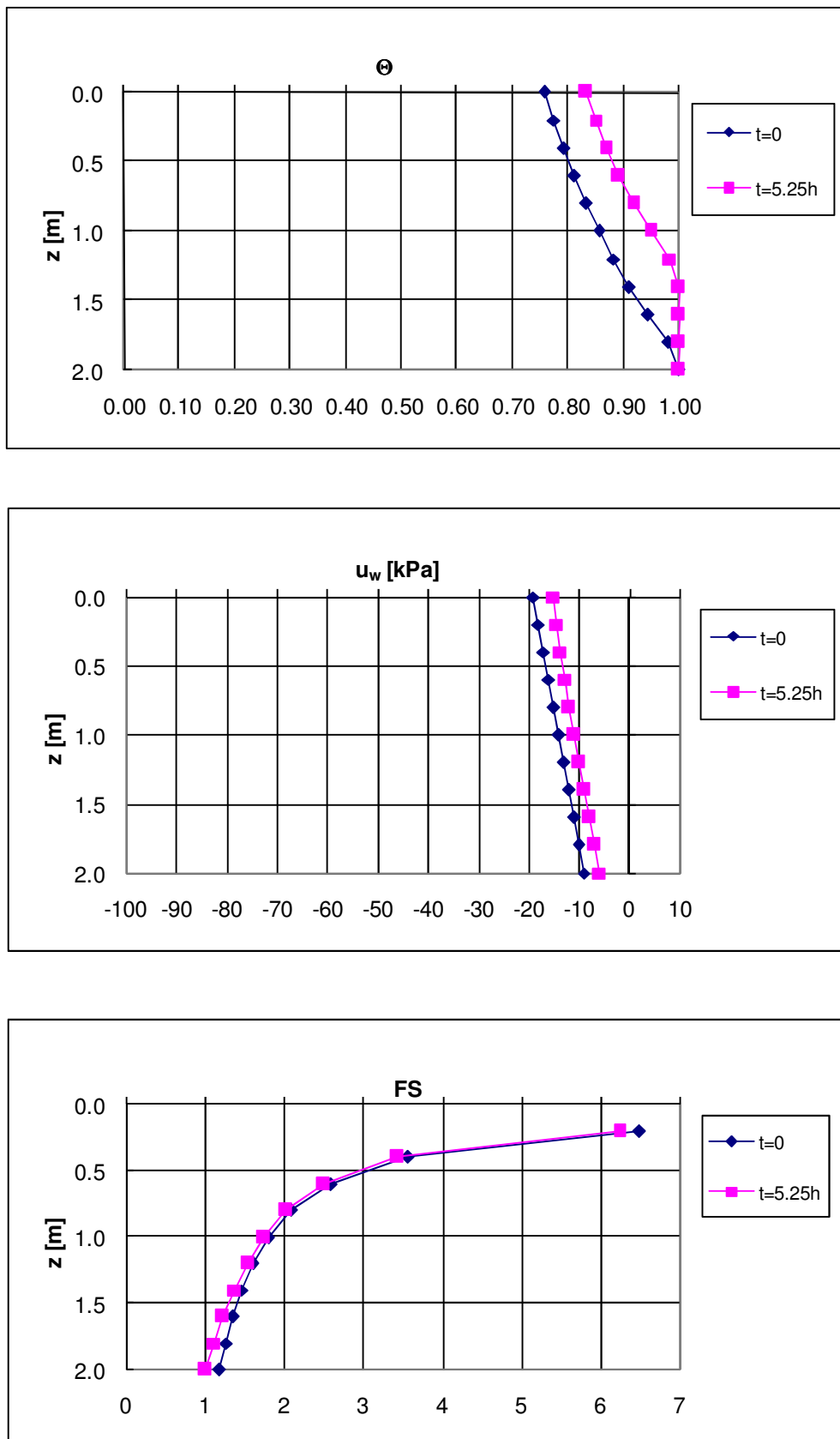


Fig. A11: $(u_a - u_w)_0 = 19 \text{ kPa}; I = 1.94 \text{ mm/h}$

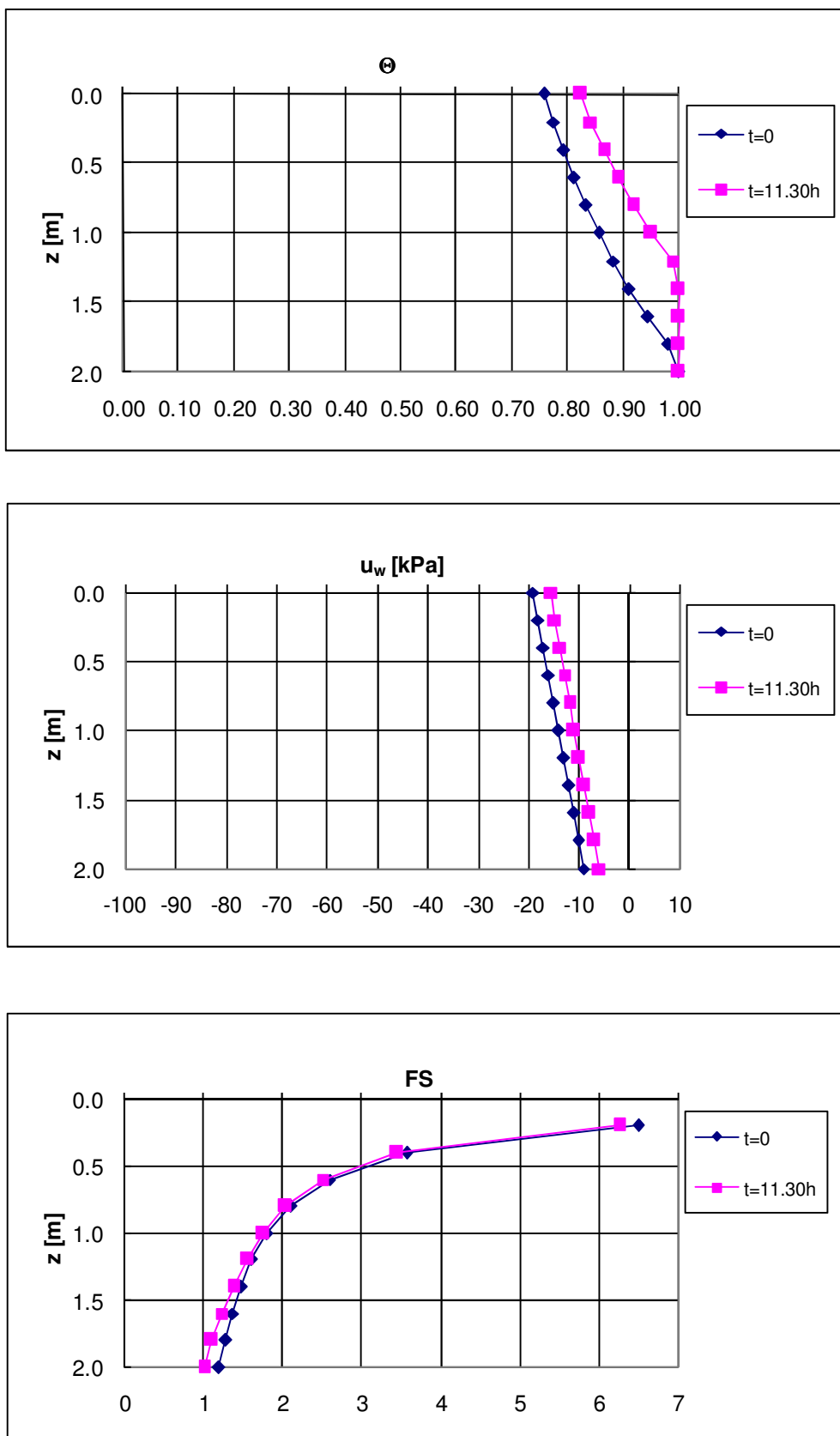


Fig. A12: $(u_a - u_w)_0 = 19 \text{ kPa}$; $I = 0.97 \text{ mm/h}$



ATTACHMENT B

Hypothesis 1

Slope angle $\beta = 45^\circ$

Soil nr.1

Case b

Thickness $h = 1$ m

Impervious bottom

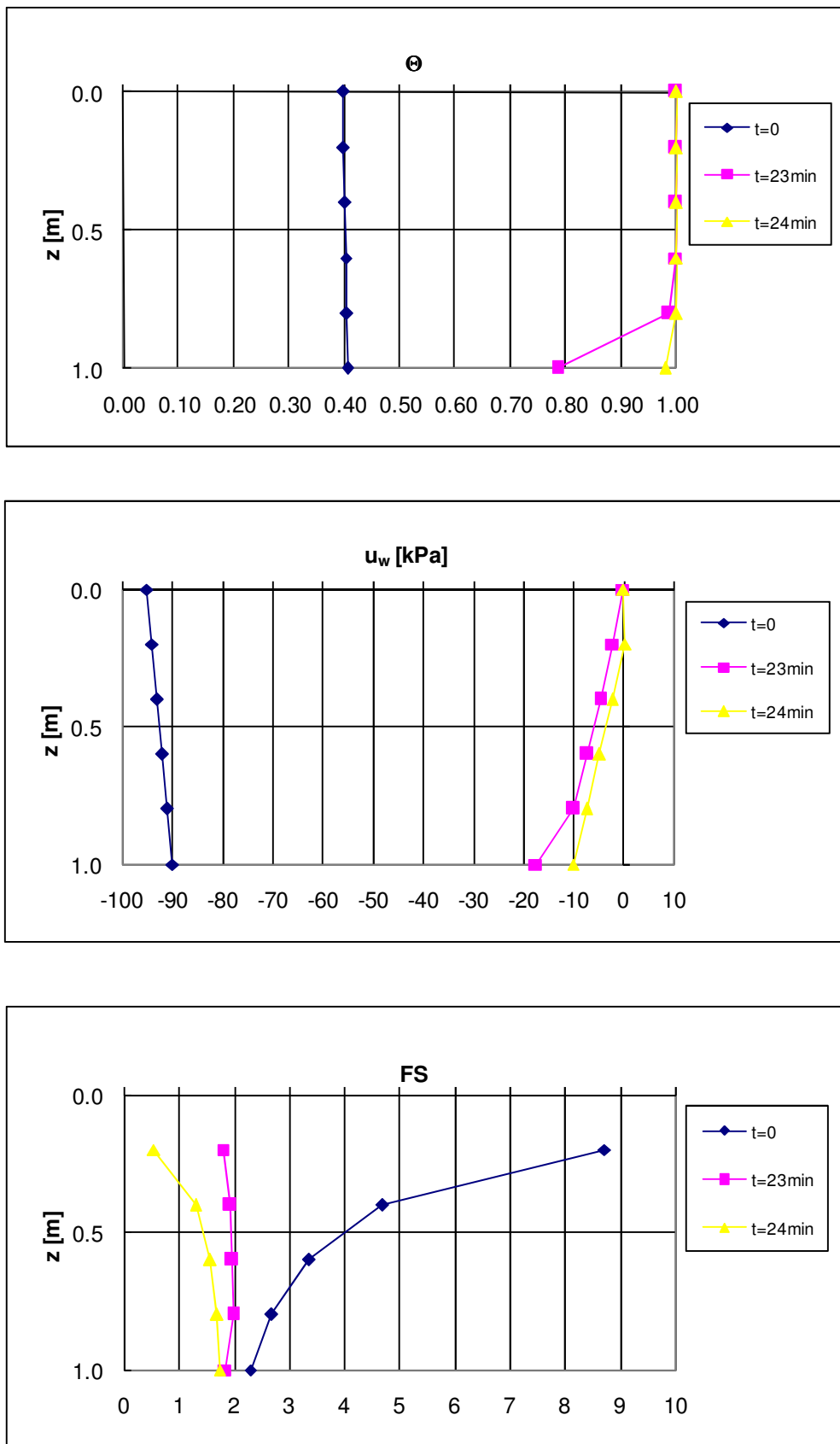


Fig. B1: $(u_a-u_w)_0 = 95 \text{ kPa}$; $I = 97.20 \text{ mm/h}$

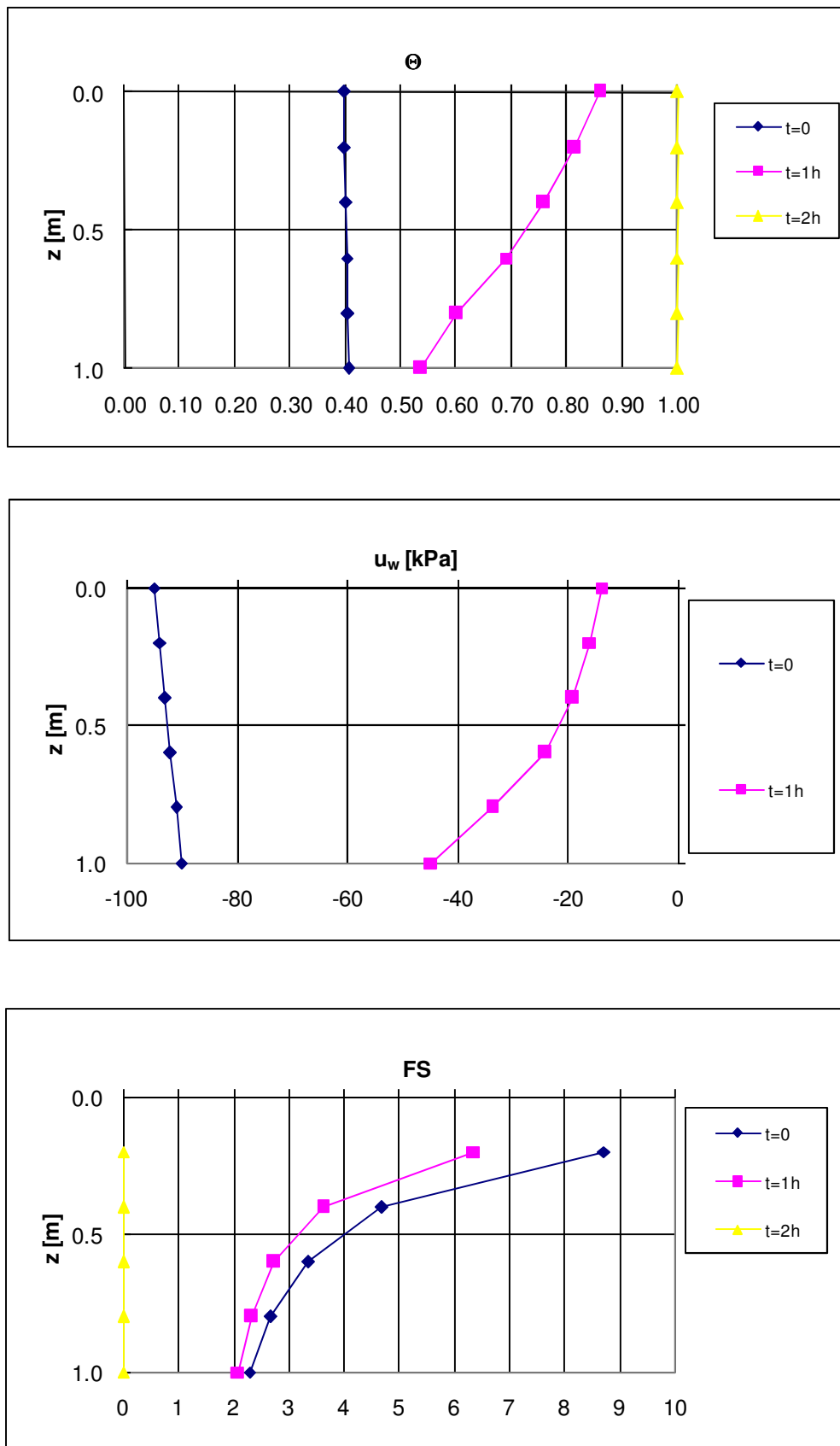


Fig. B2: $(u_a - u_w)_0 = 95 \text{ kPa}$; $I = 19.44 \text{ mm/h}$

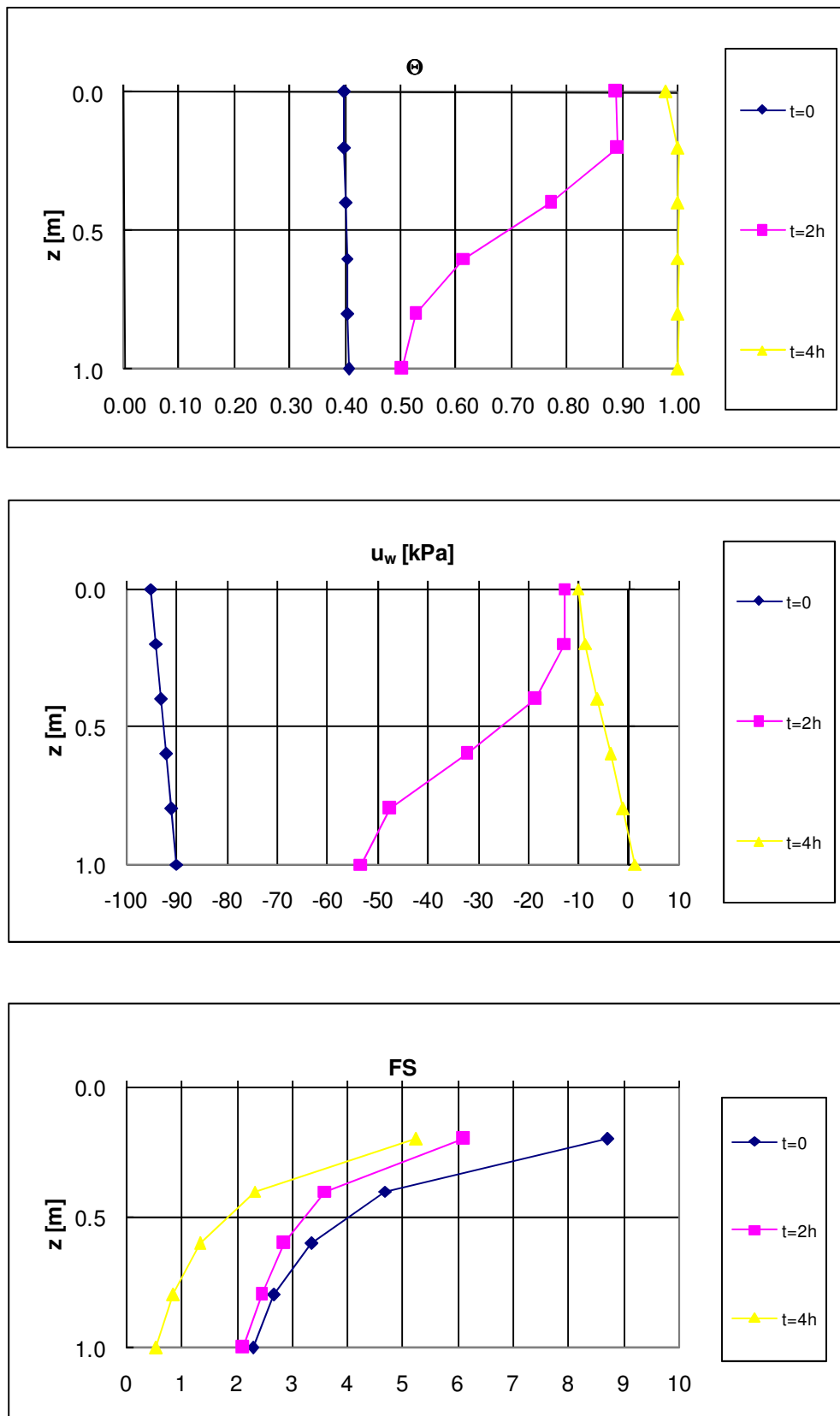


Fig. B3: $(u_a - u_w)_0 = 95 \text{ kPa}$; $I = 9.72 \text{ mm/h}$

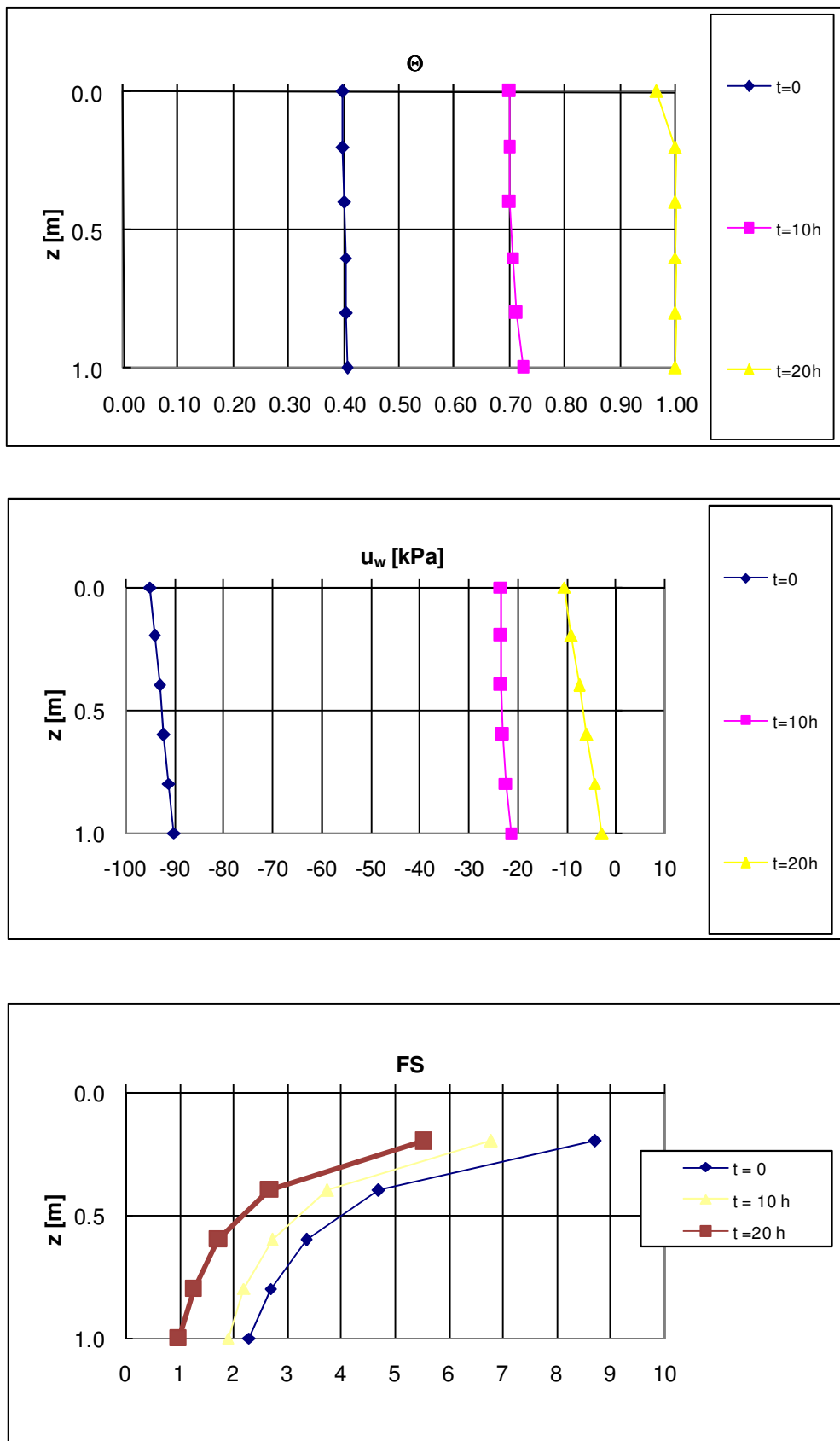


Fig. B4: $(u_a - u_w)_0 = 95 \text{ kPa}$; $I = 1.94 \text{ mm/h}$

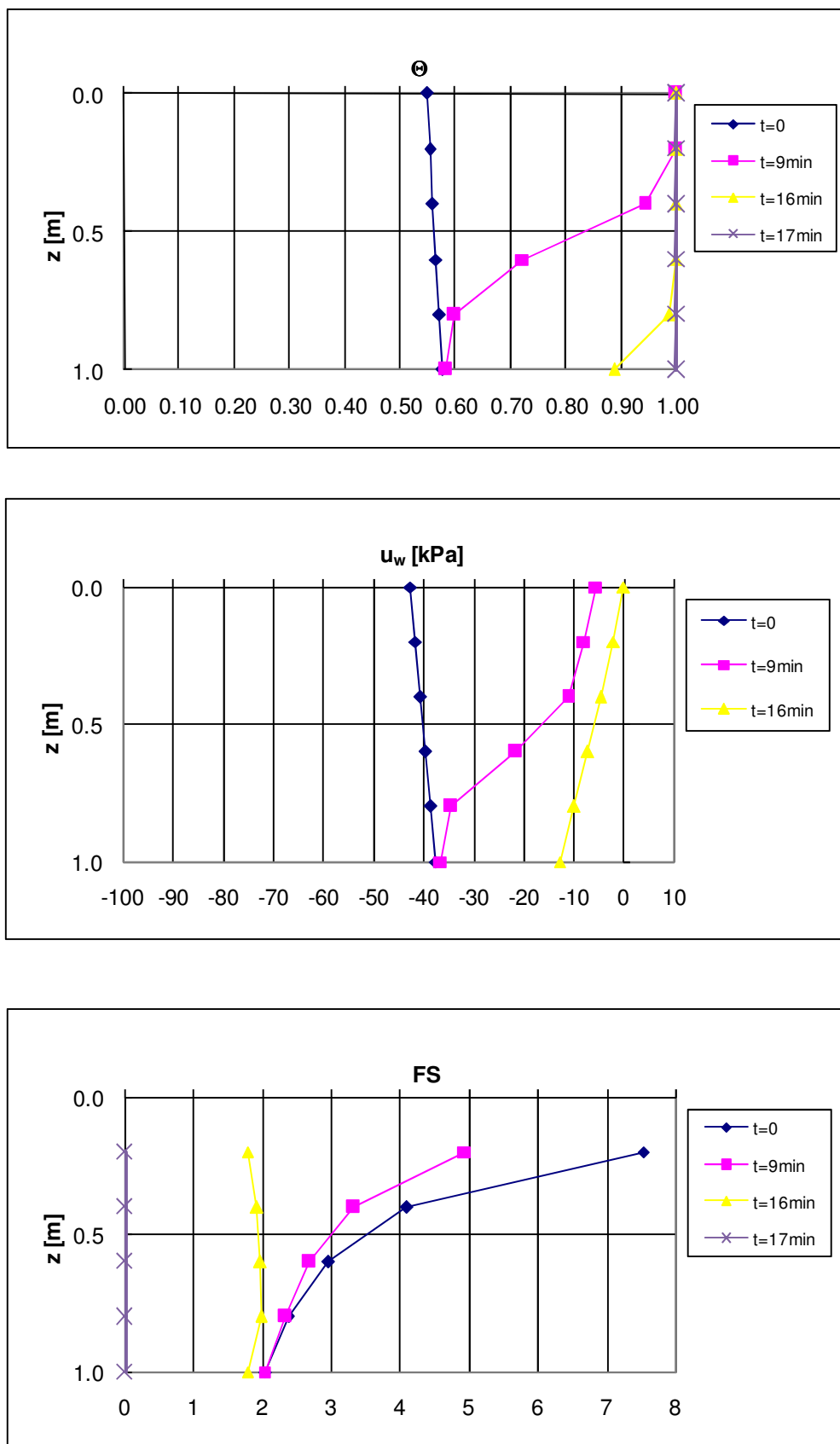


Fig. B5: $(u_a - u_w)_0 = 42.49 \text{ kPa}$; $I = 97.20 \text{ mm/h}$

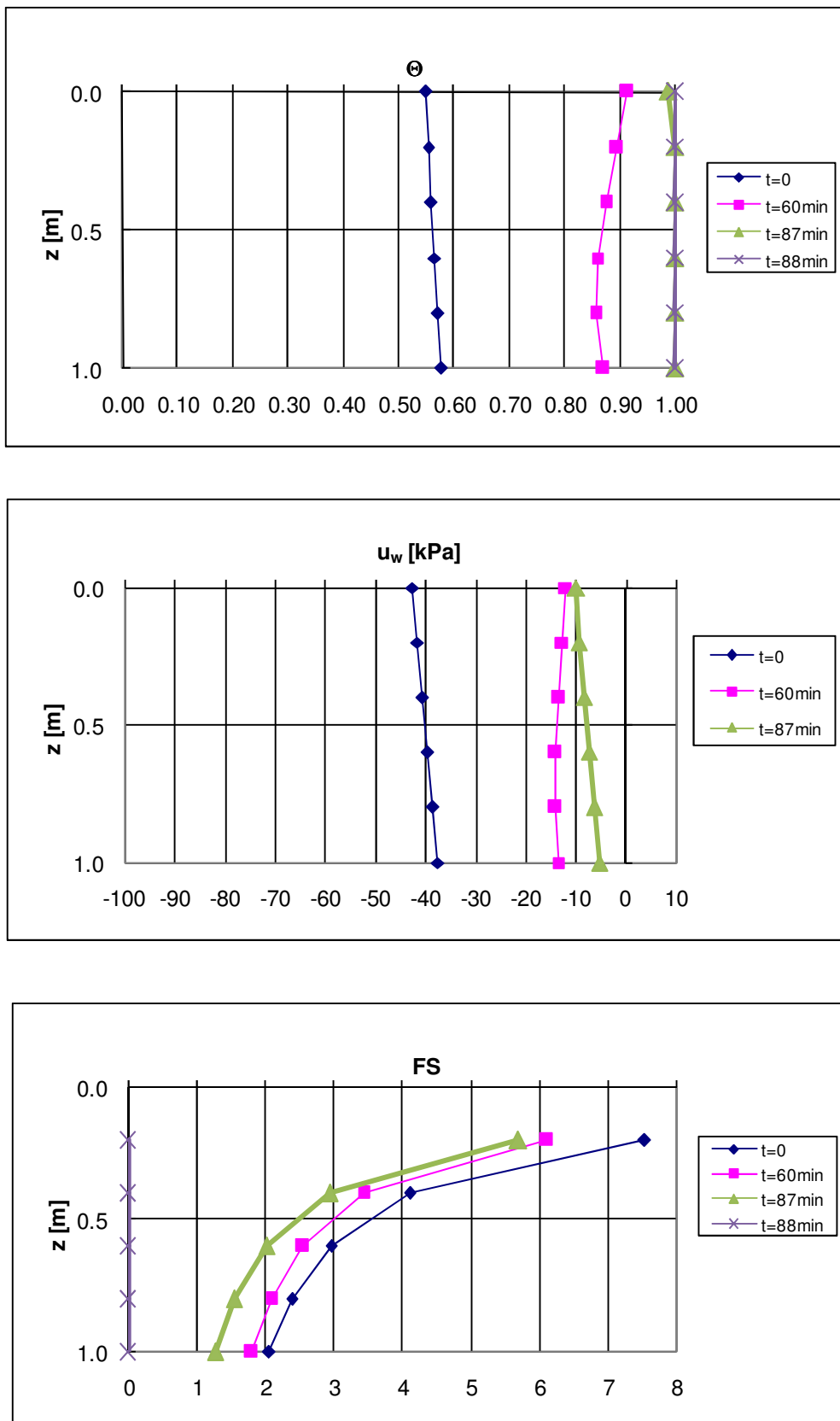


Fig. B6: $(u_a - u_w)_0 = 42.49 \text{ kPa}$; $I = 19.44 \text{ mm/h}$

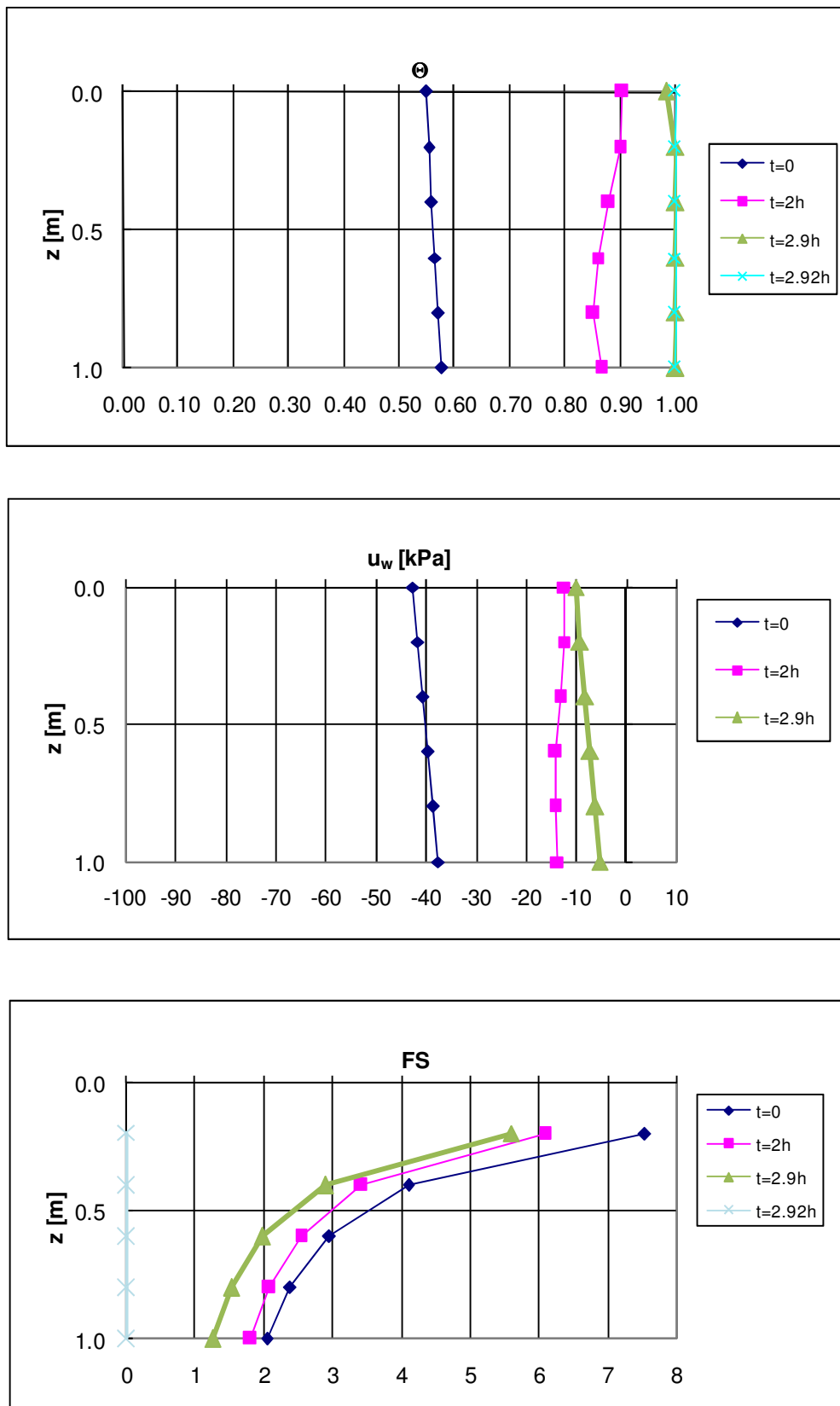


Fig. B7: $(u_a - u_w)_0 = 42.49 \text{ kPa}; l = 9.72 \text{ mm/h}$

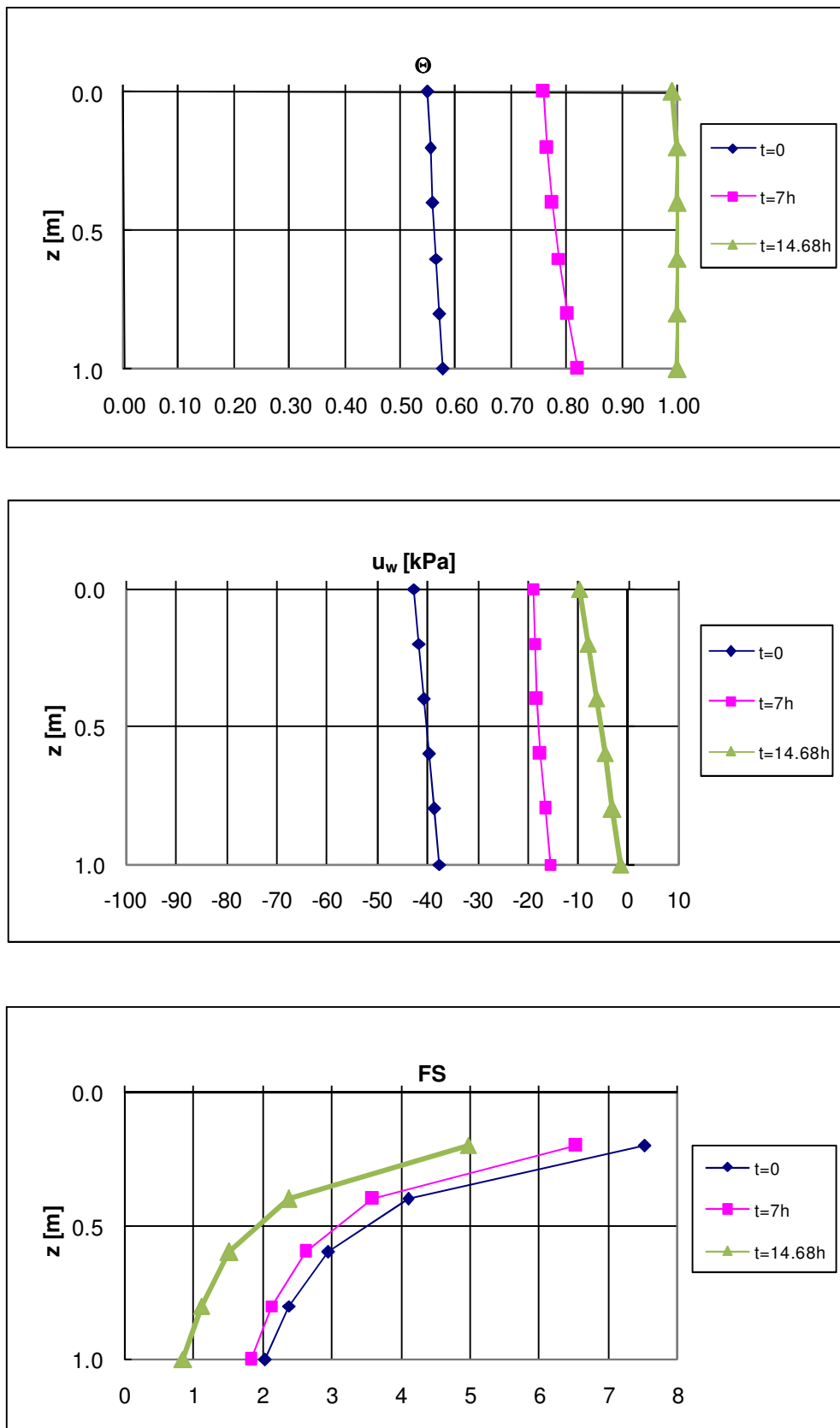


Fig. B8: $(u_a - u_w)_0 = 42.49 \text{ kPa}$; $I = 1.94 \text{ mm/h}$

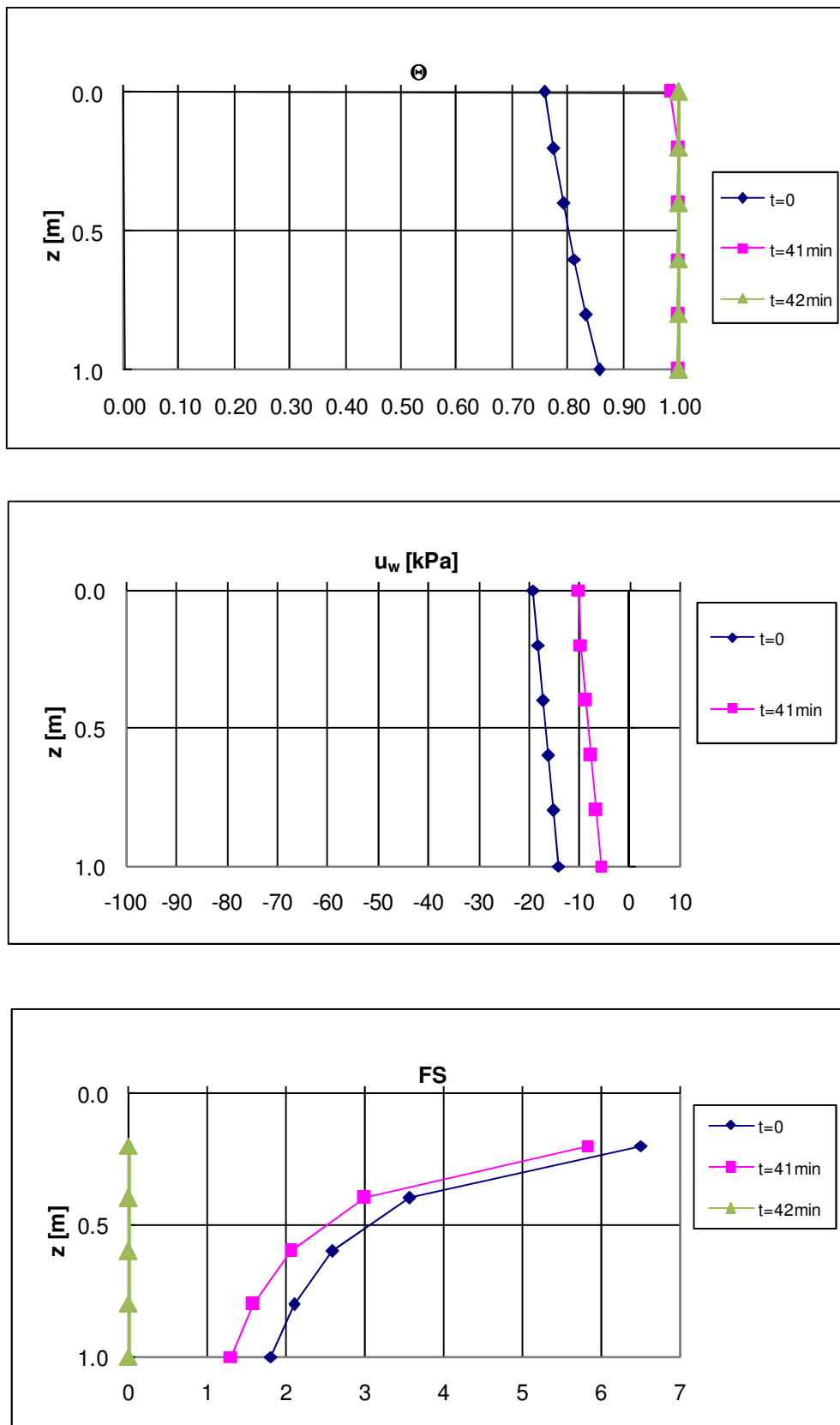


Fig. B9: $(u_a - u_w)_0 = 19 \text{ kPa}; I = 19.44 \text{ mm/h}$

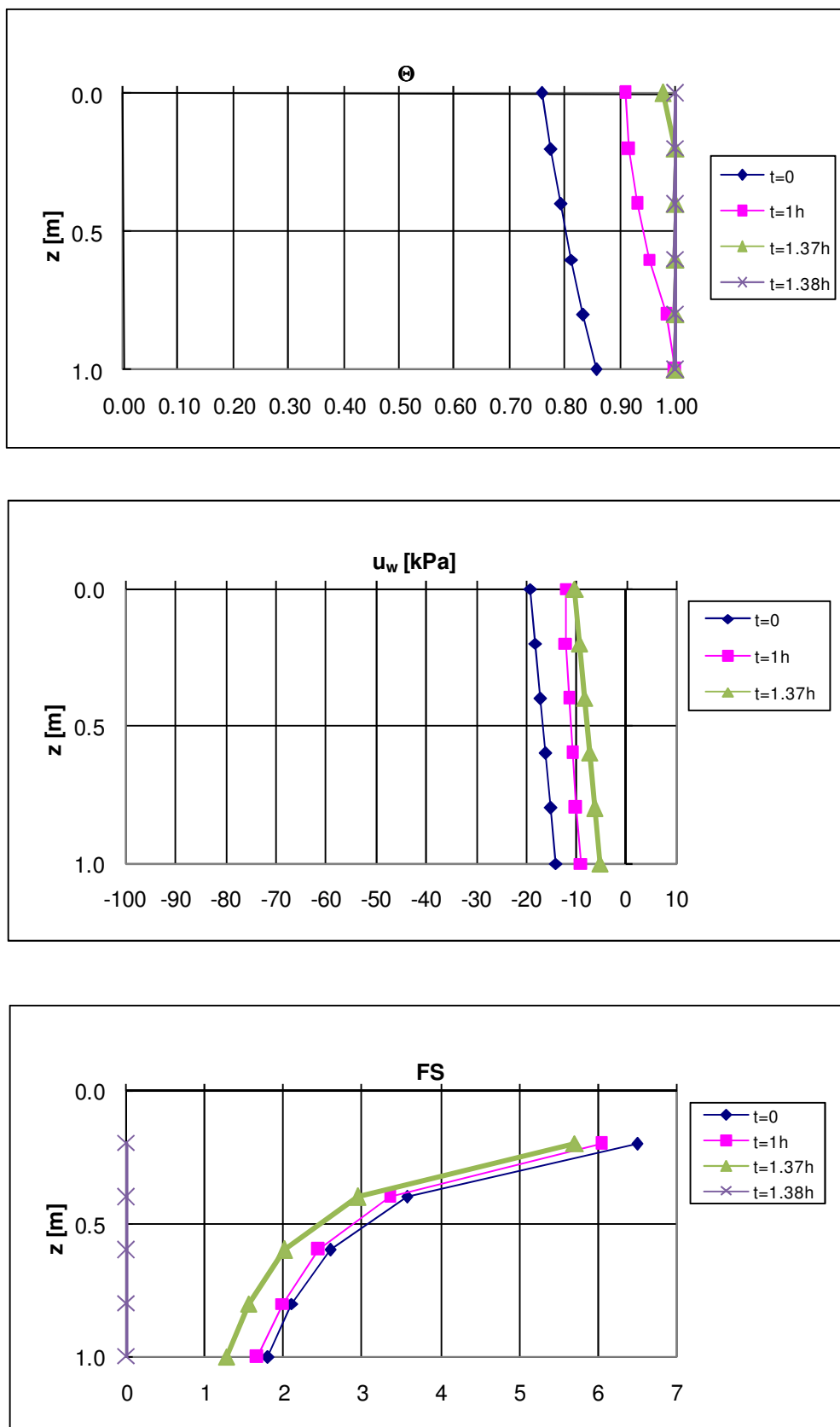


Fig. B10: $(u_a-u_w)_0 = 19 \text{ kPa}$; $I = 9.72 \text{ mm/h}$

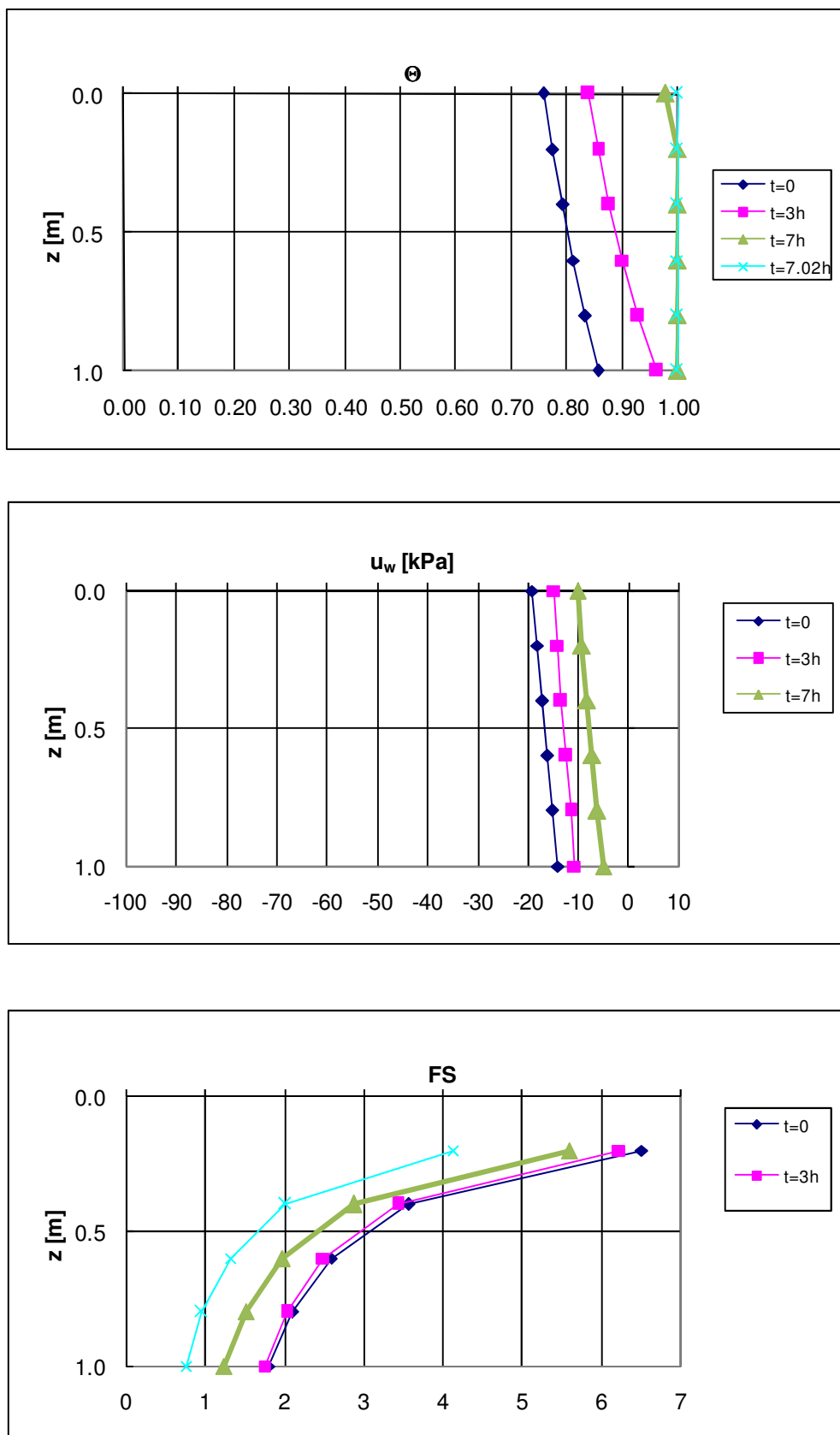


Fig. B11: $(u_a - u_w)_0 = 19 \text{ kPa}$; $I = 1.94 \text{ mm/h}$

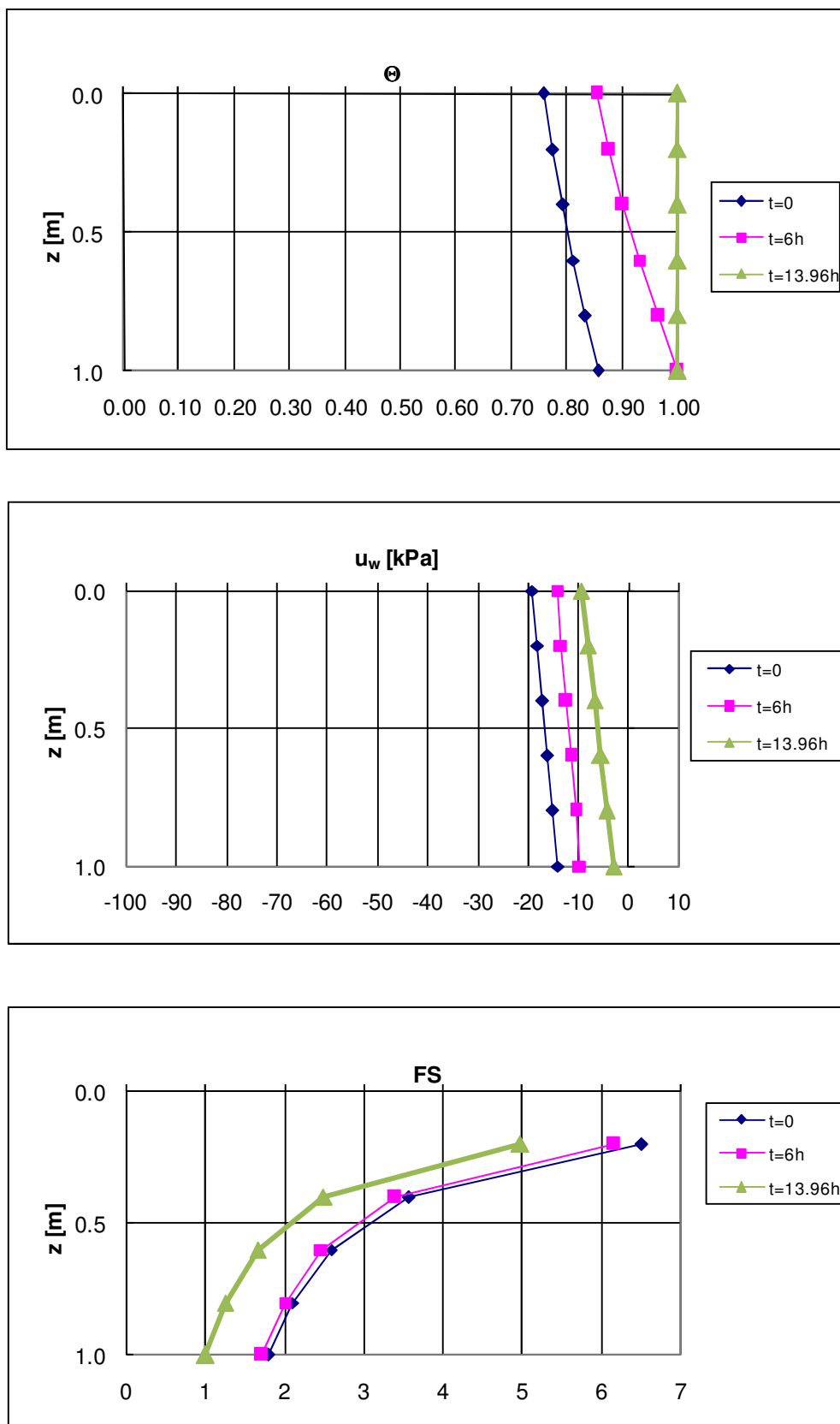


Fig. B12: $(u_a - u_w)_0 = 19 \text{ kPa}$; $I = 0.97 \text{ mm/h}$



ATTACHMENT C

Hypothesis 1

Slope angle $\beta = 45^\circ$
Soil nr.1

Case c

Thickness $h = 1$ m
Pervious bottom

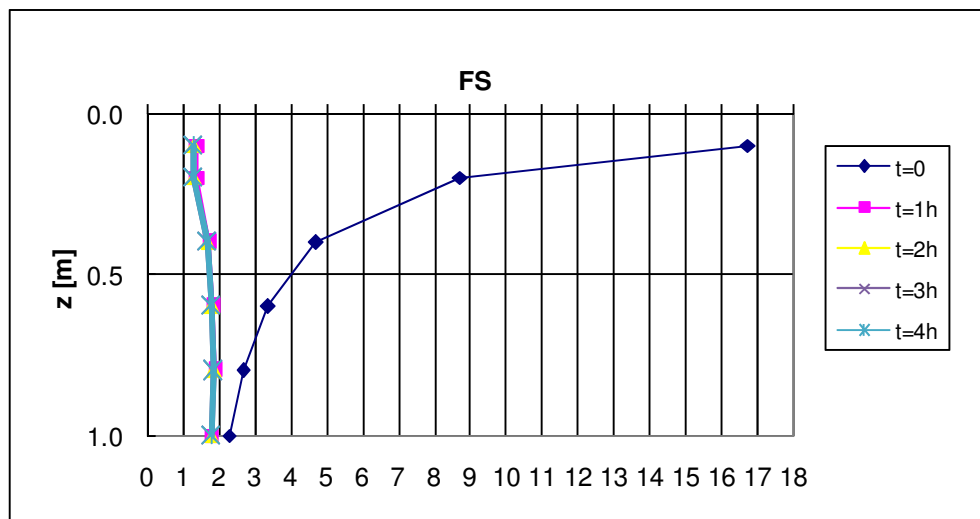
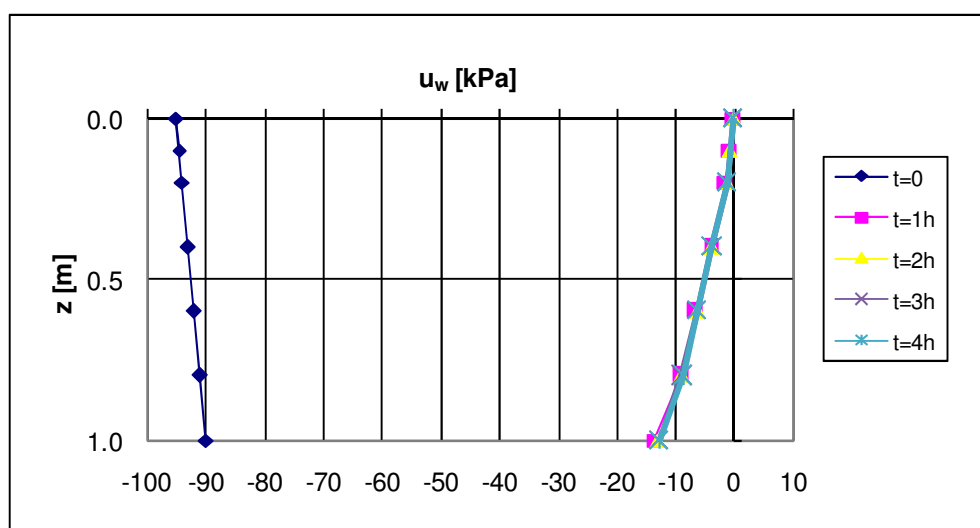
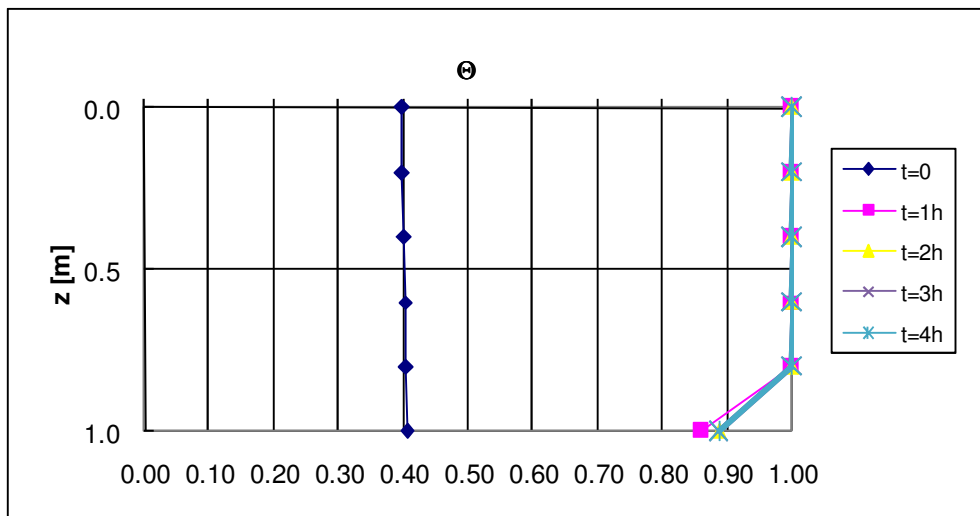


Fig. C1: $(u_a - u_w)_0 = 95 \text{ kPa}$; $I = 97.20 \text{ mm/h}$

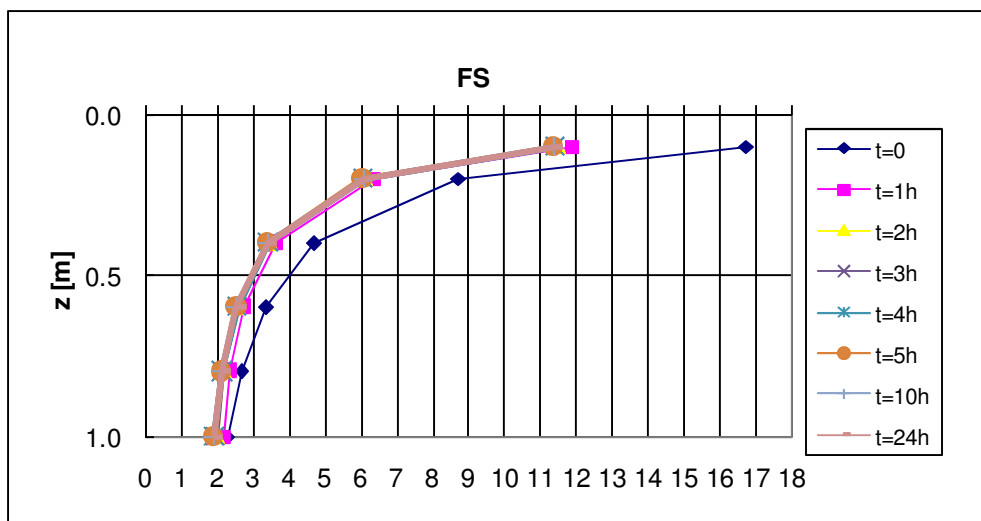
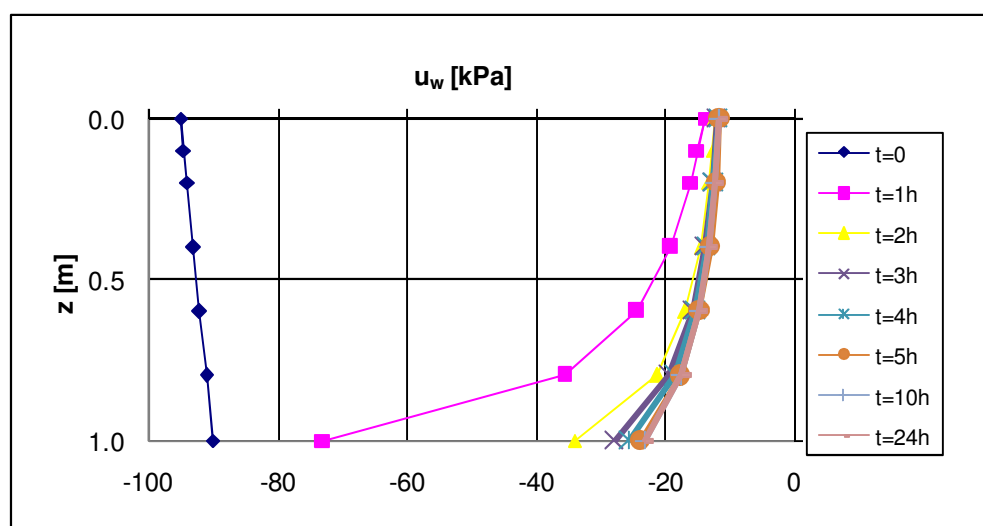
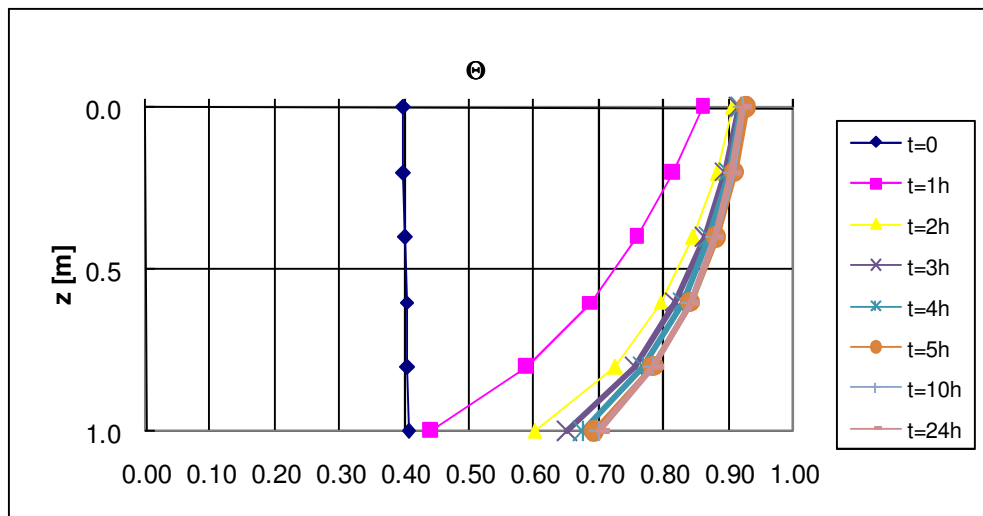


Fig. C2: $(u_a-u_w)_0 = 95 \text{ kPa}$; $I = 19.44 \text{ mm/h}$

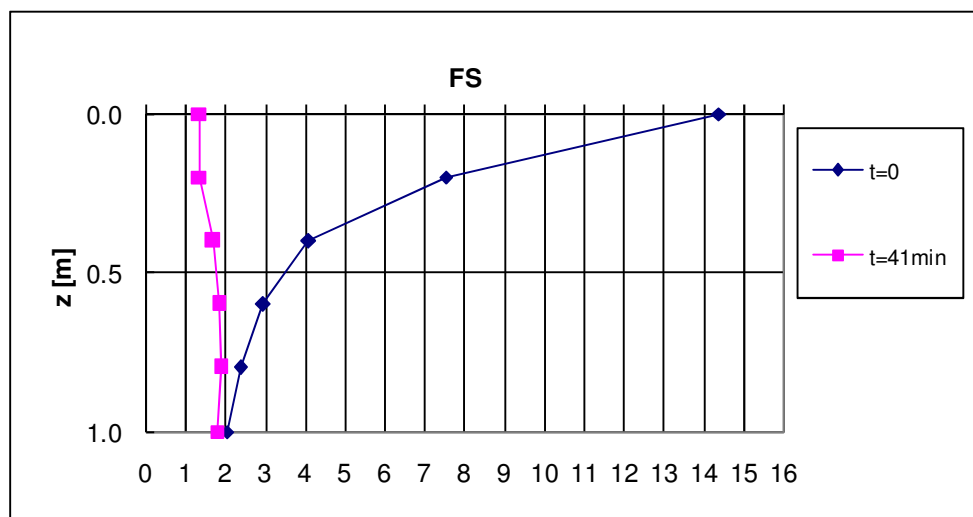
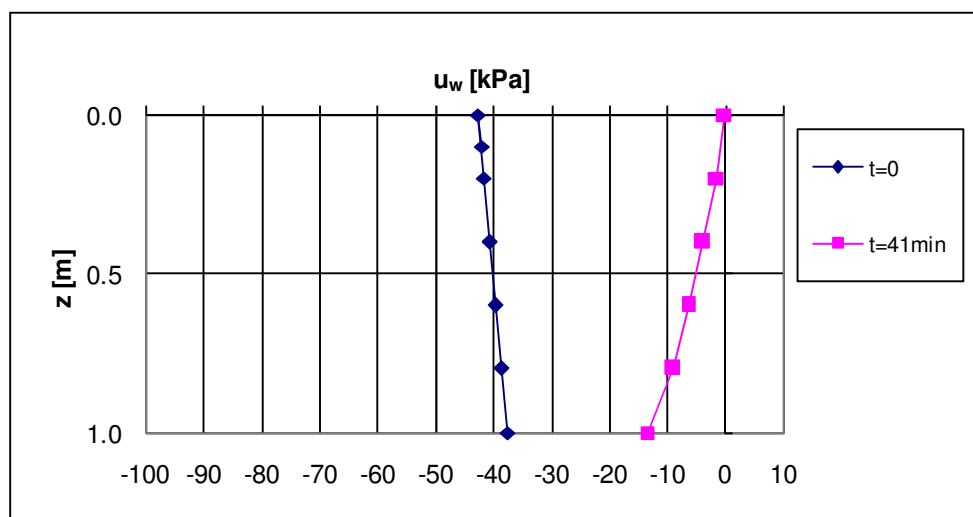
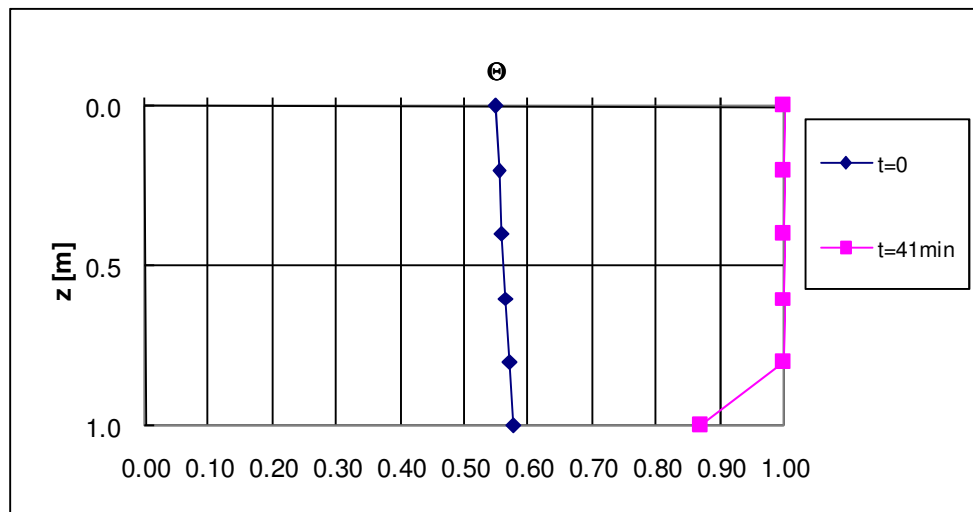


Fig. C3: $(u_a - u_w)_0 = 42.49 \text{ kPa}$; $I = 97.20 \text{ mm/h}$

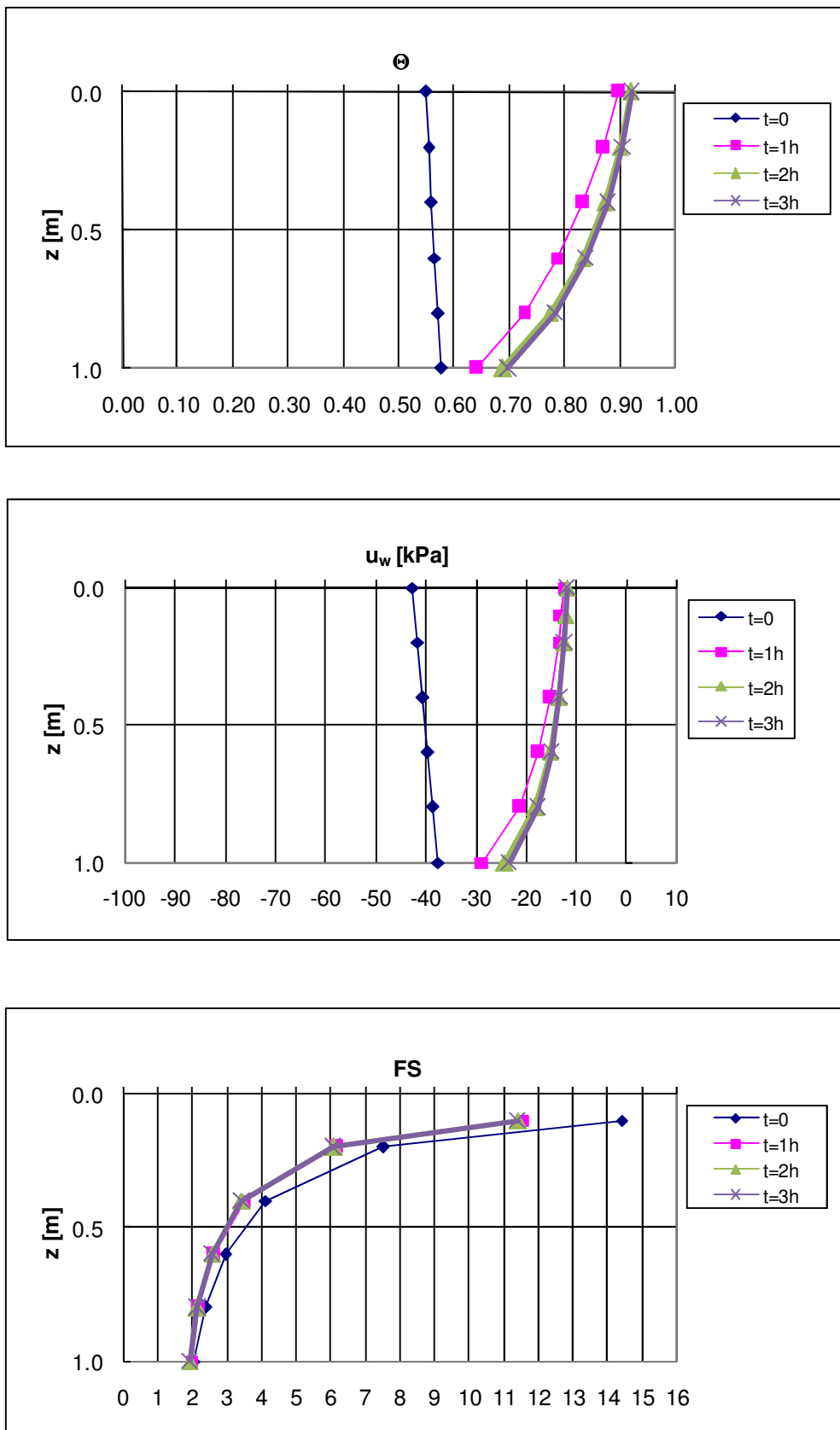


Fig. C4: $(u_a - u_w)_0 = 42.49 \text{ kPa}$; $I = 19.44 \text{ mm/h}$

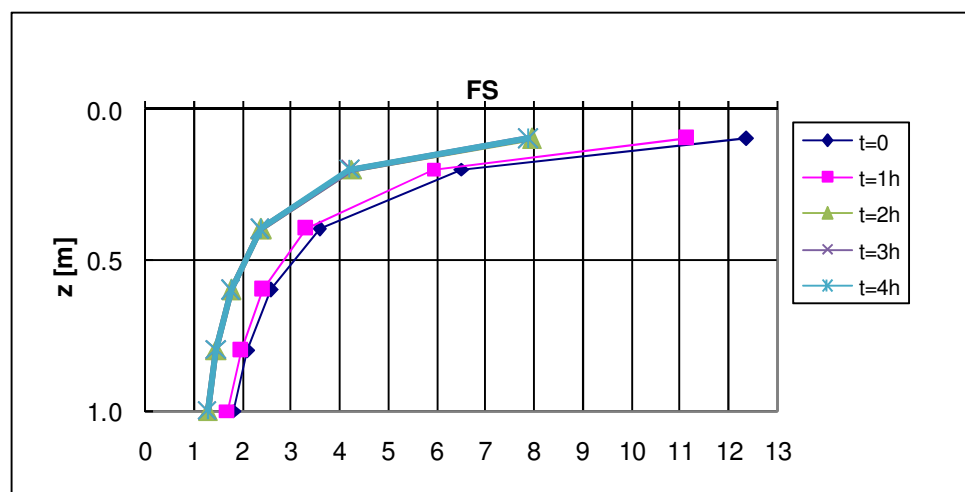
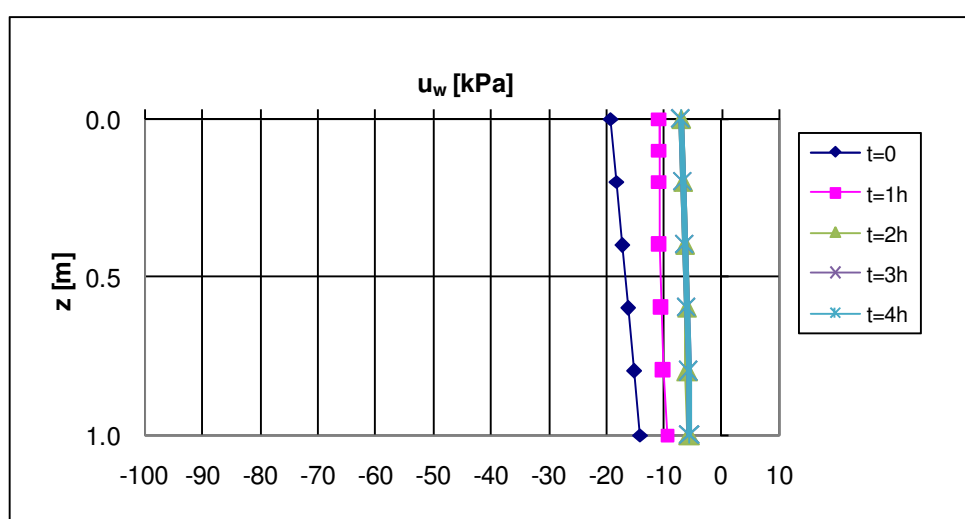
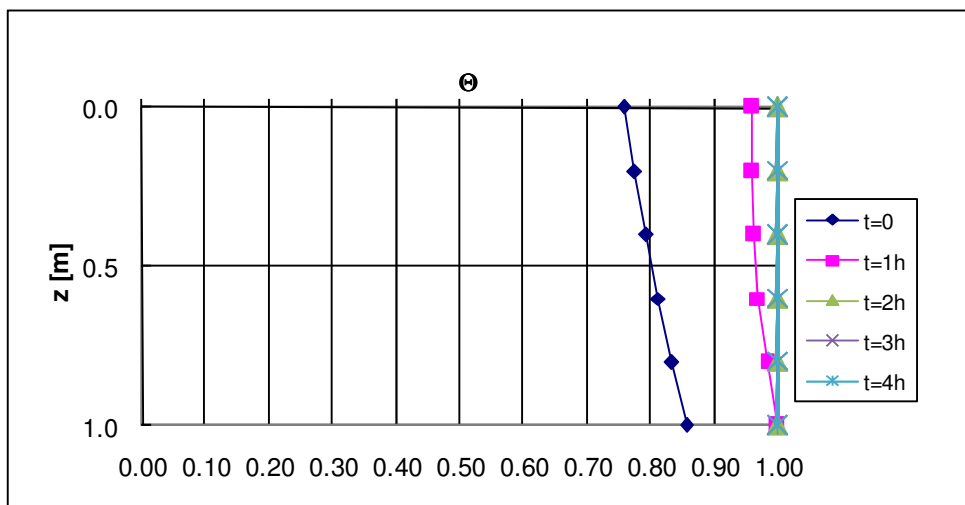


Fig. C5: $(u_a-u_w)_0 = 19 \text{ kPa}; I = 19.44 \text{ mm/h}$



ATTACHMENT D

Hypothesis 2

Slope angle $\beta = 45^\circ$
Soil nr.1

Case a

Thickness $h = 0.5$ m
Impervious bottom

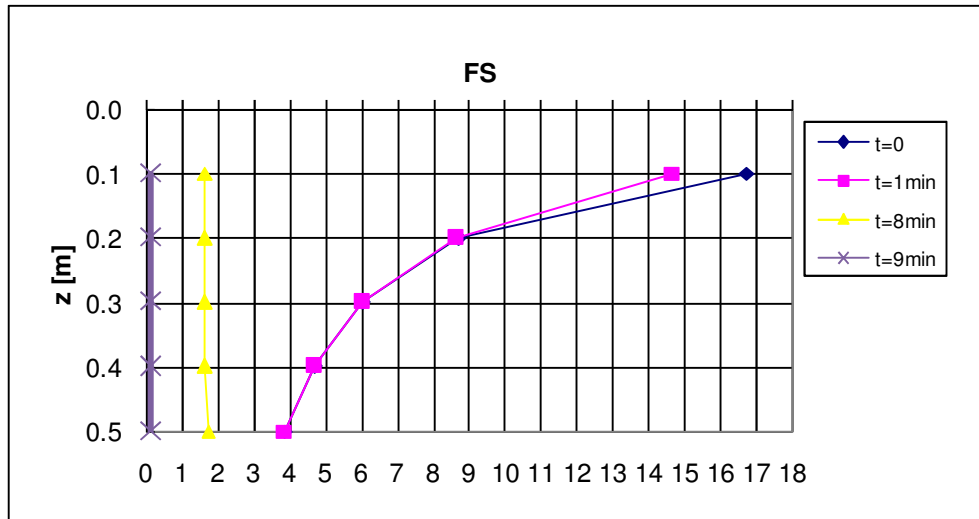
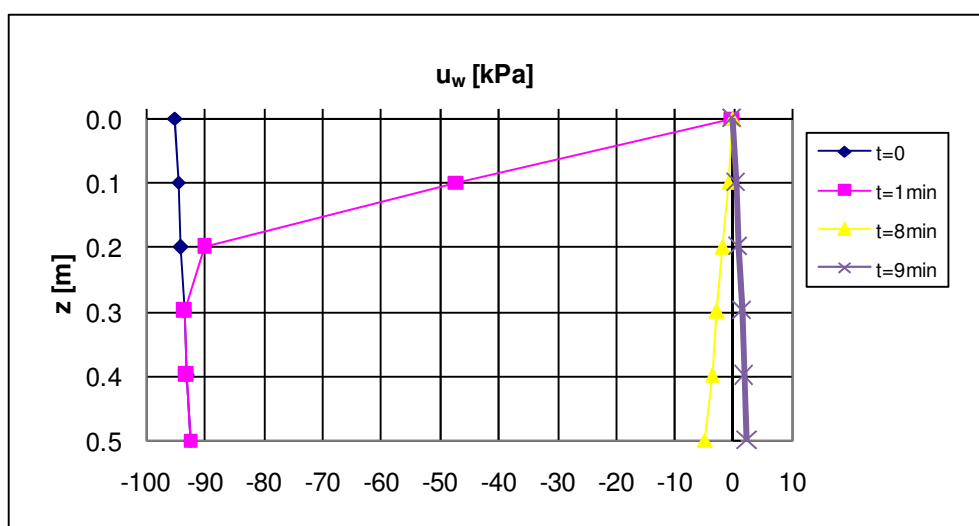
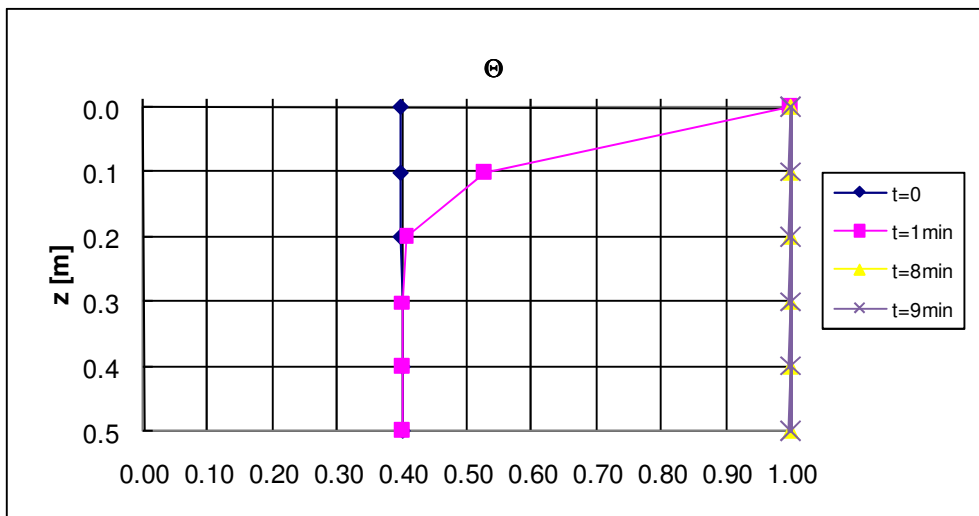


Fig. D1: $(u_a - u_w)_0 = 95$ kPa; $I = 97.20$ mm/h

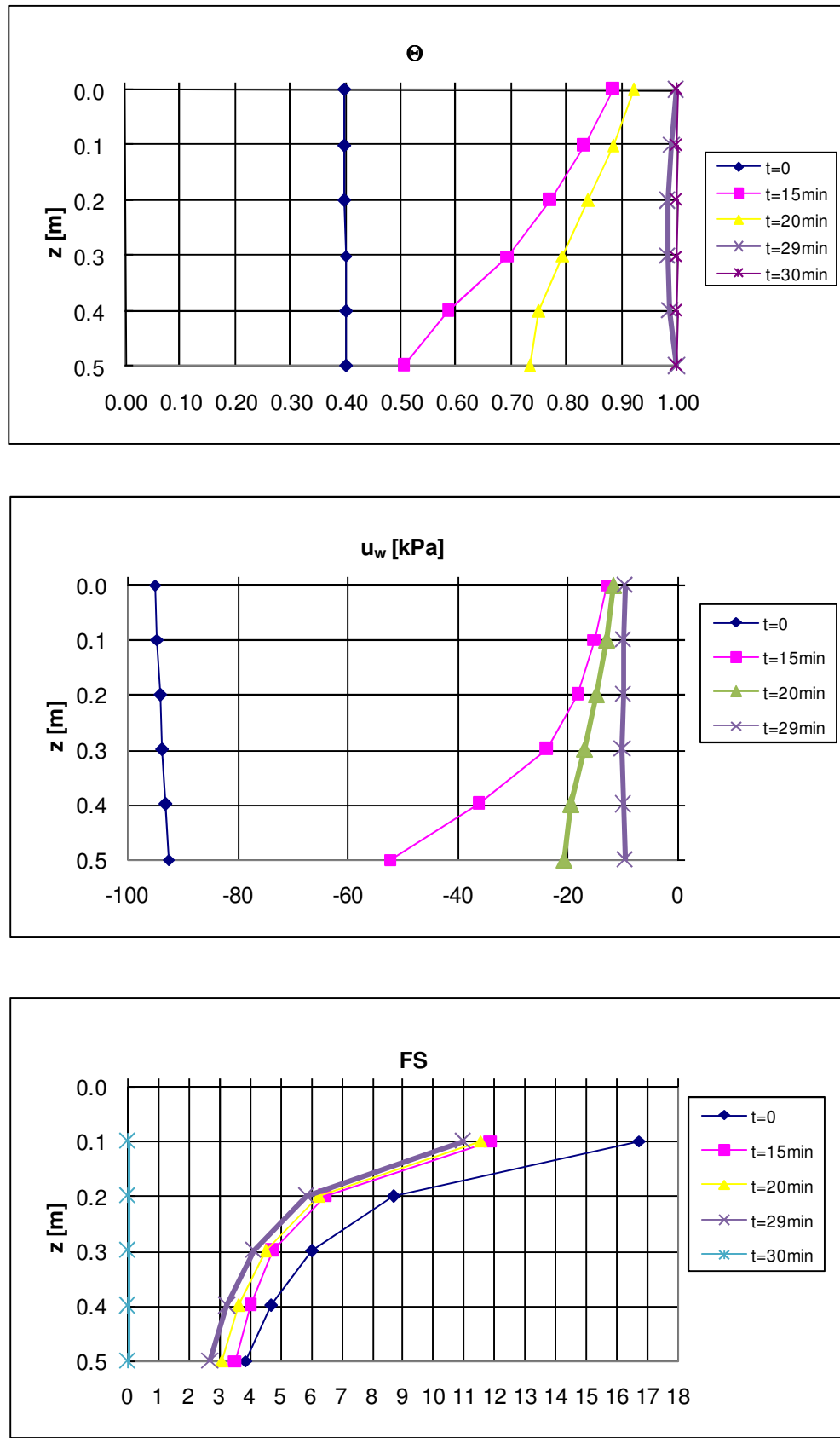


Fig. D2: $(u_a - u_w)_0 = 95 \text{ kPa}$; $I = 19.44 \text{ mm/h}$

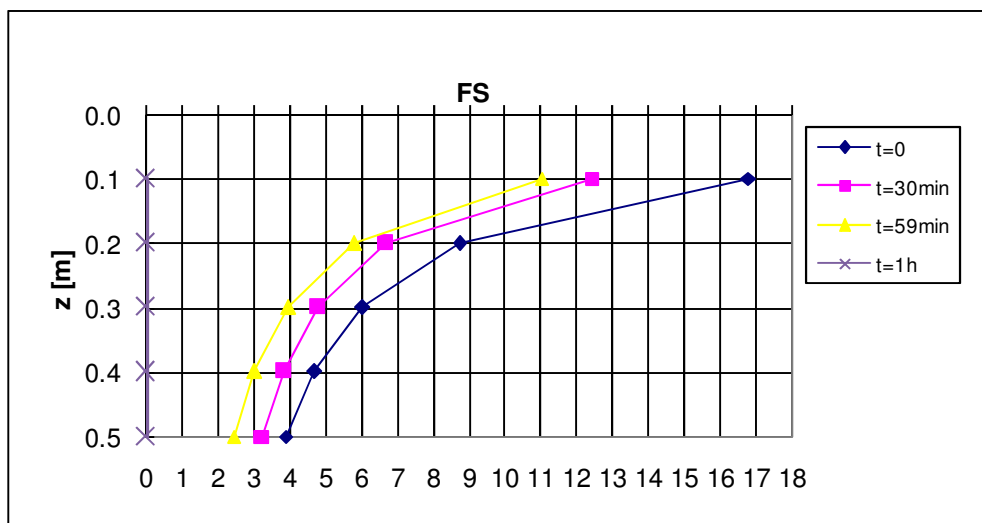
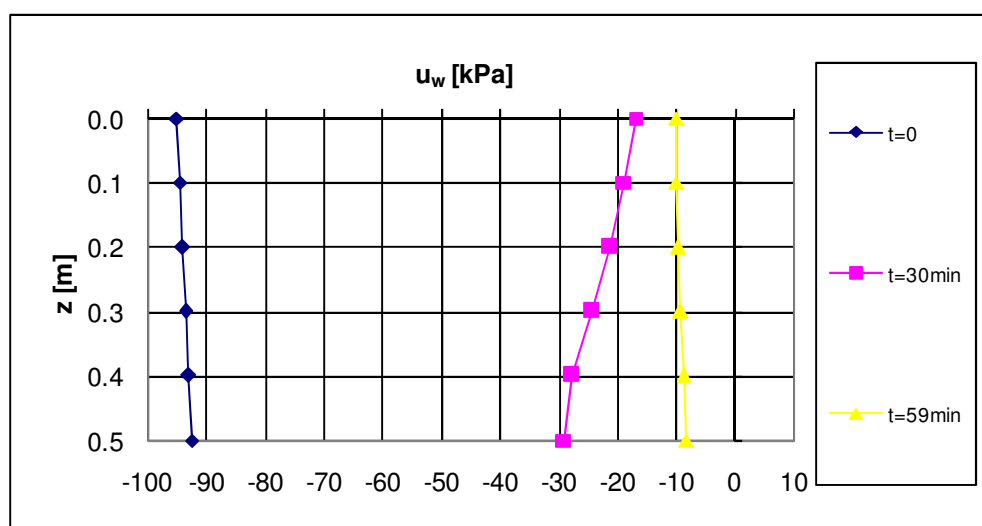
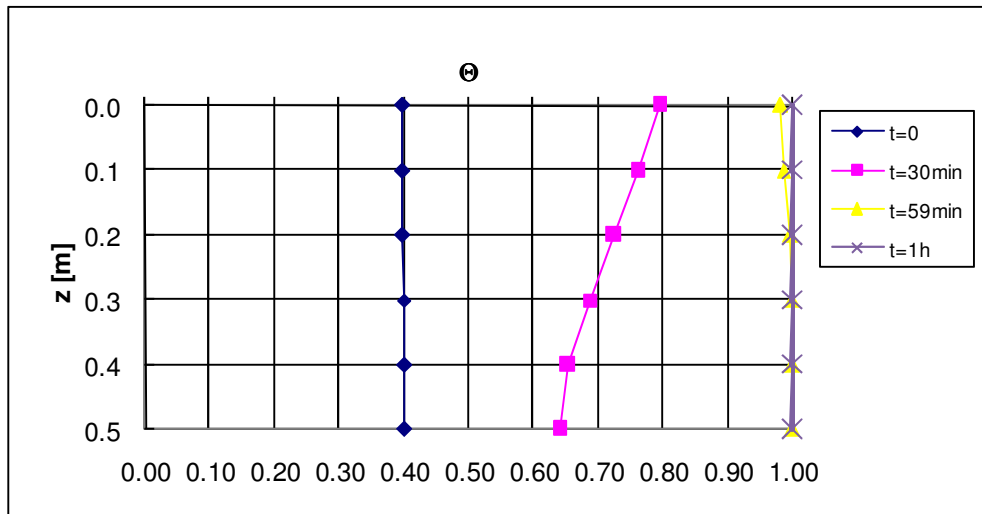


Fig. D3: $(u_a - u_w)_0 = 95$ kPa; $I = 9.72$ mm/h

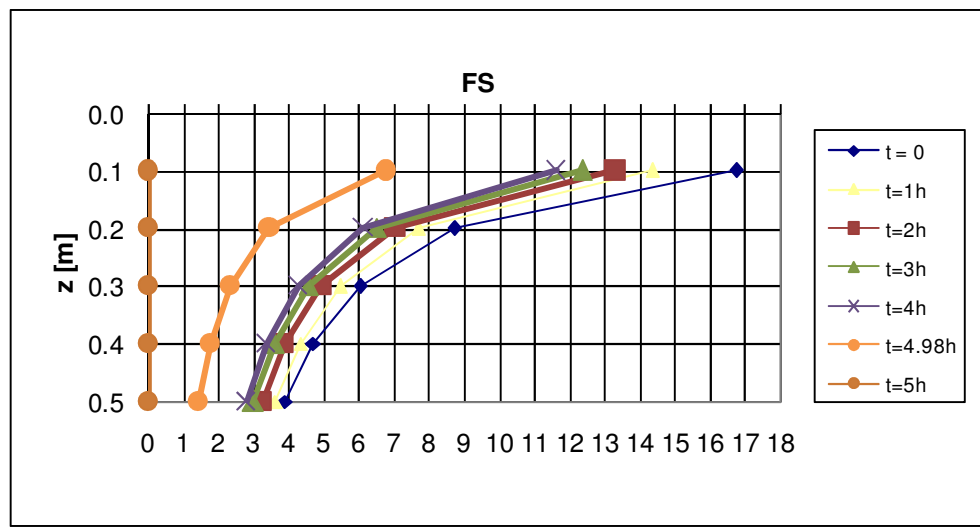
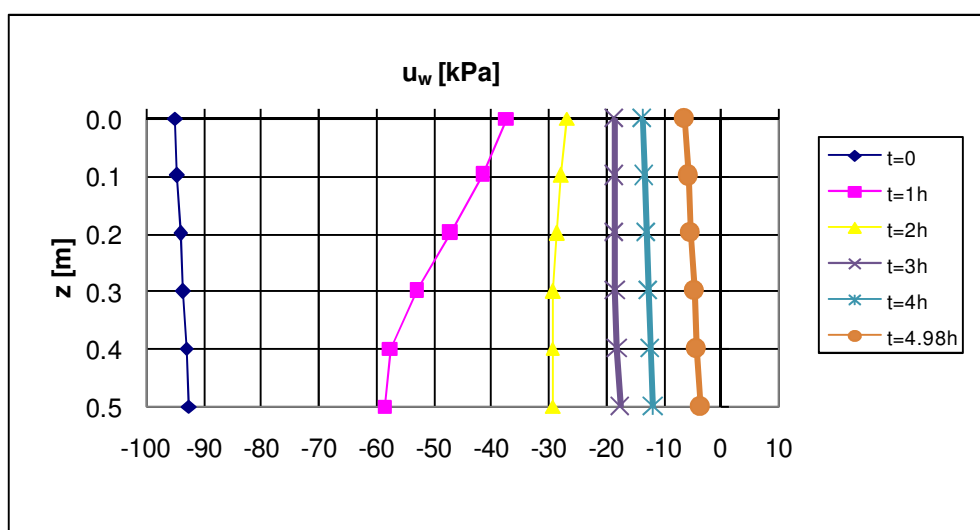
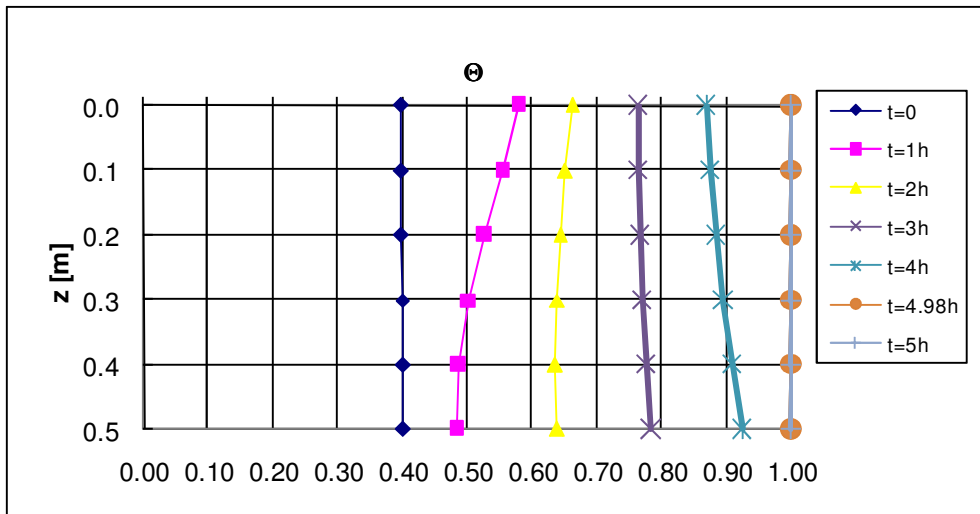


Fig. D4: $(u_a - u_w)_0 = 95 \text{ kPa}; l = 1.94 \text{ mm/h}$

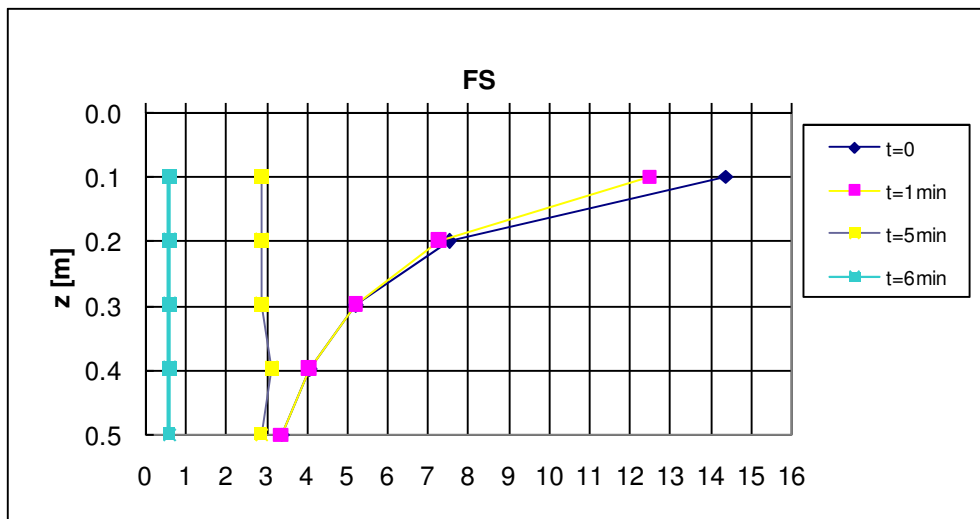
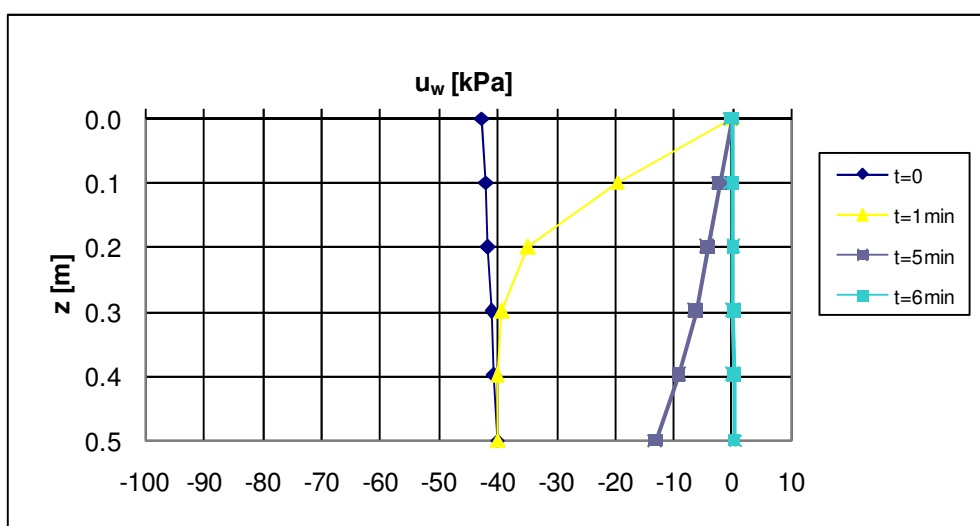
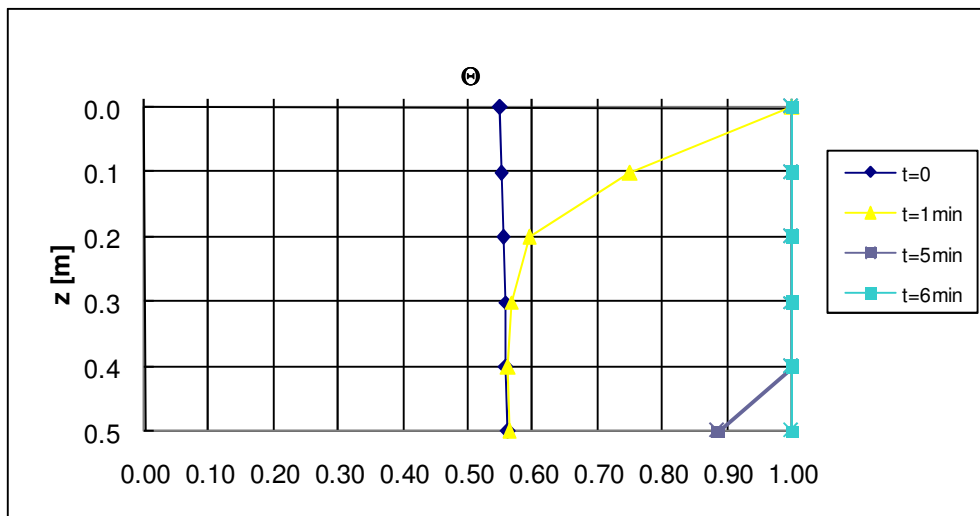


Fig. D5: $(u_a - u_w)_0 = 42.49 \text{ kPa}$; $I = 97.20 \text{ mm/h}$

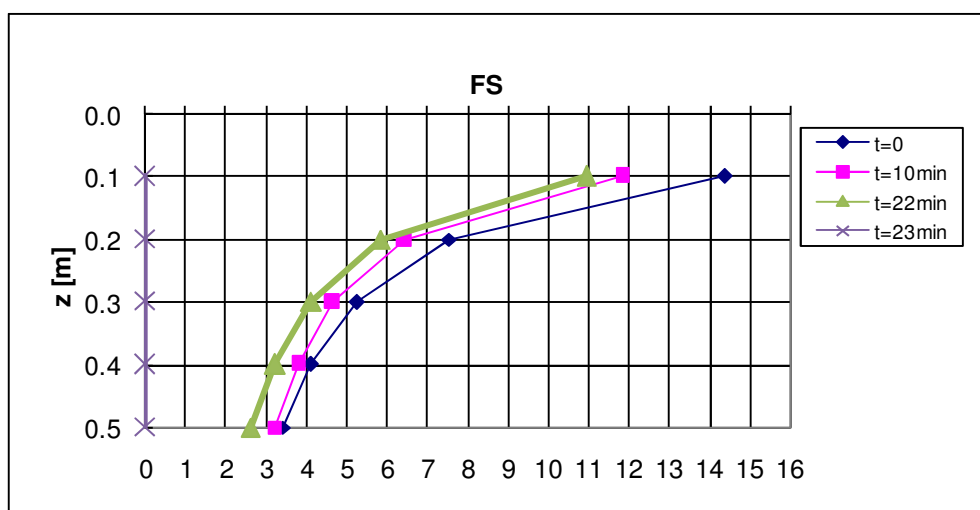
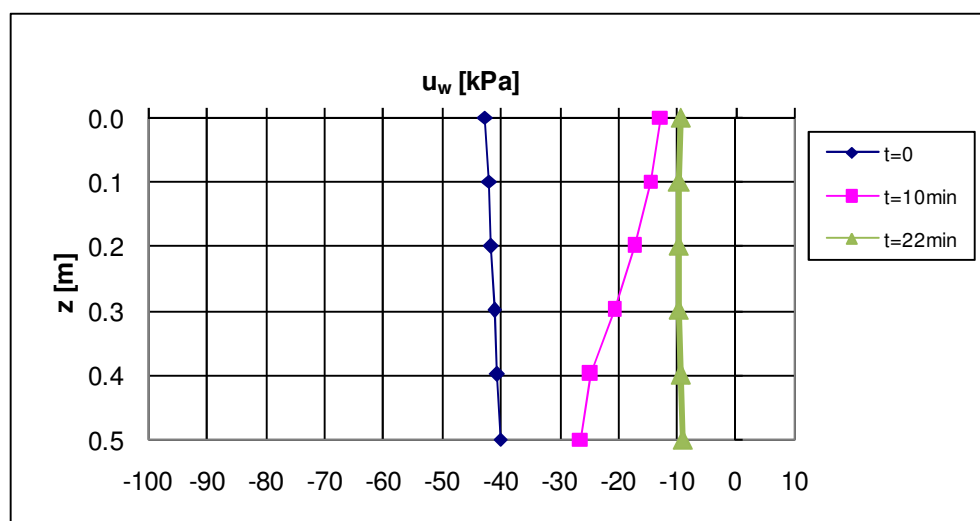
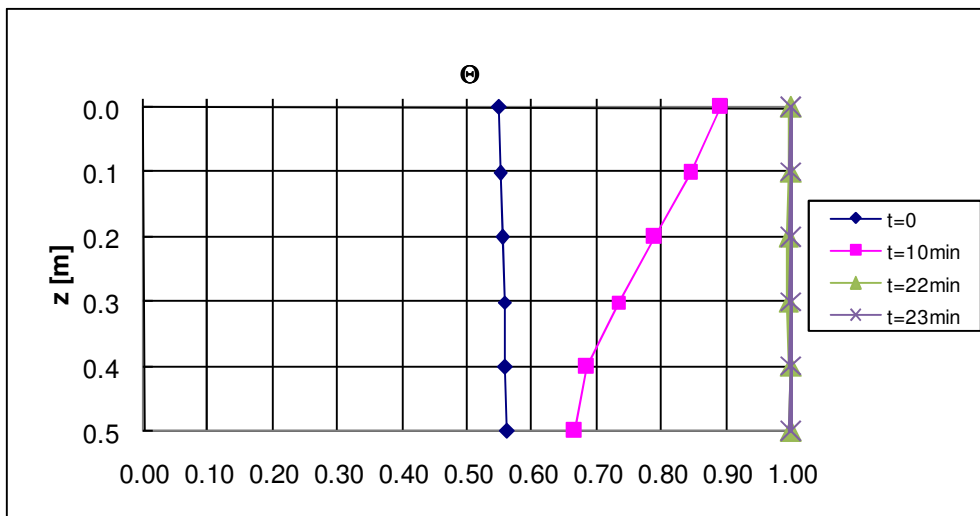


Fig. D6: $(u_a - u_w)_0 = 42.49 \text{ kPa}$; $I = 19.44 \text{ mm/h}$

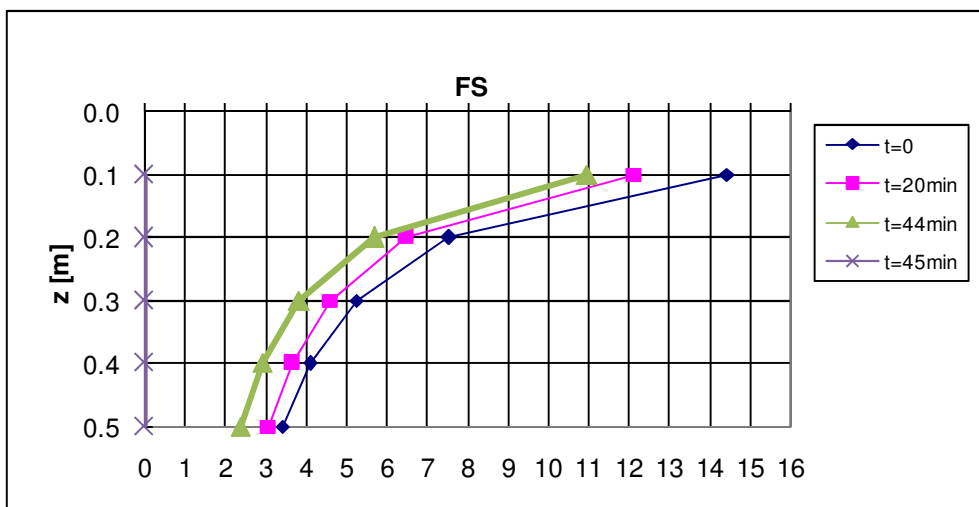
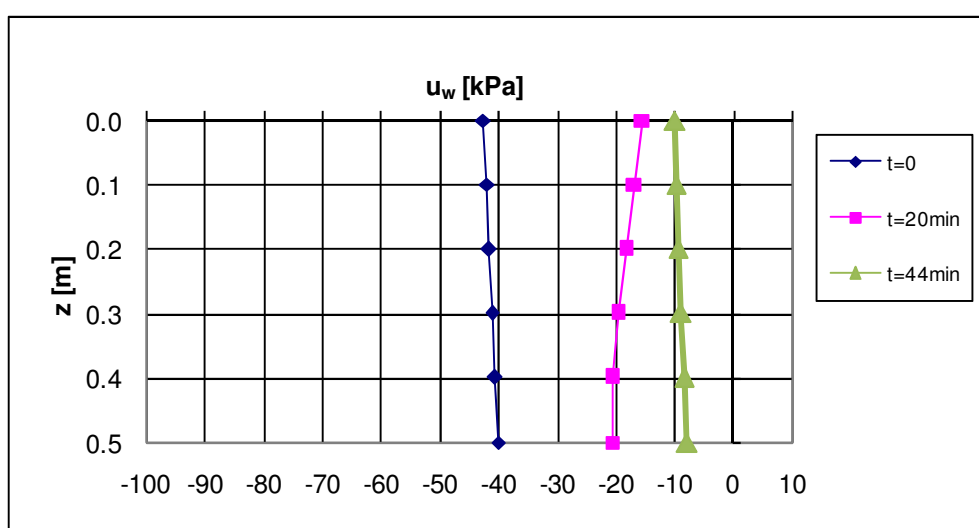
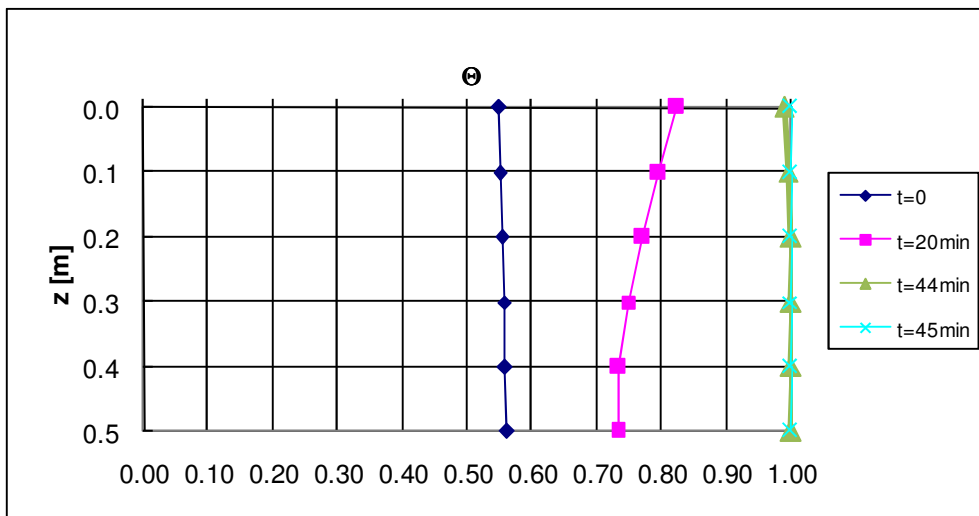


Fig. D7: $(u_a - u_w)_0 = 42.49 \text{ kPa}$; $I = 9.72 \text{ mm/h}$

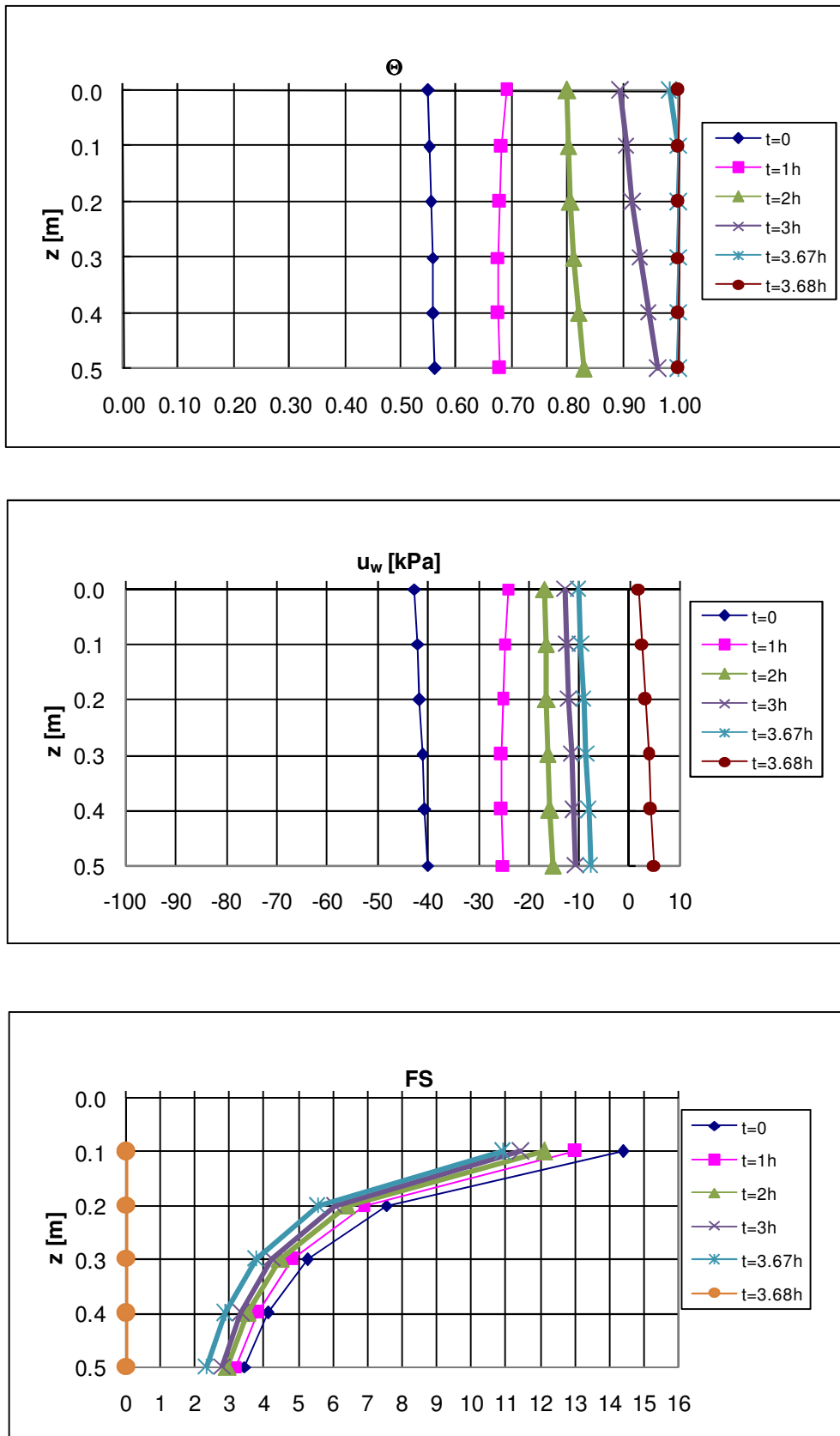


Fig. D8: $(u_a-u_w)_0 = 42.49 \text{ kPa}$; $I = 1.94 \text{ mm/h}$

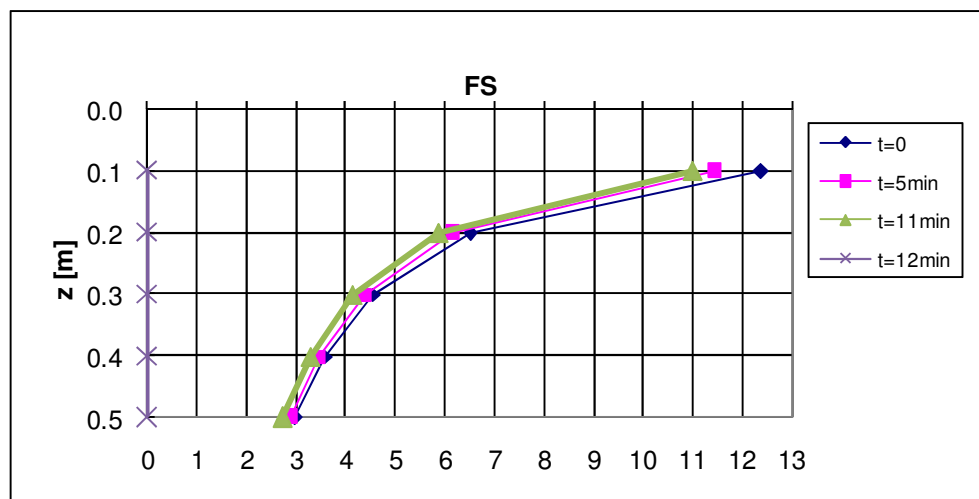
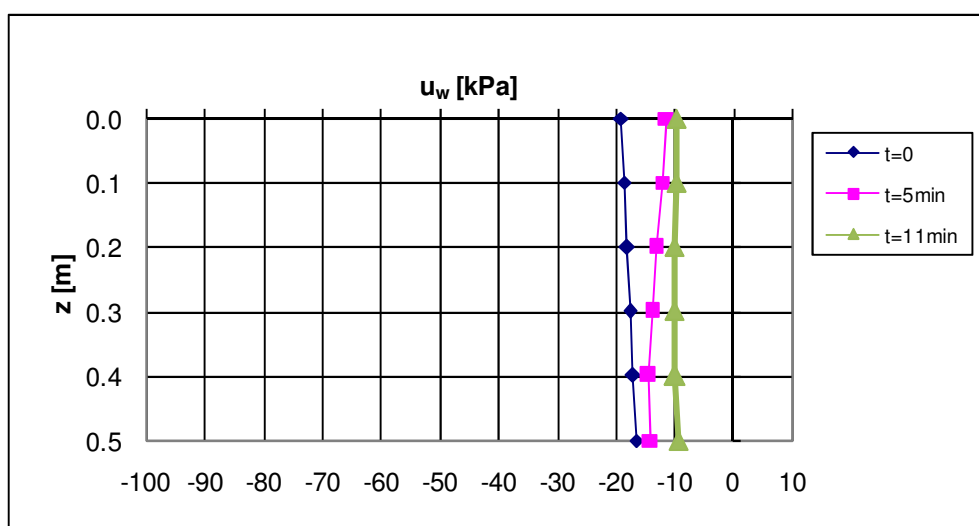
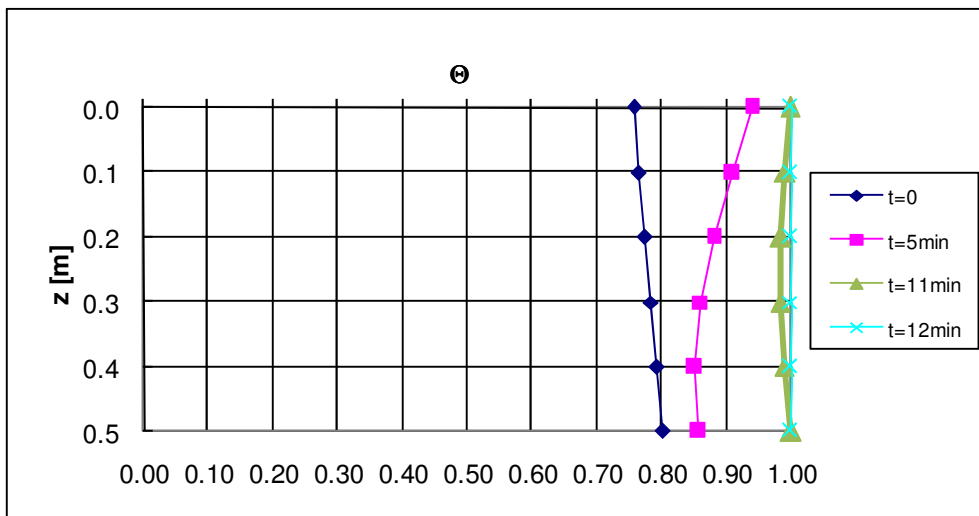


Fig. D9: $(u_a-u_w)_0 = 19 \text{ kPa}; I = 19.44 \text{ mm/h}$

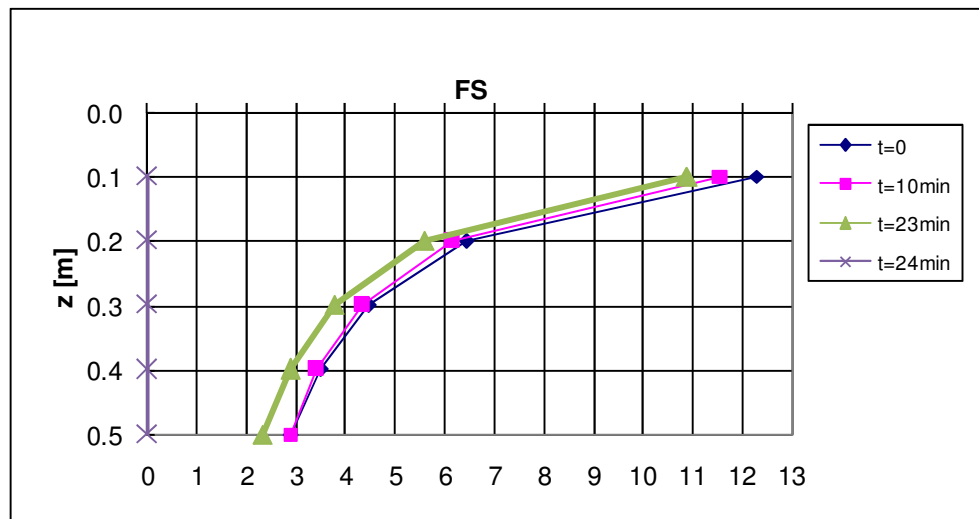
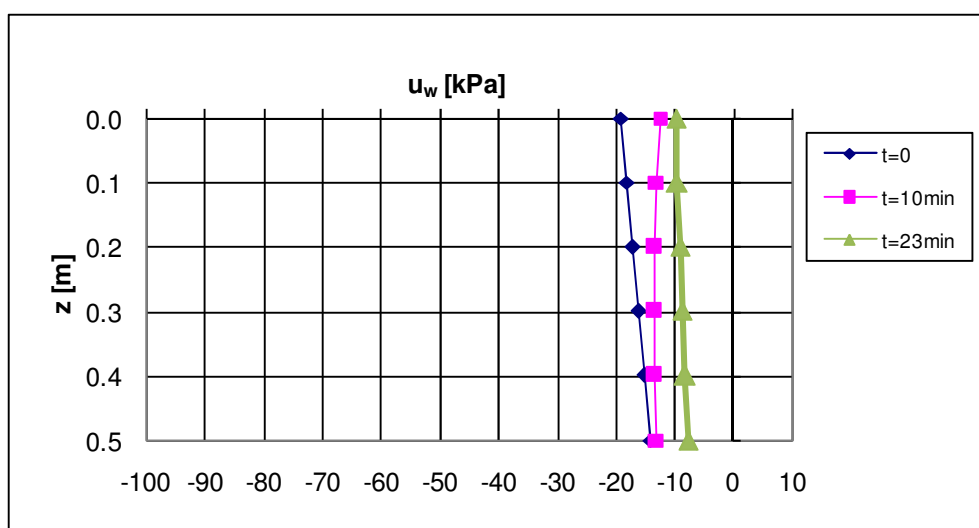
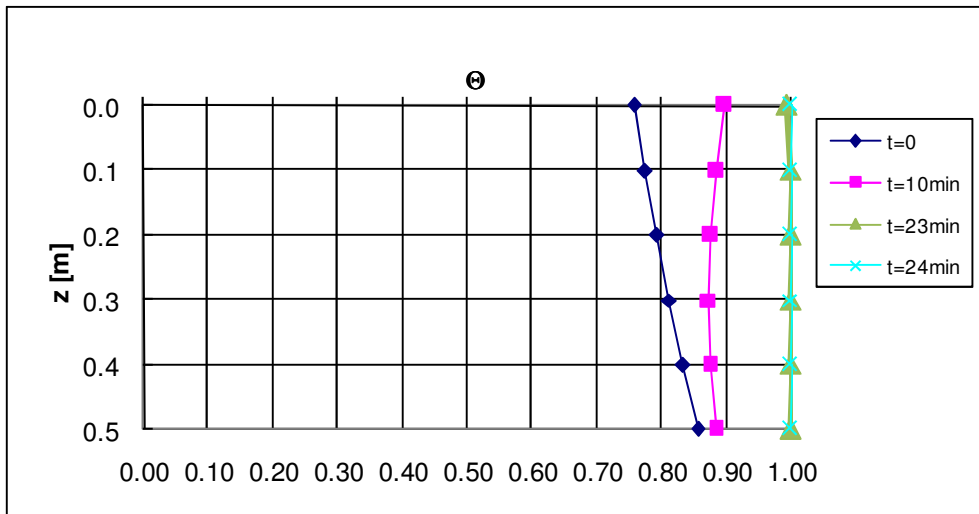


Fig. D10: $(u_a - u_w)_0 = 19 \text{ kPa}$; $I = 9.72 \text{ mm/h}$

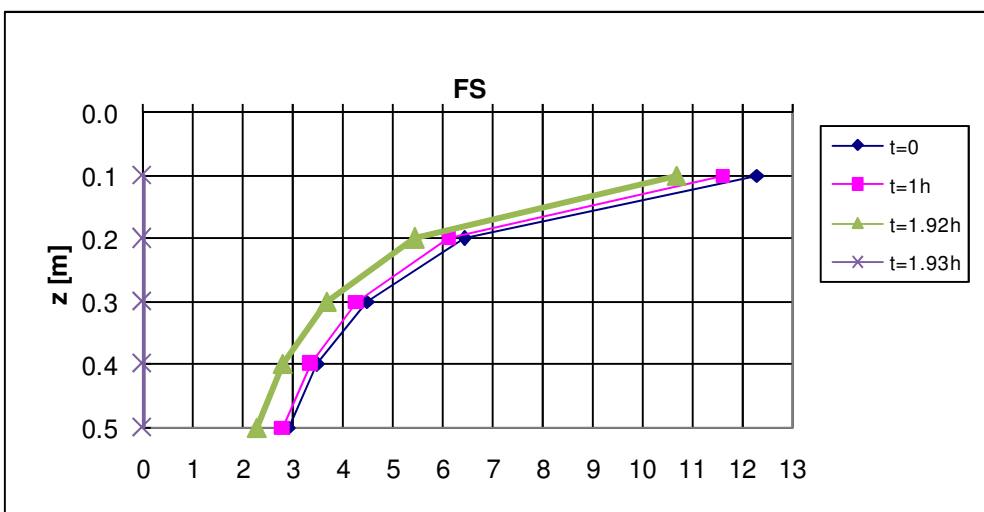
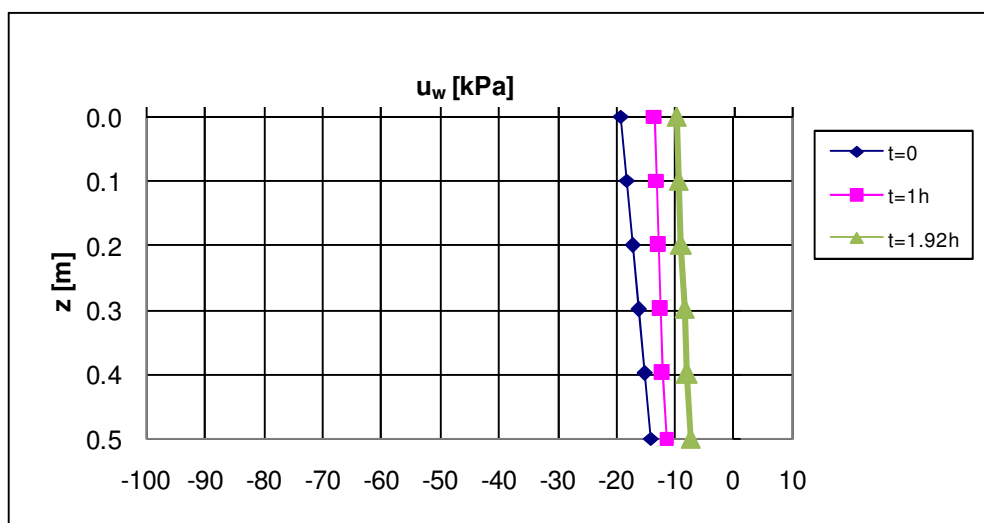
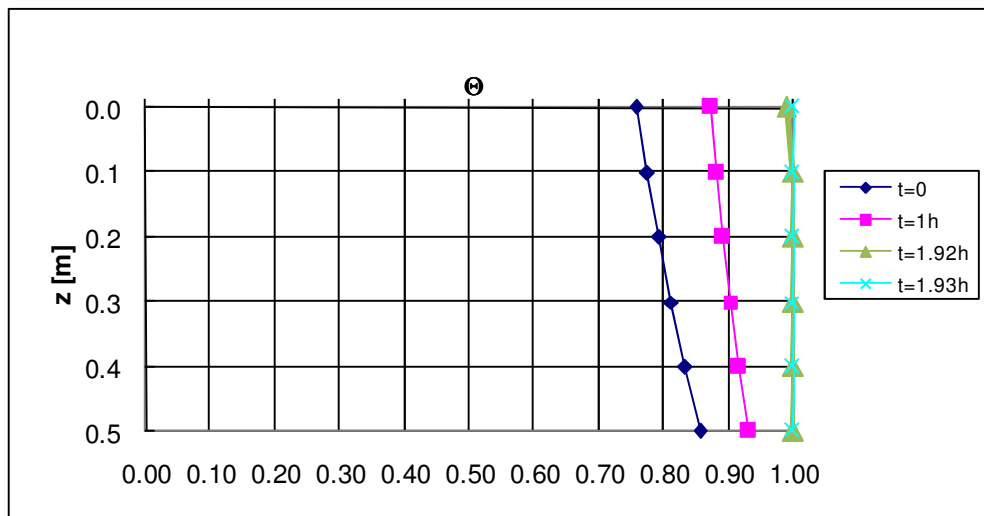


Fig. D11: $(u_a-u_w)_0 = 19 \text{ kPa}$; $I = 1.94 \text{ mm/h}$

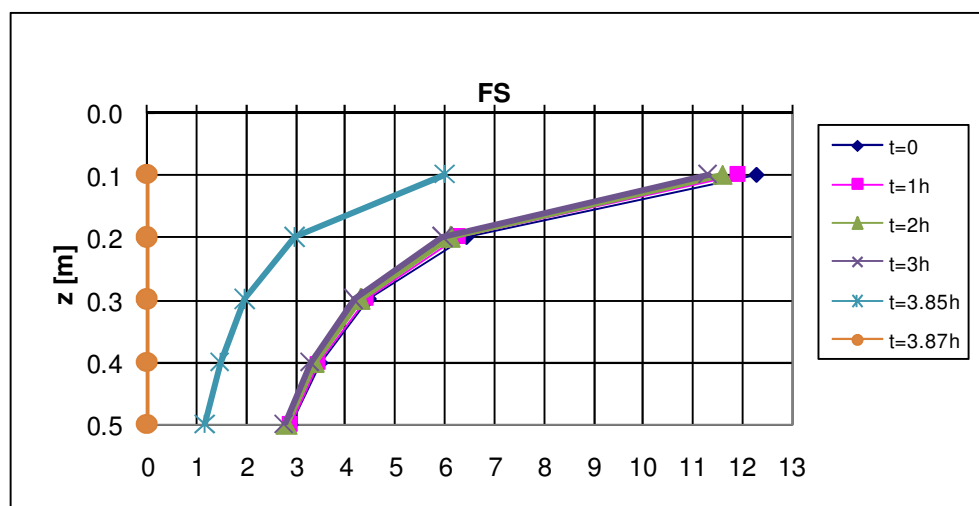
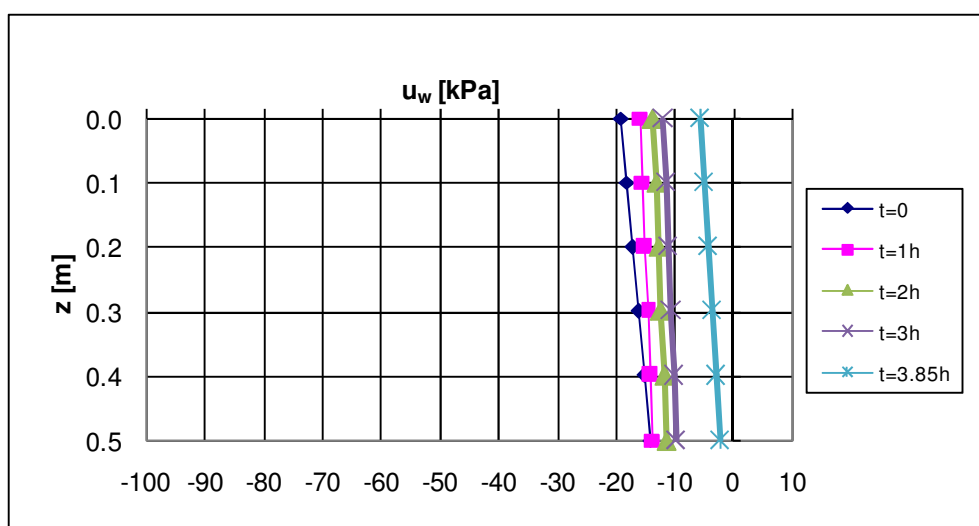
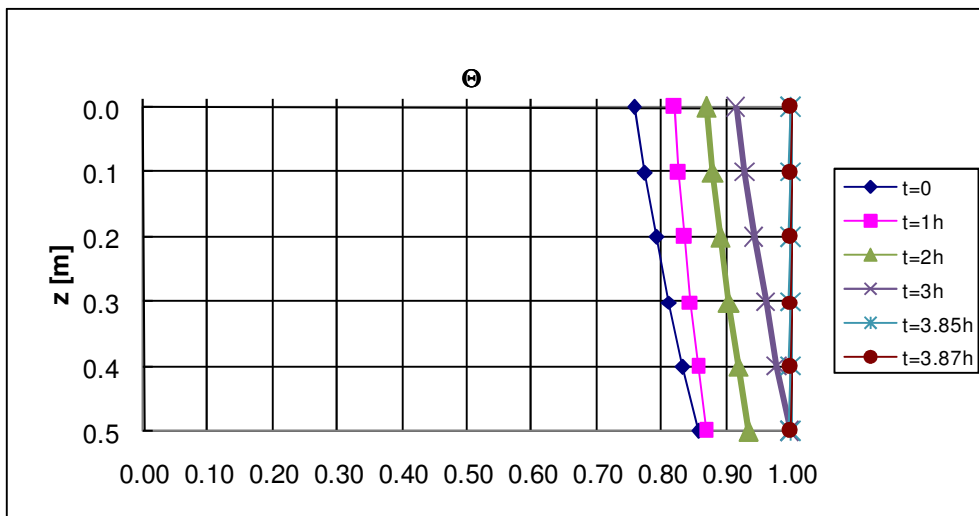


Fig. D12: $(u_a-u_w)_0 = 19 \text{ kPa}$; $I = 0.97 \text{ mm/h}$



ATTACHMENT E

Hypothesis 2

Slope angle $\beta = 30^\circ$
Soil nr.1

Case a

Thickness $h = 2$ m
Impervious bottom

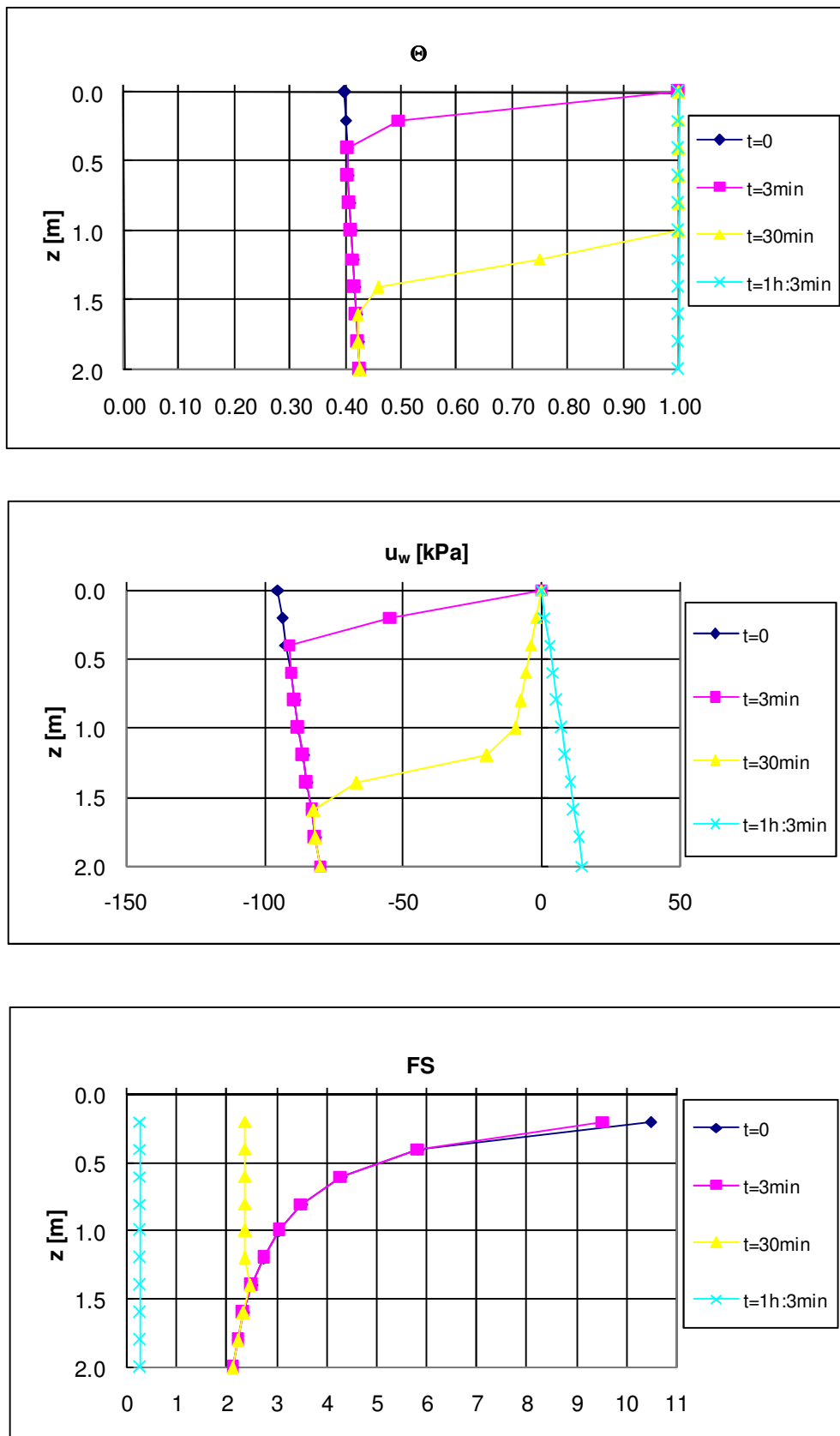


Fig. E1: $(u_a - u_w)_0 = 95 \text{ kPa}$; $I = 97.20 \text{ mm/h}$

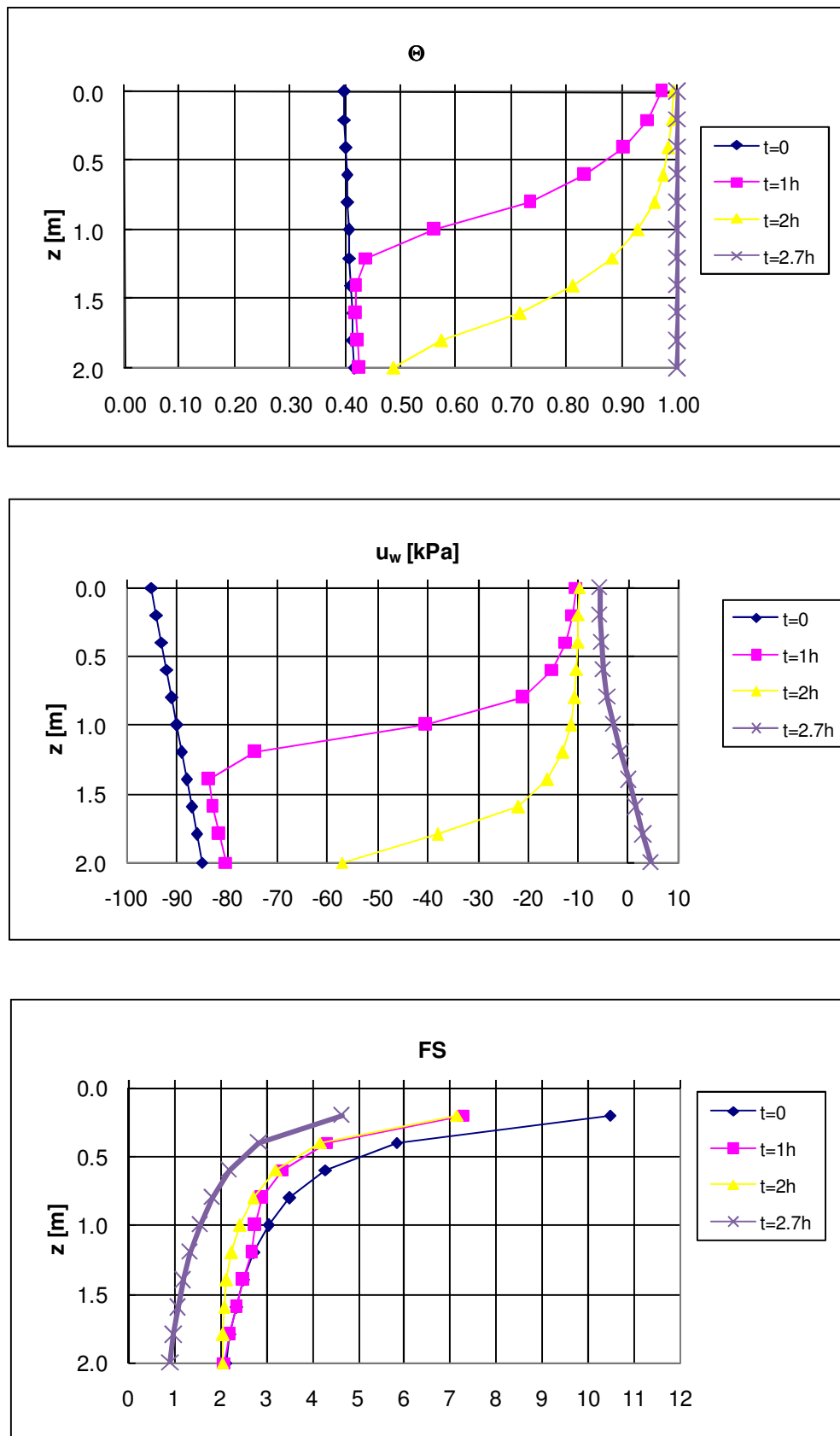


Fig. E2: $(u_a - u_w)_0 = 95 \text{ kPa}; I = 19.44 \text{ mm/h}$

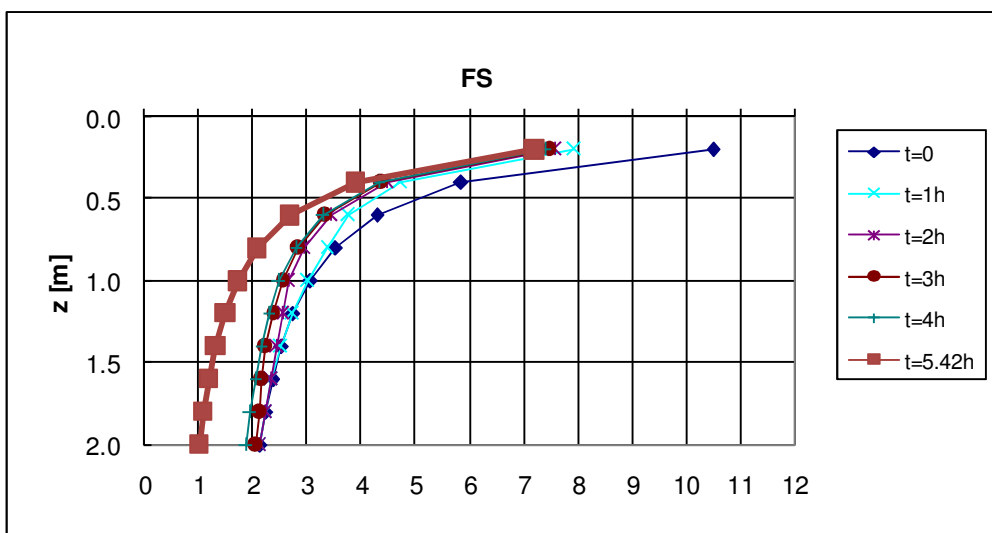
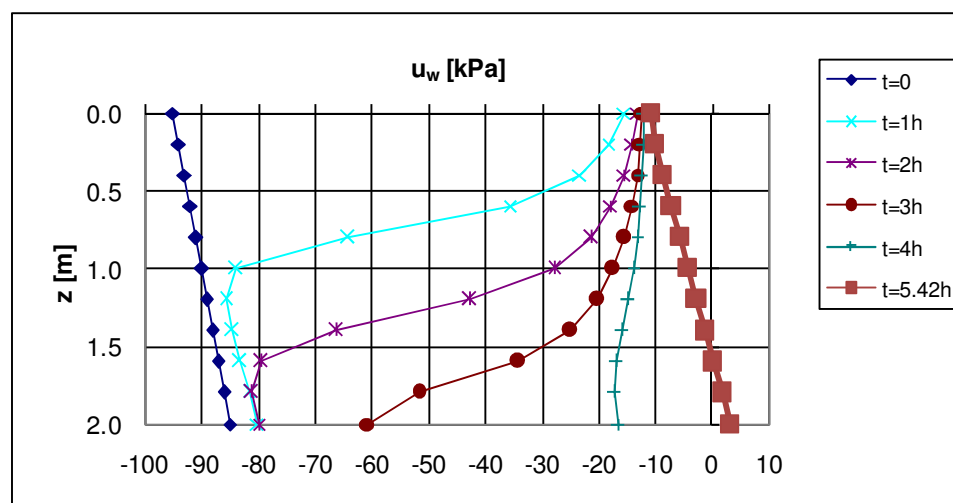
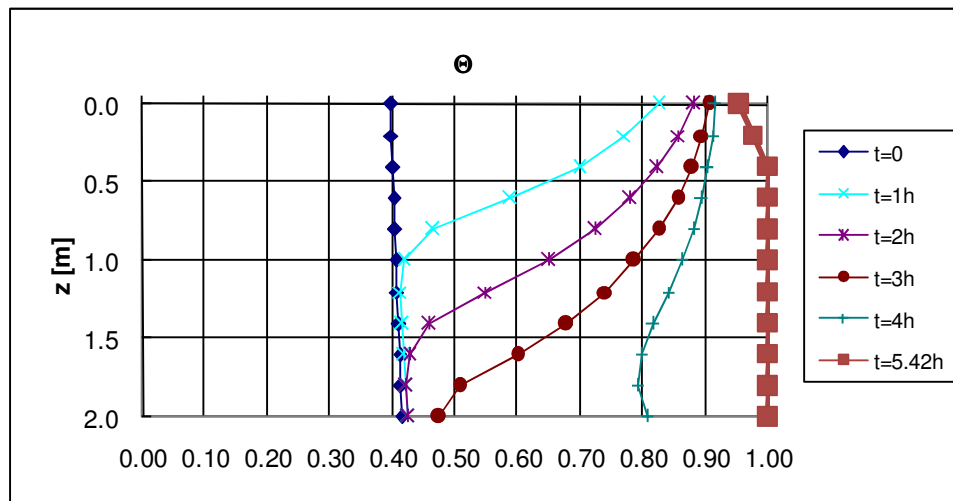


Fig. E3: $(u_a - u_w)_0 = 95 \text{ kPa}$; $I = 9.72 \text{ mm/h}$

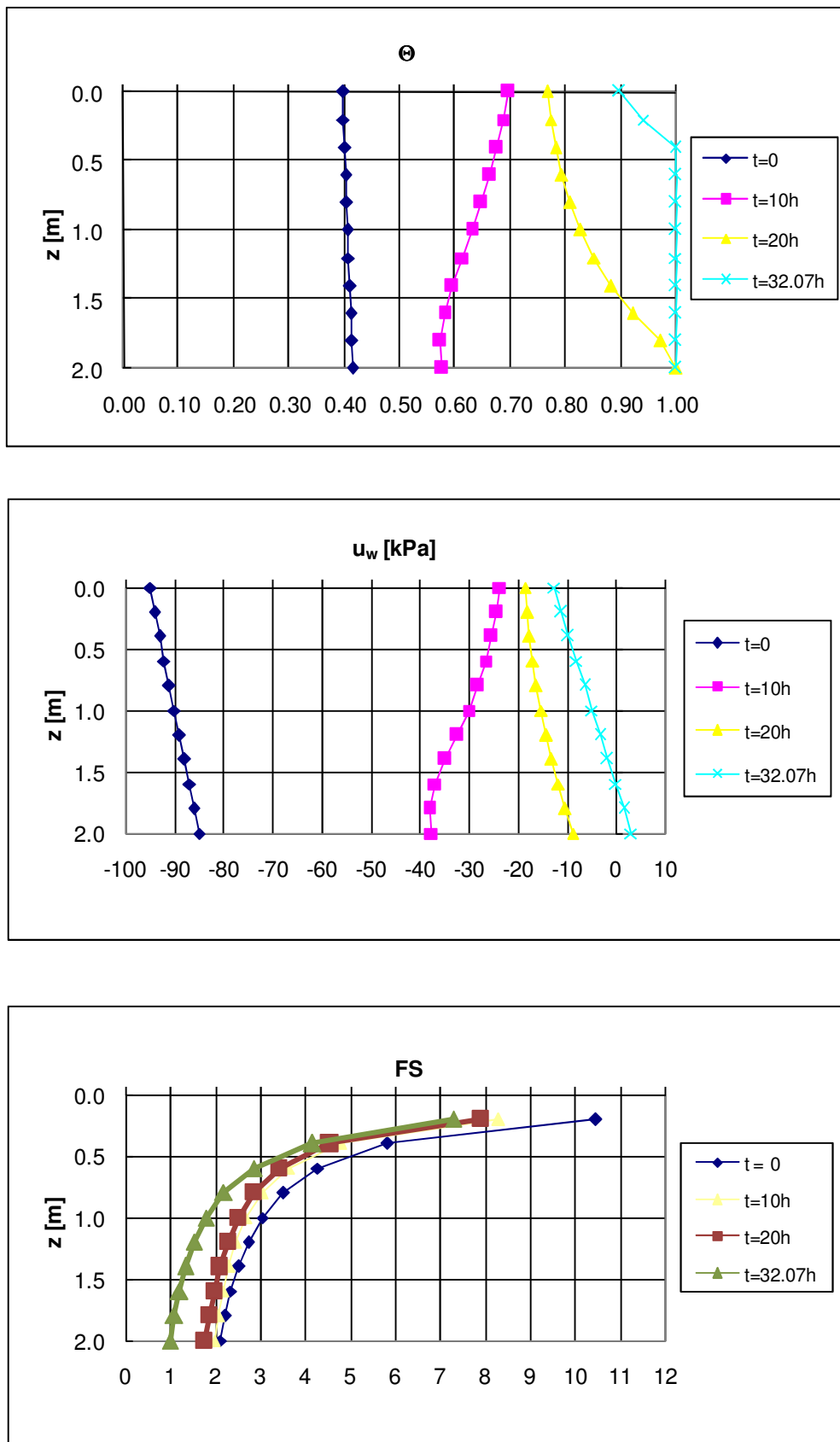


Fig. E4: $(u_a - u_w)_0 = 95 \text{ kPa}$; $I = 1.94 \text{ mm/h}$

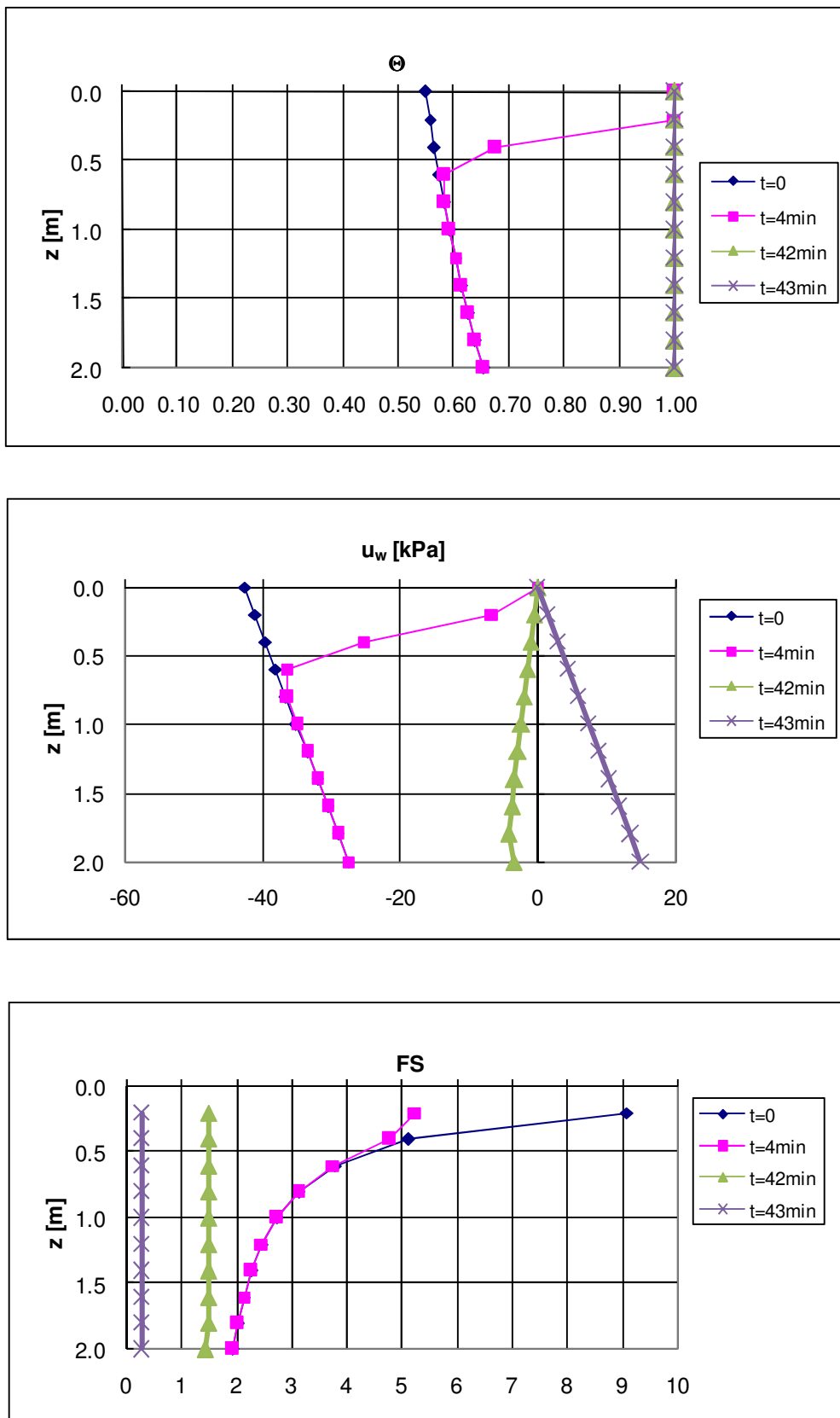


Fig. E5: $(u_a - u_w)_0 = 42.49 \text{ kPa}$; $I = 97.20 \text{ mm/h}$

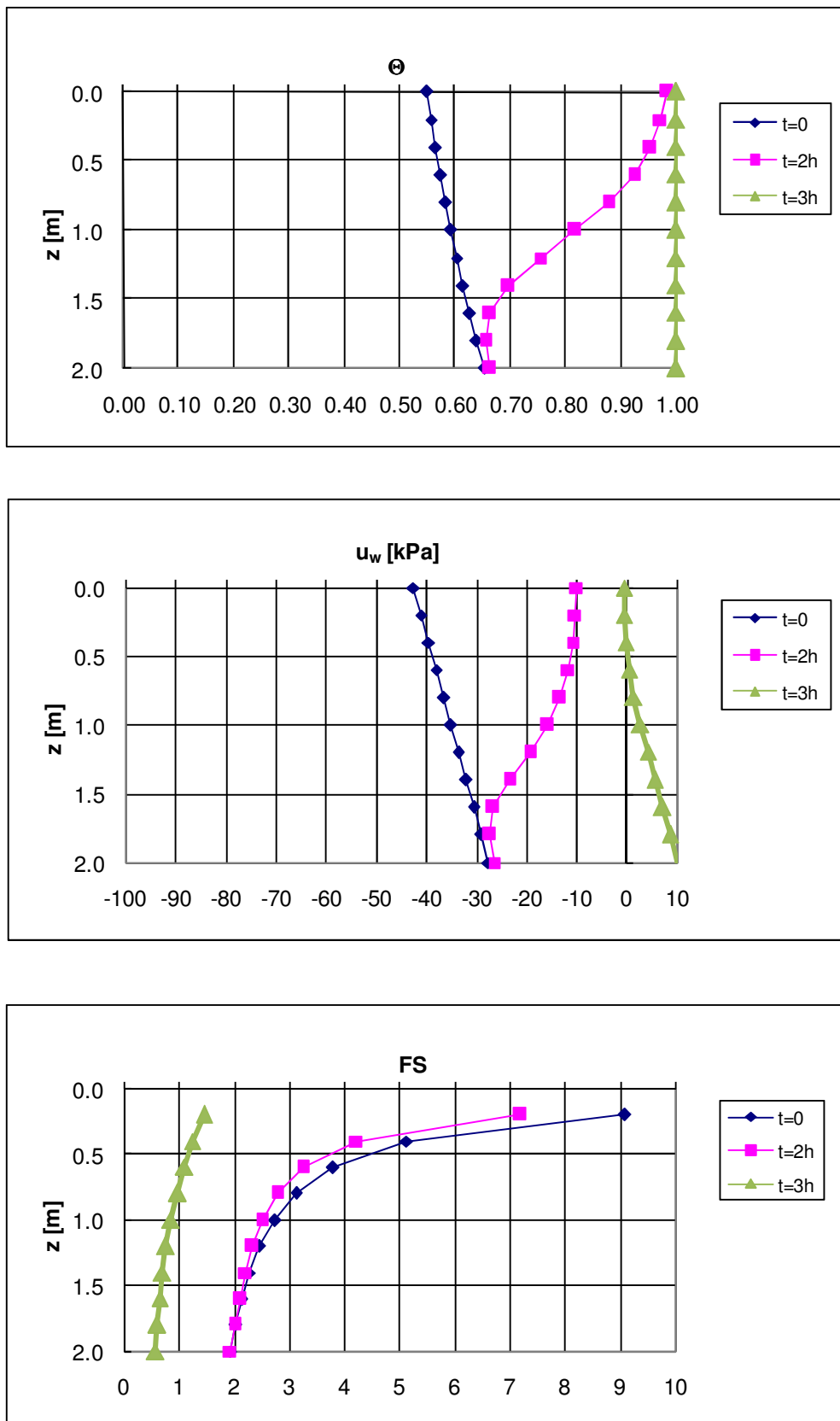


Fig. E6: $(u_a - u_w)_0 = 42.49 \text{ kPa}$; $I = 19.44 \text{ mm/h}$

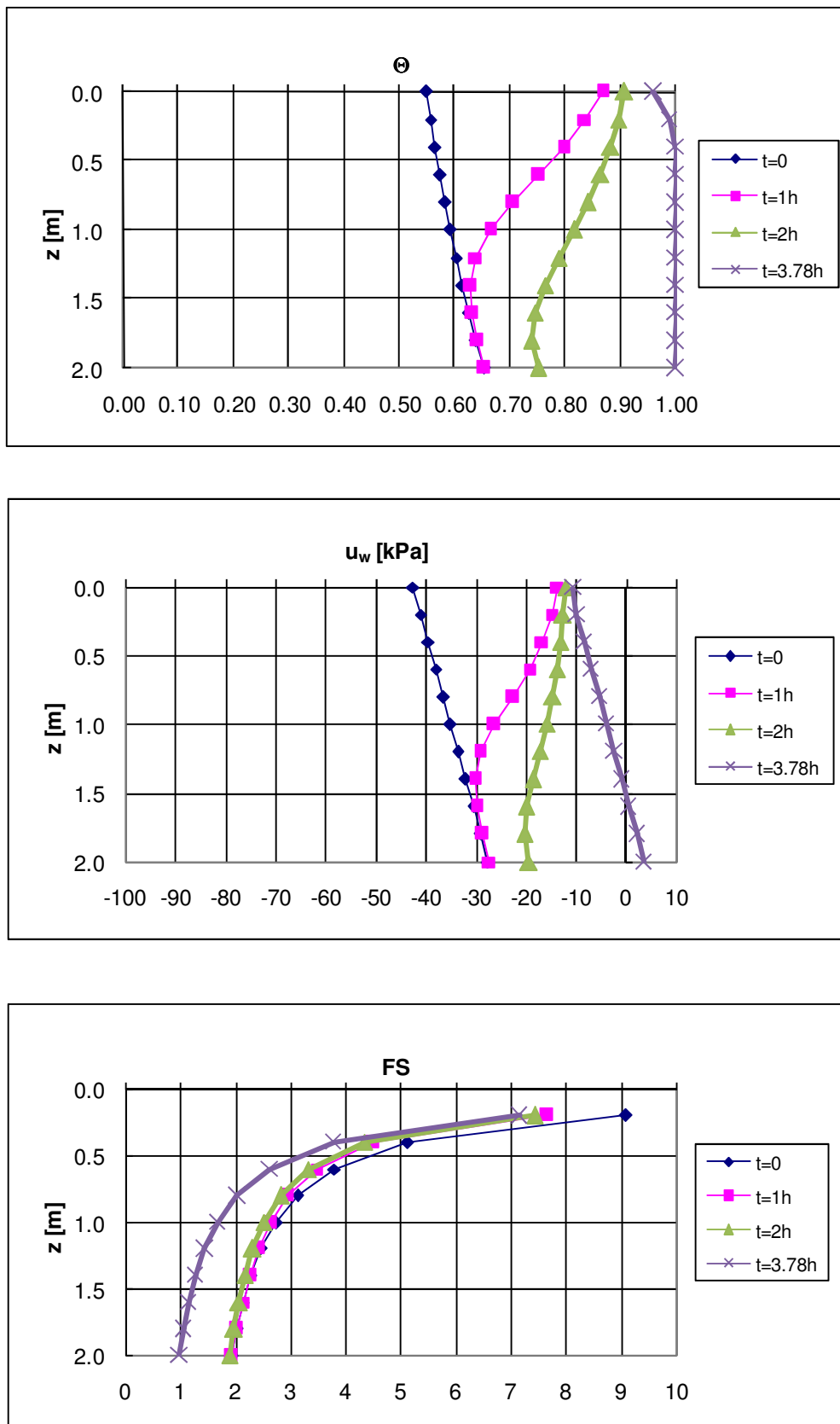


Fig. E7: $(u_a - u_w)_0 = 42.49 \text{ kPa}$; $I = 9.72 \text{ mm/h}$

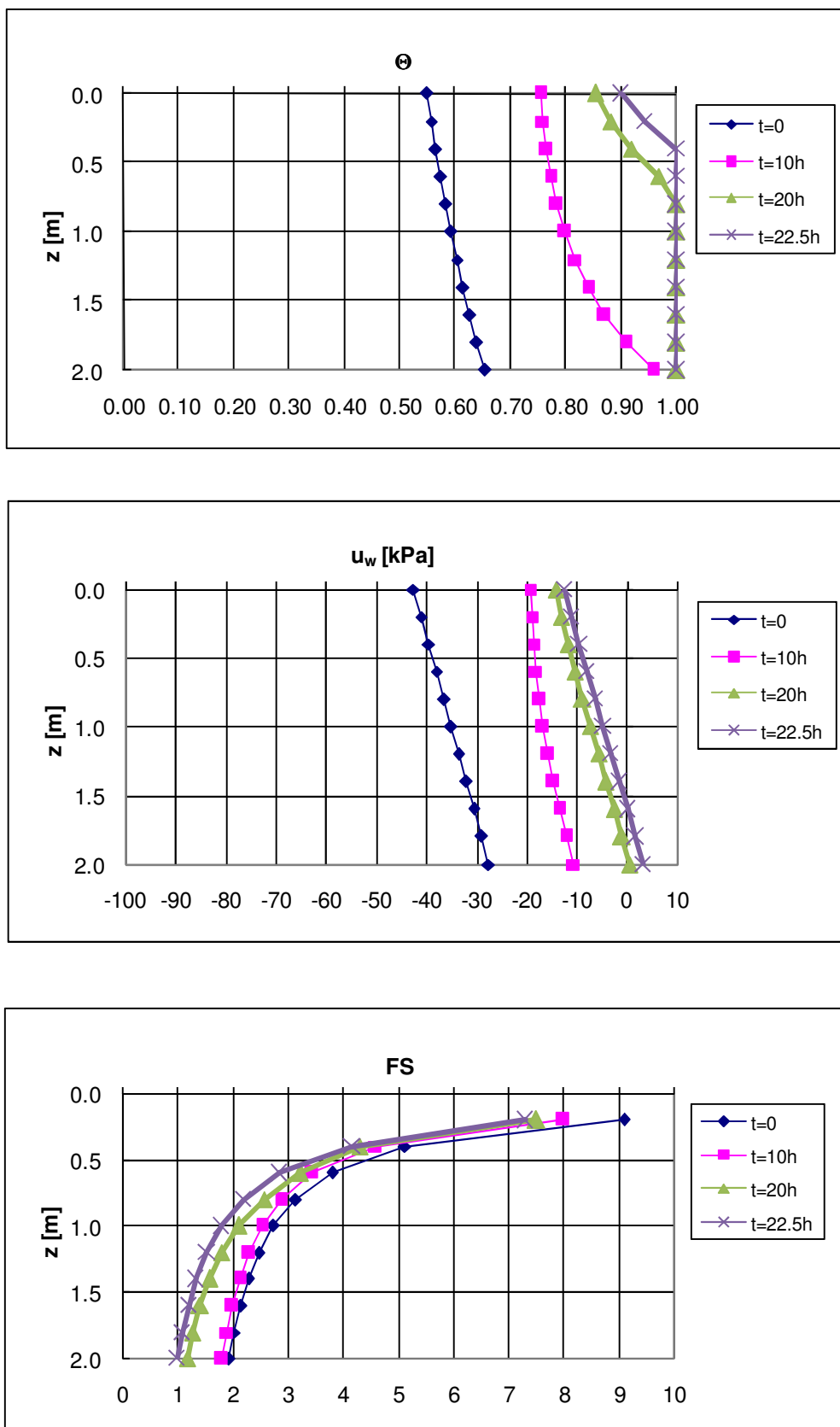


Fig. E8: $(u_a - u_w)_0 = 42.49 \text{ kPa}$; $I = 1.94 \text{ mm/h}$

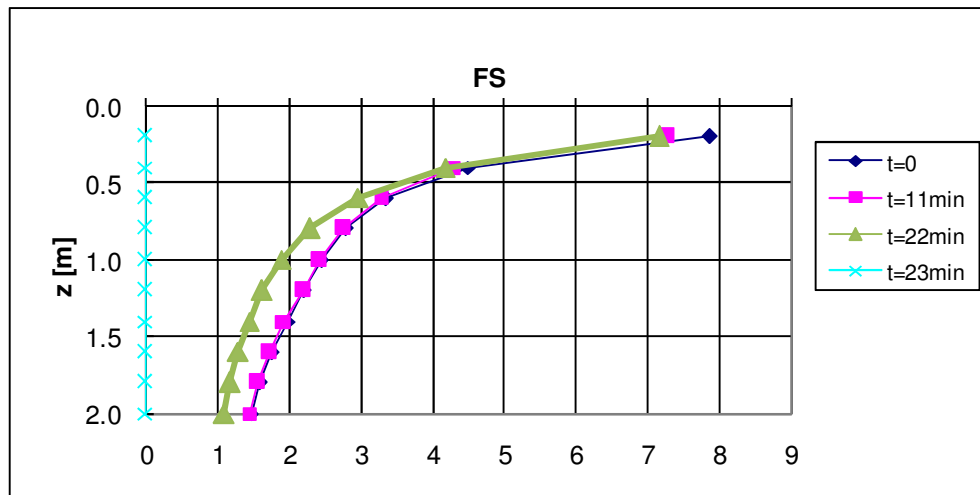
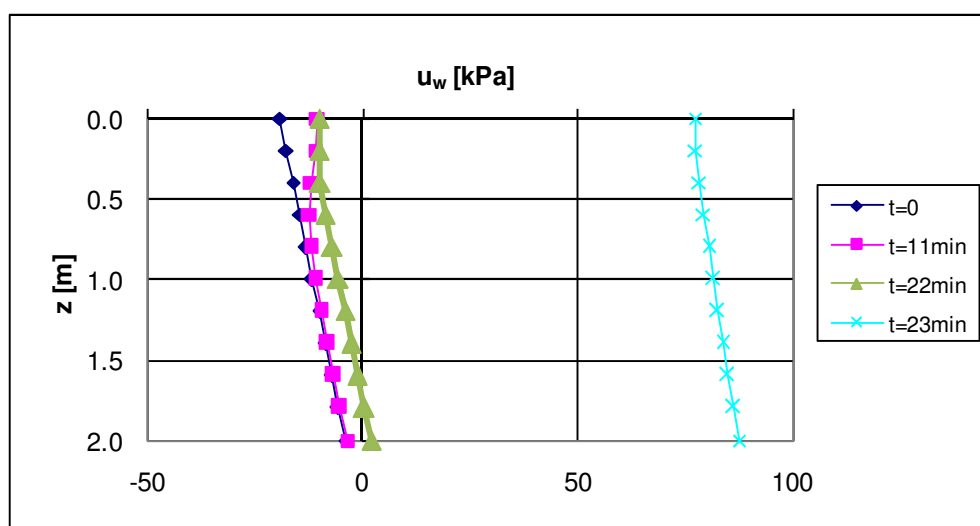
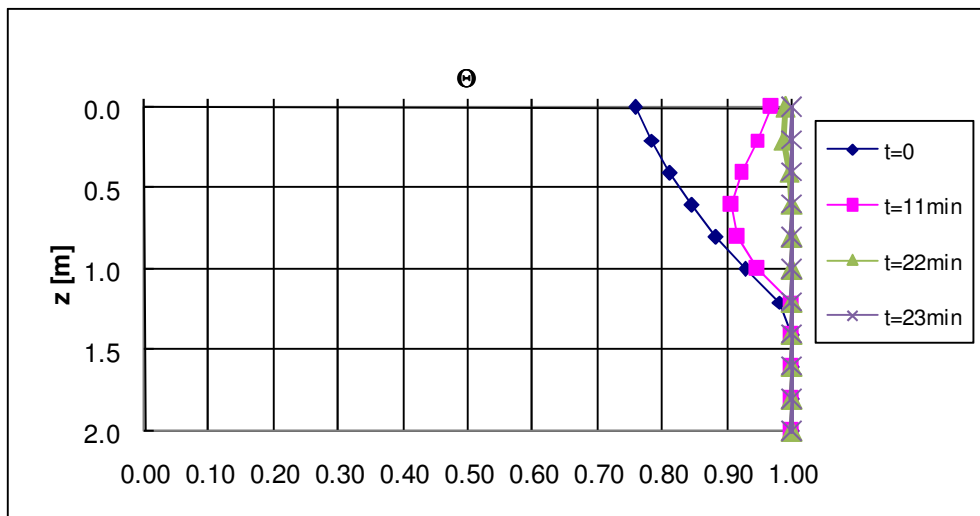


Fig. E9: $(u_a - u_w)_0 = 19 \text{ kPa}; I = 19.44 \text{ mm/h}$

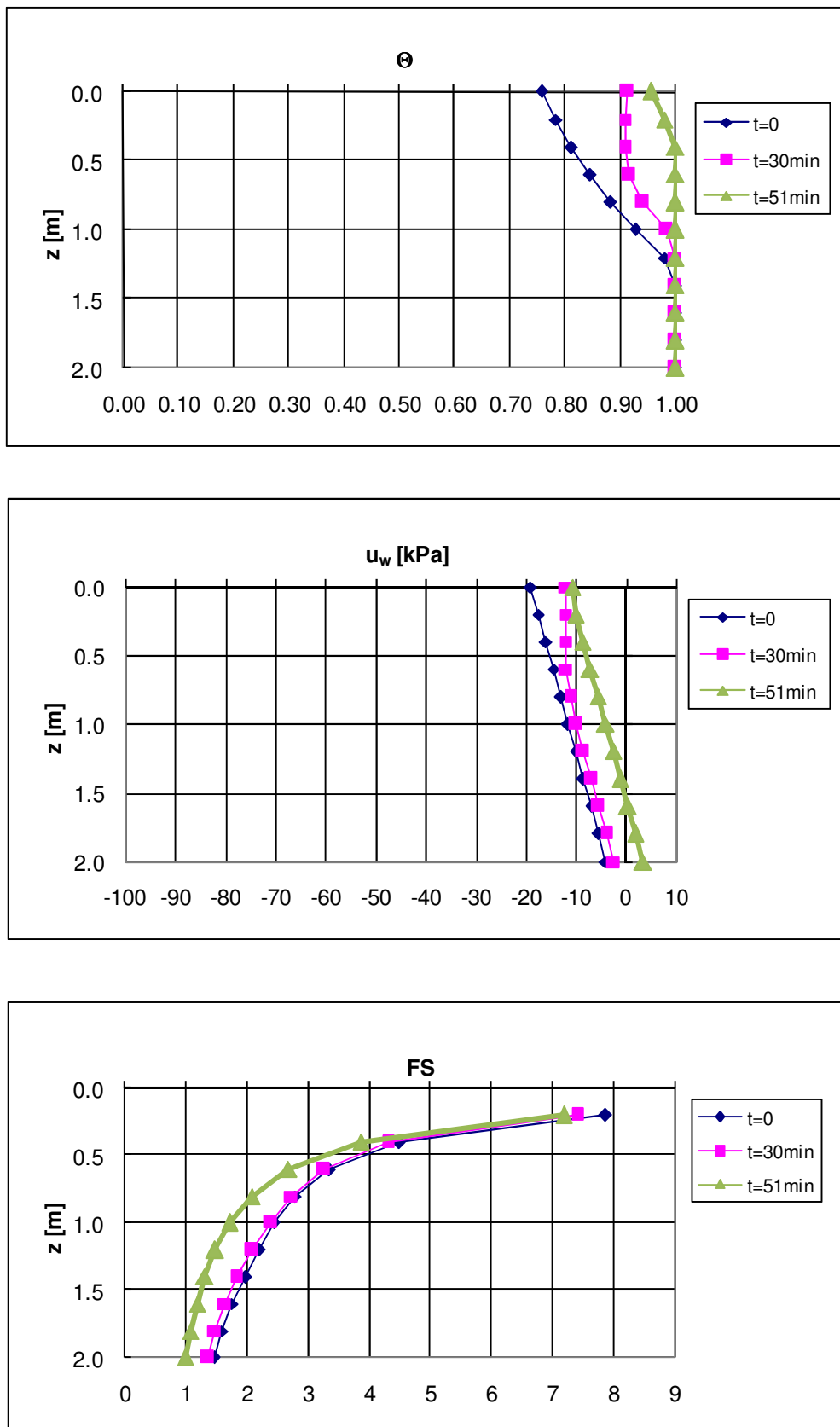


Fig. E10: $(u_a - u_w)_0 = 19 \text{ kPa}; I = 9.72 \text{ mm/h}$

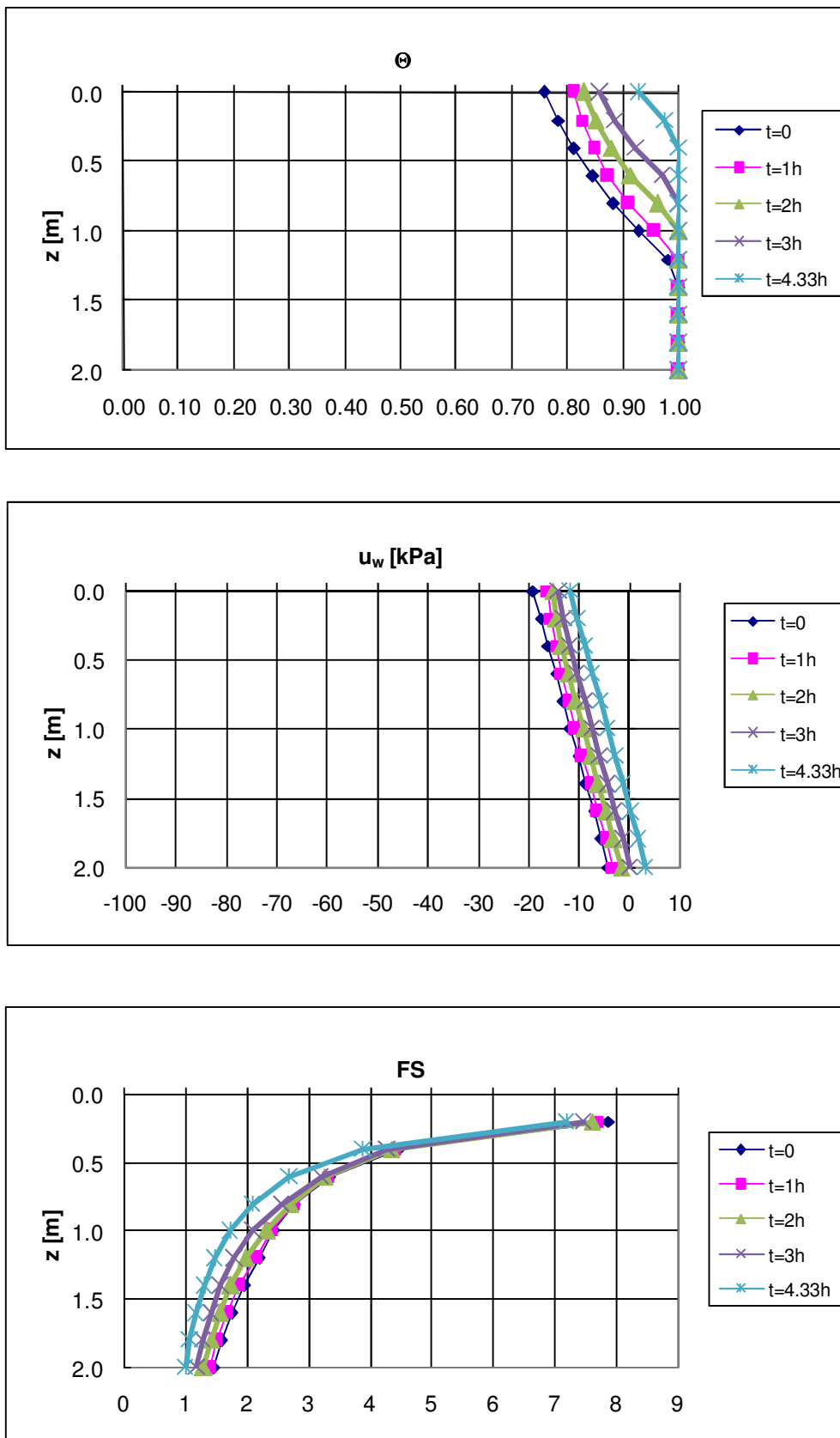


Fig. E11: $(u_a - u_w)_0 = 19$ kPa; $I = 1.94$ mm/h

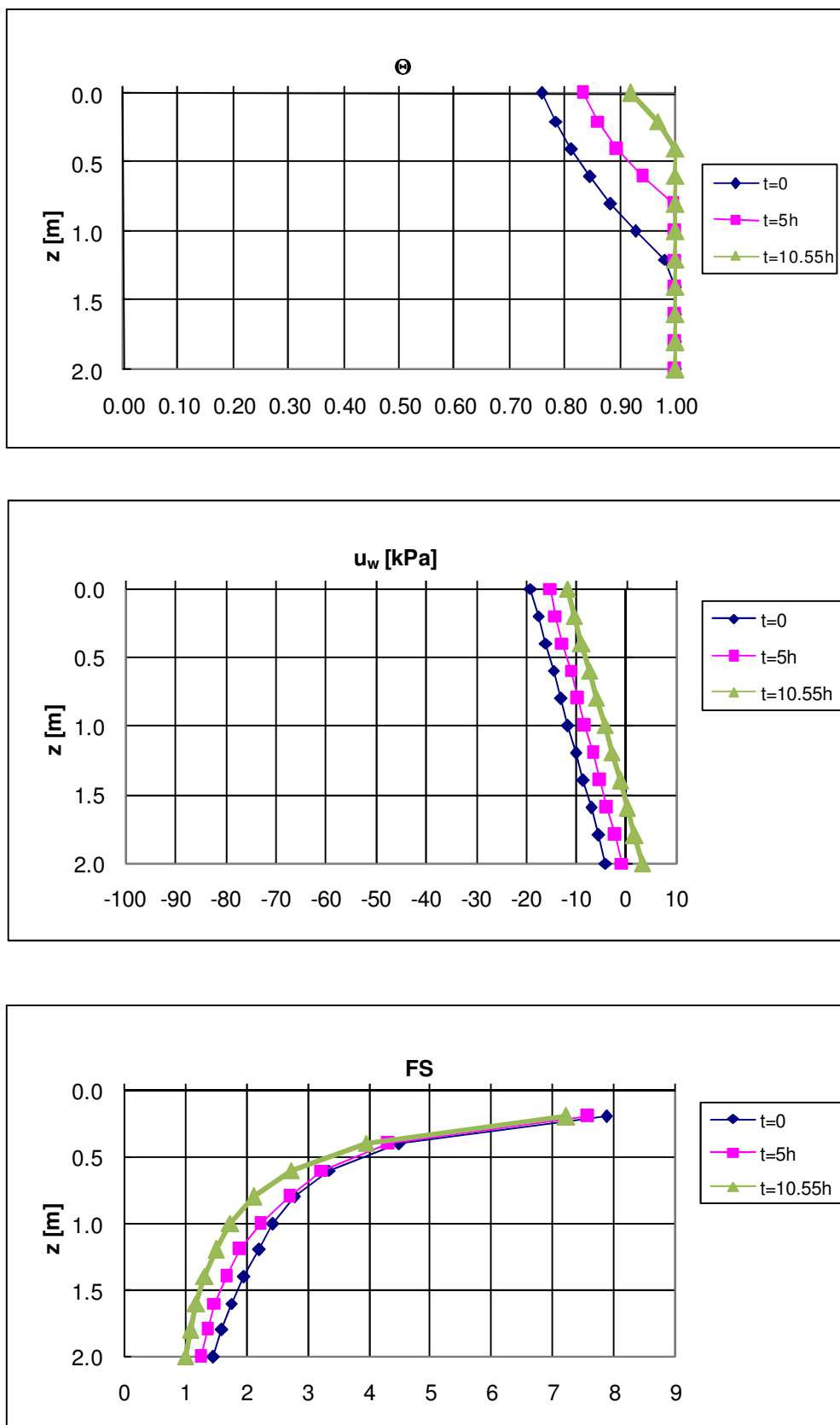


Fig. E12: $(u_a-u_w)_0 = 19 \text{ kPa}$; $I = 0.97 \text{ mm/h}$



ATTACHMENT F

Hypothesis 2

Slope angle $\beta = 30^\circ$
Soil nr.1

Case b

Thickness $h = 2$ m
Impervious bottom
Layered deposit (intermediate more pervious layer)

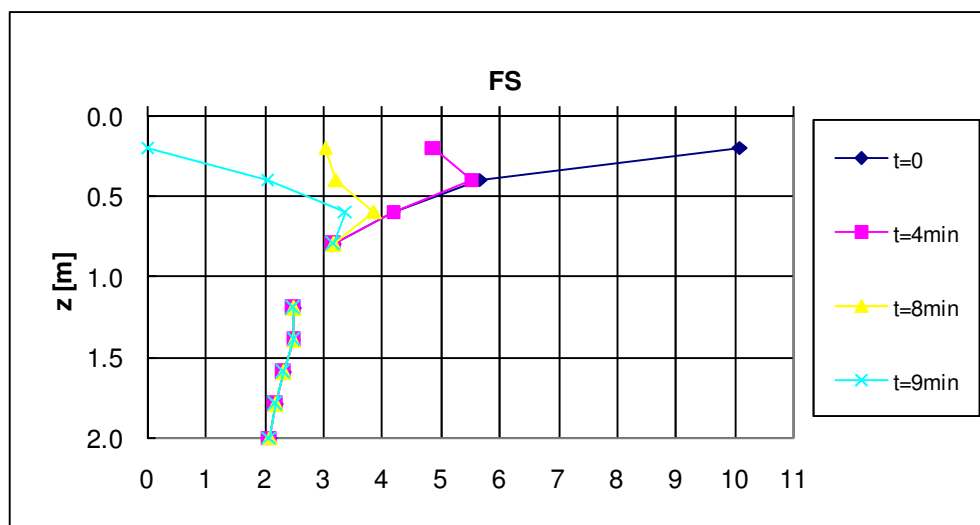
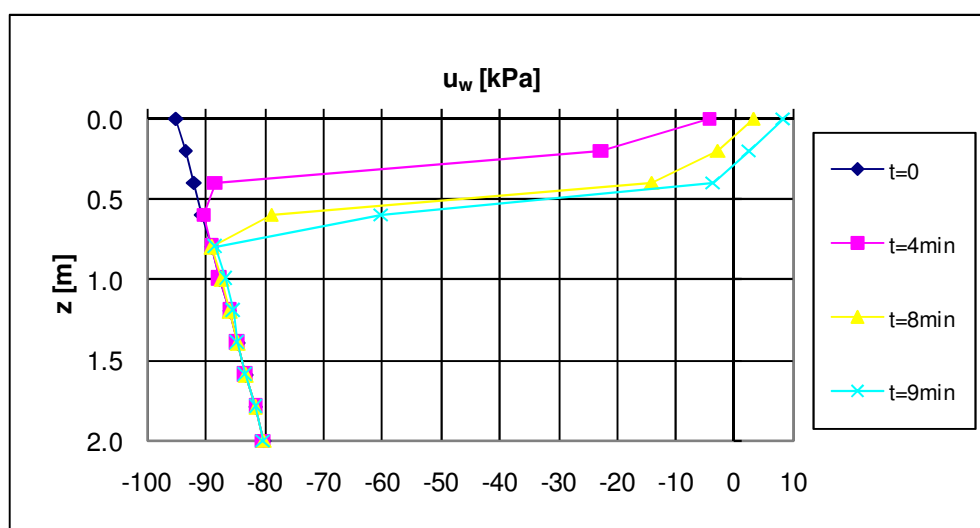
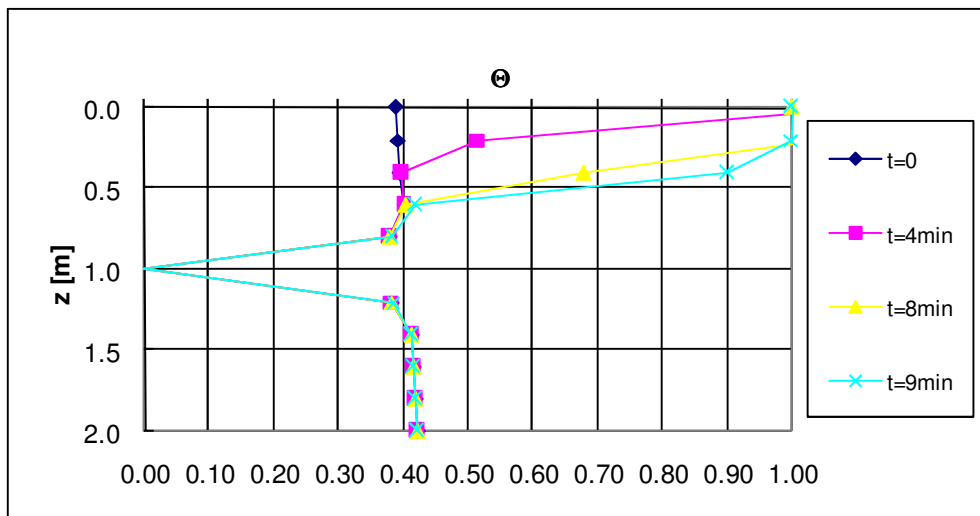


Fig. F1: $(u_a - u_w)_0 = 95 \text{ kPa}; I = 97.20 \text{ mm/h}$

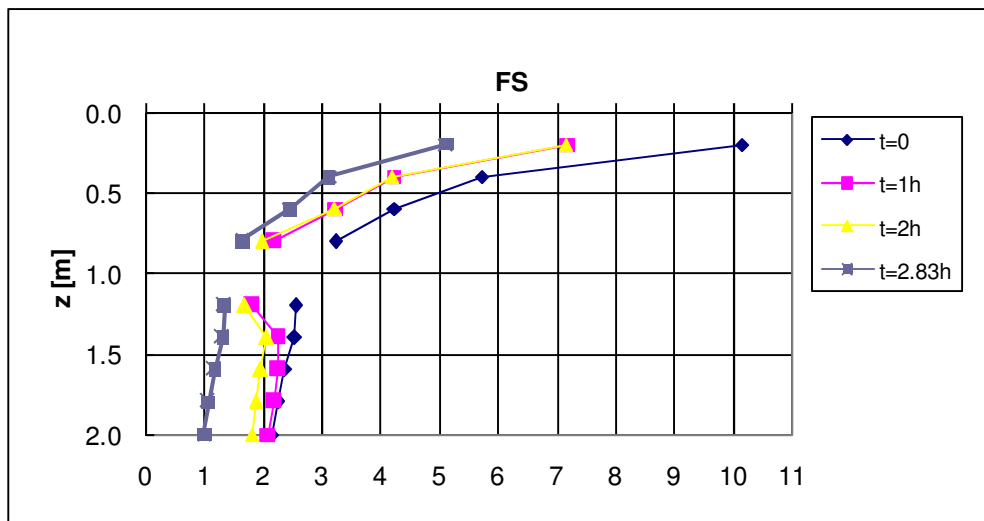
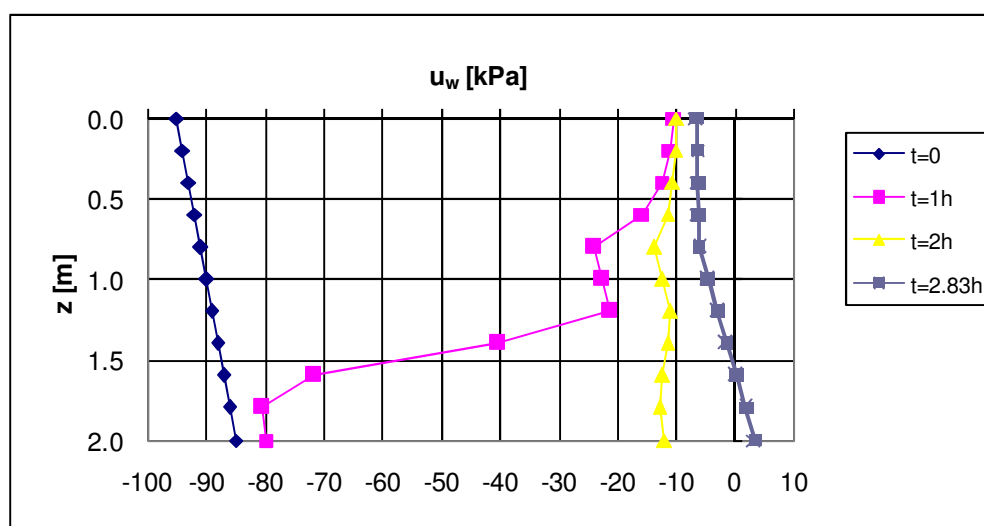
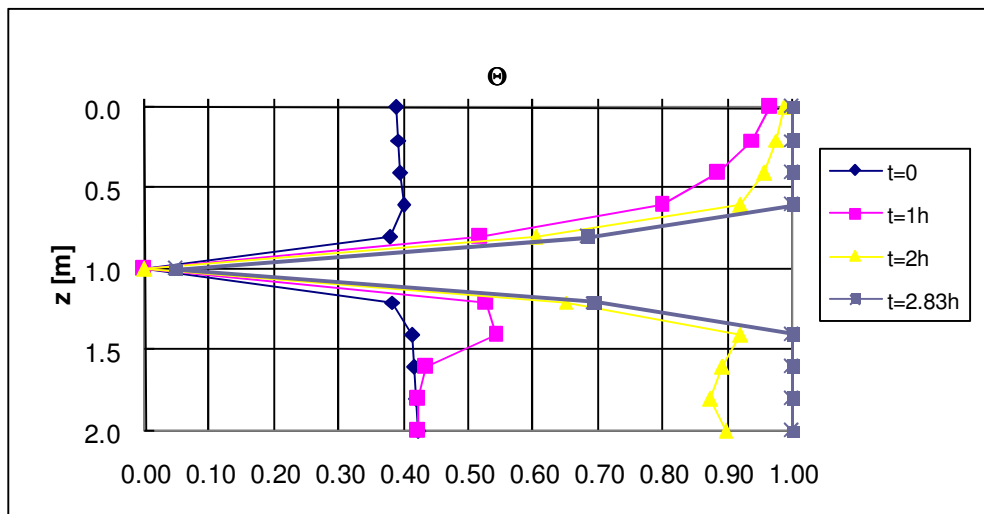


Fig. F2: $(u_a - u_w)_0 = 95 \text{ kPa}; I = 19.44 \text{ mm/h}$

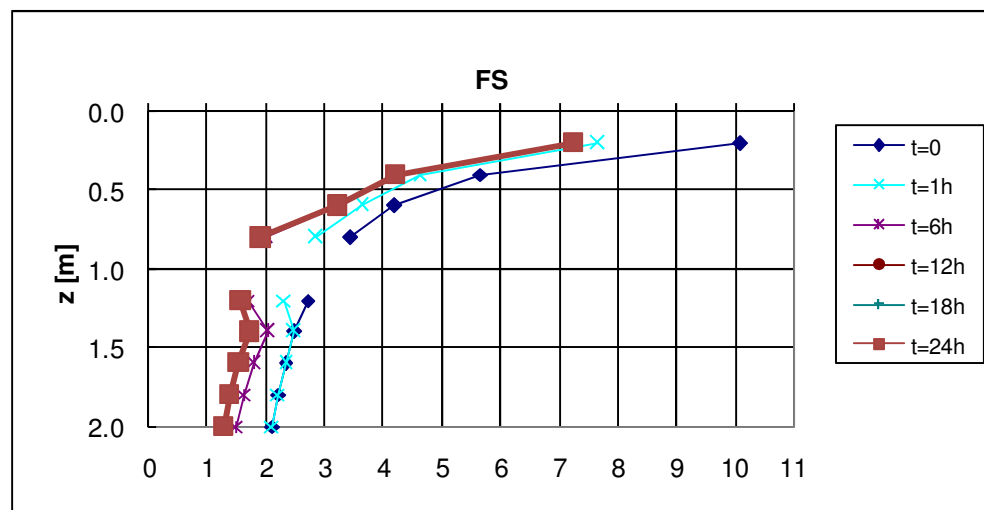
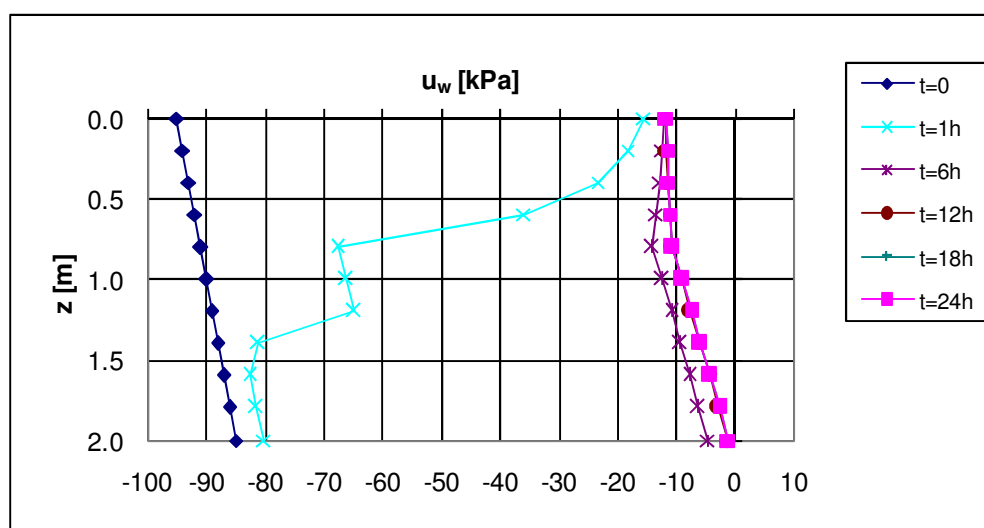
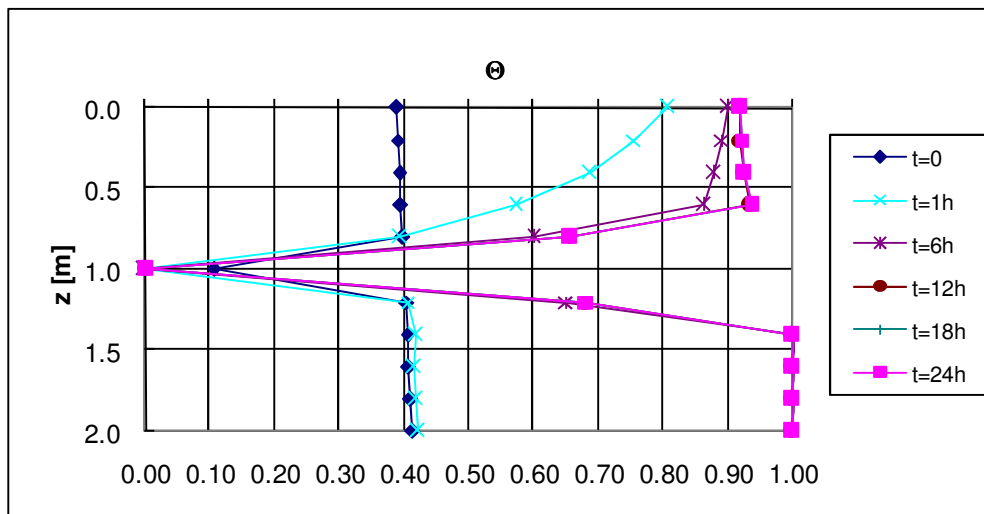


Fig. F3: $(u_a - u_w)_0 = 95 \text{ kPa}; l = 9.72 \text{ mm/h}$

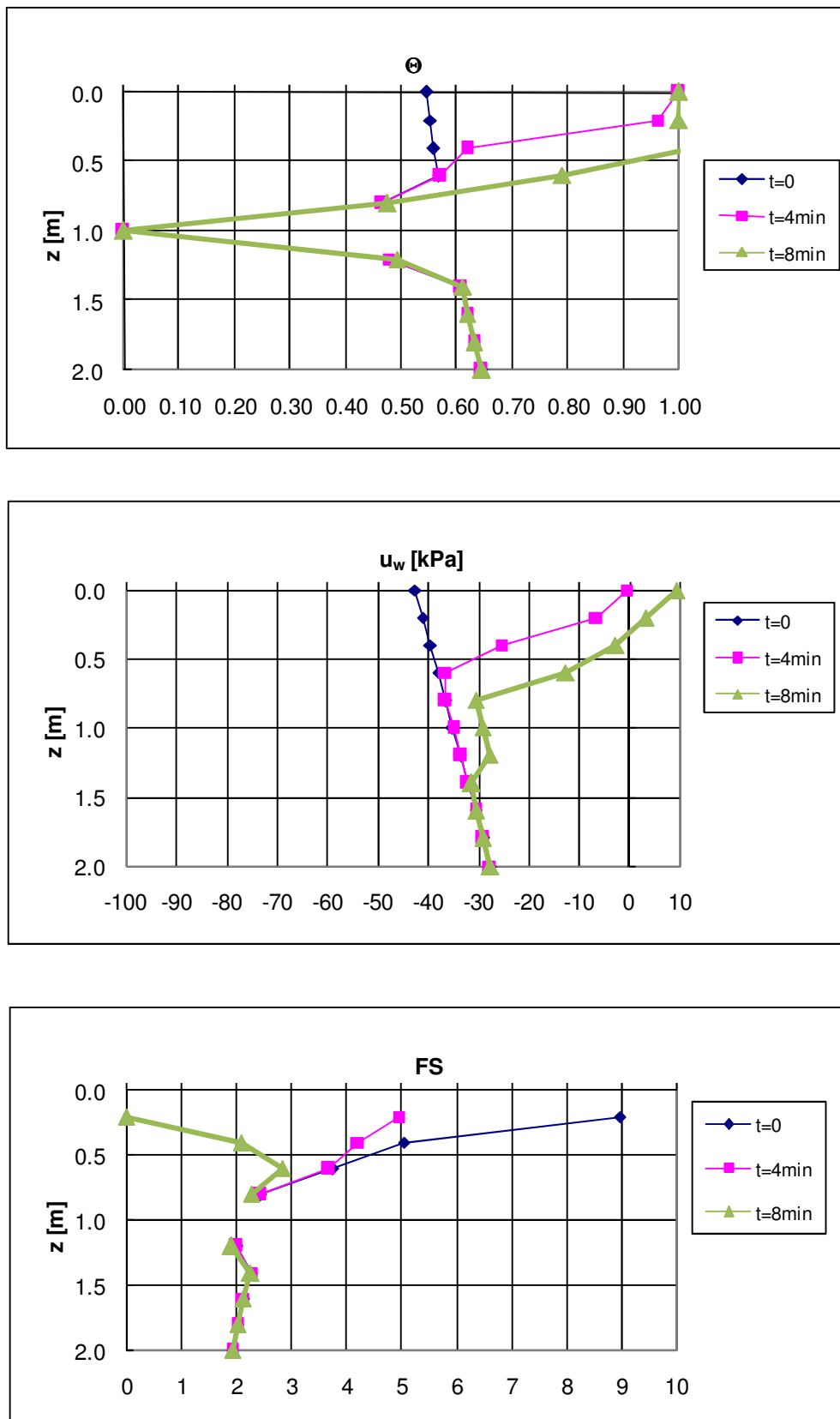


Fig. F4: $(u_a - u_w)_0 = 42.49 \text{ kPa}$; $I = 97.20 \text{ mm/h}$

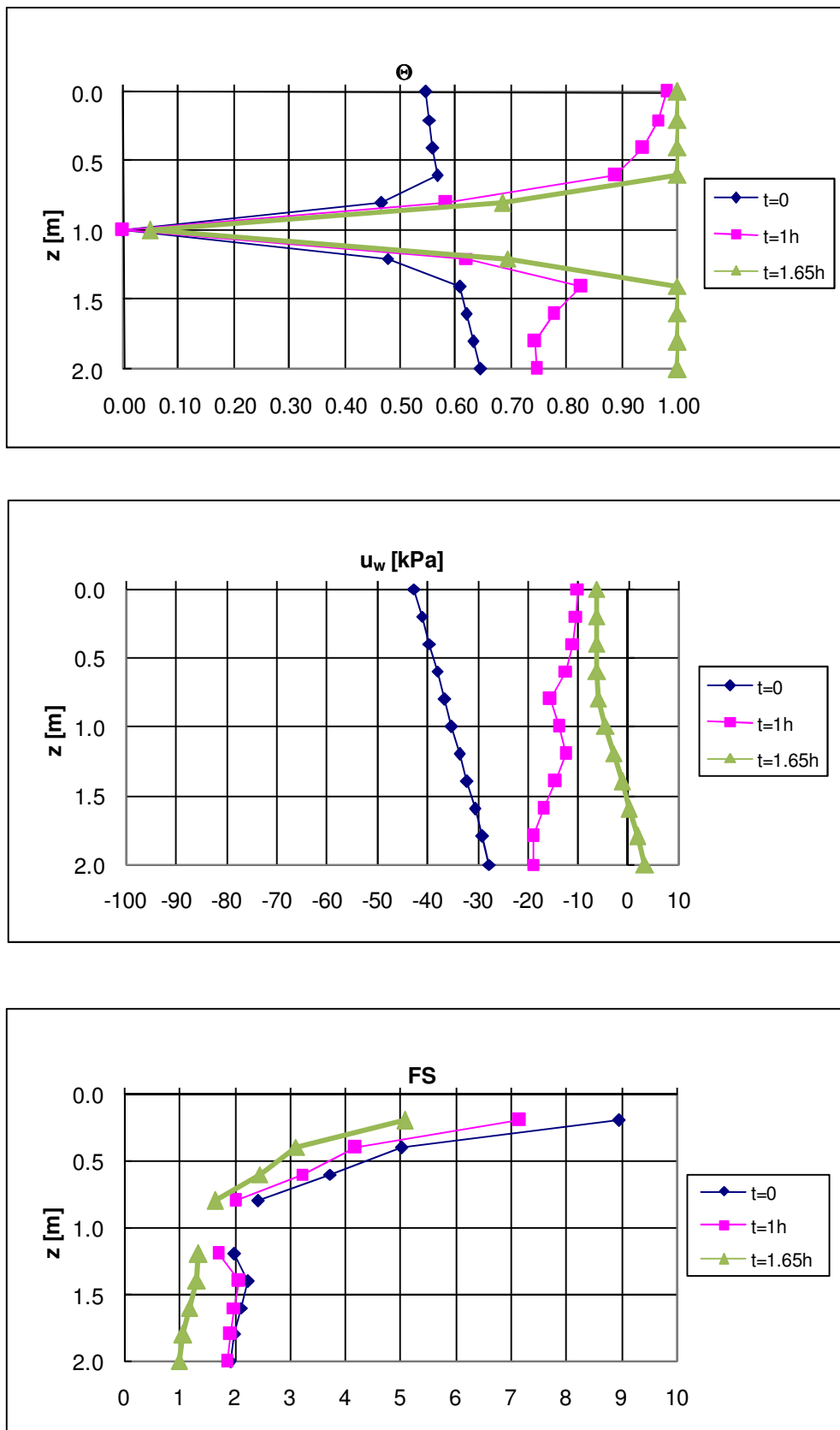


Fig.F5: $(u_a - u_w)_0 = 42.49 \text{ kPa}$; $I = 19.44 \text{ mm/h}$

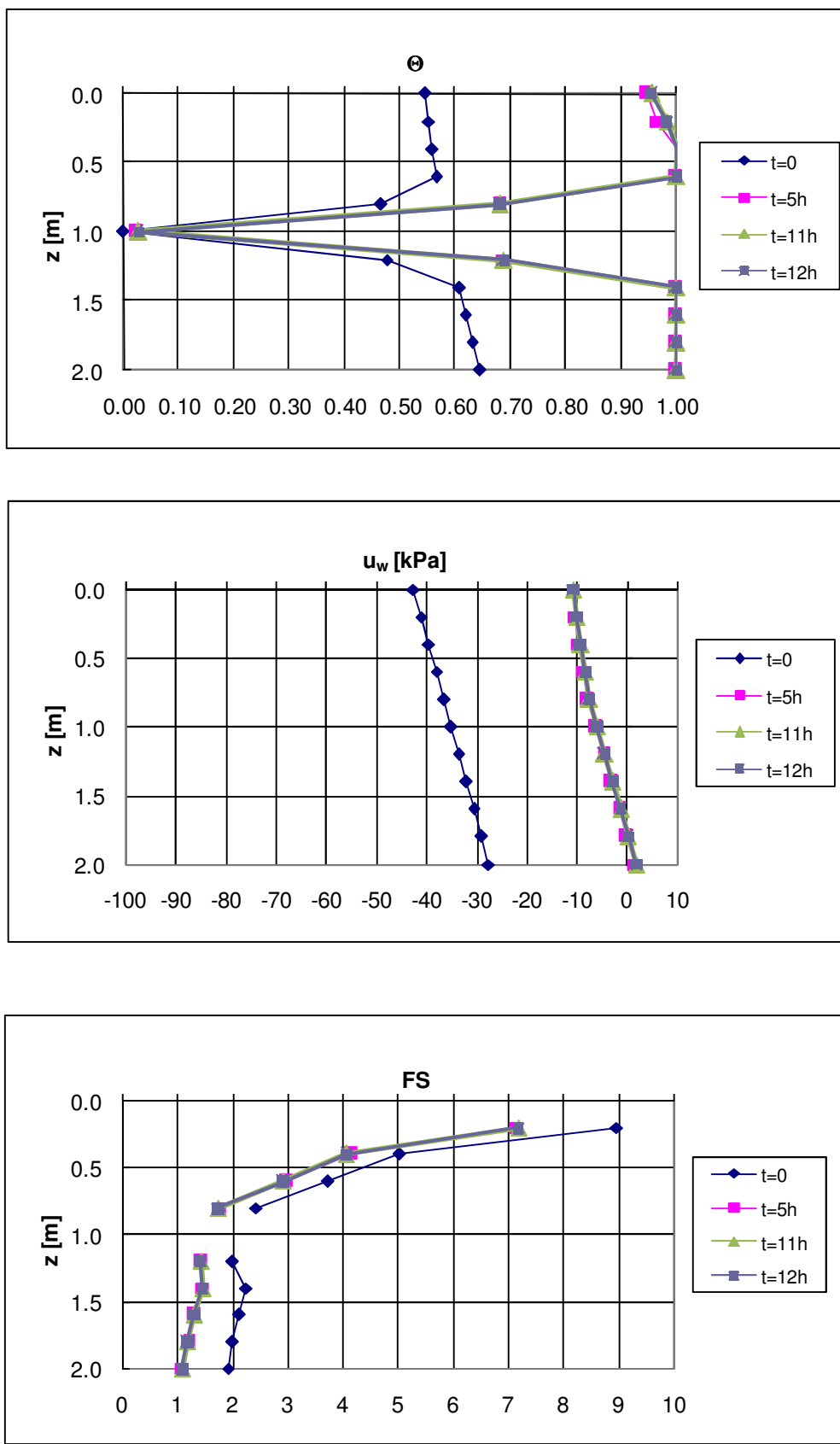


Fig. F6: $(u_a - u_w)_0 = 42.49 \text{ kPa}$; $I = 9.72 \text{ mm/h}$

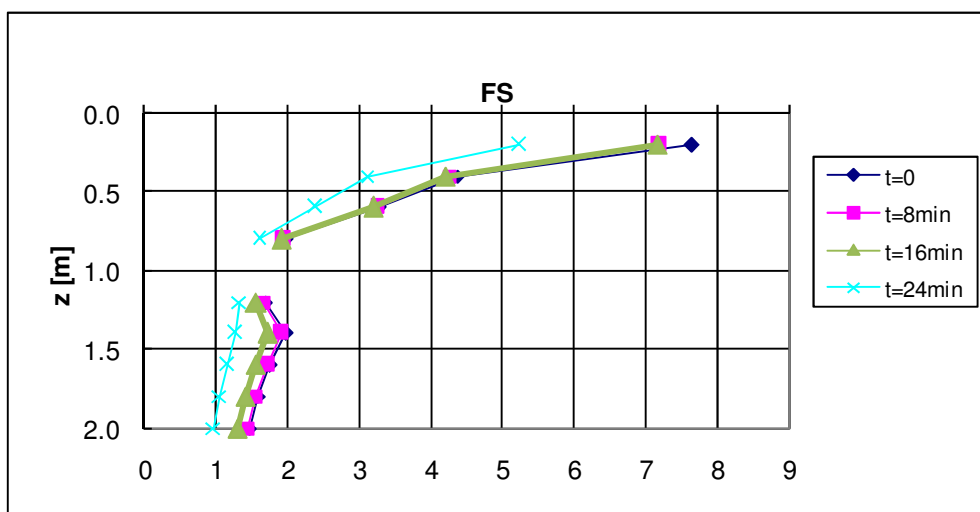
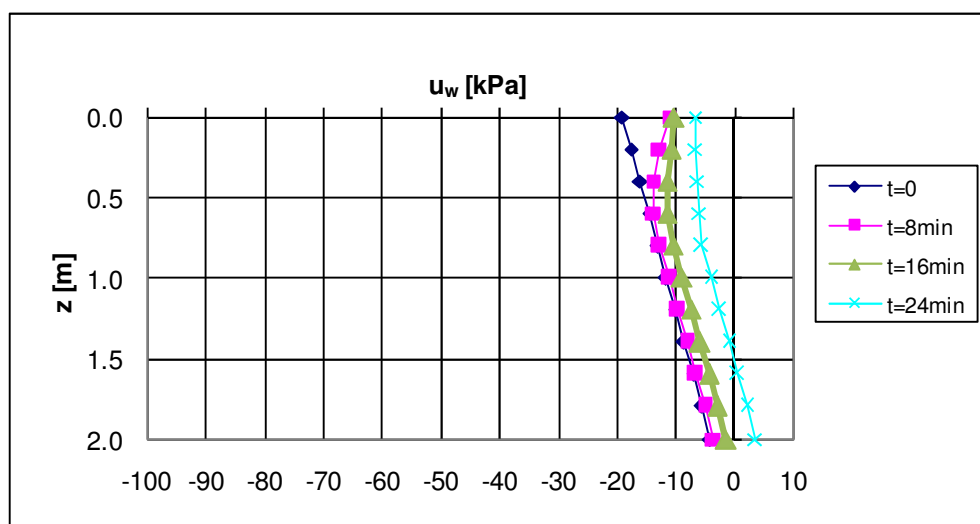
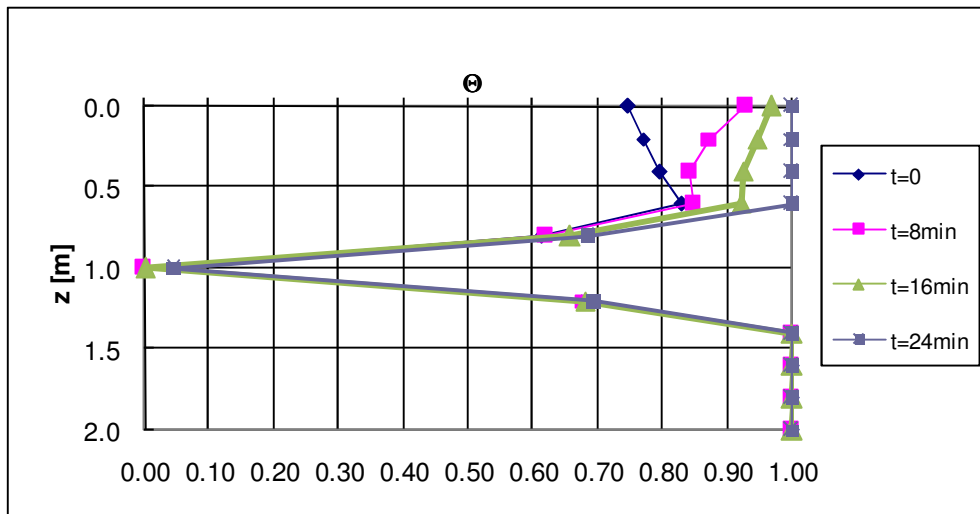


Fig. F7: $(u_a-u_w)_0 = 19 \text{ kPa}; I = 19.44 \text{ mm/h}$

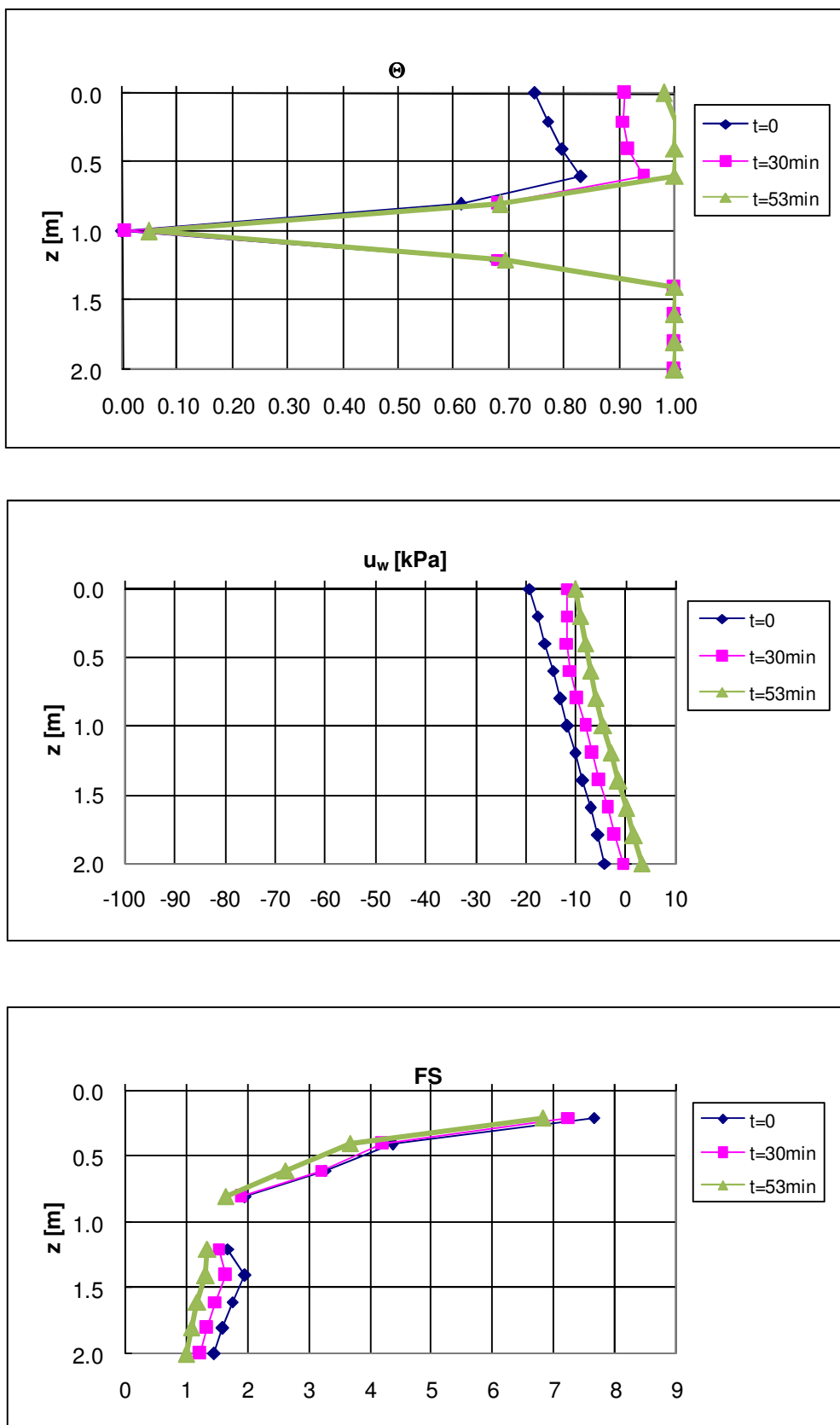


Fig. F8: $(u_a - u_w)_0 = 19 \text{ kPa}$; $I = 9.72 \text{ mm/h}$

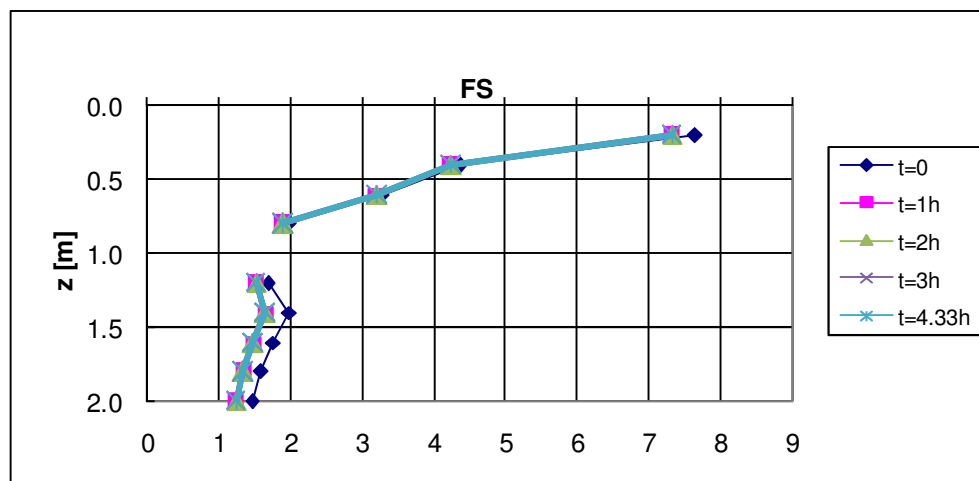
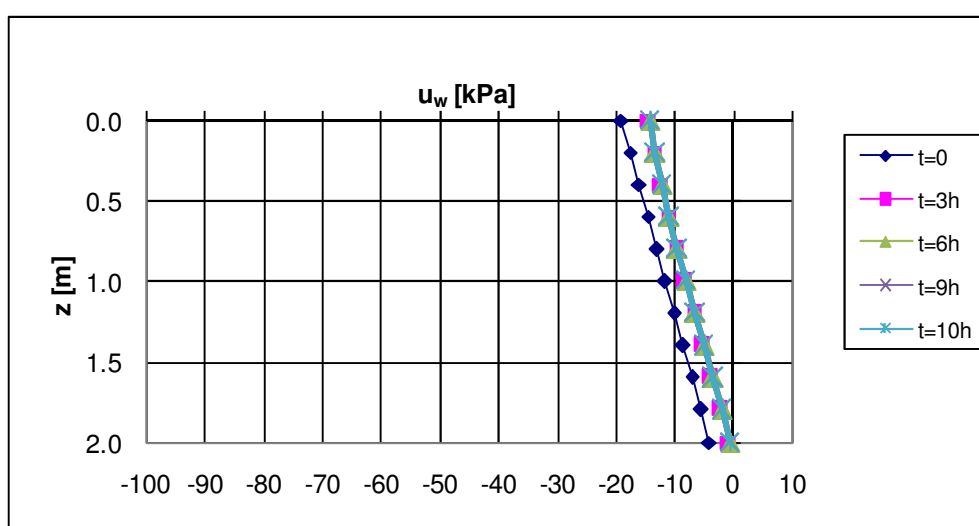
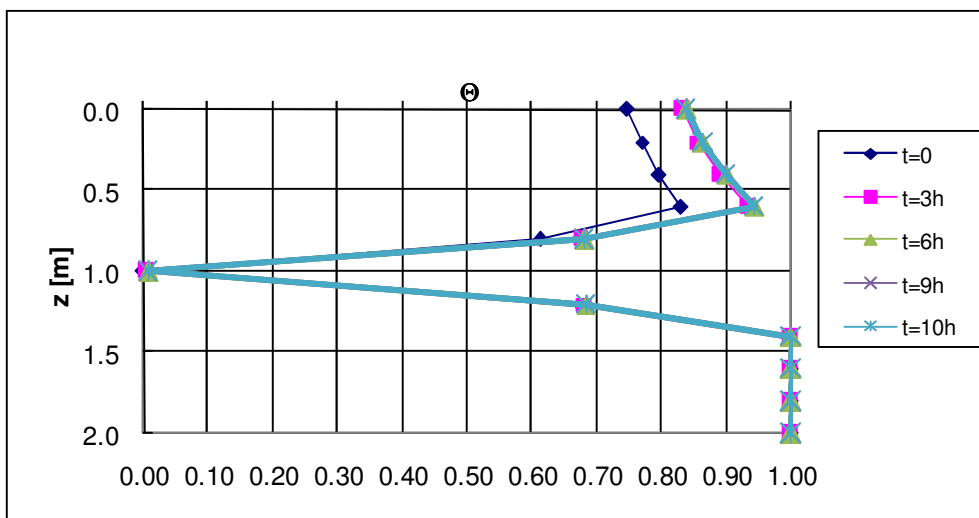


Fig. F9: $(u_a - u_w)_0 = 19$ kPa; $I = 1.94$ mm/h



ATTACHMENT G

Hypothesis 3

Slope angle $\beta = 20^\circ$
Soil nr.1

Case a

Thickness $h = 4$ m
Impervious bottom

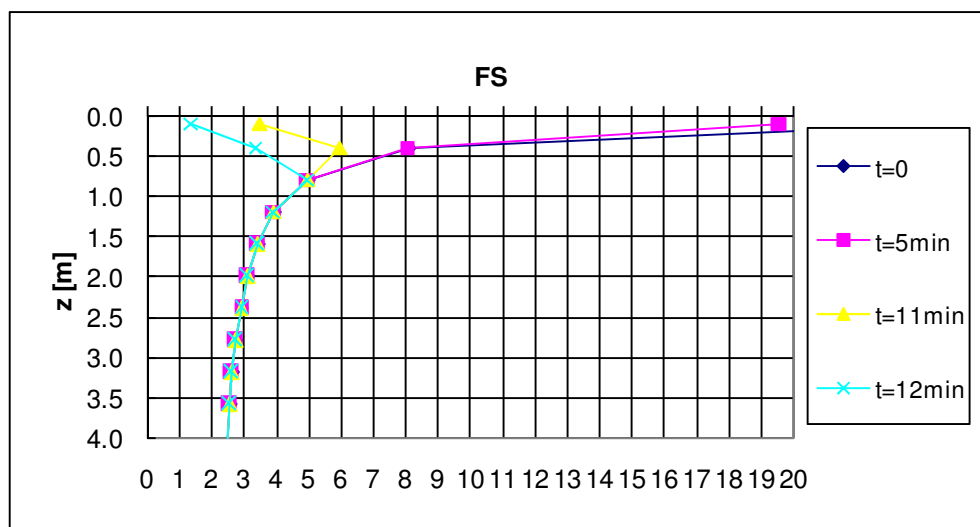
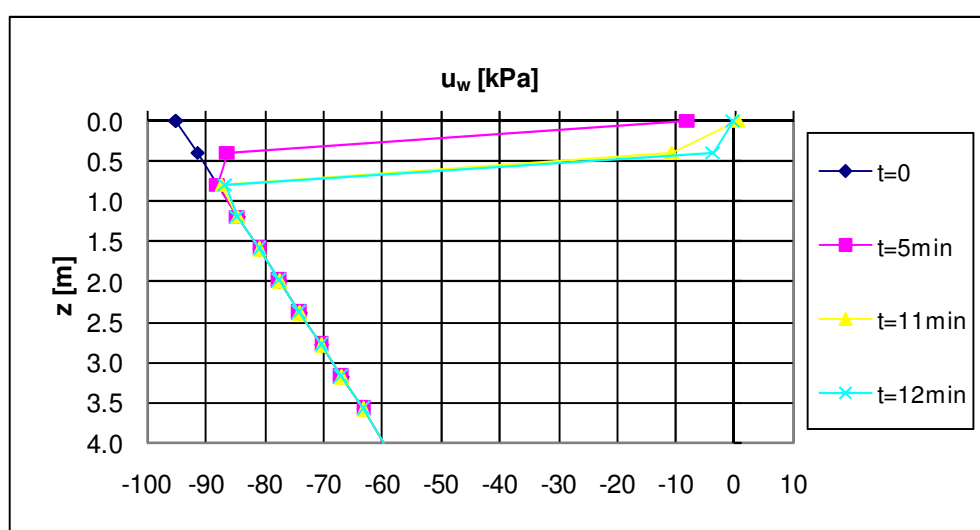
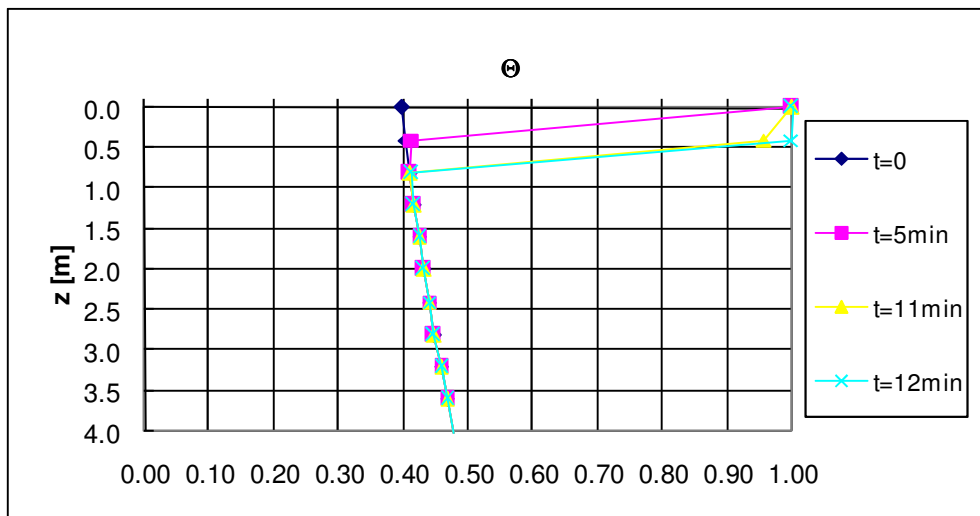


Fig. G1: $(u_a - u_w)_0 = 95 \text{ kPa}; I = 97.20 \text{ mm/h}$

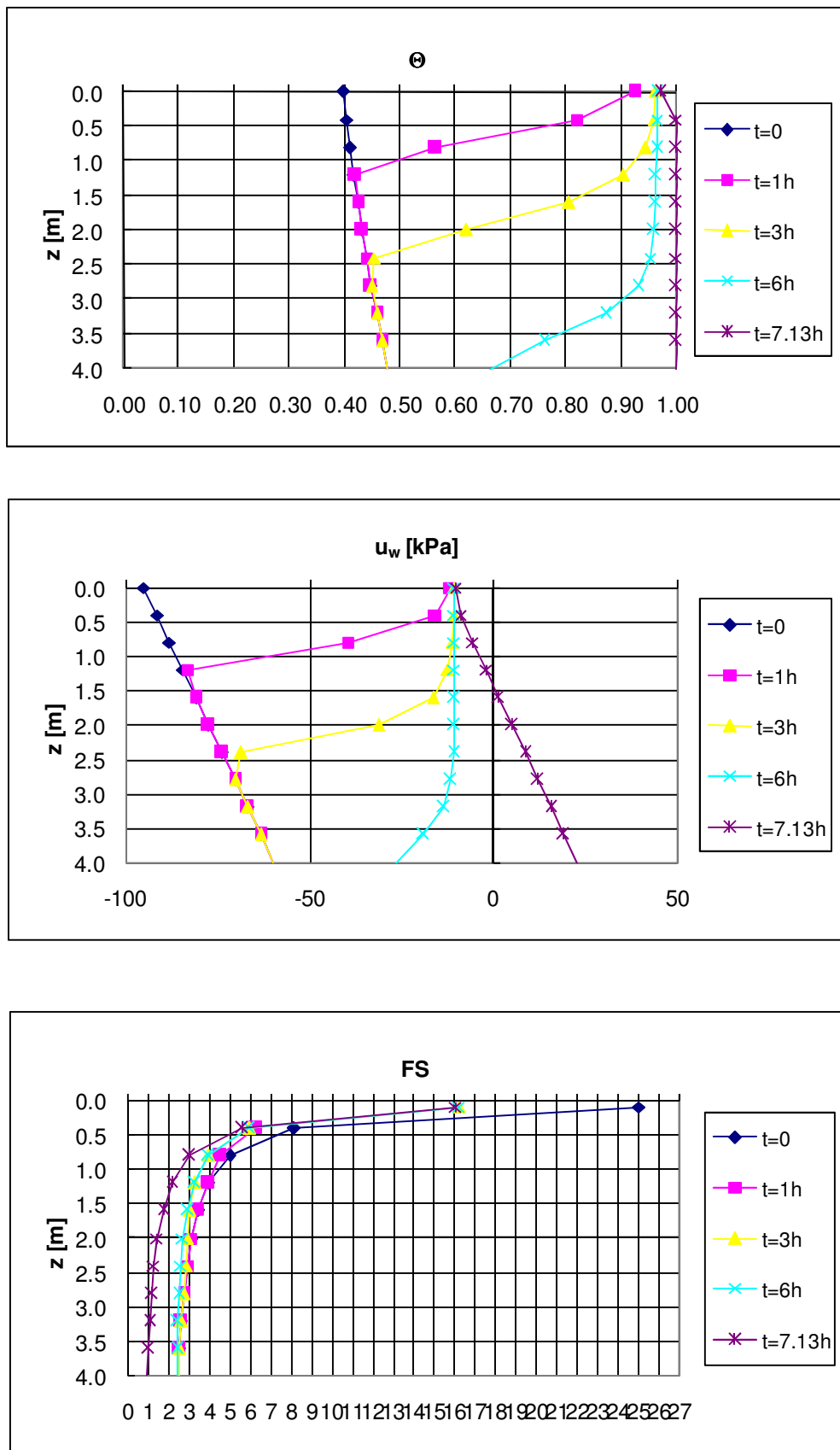


Fig. G2: $(u_a-u_w)_0 = 95 \text{ kPa}$; $I = 19.44 \text{ mm/h}$

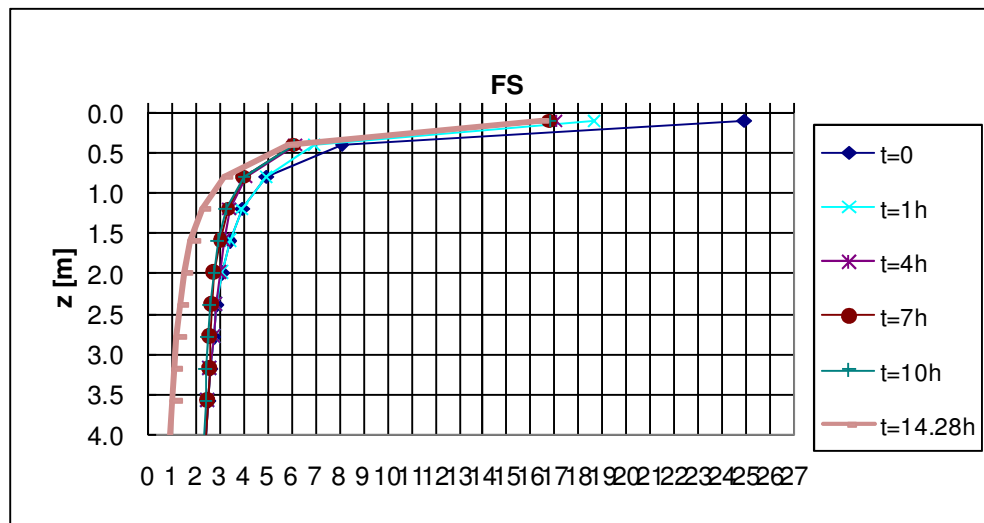
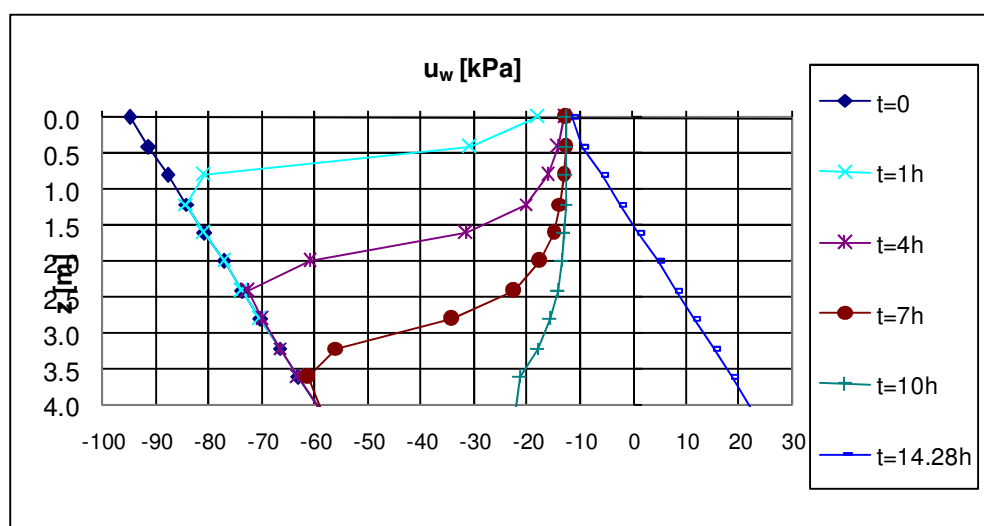
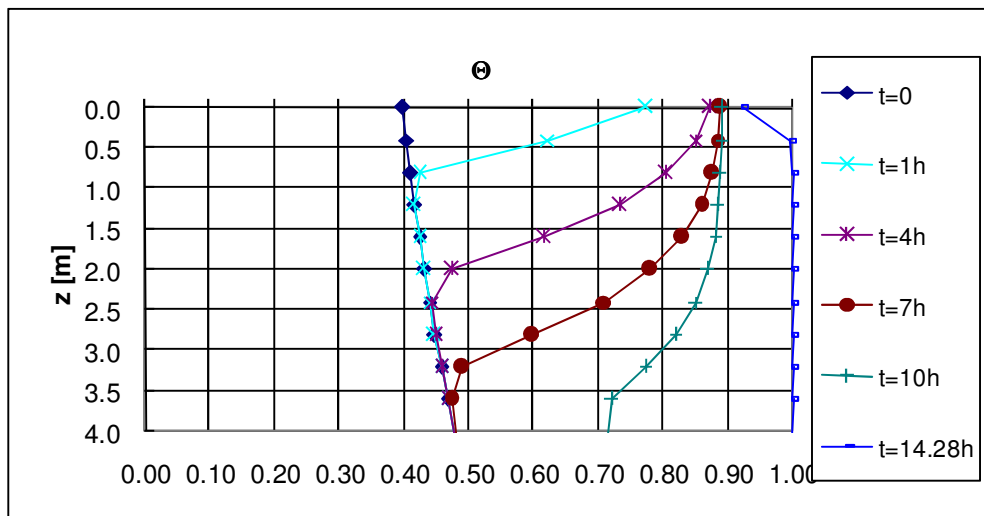


Fig. G3: $(u_a - u_w)_0 = 95 \text{ kPa}$; $I = 9.72 \text{ mm/h}$

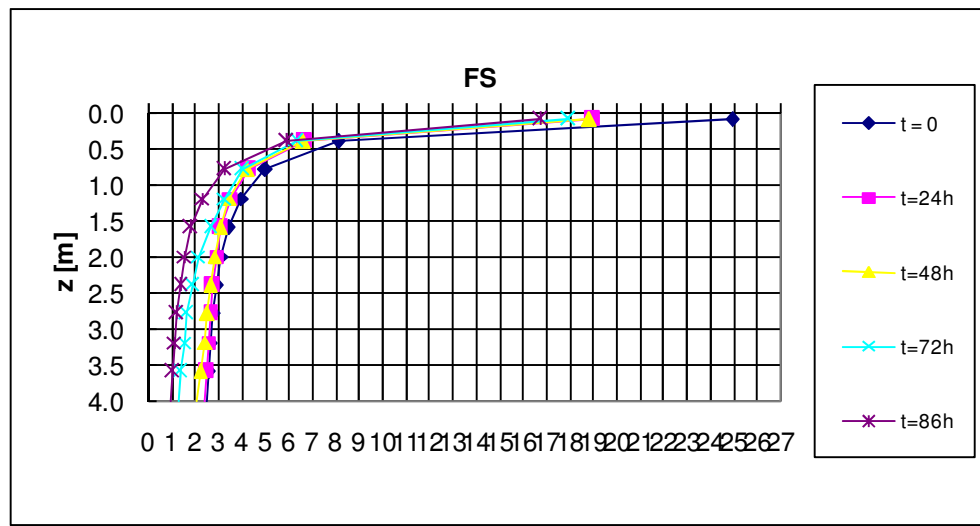
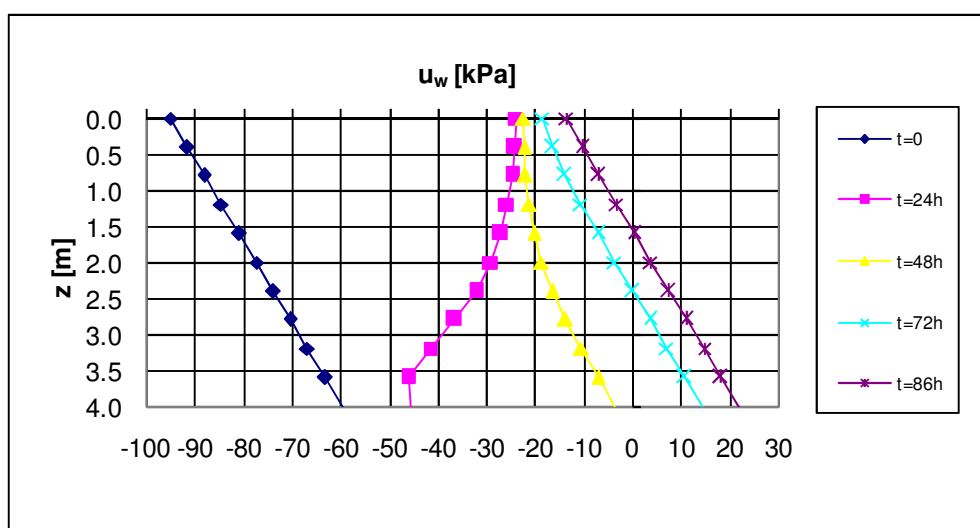
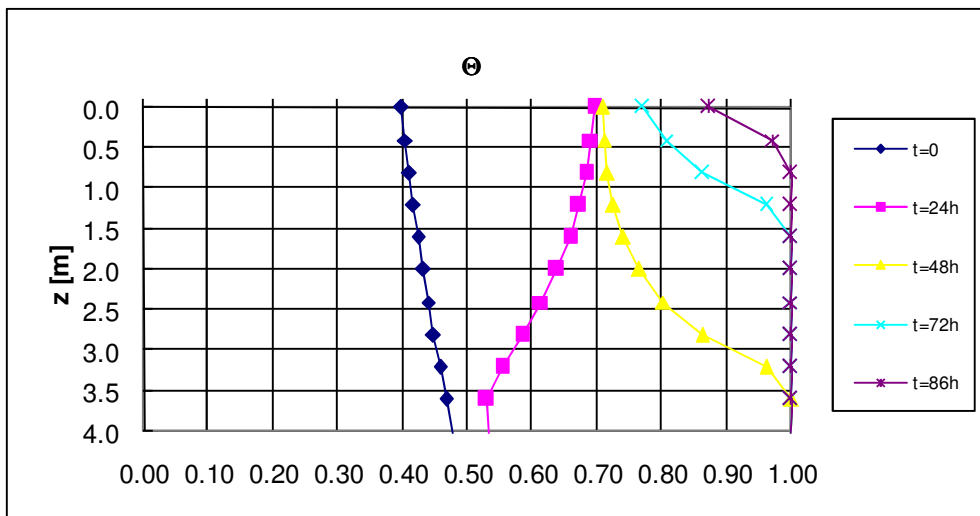


Fig. G4: $(u_a - u_w)_0 = 95 \text{ kPa}$; $I = 1.94 \text{ mm/h}$

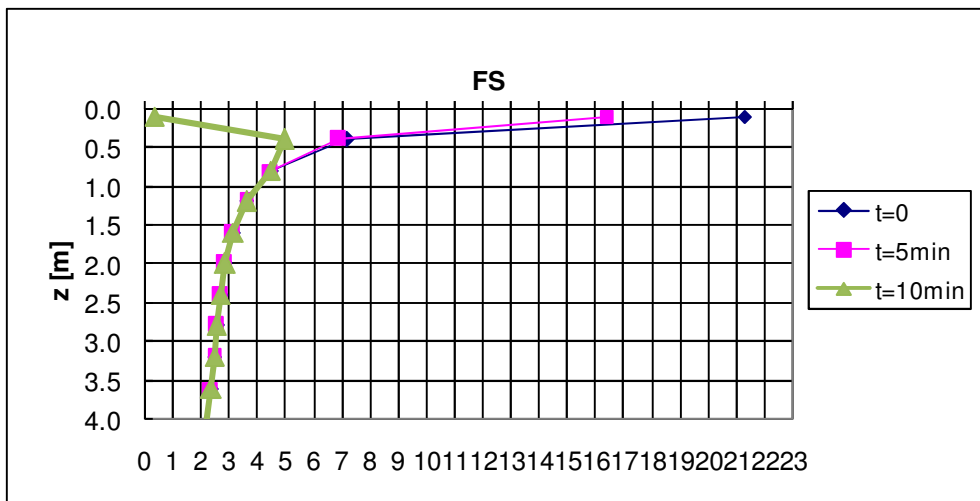
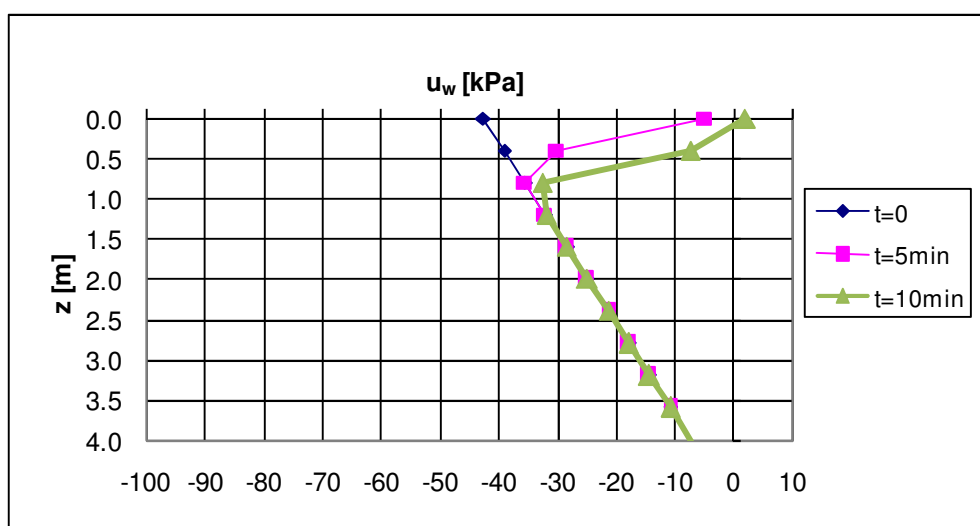
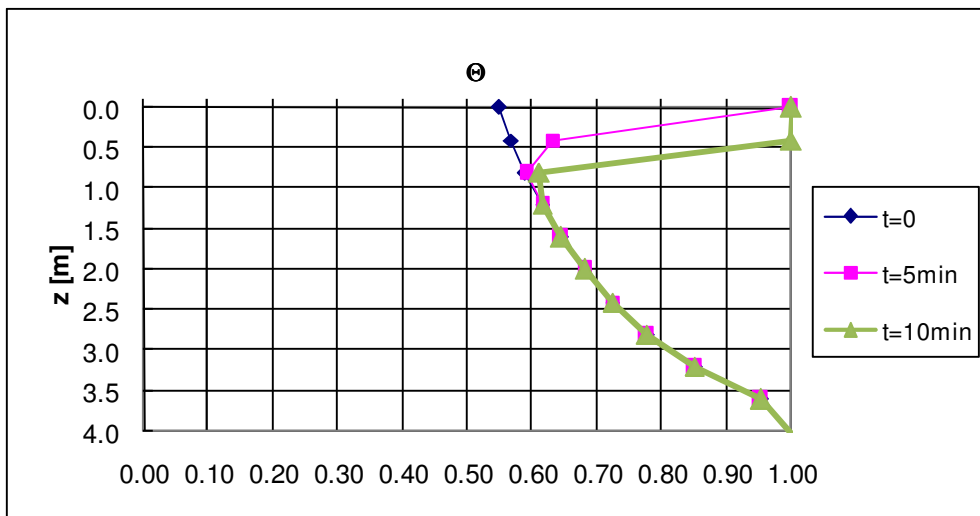


Fig. G5: $(u_a - u_w)_0 = 42.49 \text{ kPa}$; $I = 97.20 \text{ mm/h}$

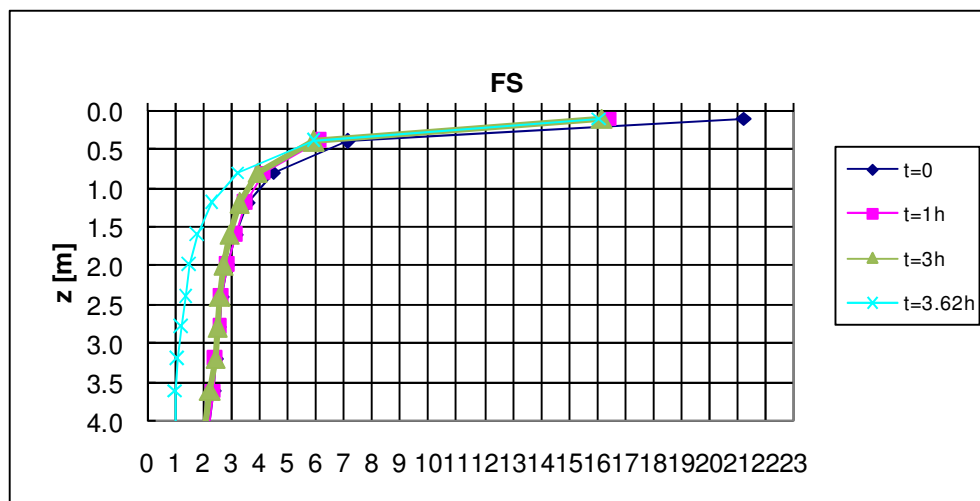
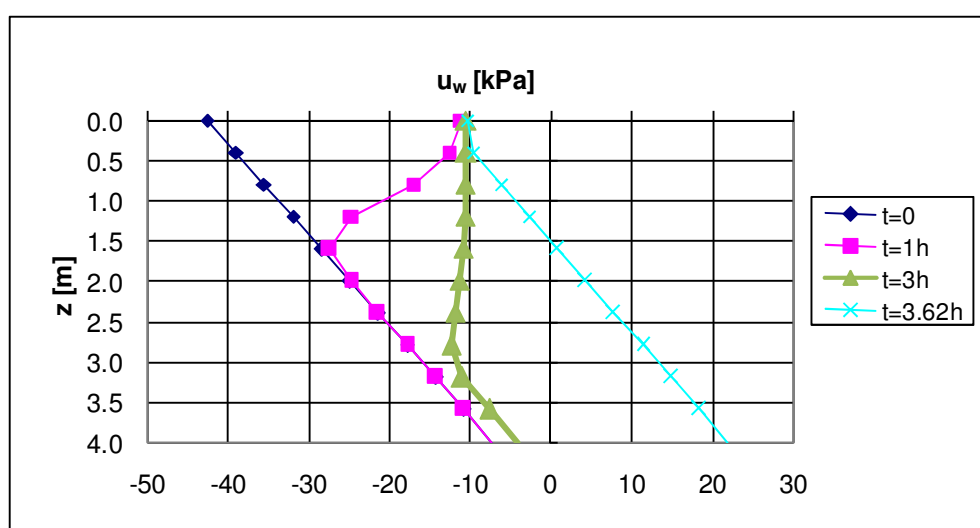
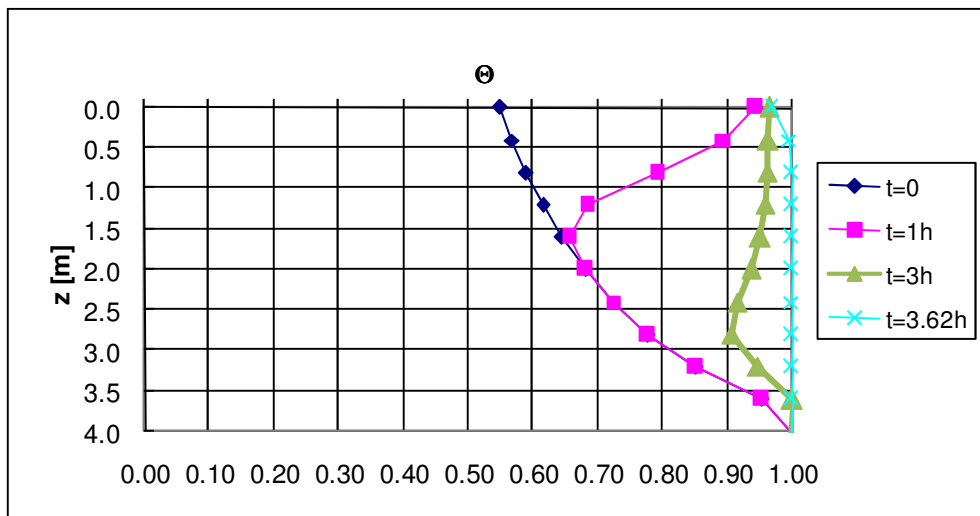


Fig. G6: $(u_a - u_w)_0 = 42.49$ kPa; $I = 19.44$ mm/h

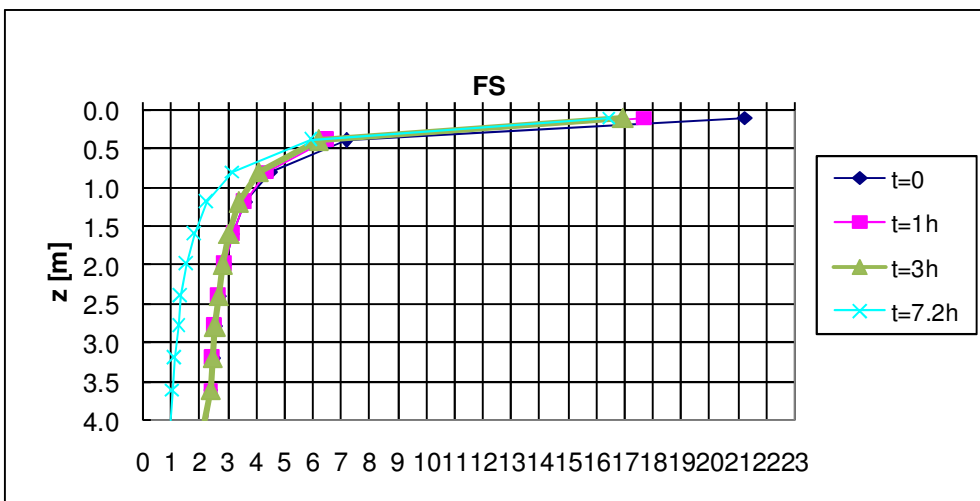
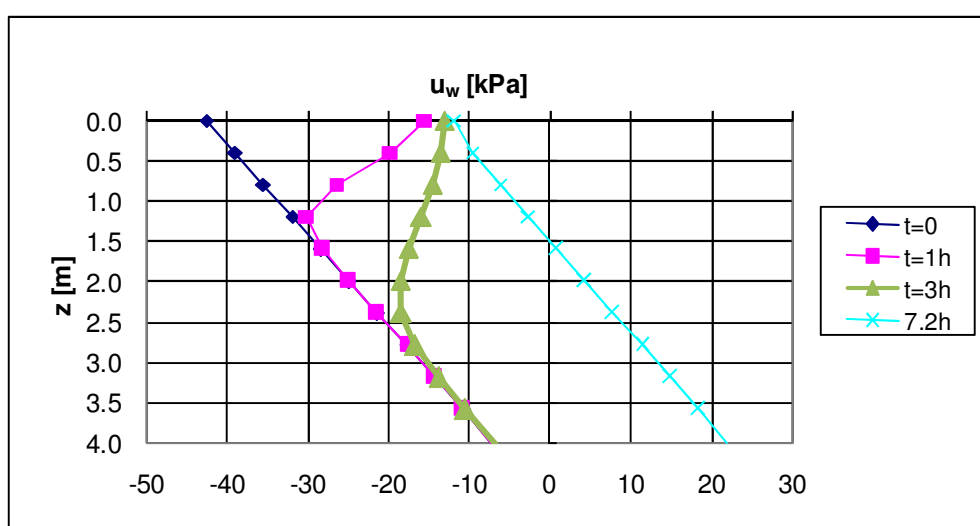
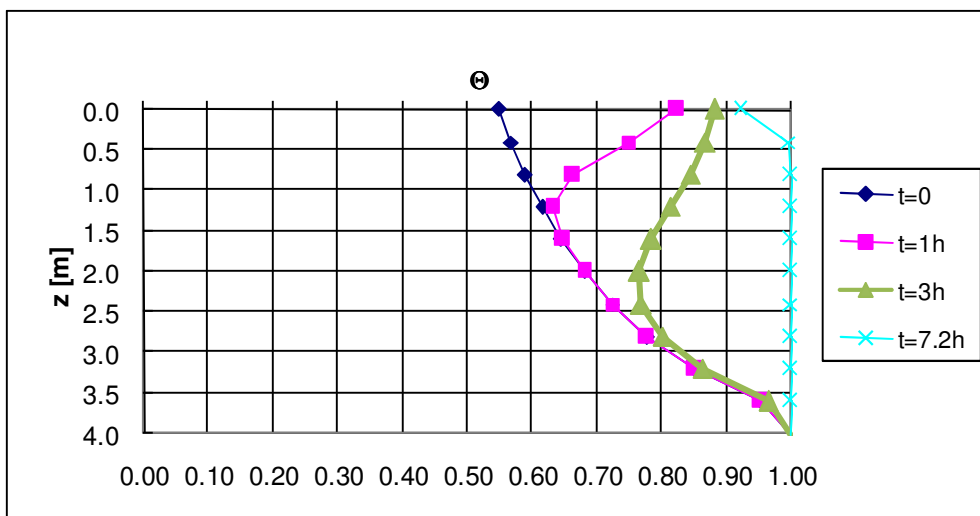


Fig. G7: $(u_a - u_w)_0 = 42.49 \text{ kPa}; l = 9.72 \text{ mm/h}$

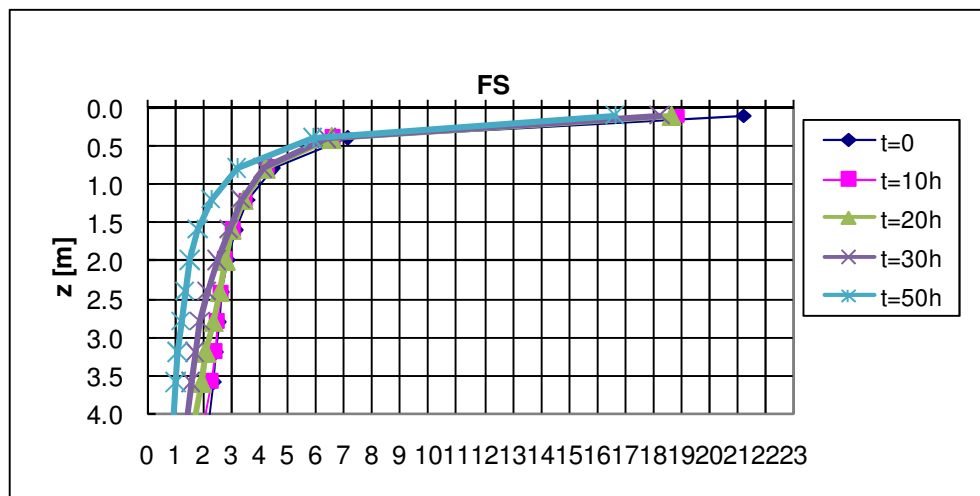
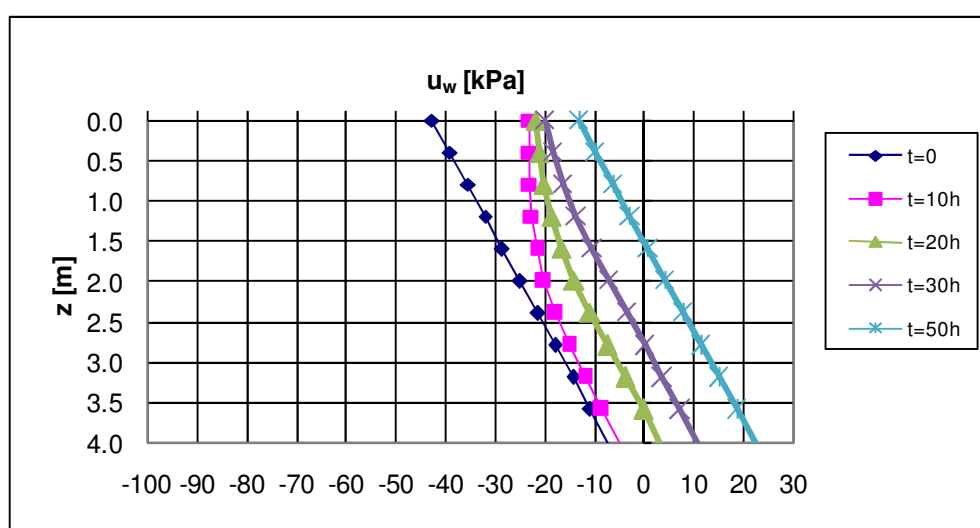
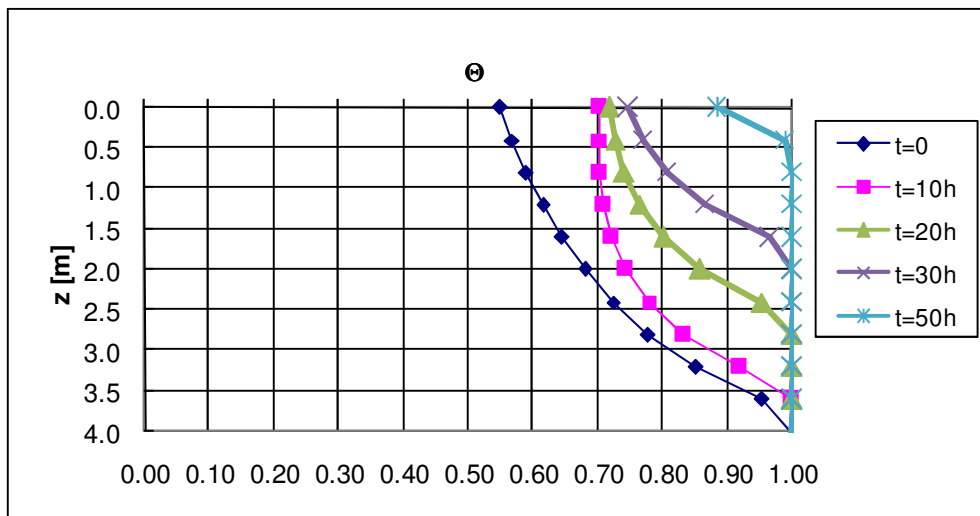


Fig. G8: $(u_a - u_w)_0 = 42.49 \text{ kPa}$; $I = 1.94 \text{ mm/h}$

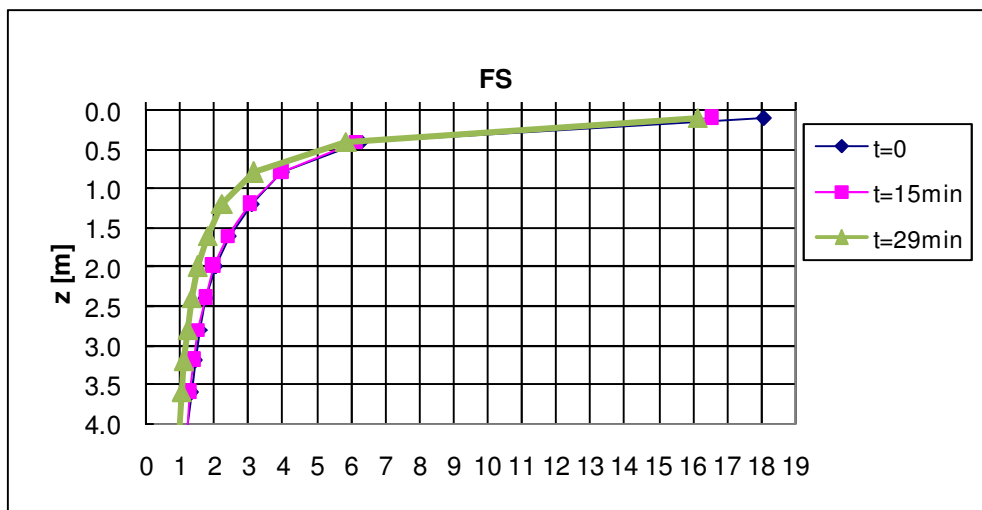
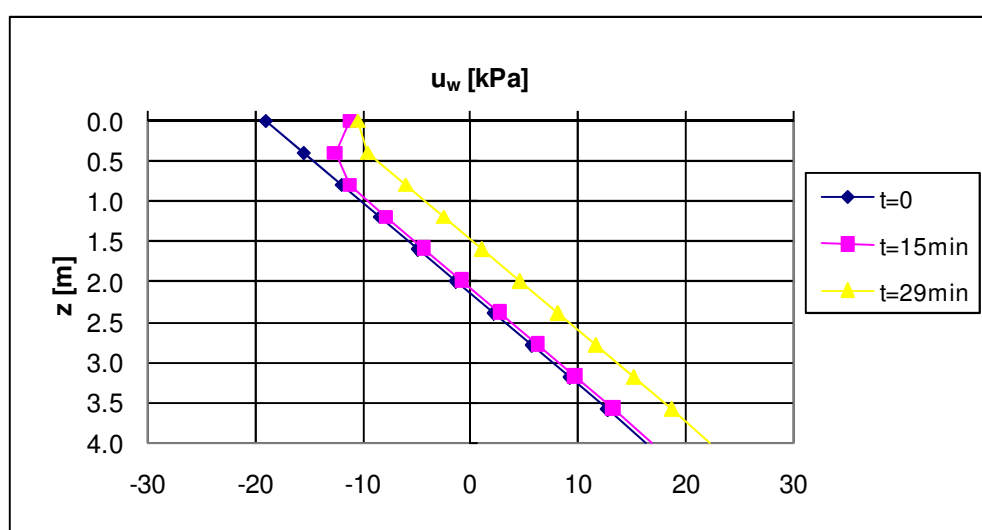
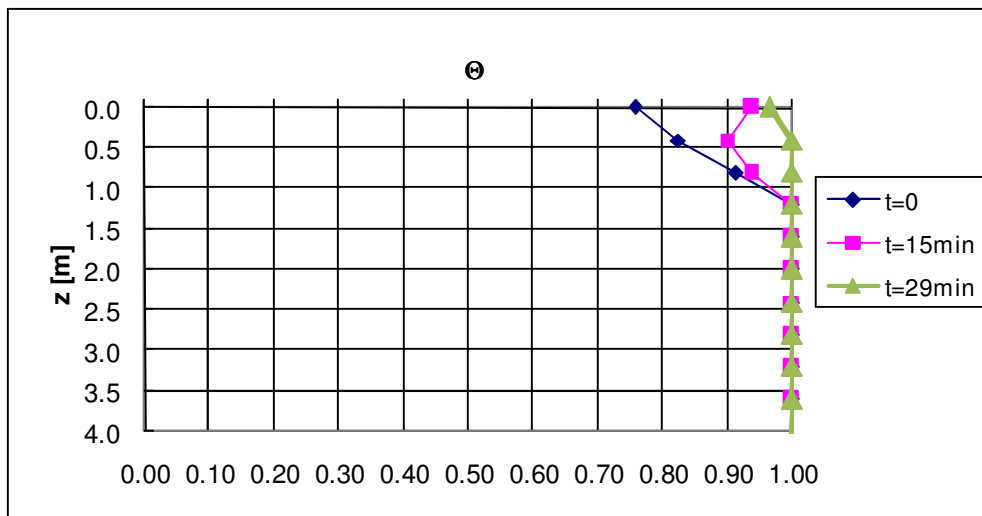


Fig. G9: $(u_a - u_w)_0 = 19 \text{ kPa}; I = 19.44 \text{ mm/h}$

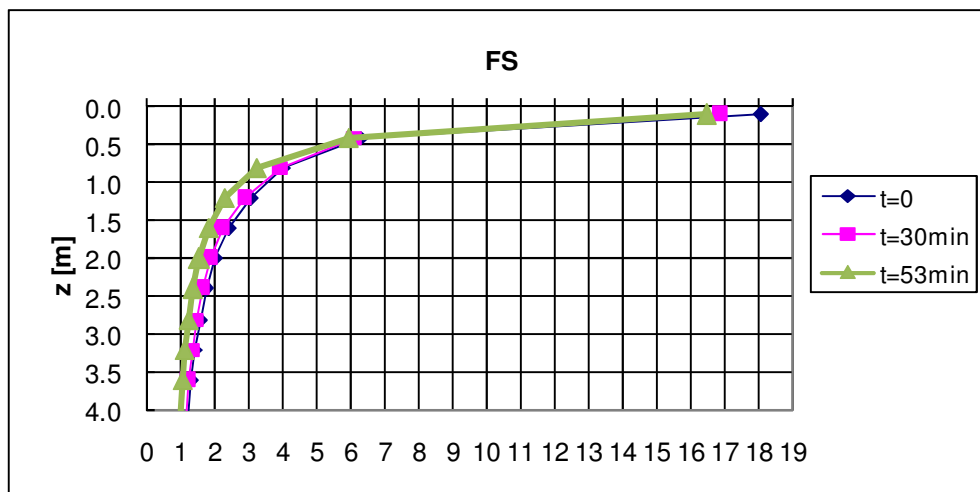
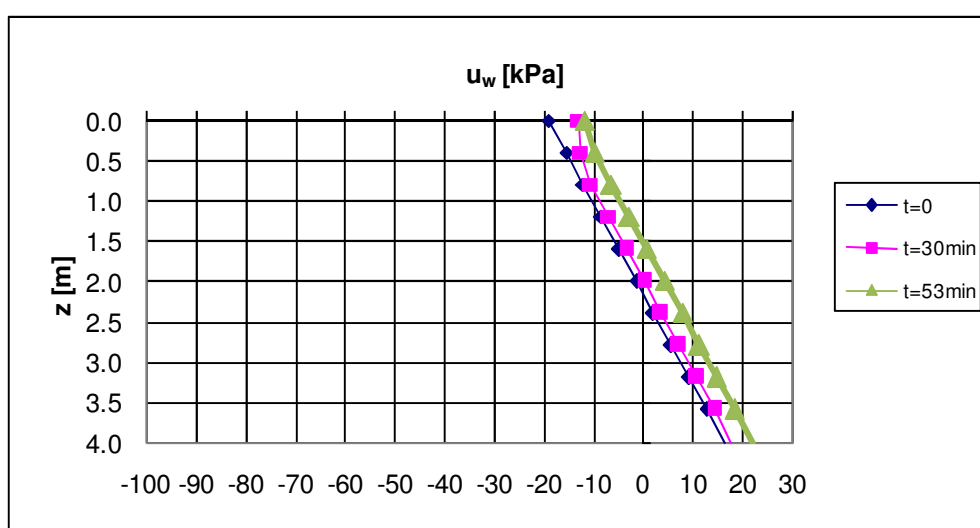
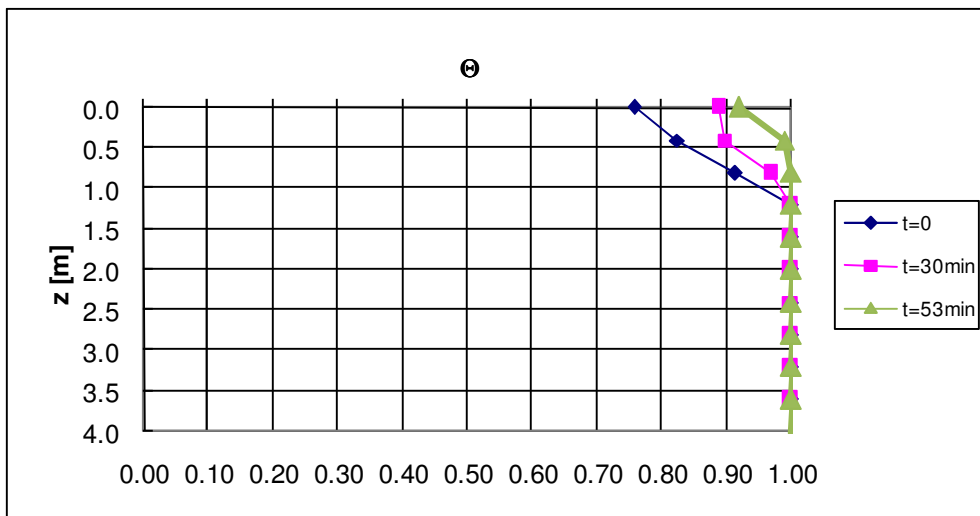


Fig. G10: $(u_a-u_w)_0 = 19 \text{ kPa}; l = 9.72 \text{ mm/h}$

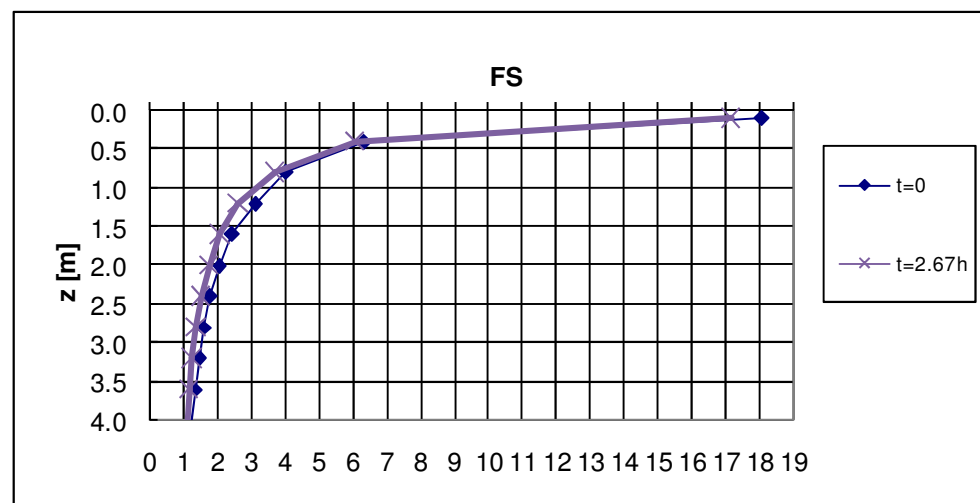
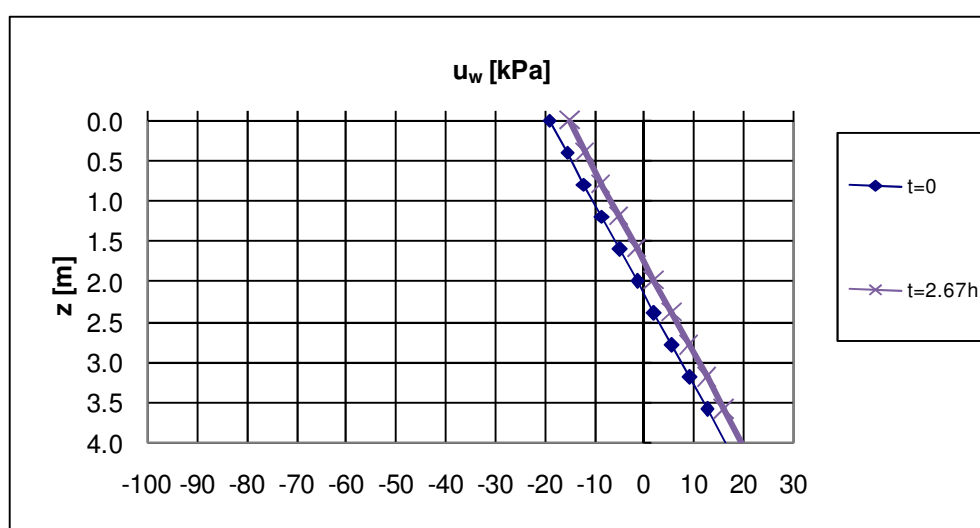
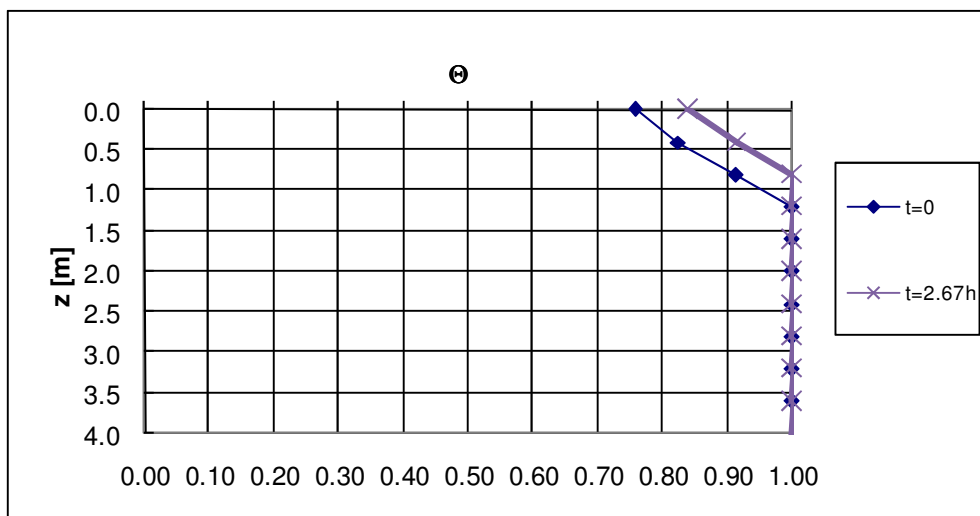


Fig. G11: $(u_a - u_w)_0 = 19$ kPa; $I = 1.94$ mm/h



ATTACHMENT H

Hypothesis 3

Slope angle $\beta = 20^\circ$
Soil nr.1

Case b

Thickness $h = 2$ m
Impervious bottom

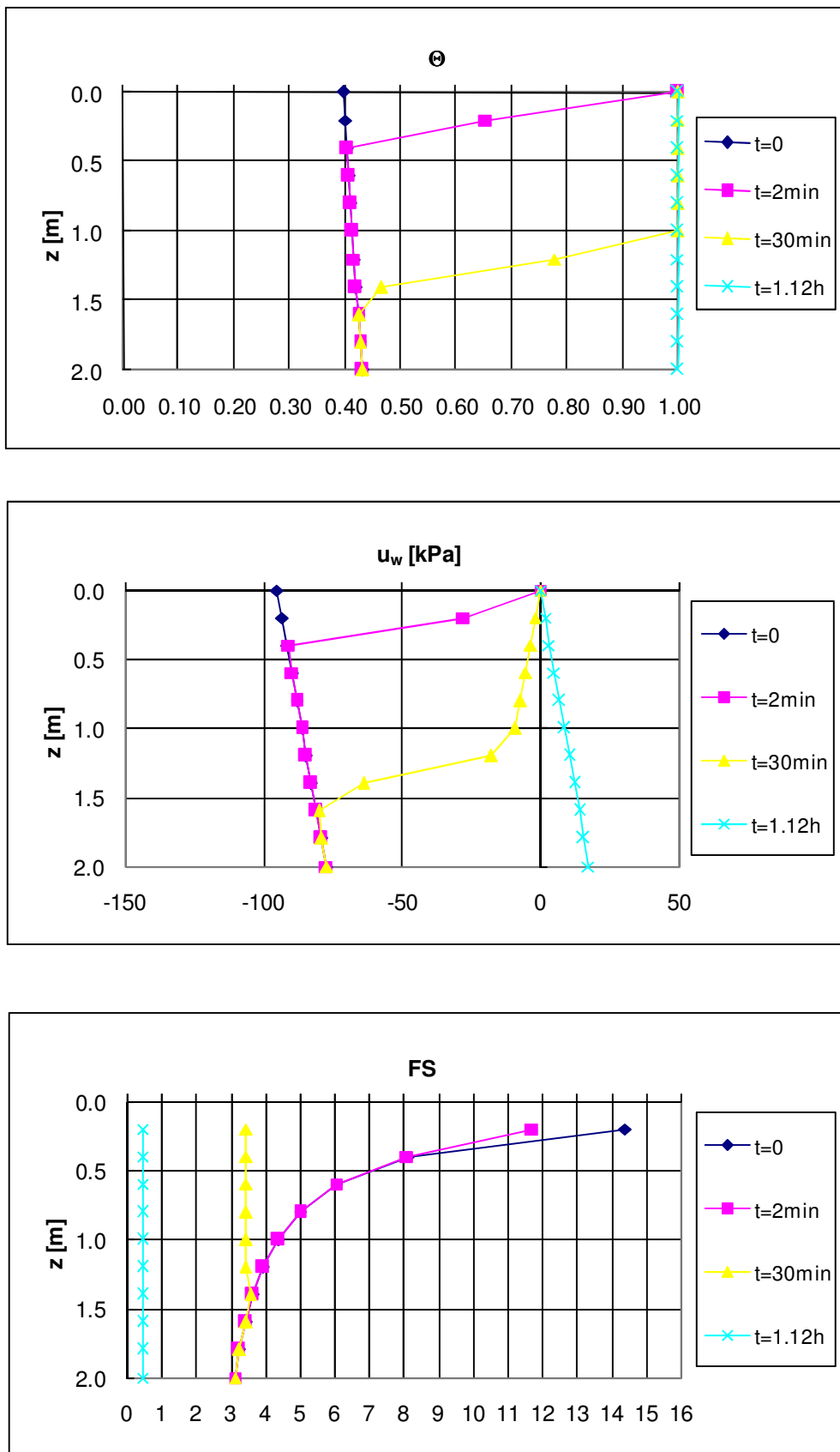


Fig. H1: $(u_a - u_w)_0 = 95 \text{ kPa}; I = 97.20 \text{ mm/h}$

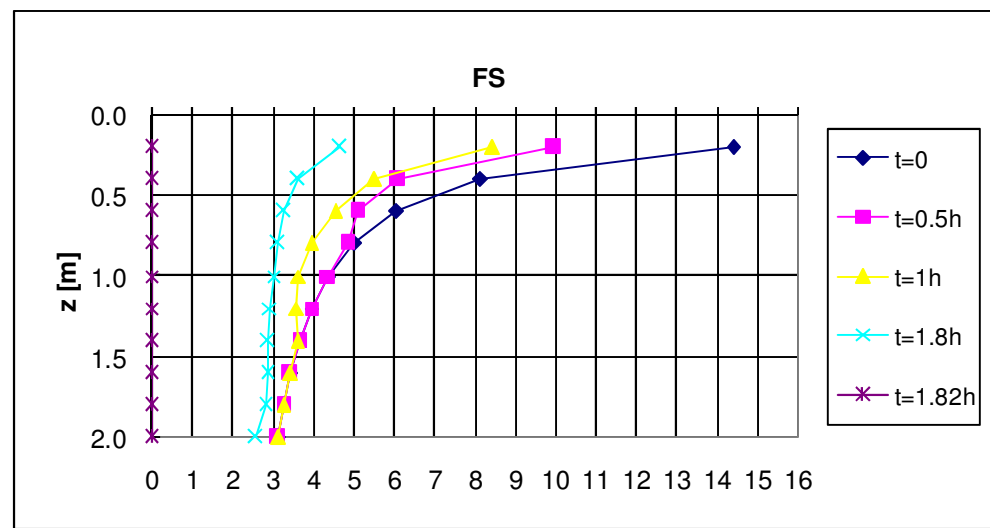
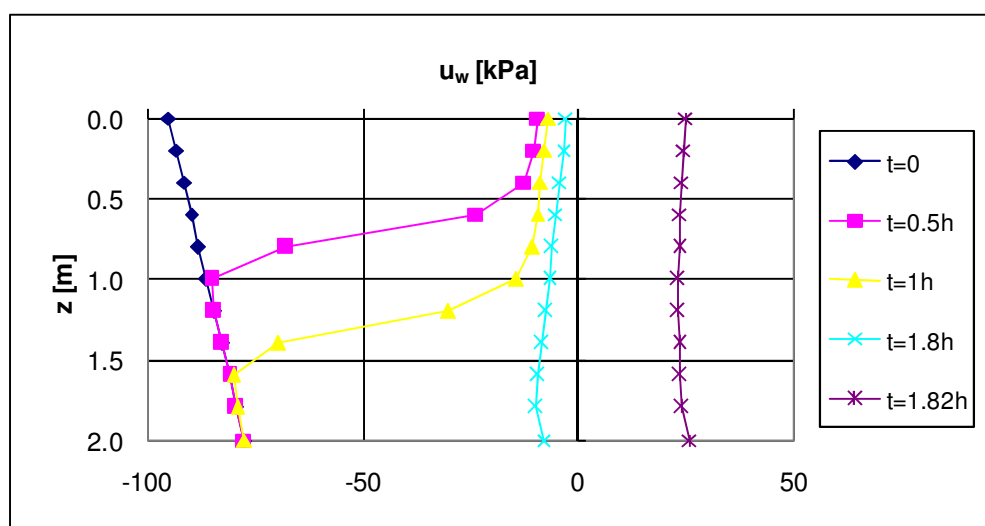
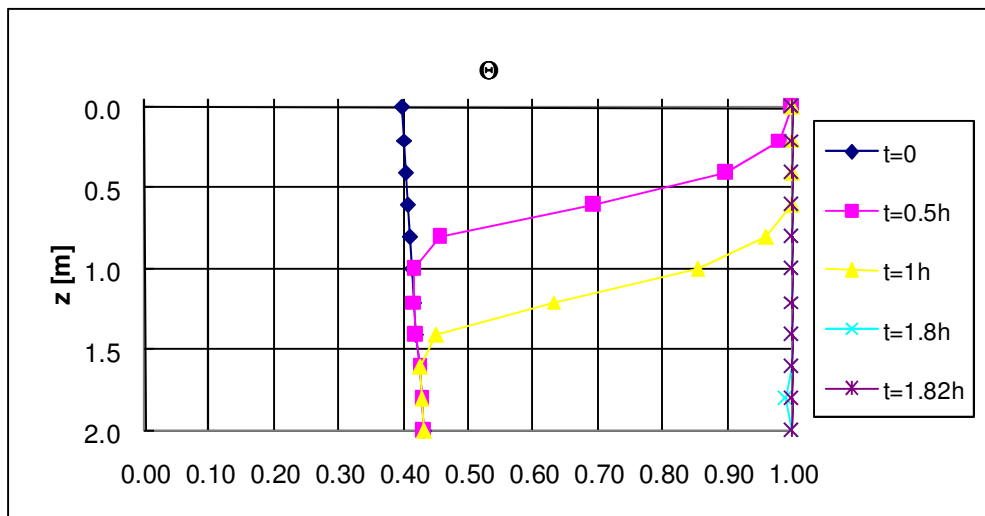


Fig. H2: $(u_a - u_w)_0 = 95$ kPa; $I = 19.44$ mm/h

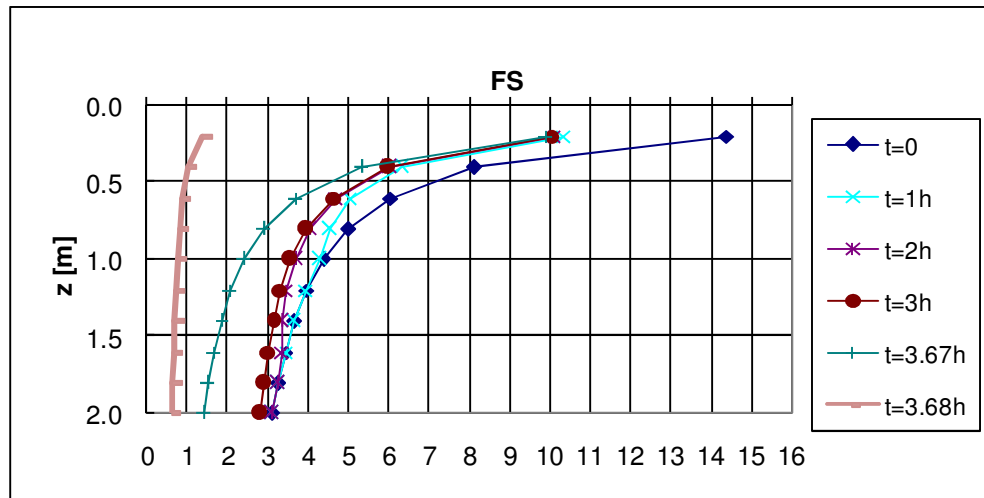
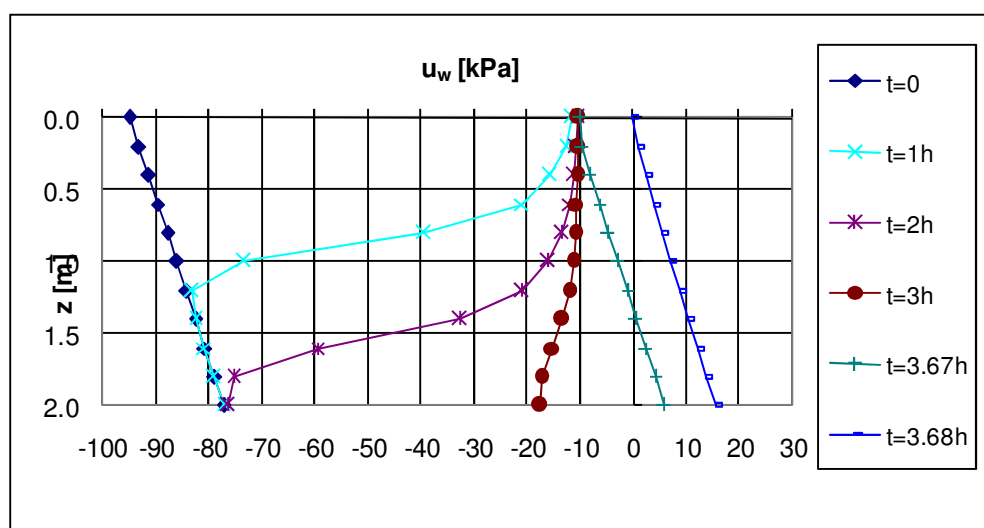
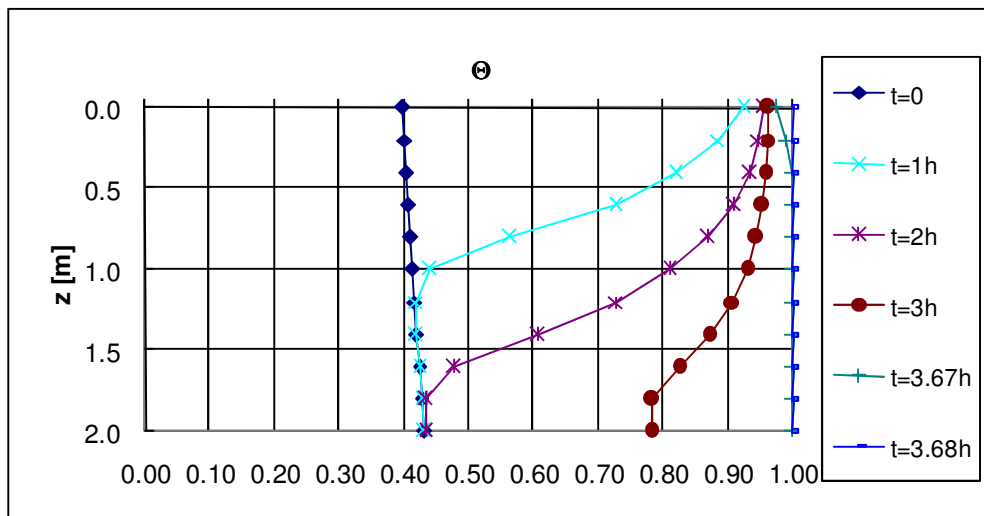


Fig. H3: $(u_a - u_w)_0 = 95 \text{ kPa}$; $I = 9.72 \text{ mm/h}$

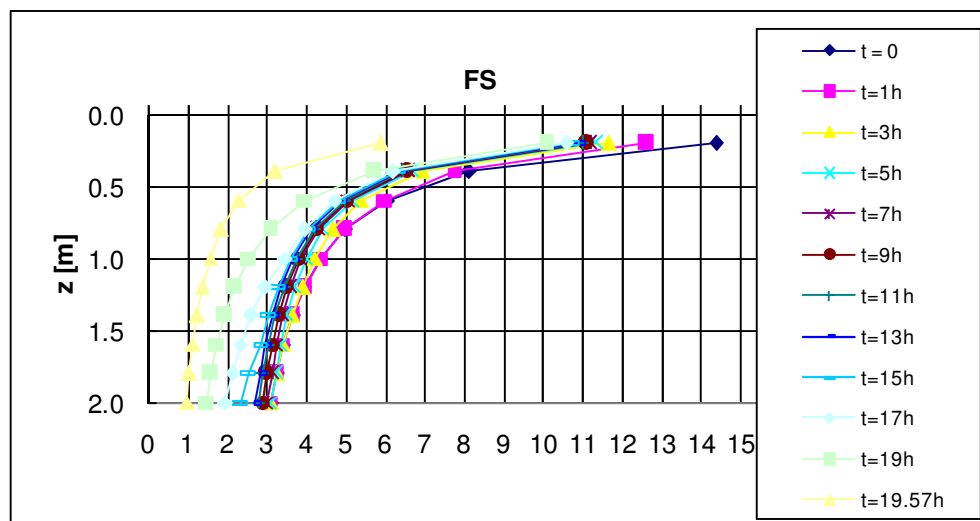
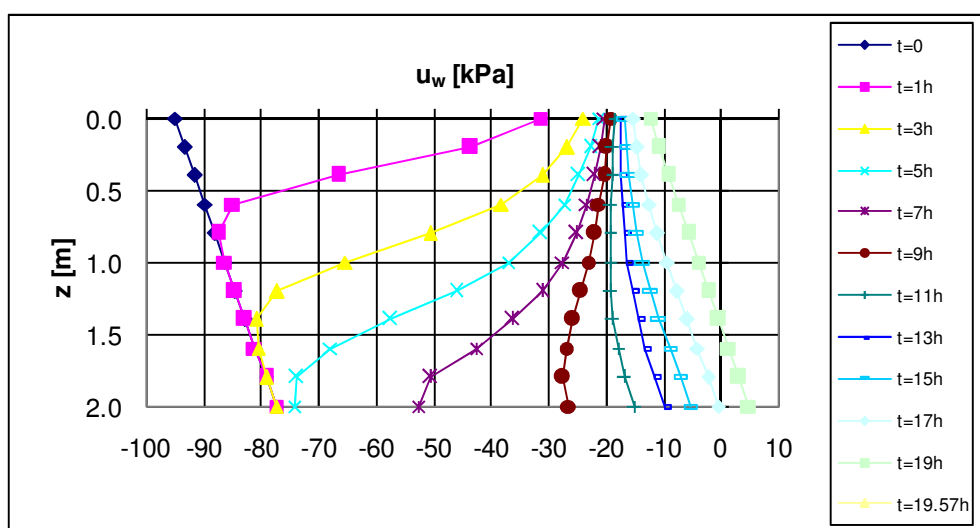
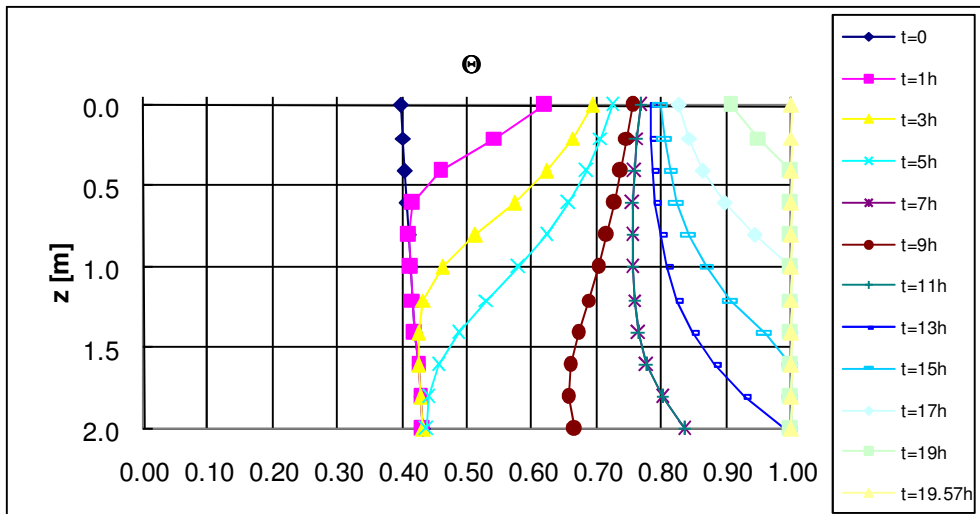


Fig. H4: $(u_a - u_w)_0 = 95 \text{ kPa}$; $I = 1.94 \text{ mm/h}$

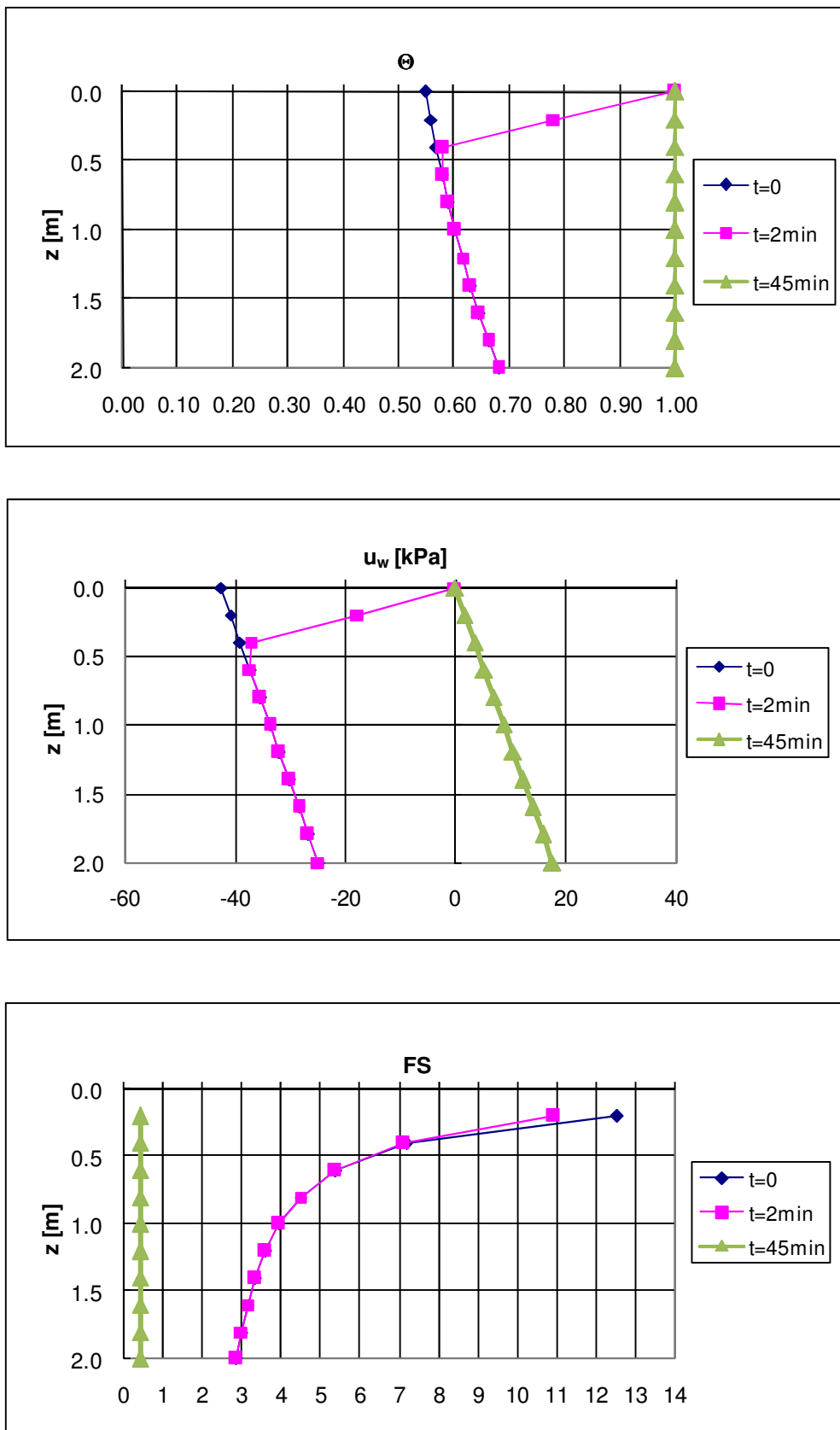


Fig. H5: $(u_a - u_w)_0 = 42.49 \text{ kPa}$; $I = 97.20 \text{ mm/h}$

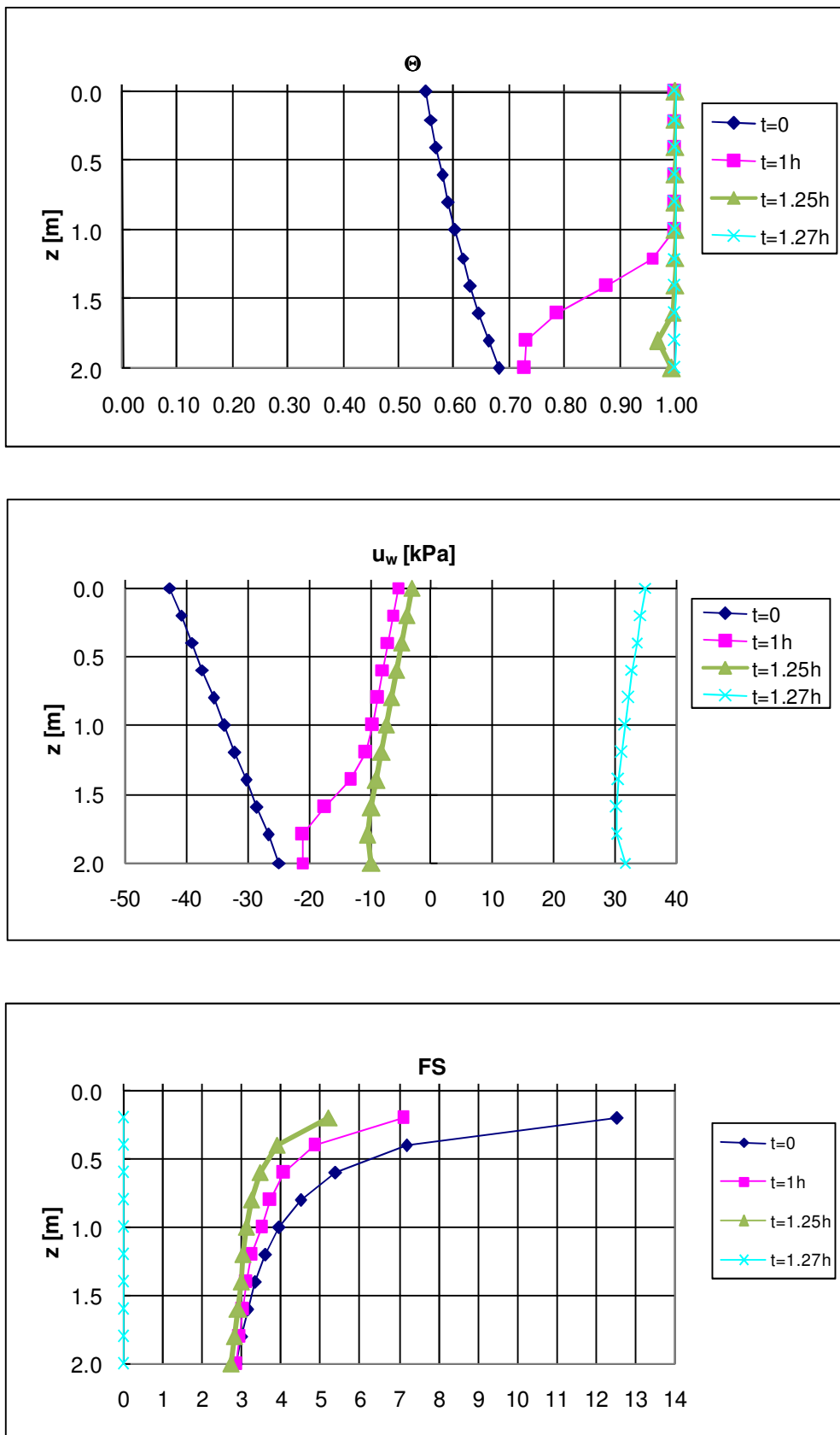


Fig. H6: $(u_a - u_w)_0 = 42.49 \text{ kPa}$; $I = 19.44 \text{ mm/h}$

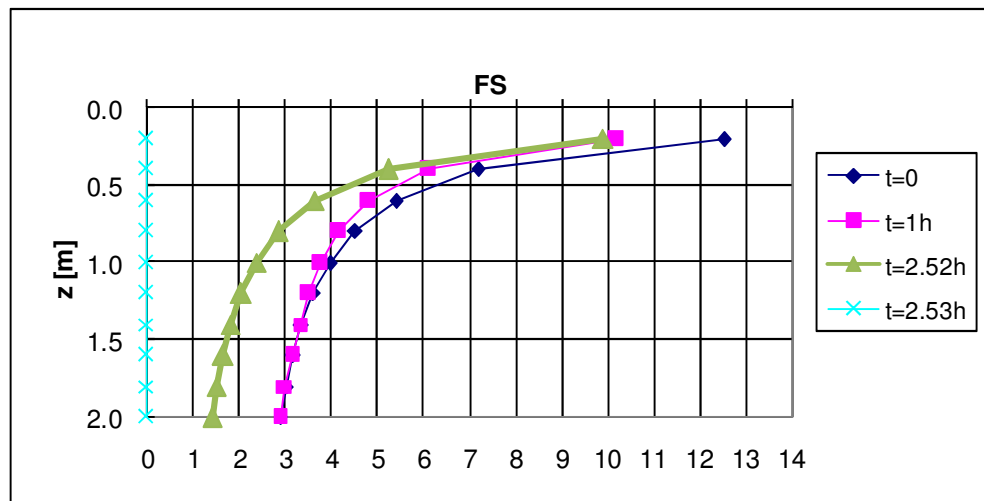
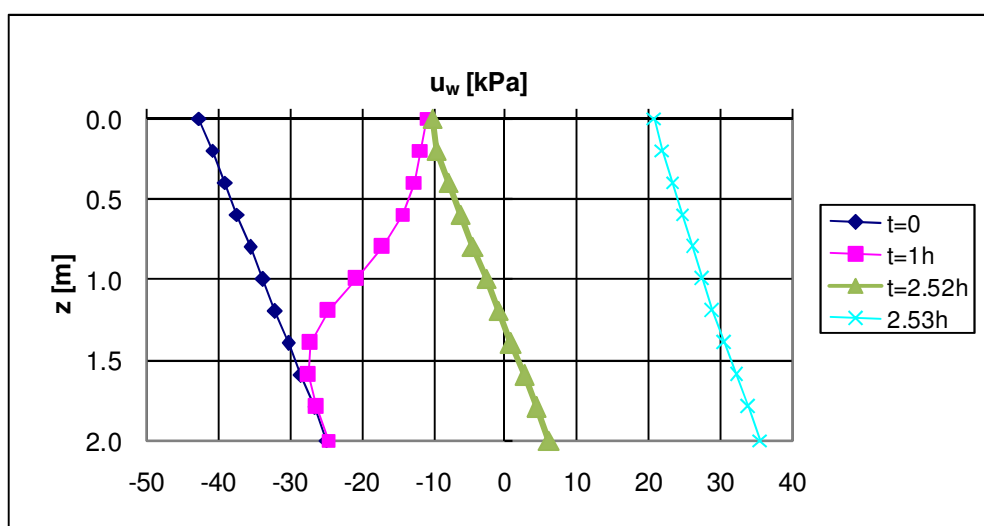
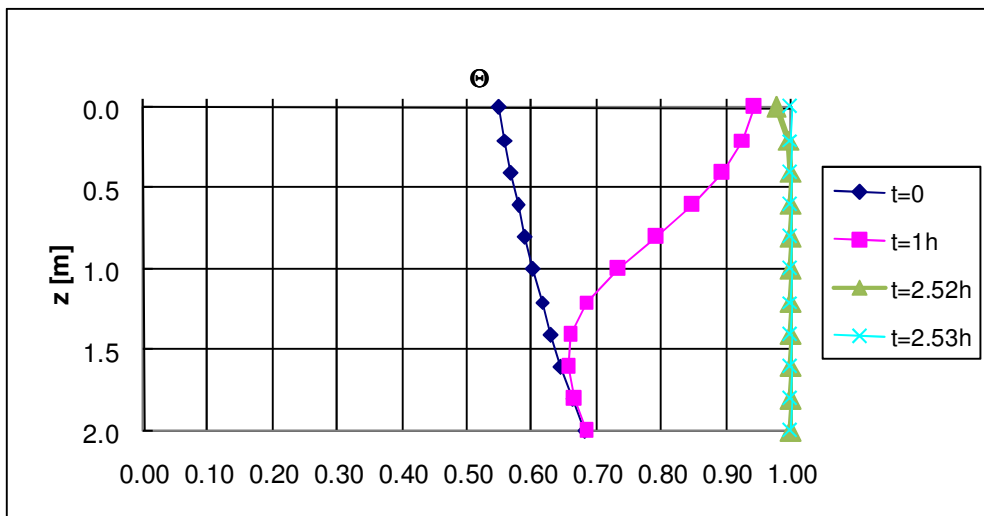


Fig. H7: $(u_a - u_w)_0 = 42.49 \text{ kPa}$; $I = 9.72 \text{ mm/h}$

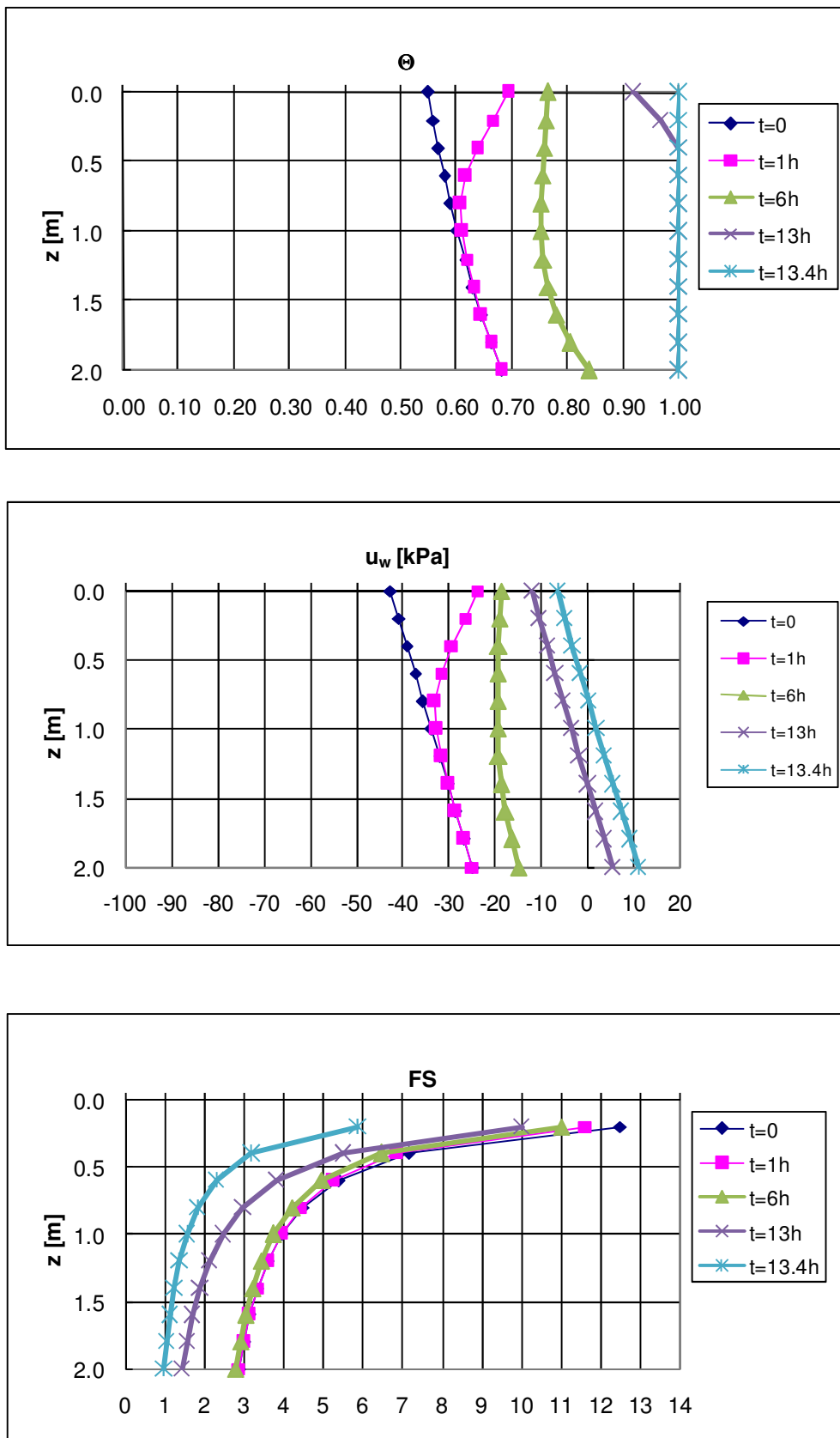


Fig. H8: $(u_a - u_w)_0 = 42.49$ kPa; $I = 1.94$ mm/h

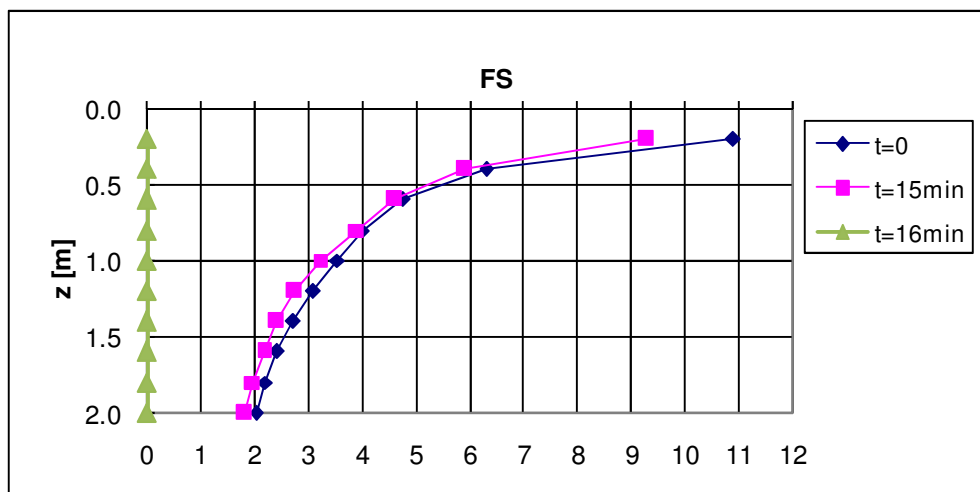
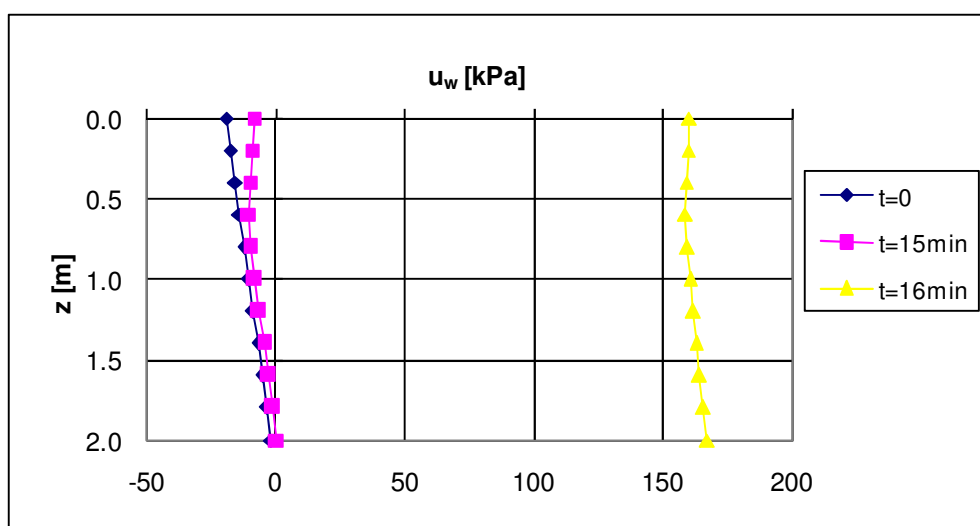
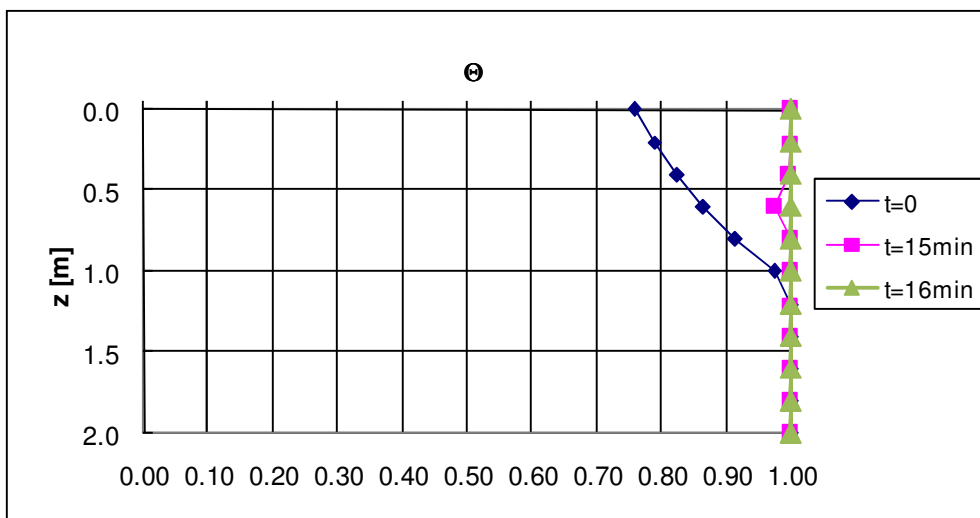


Fig. H9: $(u_a - u_w)_0 = 19$ kPa; $I = 19.44$ mm/h

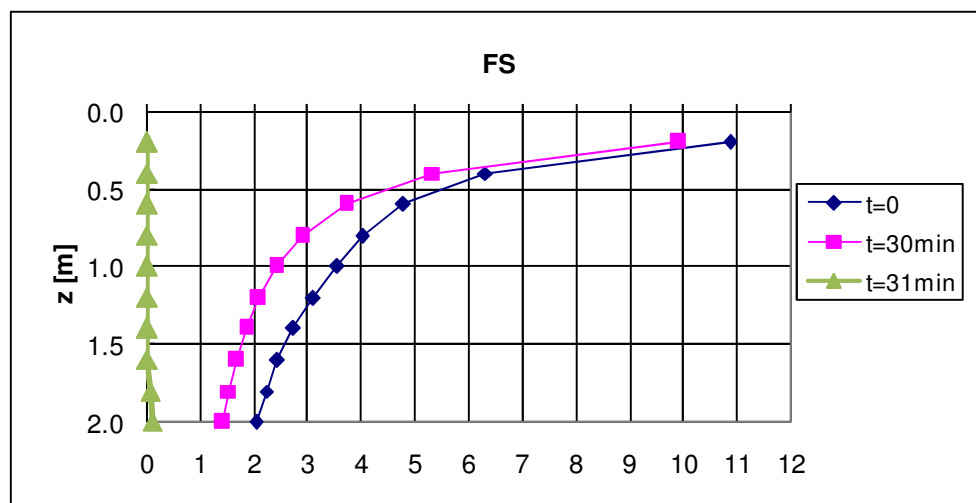
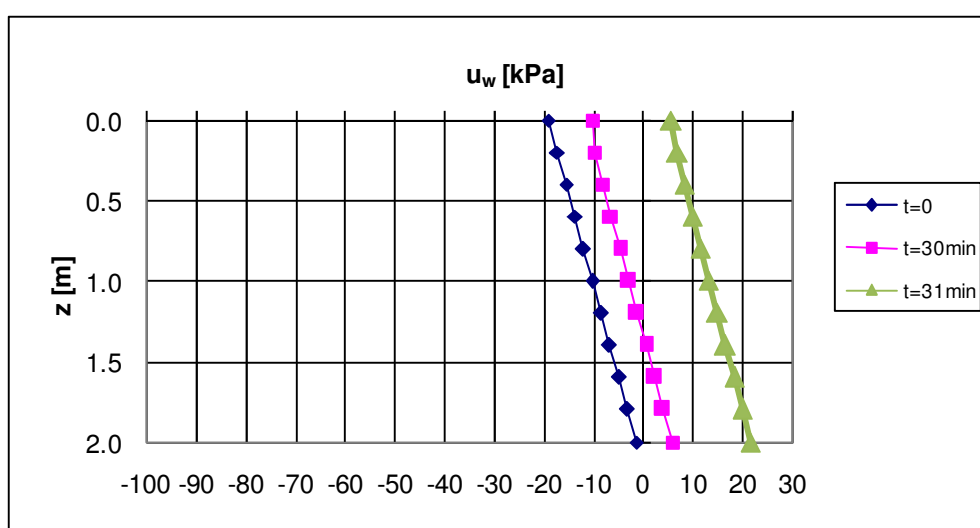
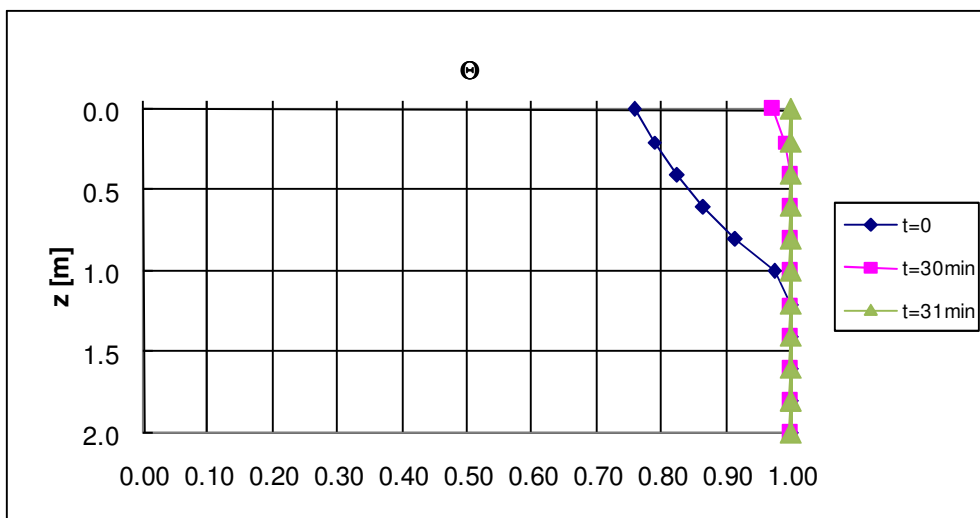


Fig. H10: $(u_a - u_w)_0 = 19 \text{ kPa}; I = 9.72 \text{ mm/h}$

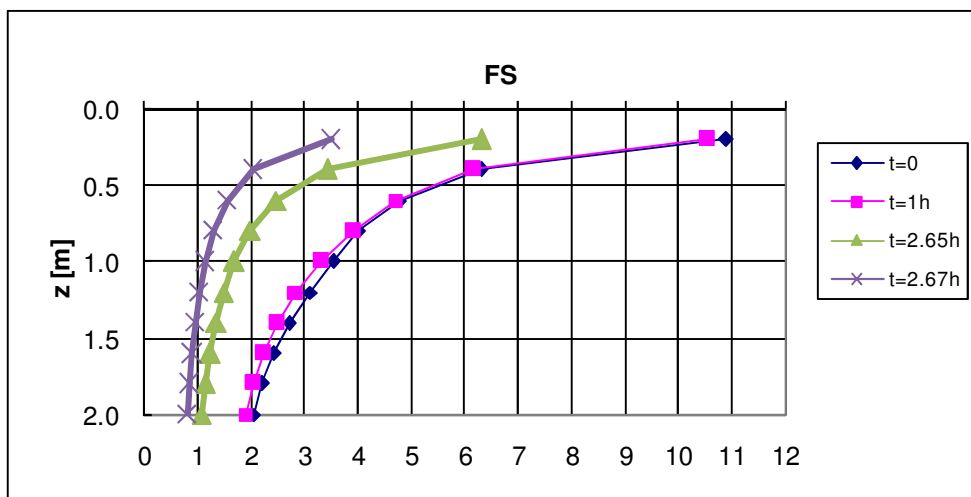
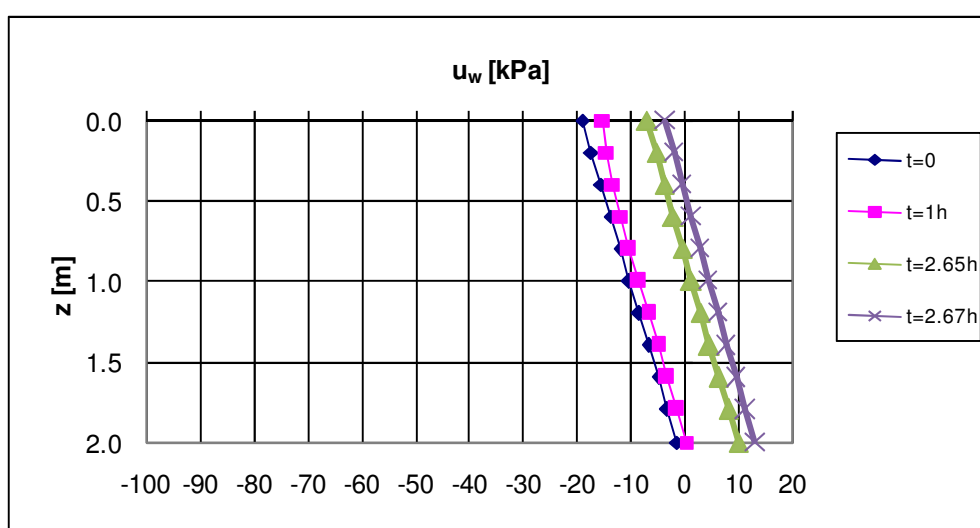
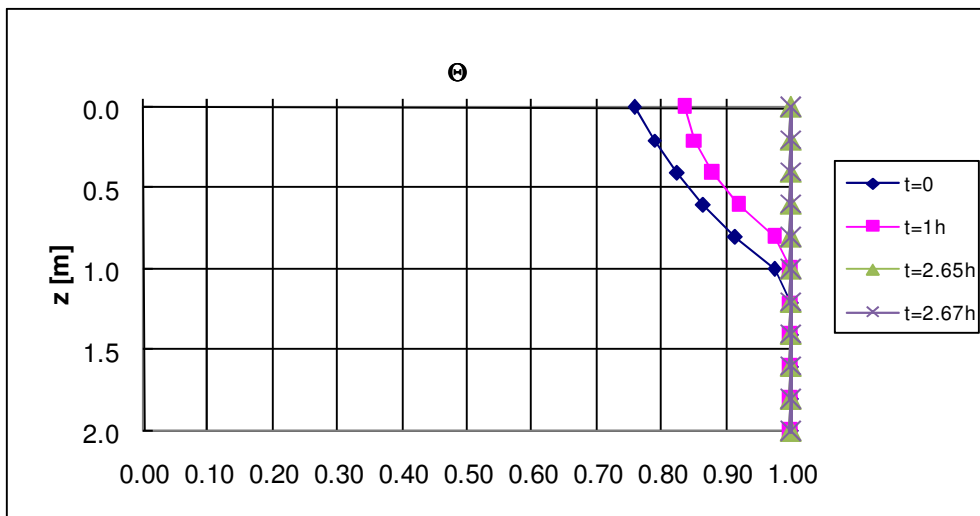


Fig. H11: $(u_a - u_w)_0 = 19 \text{ kPa}; l = 1.94 \text{ mm/h}$

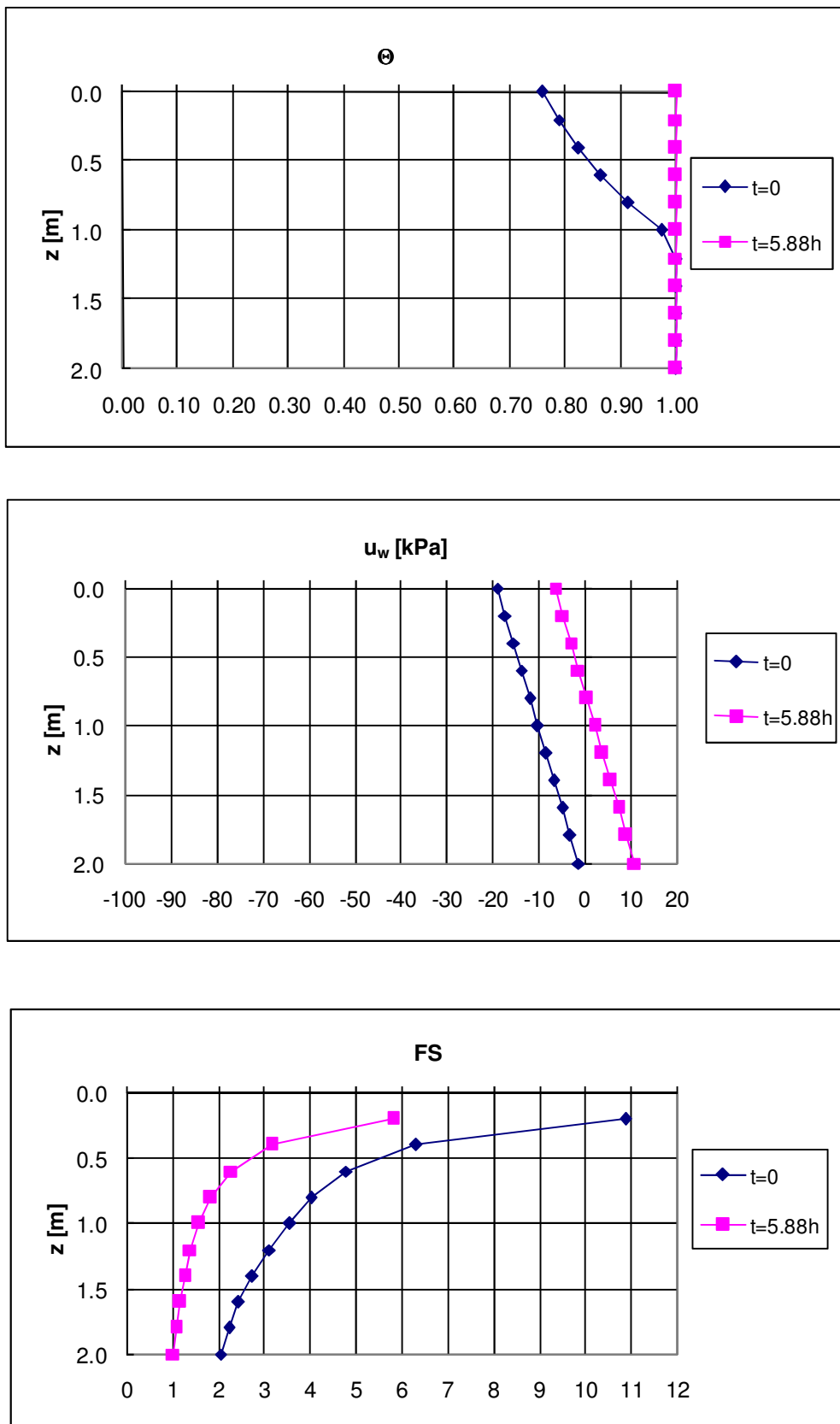


Fig. H12: $(u_a - u_w)_0 = 19 \text{ kPa}$; $I = 0.97 \text{ mm/h}$



ATTACHMENT I

Hypothesis 4

Slope angle $\beta = 40^\circ$

Soil nr.2

Thickness $h = 2$ m

Impervious bottom

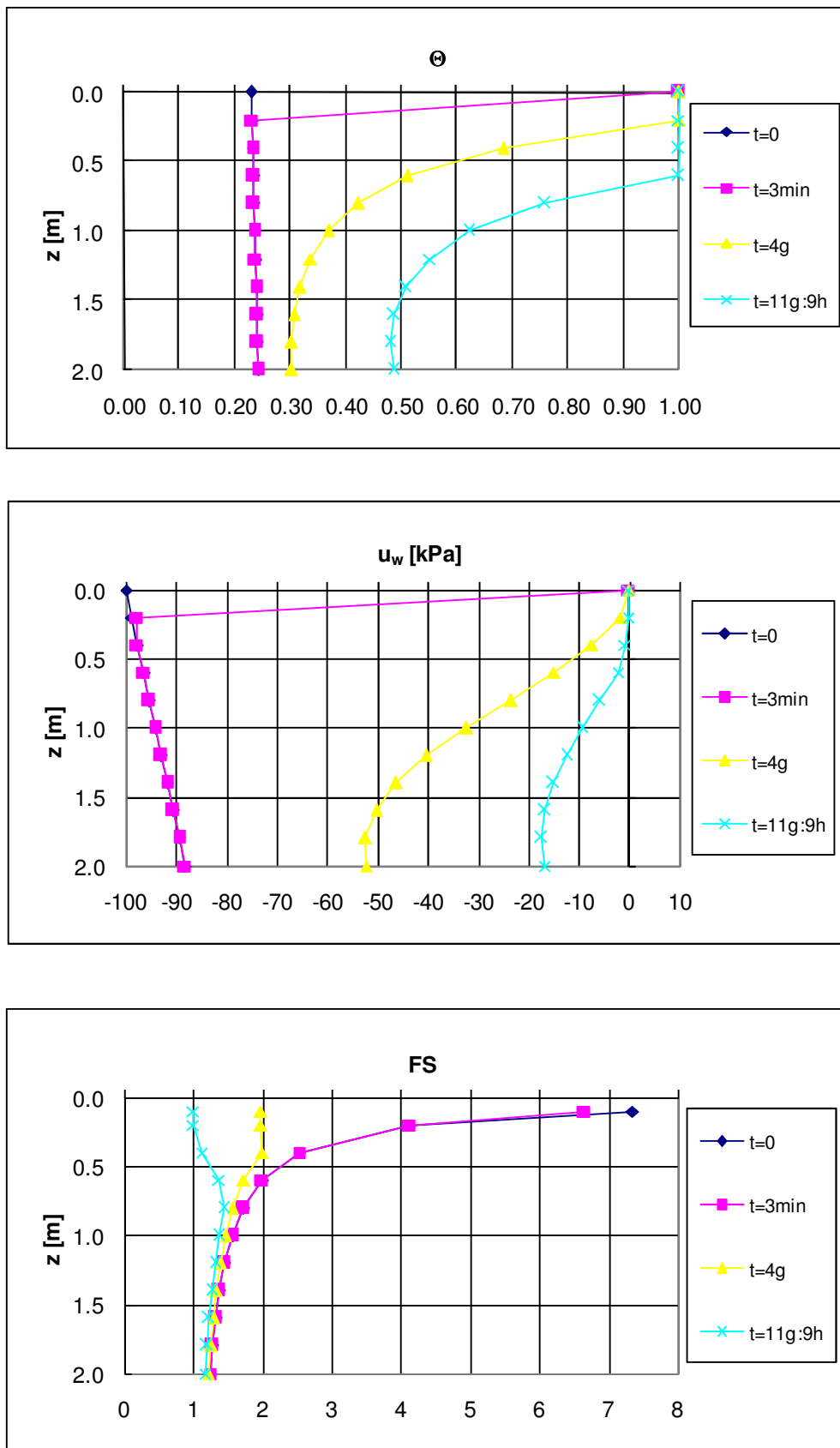


Fig. I1: $(u_a - u_w)_0 = 100 \text{ kPa}$; $I = 97.20 \text{ mm/h}$

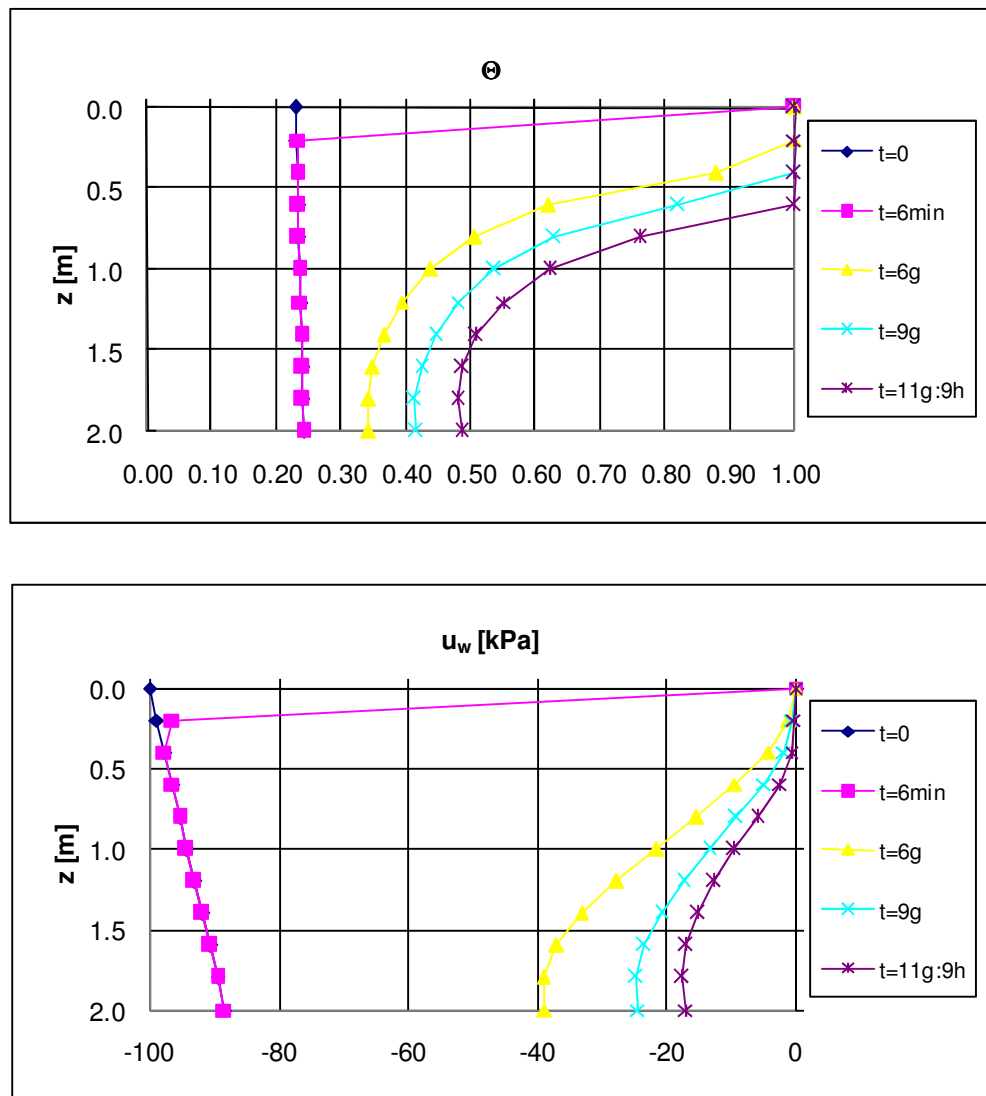


Fig. I2: $(u_a - u_w)_0 = 100 \text{ kPa}; I = 19.44 \text{ mm/h}$

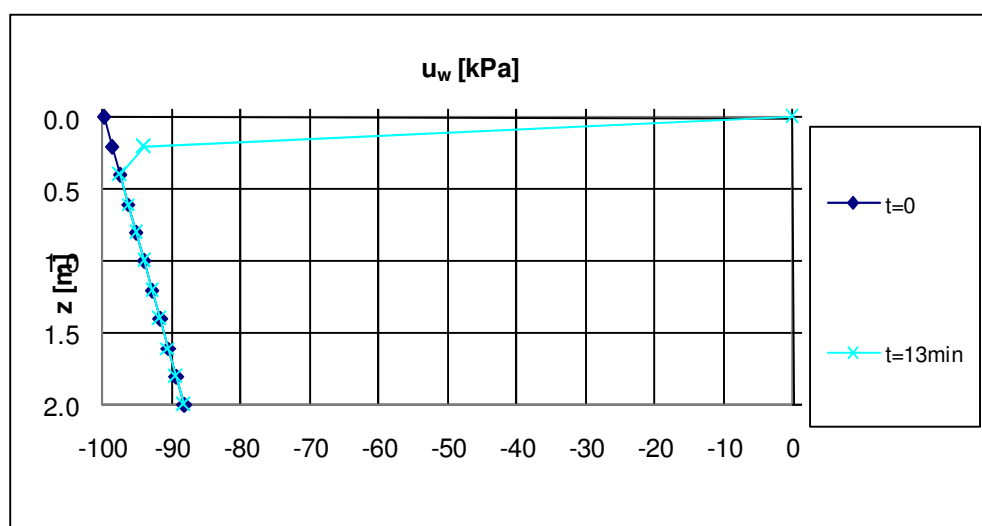
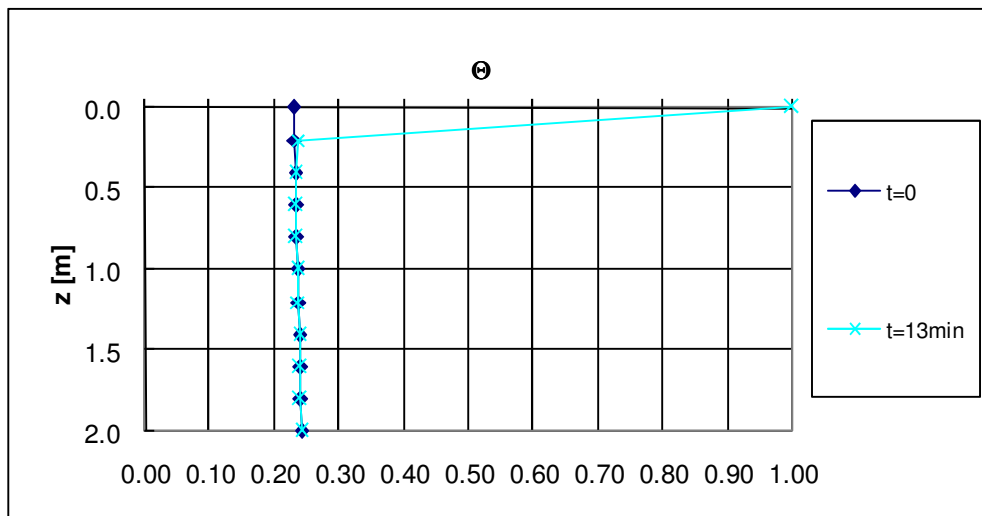


Fig. I3: $(u_a - u_w)_0 = 100 \text{ kPa}; I = 9.72 \text{ mm/h}$

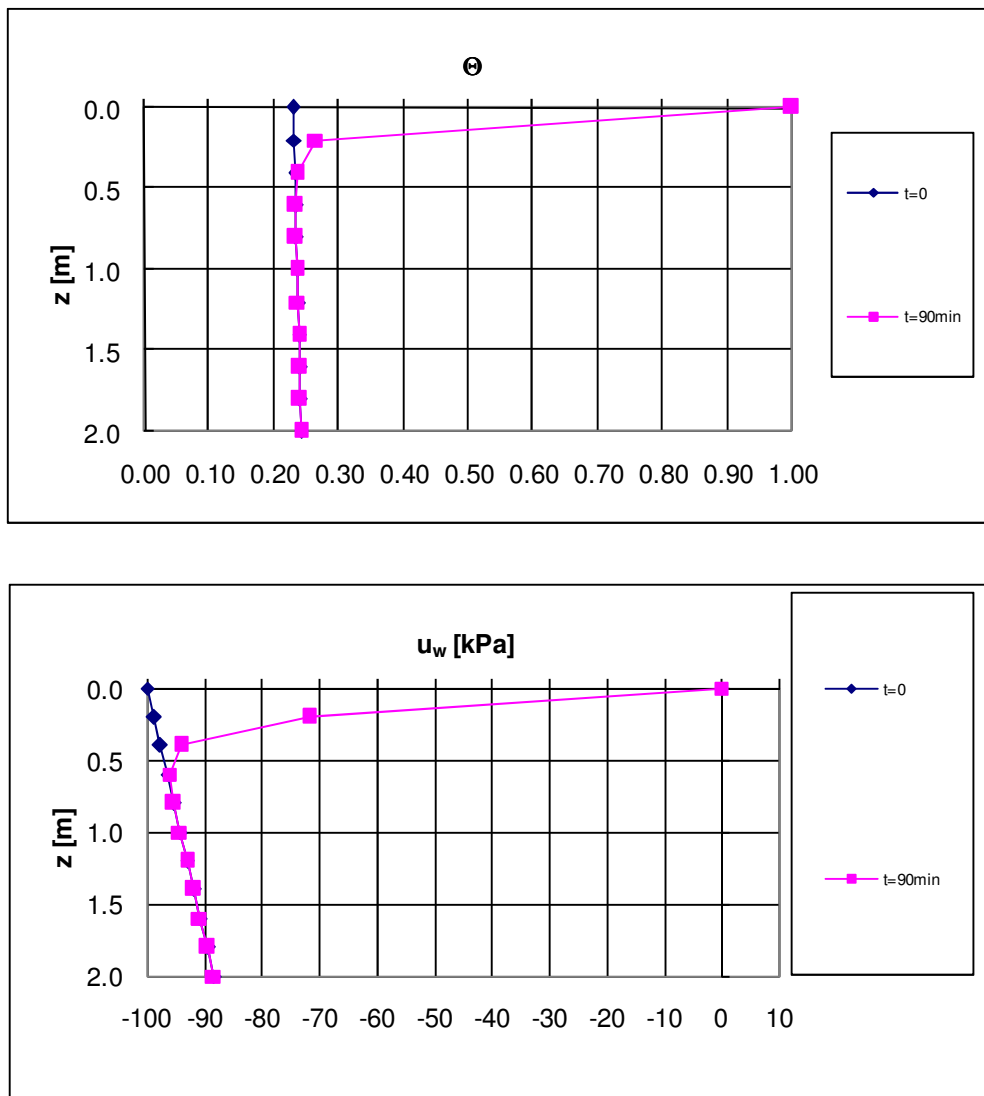


Fig. I4: $(u_a - u_w)_0 = 100 \text{ kPa}; I = 1.94 \text{ mm/h}$

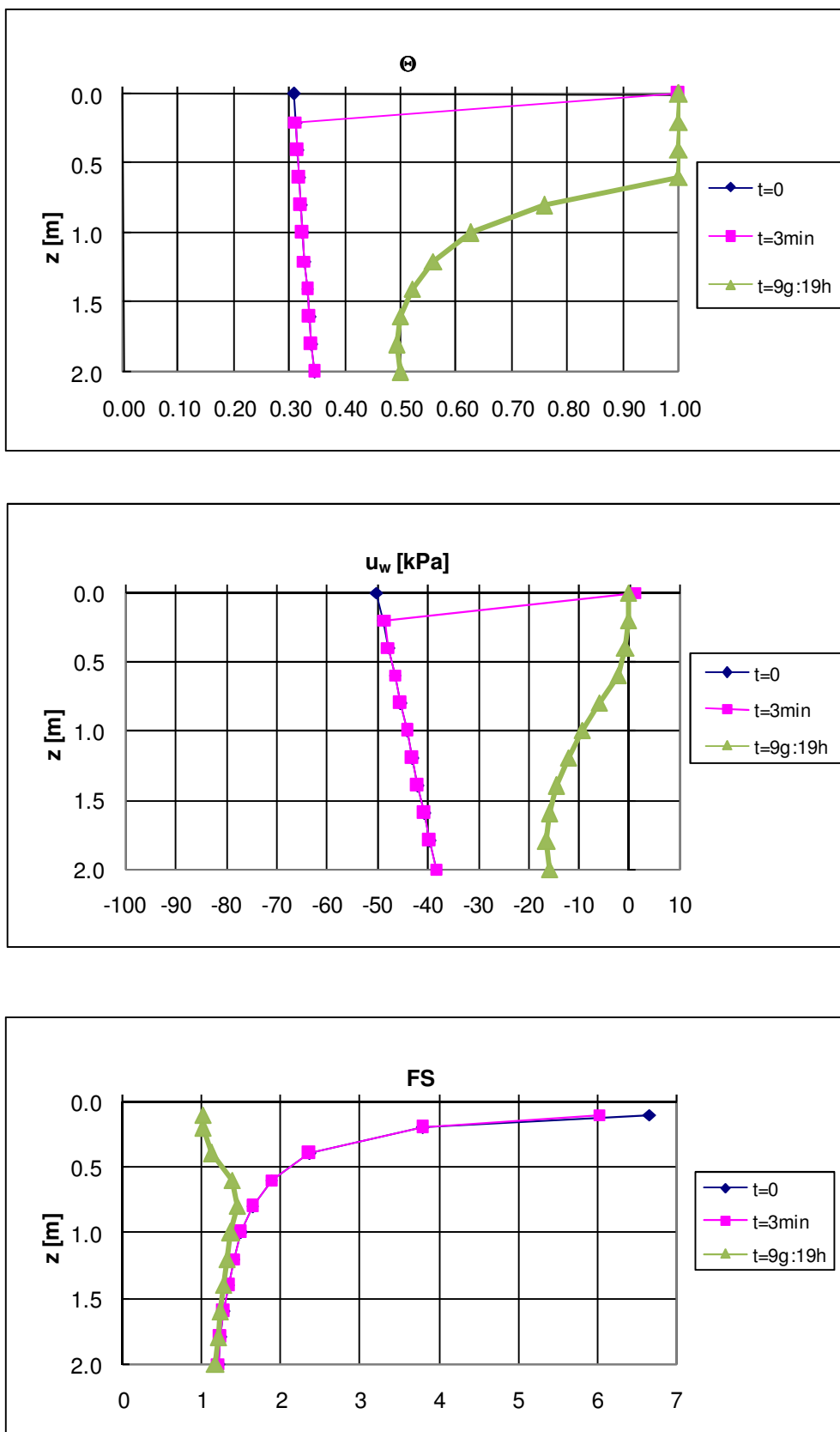


Fig. I5: $(u_a - u_w)_0 = 50 \text{ kPa}$; $I = 97.20 \text{ mm/h}$

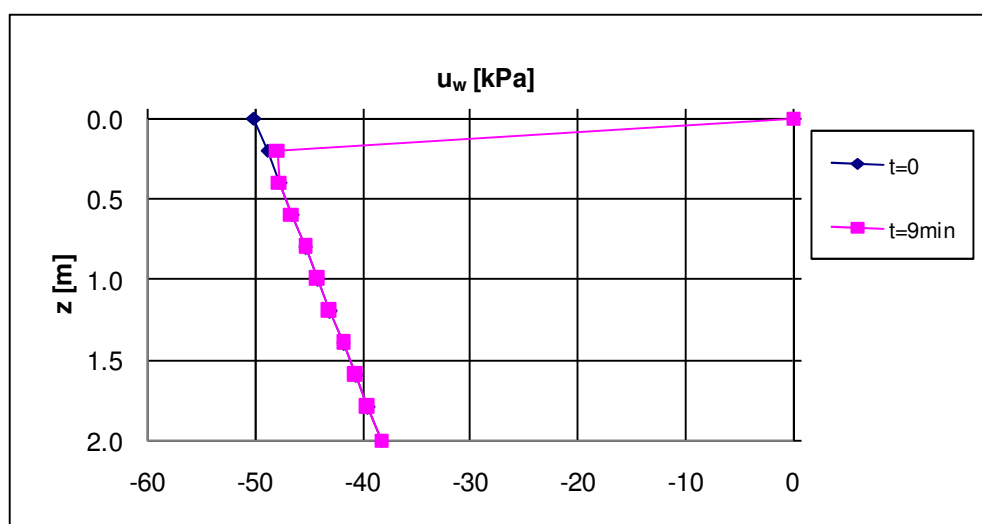
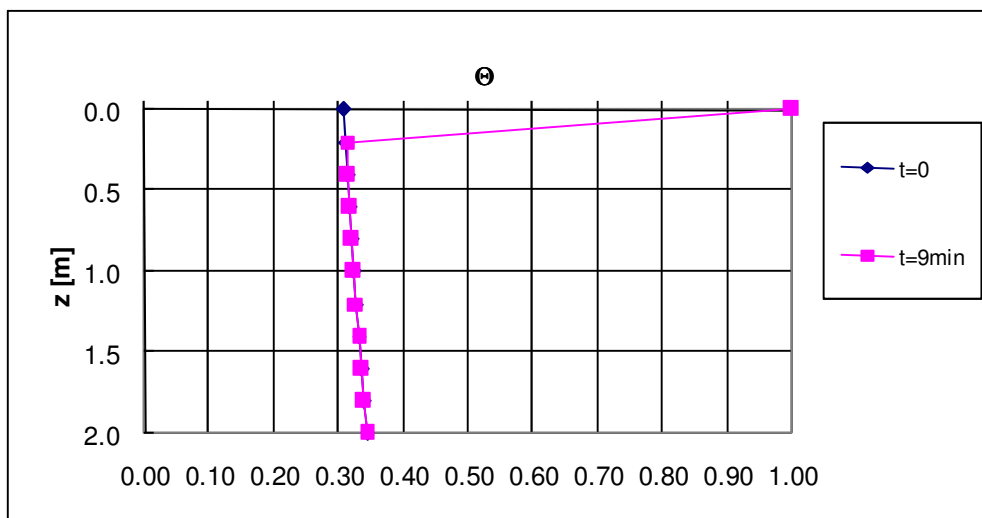


Fig. I6: $(u_a - u_w)_0 = 50 \text{ kPa}; l = 19.44 \text{ mm/h}$

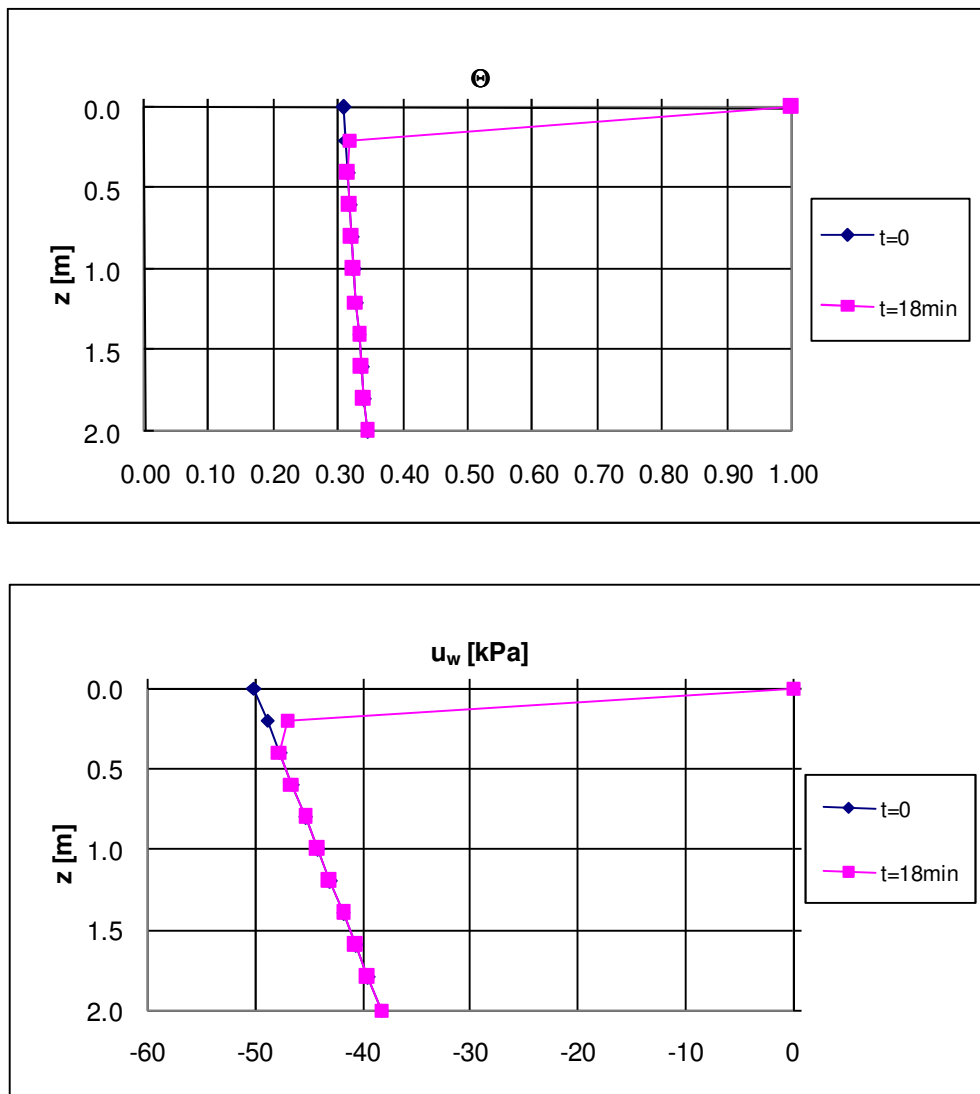


Fig. I7: $(u_a - u_w)_0 = 50 \text{ kPa}; I = 9.72 \text{ mm/h}$

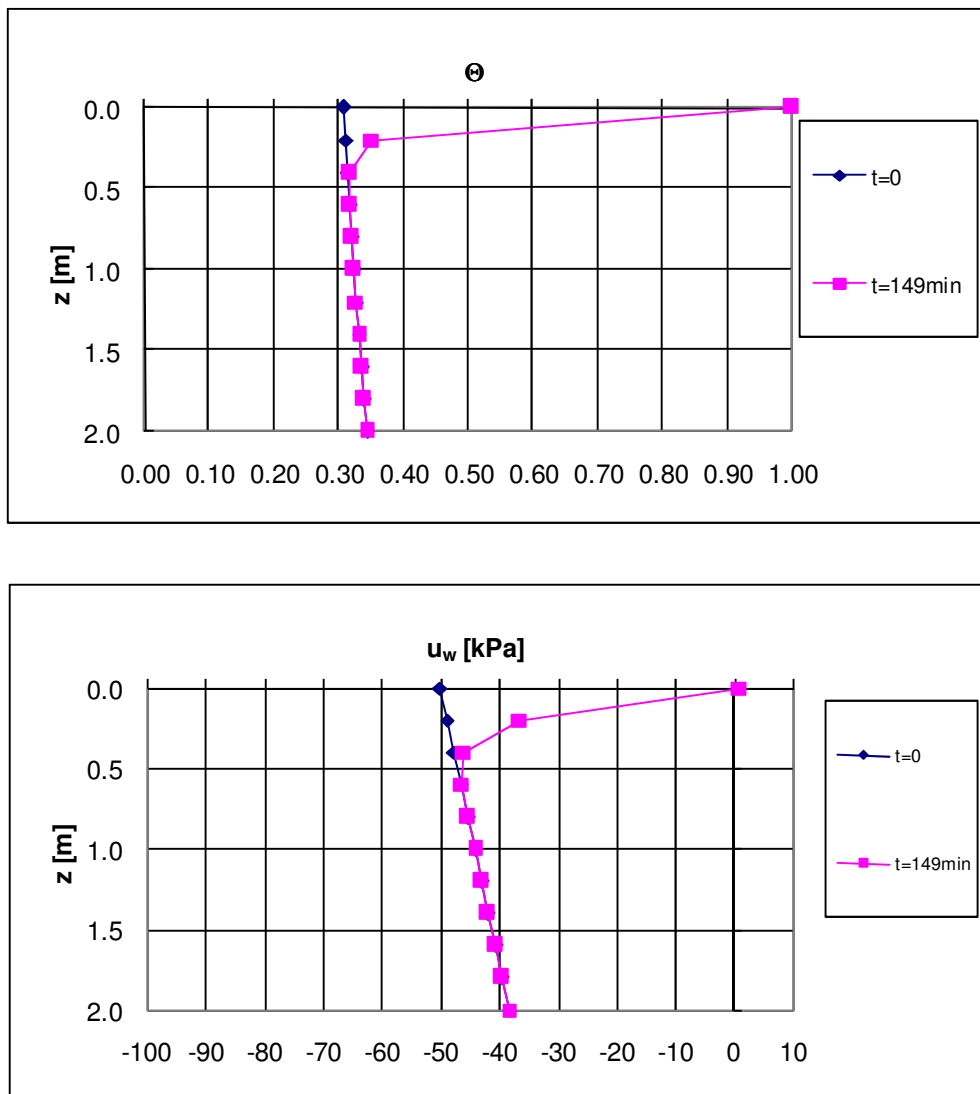


Fig. I8: $(u_a-u_w)_0 = 50 \text{ kPa}; l = 1.94 \text{ mm/h}$

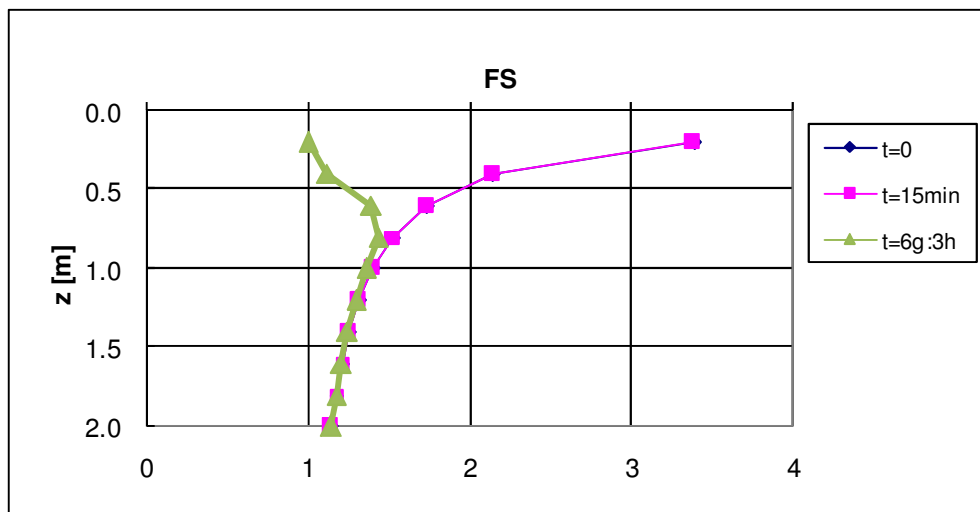
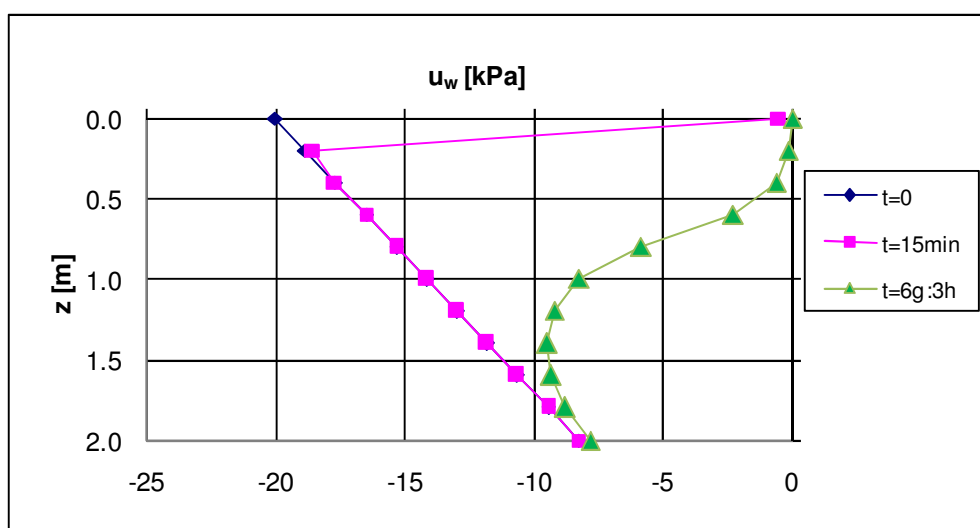
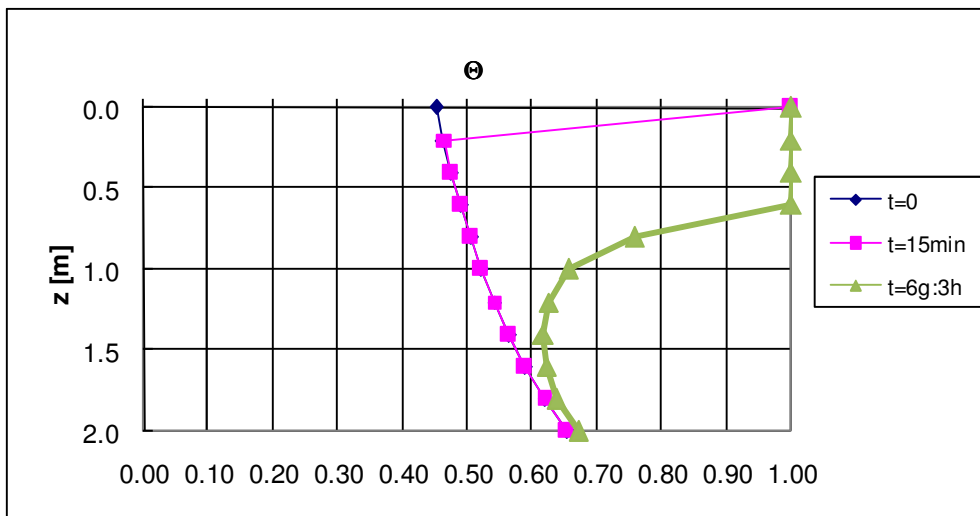


Fig. 19: $(u_a - u_w)_0 = 20 \text{ kPa}; I = 19.44 \text{ mm/h}$

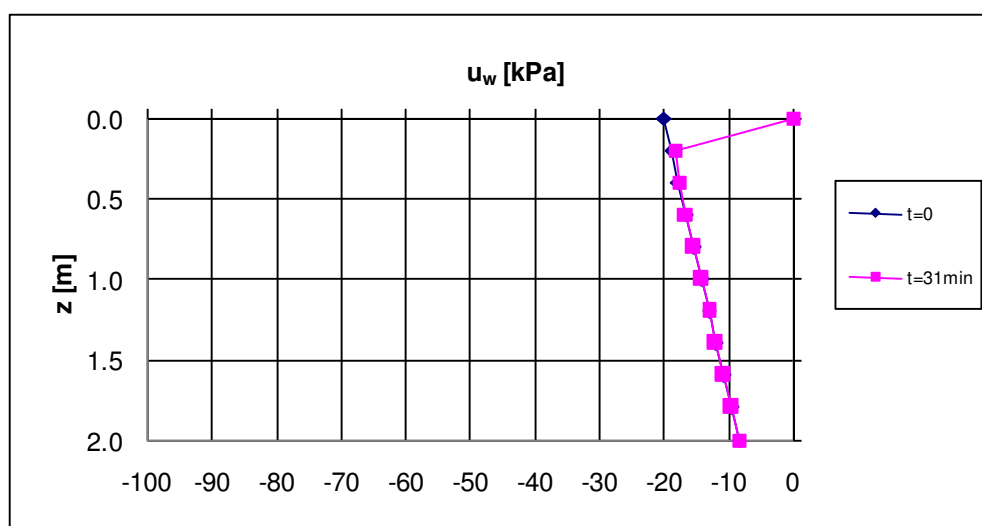
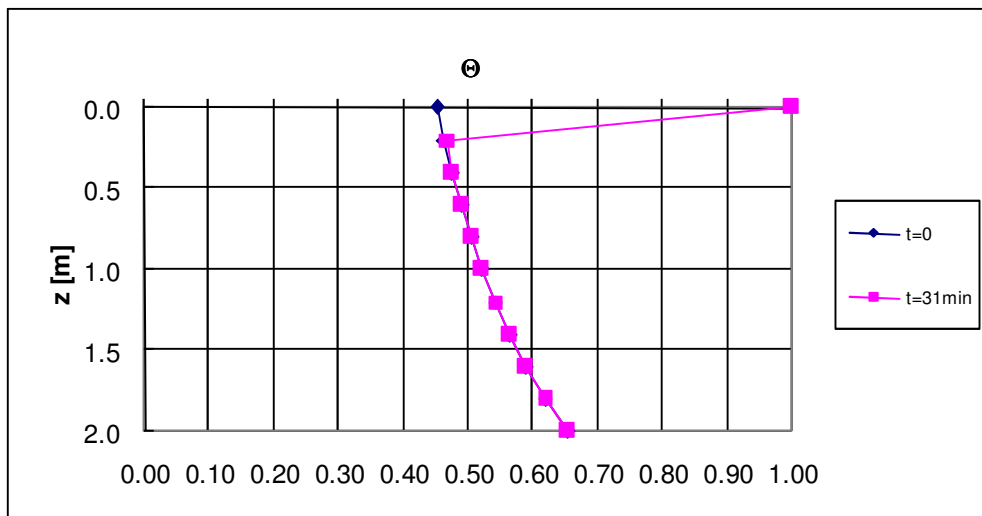


Fig. I10: $(u_a - u_w)_0 = 20 \text{ kPa}; I = 9.72 \text{ mm/h}$

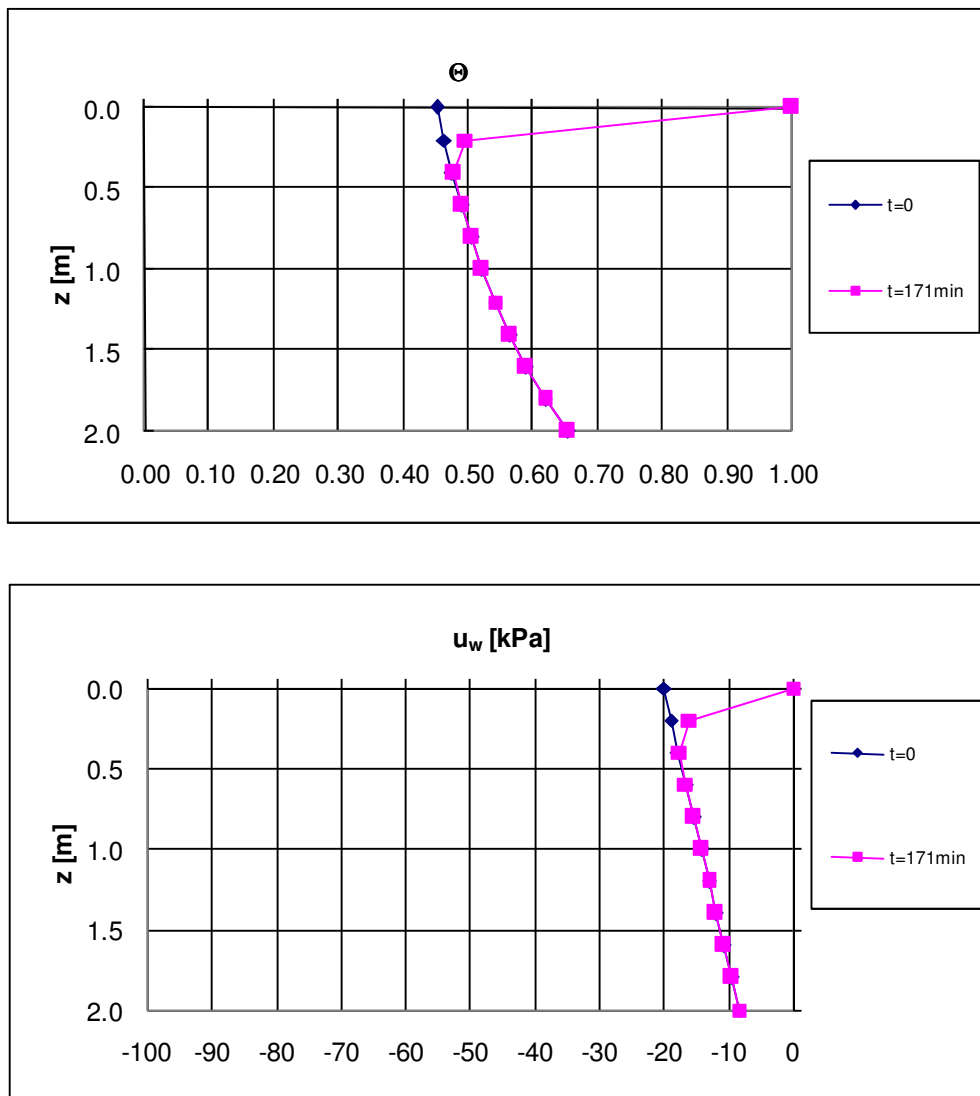


Fig. I11: $(u_a - u_w)_0 = 20 \text{ kPa}; l = 1.94 \text{ mm/h}$

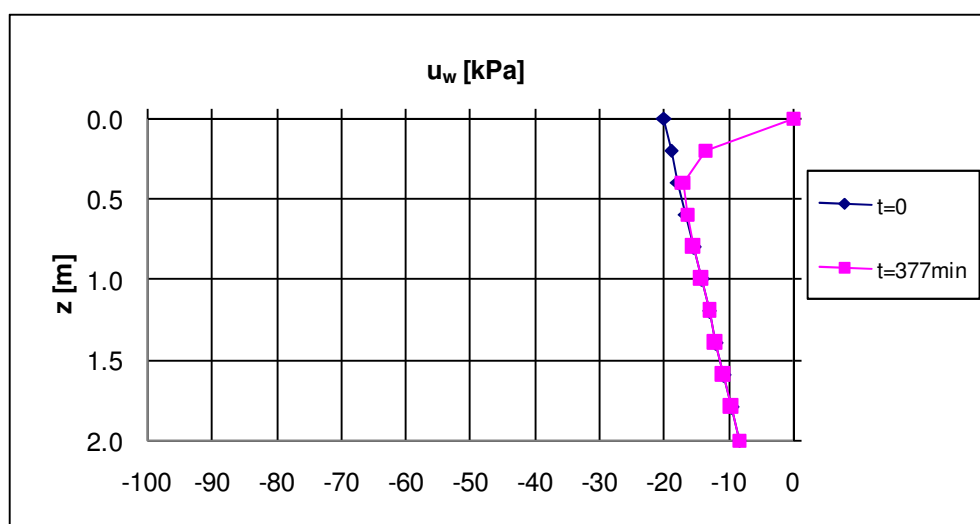
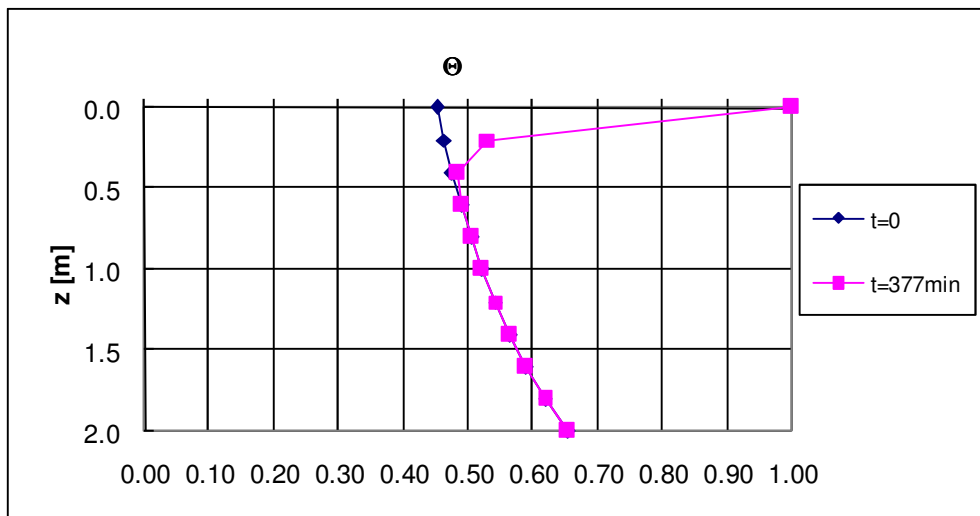


Fig. I12: $(u_a - u_w)_0 = 20 \text{ kPa}; l = 0.97 \text{ mm/h}$